The Western Wind and Solar Integration Study Phase 2

D. Lew, G. Brinkman, E. Ibanez, A. Florita,
M. Heaney, B.-M. Hodge, M. Hummon,
and G. Stark
NREL

J. King
RePPAE

S.A. Lefton, N. Kumar, and D. Agan
Intertek-APTECH

G. Jordan and S. Venkataraman
GE Energy

The Western Wind and Solar Integration Study Phase 2

D. Lew, G. Brinkman, E. Ibanez, A. Florita,
M. Heaney, B.-M. Hodge, M. Hummon,
and G. Stark
NREL

J. King
RePPAE

S.A. Lefton, N. Kumar, and D. Agan
Intertek-APTECH

G. Jordan and S. Venkataraman
GE Energy

**NREL is a national laboratory of the U.S. Department of Energy, Office of Energy
Efficiency & Renewable Energy, operated by the Alliance for Sustainable Energy, LLC.**

National Renewable Energy Laboratory
15013 Denver West Parkway
Golden, Colorado 80401
303-275-3000 • www.nrel.gov

Technical Report
NREL/TP-5500-55588
September 2013

Contract No. DE-AC36-08GO28308

NOTICE

This report was prepared as an account of work sponsored by an agency of the United States government. Neither the United States government nor any agency thereof, nor any of their employees, makes any warranty, express or implied, or assumes any legal liability or responsibility for the accuracy, completeness, or usefulness of any information, apparatus, product, or process disclosed, or represents that its use would not infringe privately owned rights. Reference herein to any specific commercial product, process, or service by trade name, trademark, manufacturer, or otherwise does not necessarily constitute or imply its endorsement, recommendation, or favoring by the United States government or any agency thereof. The views and opinions of authors expressed herein do not necessarily state or reflect those of the United States government or any agency thereof.

Acknowledgments

List of Acronyms

4HA	4-hour-ahead
BA	balancing authority
C&M	capital and maintenance
CAISO	California Independent System Operator
CC	combined-cycle
CEM	continuous emissions monitoring
CF	capacity factor
CFE	Comisión Federal de Electricidad
CG	Columbia Grid
CO_2	carbon dioxide
CSP	concentrating solar power
CT	combustion turbine
CY	calendar year
DA	day-ahead
DC	direct current
DCOE	delivered cost of energy
DG	distributed generation
DOE	U.S. Department of Energy
EFOR	equivalent forced outage rate
EIA	Energy Information Administration
EPA	Environmental Protection Agency
EPRI	Electric Power Research Institute
ERCOT	Electric Reliability Council of Texas
FFT	fast Fourier transform
GHI	global horizontal irradiance
GT	gas turbine
GW	gigawatt
GWh	gigawatt hour
HRSG	heat recovery steam generator
IID	Imperial Irrigation District
ISO	independent system operator
LAWP	Los Angeles Department of Water and Power
LRS	Loads and Resources Subcommittee
MAE	mean average error
MISO	Midwest Independent System Operator
MMBtu	million British thermal units
MW	megawatt
MWh	megawatt hour, energy
MW-h	megawatt hour, reserves
NTTG	Northern Tier Transmission Group
NO_X	nitrogen oxides
NREL	National Renewable Energy Laboratory
NWP	numerical weather prediction
O&M	operations and maintenance
PC1	Portfolio Case 1

PPA	power purchase agreement
PV	photovoltaic
RBC	reliability-based control
ReEDS	Regional Energy Deployment System
RMSE	root-mean-square error
RPS	renewable portfolio standard
SMUD	Sacramento Municipal Utility District
SO_2	sulfur dioxide
SPP	Southwest Power Pool
SPI	solar power index
ST	steam turbine
TEPPC	Transmission Expansion Planning Policy Committee
TRC	Technical Review Committee
TW	terawatt
TWh	terawatt hour, energy
TW-h	terawatt hour, reserves
VG	variable generation
VOM	variable operations and maintenance
WC	WestConnect
WECC	Western Electricity Coordinating Council
WI	Western Interconnection
WITF	Wind Integration Task Force
WWSIS-1	Western Wind and Solar Integration Study Phase 1
WWSIS-2	Western Wind and Solar Integration Study Phase 2

Executive Summary

The electric grid is a highly complex, interconnected machine, and changing one part of the grid can have consequences elsewhere. Adding wind and solar affects the operation of the other power plants and adding high penetrations can induce cycling of fossil-fueled generators. Cycling leads to wear-and-tear costs and changes in emissions. Phase 2 of the Western Wind and Solar Integration Study (WWSIS-2) evaluated these costs and emissions and simulated grid operations for a year to investigate the detailed impact of wind and solar on the fossil-fueled fleet. This built on Phase 1, one of the largest wind and solar integration studies ever conducted, which examined operational impacts of high wind and solar penetrations in the West (GE Energy 2010).

Frequent cycling of fossil-fueled generators can cause thermal and pressure stresses. Over time, these can result in premature component failure and increased maintenance and repair. Starting a generator or increasing its output can increase emissions compared to noncyclic operation. And operating a generator at part-load can affect emissions rates. Utilities are concerned that cycling impacts can significantly negate the benefits that wind and solar bring to the system. And to plan accordingly, power plant owners need to understand the magnitude of cycling impacts.

In WWSIS-2, we calculated these wear-and-tear costs and emissions impacts. These data were incorporated into commercial software that simulates operations of the western grid (which includes the United States, Canada, and Mexico) on a subhourly basis, because wind and solar output can change within the hour. We designed five hypothetical scenarios to examine up to 33% wind and solar energy penetration in the Western U.S. and to compare the impacts of wind and solar. We then examined how wind and solar affected operation, costs, and emissions from fossil-fueled generators. This work was overseen by a Technical Review Committee (TRC) to ensure that assumptions, methodologies, and analyses were realistic and credible. Our results are based on the specific characteristics of the western grid and key assumptions, including an average gas price of \$4.60/MMBtu, significant balancing authority cooperation, and least-cost economic dispatch and transmission usage that does not model bilateral transactions. The goal of WWSIS-2 is to quantify the cycling impacts that are induced by wind and solar. It does not address whether wind and solar should be built, but rather what happens if they are built.

In this study, we found that up to 33% of wind and solar energy penetration increases annual cycling costs by \$35–\$157 million in the West. From the perspective of the average fossil-fueled plant, 33% wind and solar penetration causes cycling costs to increase by \$0.47–\$1.28/MWh, compared to total fuel and variable operations and maintenance (VOM) costs of \$27–\$28/MWh. The impact of 33% wind and solar penetration on system operations is to increase cycling costs but also to displace annual fuel costs by approximately \$7 billion. WWSIS-2 simulates production or operational costs, which do not include plant or transmission construction costs. From the perspective of wind and solar, these additional cycling costs are \$0.14–0.67 per MWh of wind and solar generated compared to fuel cost reductions of \$28–\$29/MWh, based on the generator characteristics and modeling assumptions described in this report.

This study finds that up to 33% wind and solar energy penetration in the United States' portion of the Western grid (which is equivalent to 24%–26% throughout the western grid) avoids 29%–34% carbon dioxide (CO_2) emissions, 16%–22% nitrogen oxides (NO_x) emissions, and 14%–24% sulfur dioxide (SO_2) emissions throughout the western grid. Cycling had very little (<5%) impact on the CO_2, NO_X, and SO_2 emissions reductions from wind and solar. For the average fossil-fueled plant, we found that wind- and solar-induced cycling can have a positive or negative impact on CO_2, NO_x, and SO_2 emissions rates, depending on the mix and penetrations of wind and solar.

Motivation

Phase 1 of the Western Wind and Solar Integration Study (WWSIS-1) was a landmark analysis of the operational impacts of high penetrations of wind and solar power on the Western Interconnection (GE Energy 2010). The study found no technical barriers to accommodating the integration of 35% wind and solar energy on a subregional basis if adequate transmission was available and certain operational changes could be made. The two most important of the operational changes were increased balancing authority (BA) cooperation and increased use of subhourly scheduling between BAs for generation and interchanges.

The variability and uncertainty of wind and solar can have profound impacts on grid operations. Figure ES-1 shows the most challenging week of the 3 years of data studied in WWSIS-1, when high penetrations of wind and solar caused fossil-fueled plants to cycle more frequently. In this report, cycling is a broad term that means shutting down and restarting, ramping up and down, and operating at part-load.
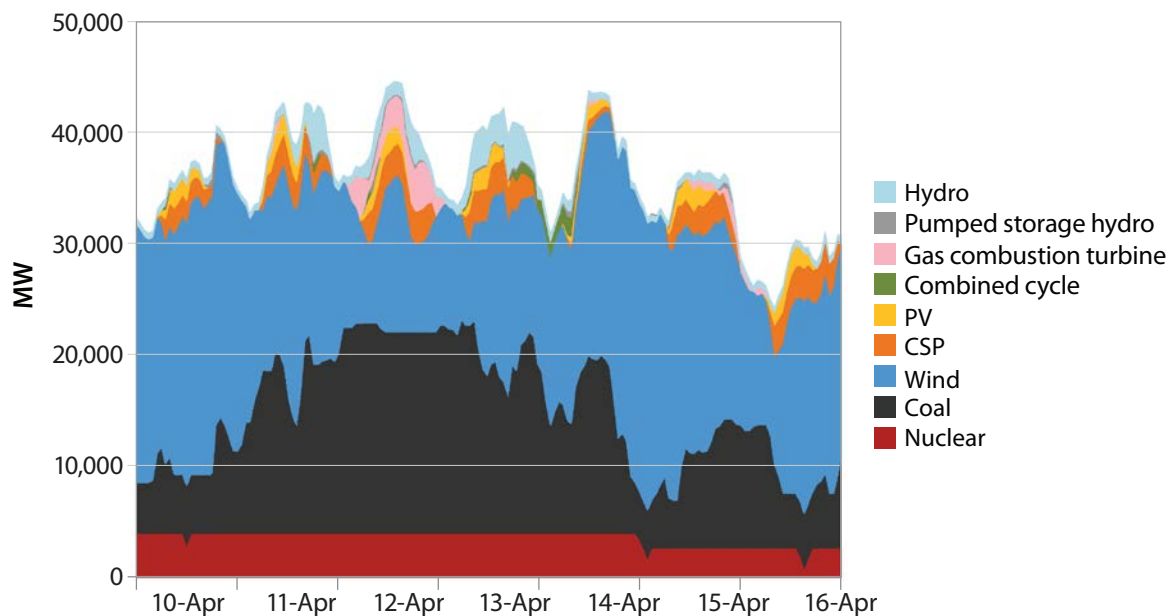
Figure ES-1. WWSIS-1 dispatch for the most challenging week of 3 years of data analyzed

Notes: PV, photovoltaic; CSP, concentrating solar power

Utilities were concerned about this type of operation and its impacts on repair and maintenance costs and component lifetimes. In addition, some analysts asserted that the emissions imposed by cycling could be a significant fraction of—or even larger than—the emissions reduced by wind and solar (Bentek Energy 2010; Katzenstein and Apt 2009).

WWSIS-2 was initiated in 2011 to determine the wear-and-tear costs and emissions impacts of cycling and to simulate grid operations to investigate the detailed impact of wind and solar on the fossil-fueled fleet. WWSIS-1 focused on whether high penetrations were technically feasible. In WWSIS-2, we analyzed the cycling impacts in detail and with a higher degree of fidelity. WWSIS-2 simulates operation of the entire Western Interconnection but wind and solar is only added to the U.S. portion of the Western Interconnection because data from outside the United States are lacking.

In WWSIS-2, we dove deep into the impacts of cycling on the operation of fossil-fueled plants. We created new data sets and simulated subhourly grid operations to answer questions such as the following:

- What are the increased costs because of wear and tear on fossil-fueled plants?

- Do these wear-and-tear costs significantly reduce the benefits of wind and solar?

- Will incorporating these costs into optimization of grid operation reduce cycling?

- What are the emissions impacts of cycling?

- How do wind impacts compare to solar impacts on cycling and grid operations?

This study focused on simulating grid operations on a subhourly basis. The results discussed here are specific to the Western Interconnection and the characteristics of the generation and transmission in the West. Adapting these results to other regions would require simulating the characteristics of those regions.

WWSIS-2 was one piece in a larger puzzle of understanding the impacts of wind and solar on the electric power grid. Although WWSIS-2 needed hypothetical scenarios of renewable energy siting and transmission expansion, these were not the main focus. System reliability and stability issues were not the focus of this study either, but are being examined in Phase 3 of WWSIS.

Background

Impacts of cycling induced by wind and solar additions can be investigated in different ways. The first is from the perspective of a fossil-fueled plant. If that plant is required to cycle more frequently, this can affect wear-and-tear costs and emission rates, which in turn affect that plant's marginal costs and emissions requirements. The second way to frame these impacts is from a system perspective. Wind and solar can impact grid operations by displacing fossil-fueled generation (and the costs and emissions associated with fossil fuels) but also increasing cycling (and the costs and emissions impacts associated with it). This study examines whether these cycling impacts significantly reduce the benefits of displacing fossil-fueled generation.

From the perspective of a power plant owner or a resource planner, the delivered cost of energy (DCOE) from a specific plant is important. From the perspective of the overall system or in terms of societal impacts, costs across the entire system are important. This report attempts to examine cycling impacts from all these perspectives.

The DCOE for a specific plant looks very different for a fossil-fueled plant than for a wind/solar plant, as shown in Figure ES-2. The DCOE for a fossil-fueled plant is a mix of fixed costs and production costs. The DCOE for a wind/solar plant is nearly all fixed capital costs. Fixed costs are those costs that do not change based on how much the plant is run, such as power plant and transmission construction costs and fixed operations and maintenance (O&M) costs. Production costs are the variable costs that increase as the plant produces more electricity and consist of fuel and VOM. VOM, in turn, comprises cycling O&M (which consists of start fuel plus wear and tear from starts and ramps) and noncyclic O&M (which are the routine overhauls and maintenance costs from the plant running at some steady-state output). The *only* capital costs included in production costs are capitalized maintenance (e.g., more frequent boiler tube replacements) because cycling and steady-state operation reduces the lifetimes of those components. Production simulation tools, such as the one used in this study, model operations of the power system. Production costs are key outputs of these tools.
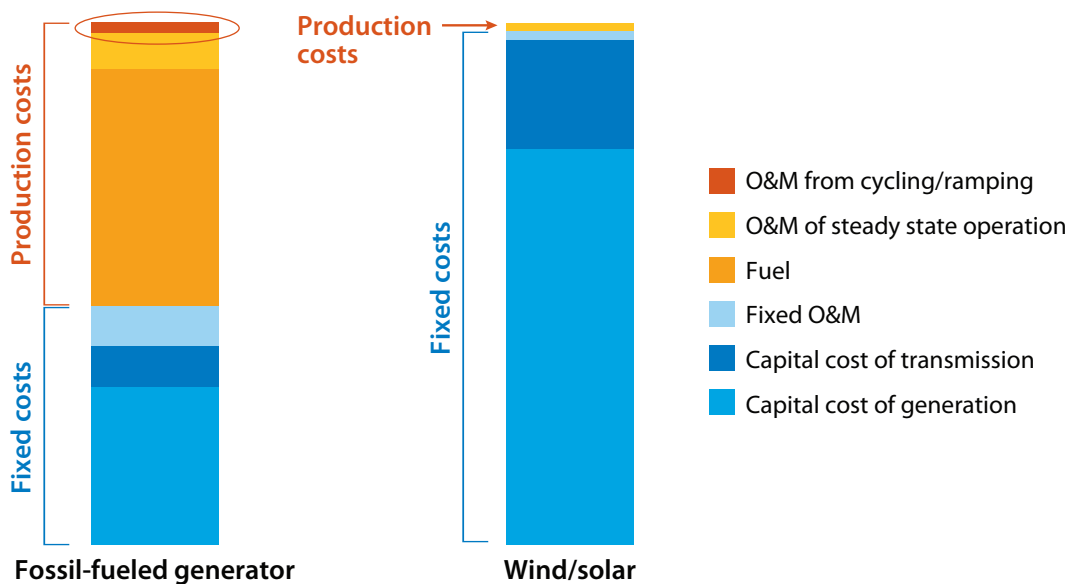

Figure ES-2. Illustrative DCOE for a fossil-fueled plant and a wind/solar plant

Adding any new generation to the power system will change the way existing plants operate. Studies show that adding wind and solar can cause existing fossil-fueled plants to cycle more and have lower capacity factors (EnerNex 2011; GE Energy 2010). Adding new, low-priced baseload generation can also cause the incumbent fossil-fueled plants to cycle more and have lower capacity factors (Milligan et al. 2011). An incumbent fossil-fueled plant that now has a lower capacity factor (and likely reduced revenue) and a higher O&M cost (because of cycling) might have a hard time remaining viable. This raises questions about who should pay for the cycling costs of incumbent plants or what happens in the marketplace to address the viability of a plant that might be needed for reliability but might no longer be profitable. These questions are not addressed in this technical report.

When O&M from cycling increases, the cost of energy component circled in red in Figure ES-2 also increases. Before this study, little wear-and-tear data for different types of cycling operation were publicly available. WWSIS-2 investigates this cost in depth. It explores the magnitude of that cost, how that cost changes when wind and solar are added to the system, how that cost changes the fuel savings that wind and solar bring to the system, and how increased wind and solar penetration affects that cost.

From a system perspective, utility planning decisions have resulted in a given portfolio of plants. Those fixed capital costs (or power purchase agreements [PPAs] if the utility is buying from an independent power producer) are now sunk costs. The system operator's job is to manage operations of that portfolio to supply reliable power at low cost to consumers. The operators do not see the fixed costs, only the production costs. If we consider the what-if scenario of this same system with a new wind/solar plant (for simplicity, ignore the bilateral transactions and incentives such as production tax credits), we can see that the near-zero production cost of wind/solar will lead the operator to dispatch the wind/solar instead of fossil-fueled generation, as long as it is within all the constraints of transmission and operating limits. This displaces the fossil-fueled generators' production costs (fuel and O&M). The change in production cost with and without wind/solar is shown in Figure ES-3. From the perspective of the system operators, this reduction in fuel cost is the benefit that wind and solar bring to the system. WWSIS-2 addresses how that benefit is affected when cycling costs are modeled in detail. The cost of wind/solar is the difference in fixed costs (capital costs of the wind/solar plants and transmission). WWSIS-2 did not conduct a cost-benefit analysis of wind and solar to determine profitability. Instead, it posited that if wind/solar is present, what benefit does it bring to the system and how much is that value reduced by cycling?
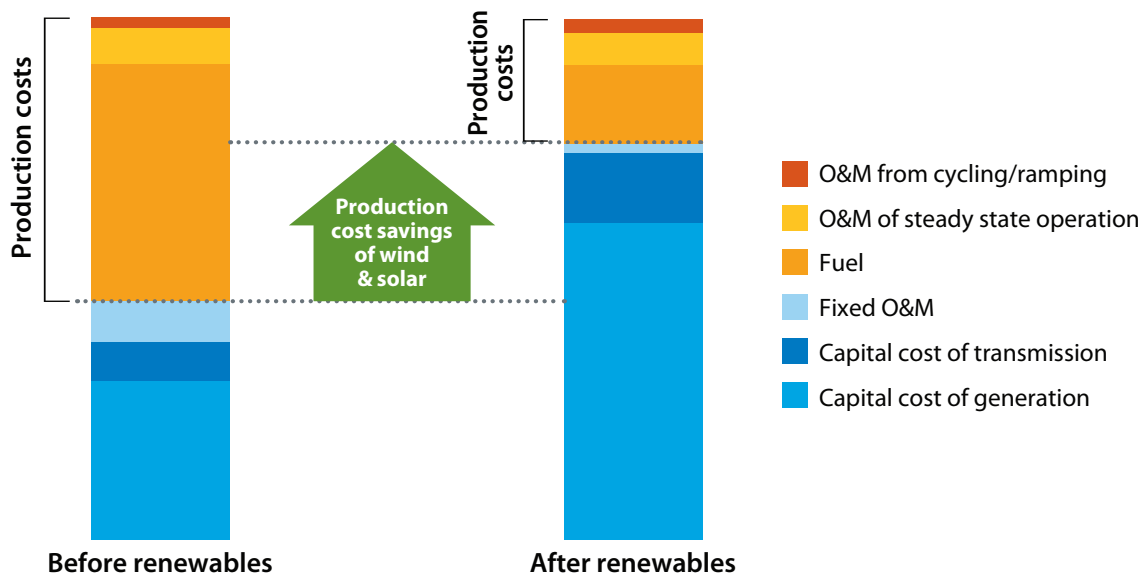
Figure ES-3. Illustrative system-wide costs before and after wind/solar

Notes: The wind/solar requires additional fixed costs but offsets production costs.
The change in production cost from wind/solar is shown by the green arrow.

Study Approach

WWSIS-2 examined the impact of up to 33% wind and solar energy penetration on the U.S. portion of the Western Interconnection. We explicitly calculated values for various types of wear-and-tear costs resulting from cycling. We used the wear-and-tear start costs to optimize detailed operations of the grid and included ramping costs in the total cost impact. We considered the impacts of both the variability and the uncertainty of wind and solar on starts, ramps, and operation of the power system. We modeled five scenarios that were designed to illuminate the impacts of increased wind and solar and compare the impacts of wind and solar on the power system.

To assess the cycling impacts on the fossil-fueled fleet induced by wind and solar, we needed the following information:

- Wear-and-tear costs and impacts for cycling

- Emissions impacts resulting from cycling

- Subhourly wind and solar plant output for future hypothetical plants

- A tool to model grid operations on a subhourly time frame.

This study was conducted by a team of researchers from the National Renewable Energy Laboratory (NREL), GE Energy, Intertek-APTECH (APTECH), and RePPAE. The TRC met every 2 months to discuss and review assumptions, data inputs, methodology, and results. TRC members included representatives from utilities, transmission planning groups, the Western Electricity Coordinating Council (WECC), and DOE and its laboratories, along with power system and fossil-fueled plant experts. As data sets or preliminary results were completed, they were vetted in public forums and peer-reviewed publications. This study has been thoroughly reviewed for technical rigor.

Wear-and-Tear Costs and Impacts Data

Cycling of thermal plants can create thermal and pressure stresses in power plant components. This leads to increased O&M costs, more frequent repairs, reduced component life, and more frequent forced outages. Power plants that were designed for baseloaded operation suffer much more wear-and-tear damage from cycling. In this report, a *start* is defined as "starting a unit that is offline." *Ramping* is defined as "load-following operation in which a generating unit increases its production." *Cycling* includes both starts and ramping.

To address the lack of public data on the wear-and-tear costs and impacts from cycling of coal and gas generators, NREL and WECC jointly retained APTECH to create a data set. APTECH had previously investigated these costs for hundreds of plants around the world. For each plant, APTECH had determined a best fit and a lower-bound and an upper-bound fit for cycling costs, where the bounds reflected the uncertainty range for that plant. APTECH statistically analyzed those proprietary data to develop generic costs and impacts for seven categories of coal and gas generators (Kumar et al. 2012). Figure ES-4 shows the statistics for the lower-bound costs for cold starts for the seven plant types. The medians of these lower-bound costs were used in the operational optimization so that the wear and tear on fossil-fueled generators was considered in the decision to commit and dispatch units. Upper-bound start costs were then applied to this dispatch to estimate the range of start costs. This may yield a conservative estimate because using those upper-bound costs in the unit commitment process could reduce cycling. On the other hand, many plant operators do not consider wear-and-tear costs in their dispatch decisions, so this may reflect a realistic view of current operations. Unless otherwise specified, ranges of wear-and-tear costs in this report reflect the uncertainty range from the lower to the upper bound. High-impact, low-probability events such as a generator failure were not included in these wear-and-tear costs because there was not enough data to assess the impact of cycling on those events.
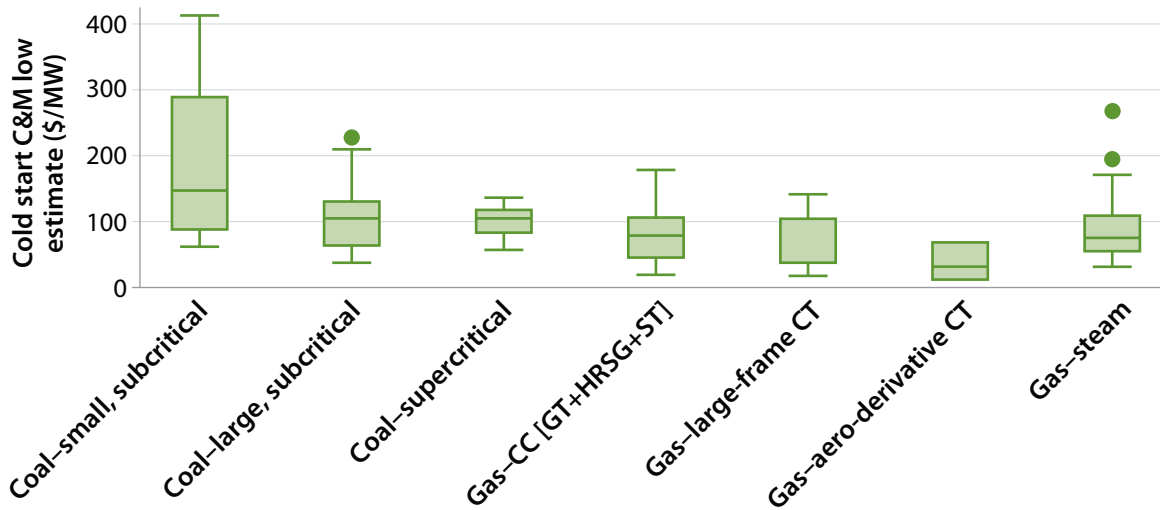
**Figure ES-4. Lower-bound costs for one cold start**

Notes: C&M, capital and maintenance; CC, combined cycle; GT, gas turbine; HRSG, heat recovery steam generator; ST, steam turbine; CT, combustion turbine. The range shows the 25th to 75th percentile, with the median shown within that range. Nonoutlier extrema are depicted by the whiskers in the plots. Outliers are represented as dots.

CO_2, NO_X, and SO_2 Emissions Data

Starts, ramping, and part-loading also have impacts on emissions. To address the lack of emissions data from cycling, NREL analyzed unit-specific measured emissions from the U.S. Environmental Protection Agency (EPA) Continuous Emissions Monitoring (CEM) data set (EPA 2009) to develop refined emissions rates for most units in the U.S. portion of the Western Interconnection for CO_2, NO_x, and SO_2. Figure ES-5 shows an example of how heat rates and emissions rates were calculated for part-load. In addition, unit-specific incremental emissions from starts and ramps were calculated using these measured emissions data. Part-loading generally results in a higher emission rate overall, except for NO_x emission rates, which decrease for coal and gas steam units. Compliance with existing or proposed emissions regulations was not analyzed.

Wind and Solar Power Output Data

In WWSIS-2, we updated the wind and solar plant output and forecast data sets from WWSIS-1 to best represent current technologies and methodologies. For example, we capitalized on recent advances in modeling of utility-scale PV plants on a subhourly timescale. The following types of plants were modeled in WWSIS-2: utility-scale wind, rooftop distributed generation PV, utility-scale PV, and CSP with 6 hours of thermal storage.
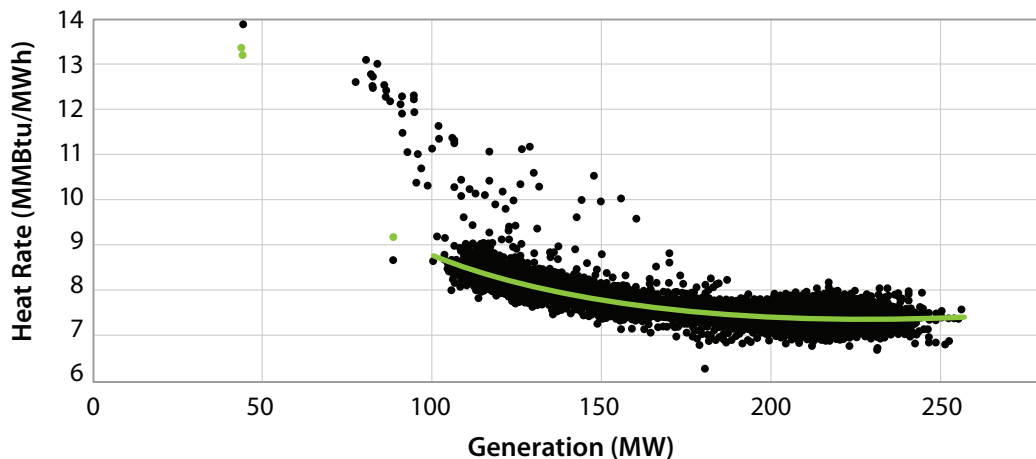
Figure ES-5. Heat-rate curve for a typical gas CC unit

Notes: The black dots show measured emission rates for every hour of the year. The green line shows a local linear fit.

Production Simulations and Scenarios

Production simulations were used as the primary tool to examine operations of the power system. These simulations produce extensive data outputs including generator commitment and dispatch, emissions, costs, and transmission path flows for each time step. Production costs are a key output. Fixed capital costs and PPAs are not included in these simulations.

We simulated scenarios in 2020 using the WECC Transmission Expansion Planning Policy Committee's (TEPPC's) 2020 Portfolio Case 1 as the basis for the production simulation modeling (WECC 2011). Because that case had a relatively high ($7.28/MMBtu) average gas price, we used the gas price projections from WECC TEPPC 2022, which averages $4.60/MMBtu, for the base runs. Load and weather data from 2006 were used. The following five scenarios were created, with penetrations by energy:

- No Renewables—0% wind, 0% solar
- TEPPC—9.4% wind, 3.6% solar
- High Wind—25% wind, 8% solar
- High Solar—25% solar, 8% wind
- High Mix—16.5% wind, 16.5% solar.

Table ES-1 shows installed capacities. NREL's Regional Energy Deployment System (ReEDS) model was used to select which regions were optimal locations for siting the wind and solar based on resources, load, and transmission (Short et al. 2011). We used the commercial production simulation tool PLEXOS to model unit commitment, dispatch, and power flow for the system for a year. The power flow was an optimal direct current (DC) power flow, respecting transmission constraints and using power transfer distribution factors, not a simplified pipeline model. We added capacity to interfaces with high shadow prices and iterated until all shadow prices were within a consistent cutoff. The shadow price is the marginal value of relaxing the interface limit constraint. It defines the potential value of new transmission along each interface (but not the cost). The nearly 40 BAs in the Western Interconnection were modeled using the 20 WECC Load and Resource Subcommittee zones, which were the most granular we could obtain from WECC. The production simulation was run zonally so that collector systems would not need to be designed for each plant. This means that we assumed that sufficient intrazonal transmission was built for each plant and ignored local congestion that could result in curtailment.

Table ES-1. Installed Solar and Wind Capacity and Average Capacity Factor for Each State for Each Scenario

TEPPC

State	Rooftop PV Capacity (MW)	CF	Utility Scale PV Capacity (MW)	CF	CSP Capacity (MW)	CF	Wind Capacity (MW)	CF	Total Capacity (MW)	CF
Arizona			1,171	22%	472	43%	3,681	30%	5,324	30%
California			3,545	25%	3,221	44%	7,299	30%	14,065	32%
Colorado			1,342	20%	169	37%	3,256	29%	4,767	27%
Idaho							523	27%	523	27%
Montana							838	34%	838	34%
Nevada			304	22%	334	42%	150	25%	788	31%
New Mexico			140	27%	156	39%	494	28%	790	30%
Oregon							4,903	26%	4,903	26%
South Dakota										
Texas										
Utah			571	20%			323	31%	894	24%
Washington							4,652	27%	4,652	27%
Wyoming							1,784	42%	1,784	42%
Total			7,074	23%	4,352	43%	27,900	29%	39,326	30%

High Solar

State	Rooftop PV		Utility Scale PV		CSP		Wind		Total	
	Capacity (MW)	CF	Capacity (MW)	CF	Capacity (MW)	CF	Capacity (MW)	CF	Capacity (MW)	CF
Arizona	4,498	19%	9,570	23%	9,644	42%	270	33%	23,982	30%
California	9,006	18%	14,258	23%	9,197	43%	5,203	33%	37,663	28%
Colorado	1,127	18%	4,437	22%	1,440	35%	3,617	31%	10,620	27%
Idaho	3	15%	2	16%			583	28%	588	28%
Montana	25	15%	34	17%			988	35%	1,047	34%
Nevada	772	19%	6,503	24%	672	40%	150	25%	8,098	25%
New Mexico	943	20%	2,874	24%	574	38%	644	32%	5,034	26%
Oregon	101	14%	126	21%			4,665	26%	4,892	26%
South Dakota	4	17%	6	19%			330	37%	340	37%
Texas	233	20%	335	23%					568	22%
Utah	2,132	17%	3,759	21%			323	31%	6,214	20%
Washington	405	13%	759	19%			4,952	27%	6,116	25%
Wyoming	10	18%	18	21%			1,634	43%	1,662	42%
Total	19,261	18%	42,680	23%	21,526	42%	23,357	31%	106,824	27%

High Wind

State	Rooftop PV		Utility Scale PV		CSP		Wind		Total	
	Capacity (MW)	CF	Capacity (MW)	CF	Capacity (MW)	CF	Capacity (MW)	CF	Capacity (MW)	CF
Arizona	1,975	19%	2,330	25%	3,303	43%	4,941	30%	12,548	31%
California	4,875	18%	5,372	25%	2,469	45%	11,109	30%	23,824	28%
Colorado	1,059	18%	1,128	22%	169	37%	6,226	35%	8,581	31%
Idaho	3	15%	2	16%			1,333	29%	1,338	29%
Montana	22	15%	34	17%			6,658	36%	6,714	36%
Nevada	398	19%	344	22%	439	42%	3,270	31%	4,452	30%
New Mexico	172	20%	209	27%	156	39%	4,784	38%	5,321	37%
Oregon	91	14%	101	22%			5,473	26%	5,665	26%
South Dakota	4	17%	6	19%			2,640	36%	2,650	36%
Texas	76	20%	122	27%					198	24%
Utah	361	17%	489	21%			1,343	32%	2,193	27%
Washington	371	13%	492	20%			5,882	27%	6,745	26%
Wyoming	9	18%	18	21%			10,184	43%	10,211	43%
Total	9,417	18%	10,647	24%	6,536	43%	63,840	34%	90,439	32%

High Mix

State	Rooftop PV Capacity (MW)	CF	Utility Scale PV Capacity (MW)	CF	CSP Capacity (MW)	CF	Wind Capacity (MW)	CF	Total Capacity (MW)	CF
Arizona	3,655	19%	5,394	25%	9,374	42%	1,440	32%	19,863	33%
California	8,412	18%	9,592	23%	3,594	44%	6,157	31%	27,754	26%
Colorado	1,127	18%	1,653	22%	169	37%	4,396	33%	7,344	29%
Idaho	3	15%	2	16%			1,093	29%	1,098	29%
Montana	25	15%	34	17%			4,288	36%	4,347	36%
Nevada	772	19%	3,282	26%	562	40%	1,560	32%	6,177	28%
New Mexico	943	20%	1,280	27%	298	40%	3,134	38%	5,654	33%
Oregon	101	14%	126	21%			5,413	26%	5,640	26%
South Dakota	4	17%	6	19%			1,950	36%	1,960	36%
Texas	208	20%	193	25%					401	22%
Utah	1,204	17%	1,216	22%			683	33%	3,102	22%
Washington	405	13%	709	19%			5,762	27%	6,876	26%
Wyoming	10	18%	18	21%			7,244	44%	7,272	44%
Total	16,870	18%	23,504	24%	13,997	42%	43,118	34%	97,489	30%

Note: CF, capacity factor

Operations of the entire Western Interconnection were modeled in detail in PLEXOS. We ran a day-ahead (DA) unit commitment for all generation using DA wind and solar forecasts. Coal and nuclear units were committed during the DA market. We next ran a 4-hour-ahead (4HA) unit commitment to commit CC and gas steam units, using 4HA wind and solar forecasts. Finally, we ran a real-time economic dispatch on a 5-minute interval to dispatch all units (i.e., gas CT and internal combustion units were allowed to start during the real-time dispatch).

Load forecasts were assumed to be perfect because we lacked a consistent set of load forecasts; as a result, all the uncertainty in operations came from wind and solar. This assumption may result in putting more of a burden on wind/solar than is realistic. Variability, on the other hand, came from both load and wind/solar.

Three types of operating reserves were held: contingency, regulating, and flexibility (or load-following). Contingency reserves were unchanged with wind and solar because no wind or solar plant was the single largest contingency. Regulating reserves covered 1% of load and 95% of the 10-minute forecast errors of wind and PV. Increases in regulation requirements were modest in the high-penetration scenarios: up to 10% greater than in the No Renewables Scenario. Finally, flexibility reserves, specifically to address load-following needs for wind and PV, were held to cover 70% of the 60-minute forecast errors of wind and PV.

We conducted statistical analysis to examine the geographic diversity of wind, solar, and load. We investigated monthly, diurnal, hourly, and subhourly variability to determine increased ramping needs and correlations between load, wind, and PV. Extreme event analysis determined maximum ramping needs and tail events.

Production simulation models are not a perfectly accurate representation of operations. As much as possible, we used WECC TEPPC assumptions, data, and scenarios because they have been widely vetted. It is important to note the following:

- Most of the Western Interconnection (except California and Alberta) today operates on the basis of a combination of short-term and long-term bilateral contracts. This information is confidential and could not be used in this study. As a result, the grid was assumed to be operated on the basis of least-cost economic dispatch.

- Most of the Western Interconnection today primarily uses contractual obligations to schedule transmission. Transmission that is not accessible to other generation might be available. In this study, we did not model these contracts; instead, we assumed that existing available transmission capacity was used in a way that minimized production costs across the Western Interconnection.

What are the impacts of these assumptions? If a bilateral contract results in operating a less economic plant, that increases production cost. It might also result in more wind/PV curtailment or less flexibility available to balance the system, which could increase cycling. If sufficient transmission capacity is not available, that might also result in more wind/PV curtailment.

Key Findings

Our analysis in WWSIS-2 yielded a tremendous amount of noteworthy results, which are detailed in the main report. All study results are in 2011 nominal dollars. Under the scenarios studied, we found the following for the Western Interconnection:

- High penetrations of wind and solar increase annual wear-and-tear costs from cycling by \$35–\$157 million[1]. This represents an additional \$0.47–\$1.28/MWh of cycling costs for the average fossil-fueled generator. Cycling diminishes the production cost reduction of wind and solar by \$0.14–\$0.67/MWh, based on the specific system and generator characteristics modeled. These costs are a small percentage of annual fuel displaced across the Western Interconnection (approximately \$7 billion) and the reduction in fuel costs (\$28–\$29/MWh of wind and solar generated). The costs are, however, significant compared to the average steady-state VOM and cycling costs of fossil-fueled plants (\$2.43–\$4.68/MWh, depending on scenario). Production costs do not include the capital or PPA costs to construct power plants or transmission.

- CO_2, NO_X, and SO_2 emissions impacts resulting from wind- and solar-induced cycling of fossil-fueled generators are a small percentage of emissions avoided by the wind and solar generation. Wind- and solar-induced cycling has a negligible impact on avoided CO_2 emissions. Wind- and solar-induced cycling will cause SO_2 emissions reductions from wind and solar to be 2%–5% less than expected and NO_x emissions reductions to be 1%–2% larger than expected. From a fossil-fueled generator perspective, this cycling can have a positive or negative impact on CO_2, NO_X, and SO_2 emissions rates.

- Solar tends to dominate variability challenges for the grid; wind tends to dominate uncertainty challenges. Both of these challenges can be mitigated. Because we know the largest component of solar variability, the path of the sun through the sky, we can plan for this in the unit commitment. The DA wind forecast error can be mitigated with a 4HA commitment of gas units to take advantage of the improved forecasts.

- Although wind and solar affect the grid in very different ways, their impacts on system-wide production costs are remarkably similar.

Wind and Solar Displace Primarily Gas Generation and Increase Coal Ramping

As the quantity of resources with zero or very low marginal cost (such as wind and solar, but also possibly hydropower [hydro] or nuclear) increases, the new resources displace higher-cost resources (such as gas). The new resources can, however, also start to displace more traditional low-cost resources (such as coal). Figure ES-6 shows the dispatch stacks in the summer, depicting the high loads that lead the increased wind/solar to displace mostly gas CC units. The significant solar output in the High Solar Scenario, though, resulted in some displacement of coal generation even in the summer.

The impacts on other resources were amplified in the spring, when loads are low and both wind and solar generation are high. Figure ES-7 shows the most challenging week, defined by the minimum net load condition (net load is load minus wind minus solar). In the High Wind Scenario, the significant wind on March 29 displaced nearly all the gas output and severely cut into the coal output. Some wind and PV was curtailed, as shown by the dashed line in the dispatch stack on March 29 and 30. The curtailment occurred when the other types of generation hit their minimum generation levels. Coal was cycled, but without any periodicity and relatively slowly over days. The High Solar Scenario had a very different impact. Solar generation was high enough at midday to lead to significant curtailment of wind/PV and ramping of coal up and down on a daily basis. Impacts from wind- and solar-induced cycling are likely to be greater during the spring than during the summer.

---

[1] The low and high ends of this range give an uncertainty range for cycling costs and represent application of the lower-bound and upper-bound cycling costs, respectively. The high end of the uncertainty range is an overestimate because of the method used.
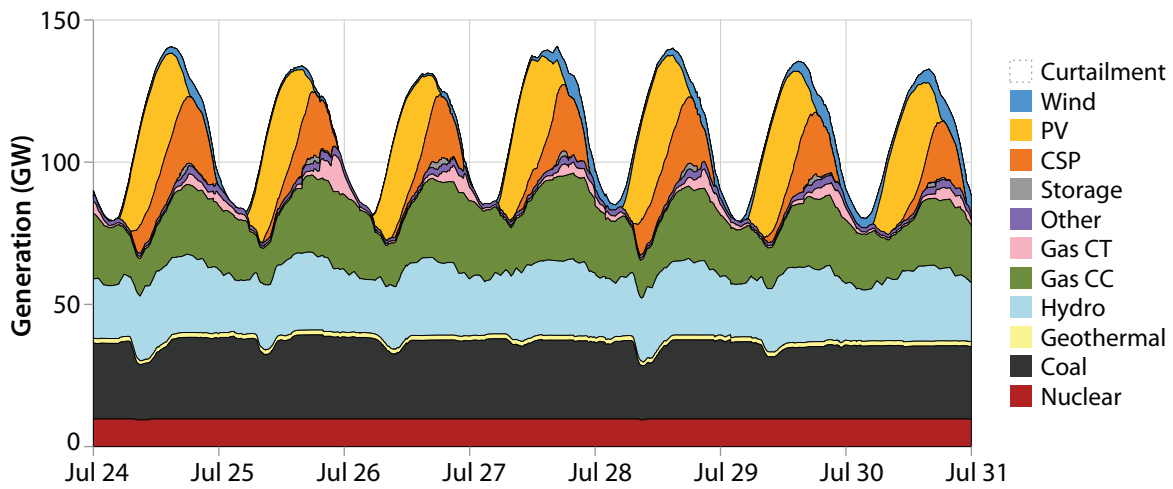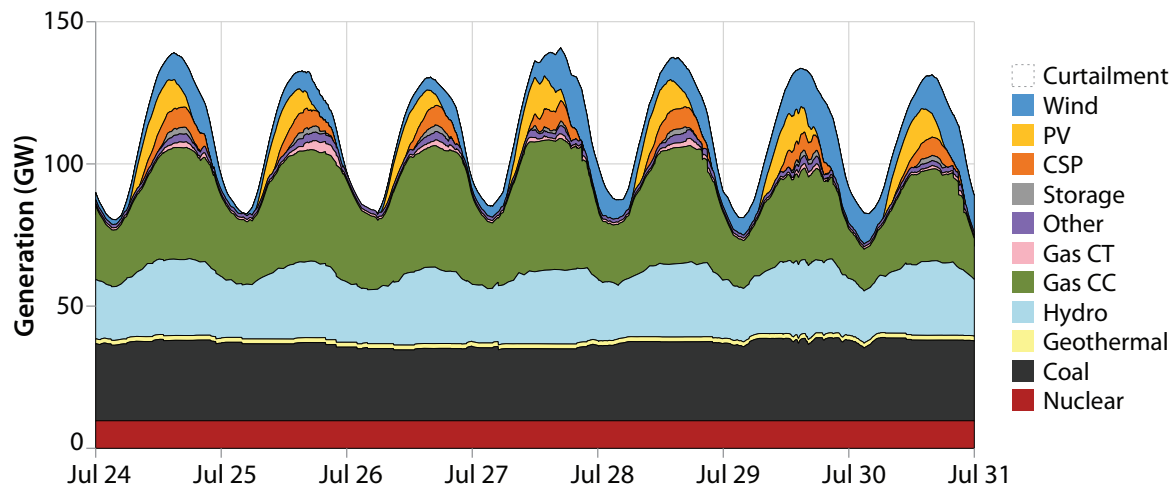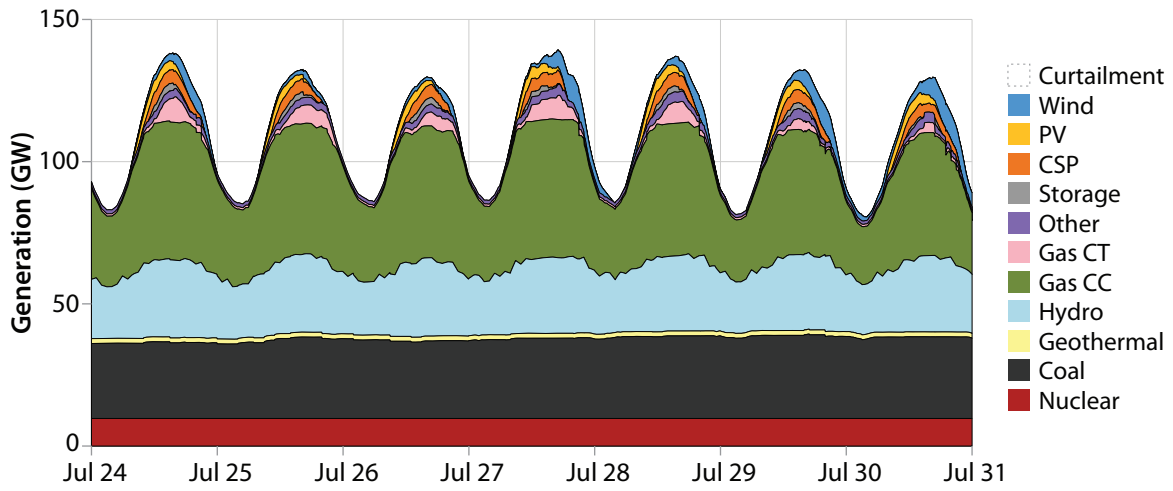
Figure ES-6. Five-minute dispatch stacks for the (top) TEPPC, (middle) High Wind, and (bottom) High Solar Scenarios for a week in July
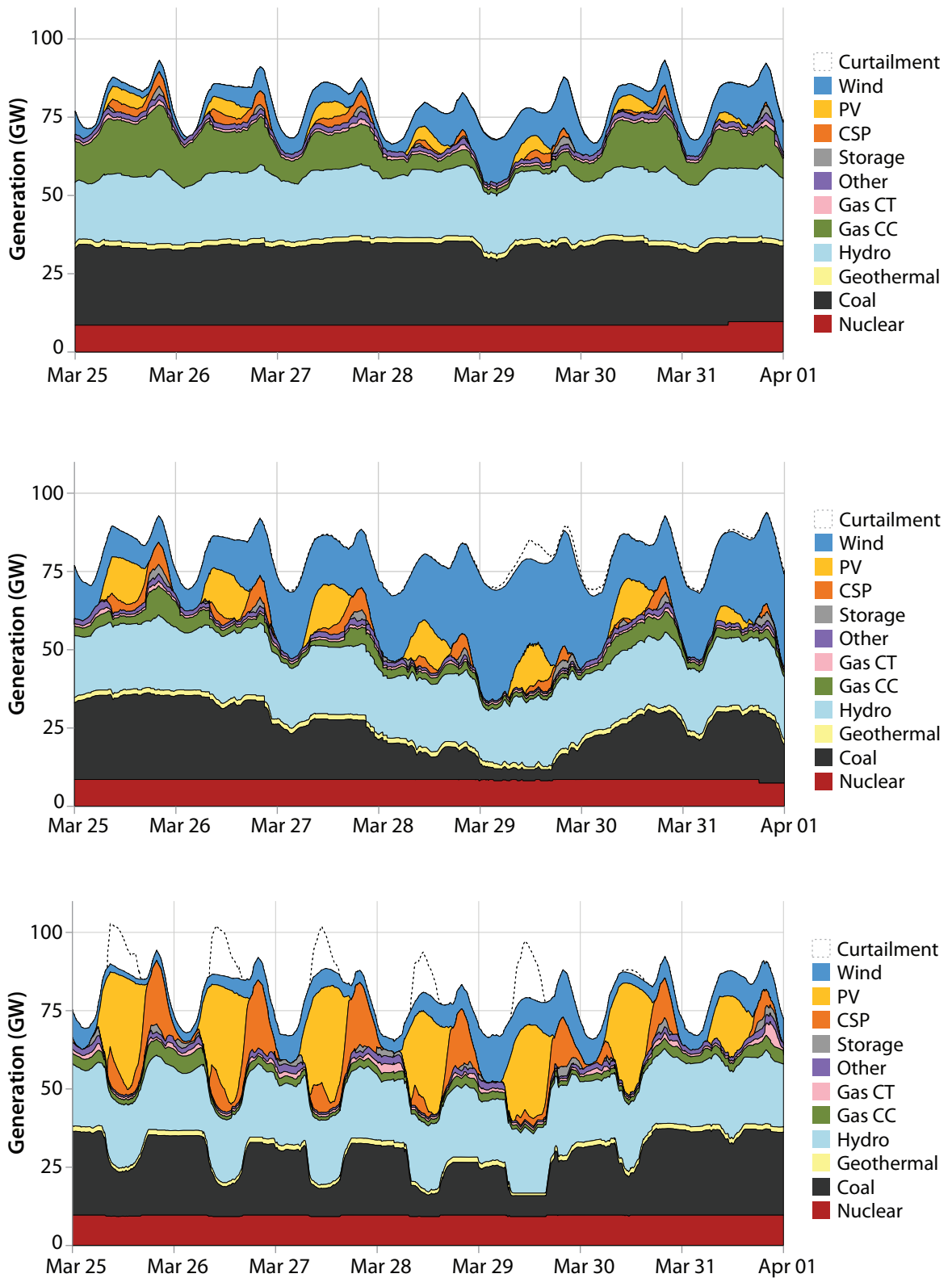
Figure ES-7. Five-minute dispatch stacks for the (top) TEPPC, (middle) High Wind, and (bottom) High Solar Scenarios for a week in March

Note: This week represented the minimum net load condition.

Despite these challenges, the 5-minute production simulation results showed that the system can operate and balance load and generation. Operational results for contingency, regulating, and flexibility reserves were examined, and issues were minimal. There were no regulating reserve violations and very few contingency reserve violations. Figure ES-8 shows that wind and solar mostly displace gas CC generation. Displacement of coal increased with increasing penetrations of wind, because gas already tends to be decommitted or backed down at night when there are high levels of wind.

The dispatch stacks showed that the system used the least expensive methods for flexibility from various types of generators to serve load and reserves. In the summer, capacity was required more than flexibility. In the spring, balancing the load with high instantaneous wind/solar penetrations required a lot of flexibility. Ramping hydro within its constraints was one source for flexibility; wind/PV curtailment was another. Cycling of fossil-fueled plants was a third, and we delve into that here. The High Solar Scenario ramped coal up and down on a daily basis. In the High Wind Scenario, coal was shut down and restarted on a weekly or longer frequency, especially during the low net load event on March 29. In all scenarios, CTs are shut down and restarted frequently, running for only several hours per start.

Over the course of 1 year, Figure ES-9 shows the cycling impact by plant type by scenario. Coal starts do not change appreciably but the High Wind Scenario decreased the average coal runtime per start by a third and the High Solar Scenario increased the number of ramps by an order of magnitude compared to the No Renewables Scenario. The High Wind Scenario required somewhat less ramping of coal units compared to the High Solar Scenario.

Wind and solar generation displaced primarily gas generation, based on an average gas price of $4.60/MMBtu.
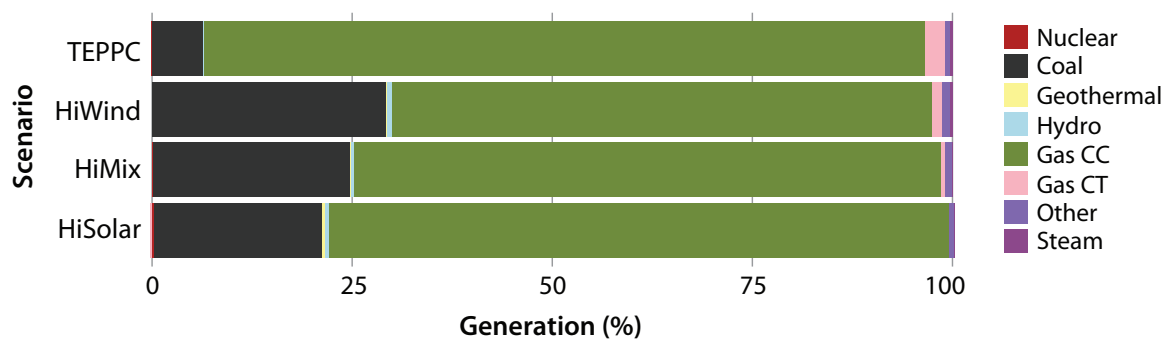

Figure ES-8. Generation displaced by wind/solar, compared to the No Renewables Scenario

Increasing wind/solar first increased and then decreased the number of CC starts. Even moderate penetrations halved the CC runtime per start, where it basically remained even at high penetrations. CC ramps actually decreased in the high-penetration scenarios.

Wind causes a significant reduction in CT cycling (and generation). The High Solar Scenario, however, shows more CT capacity started compared to the No Renewables Scenario, partly because of the correlation of evening peak load with decreased PV output at sunset.

(a)

(b)

Scenario
- ■ NoRenew
- ■ TEPPC
- ■ HiWind
- ■ HiMix
- ■ HiSolar

(c)
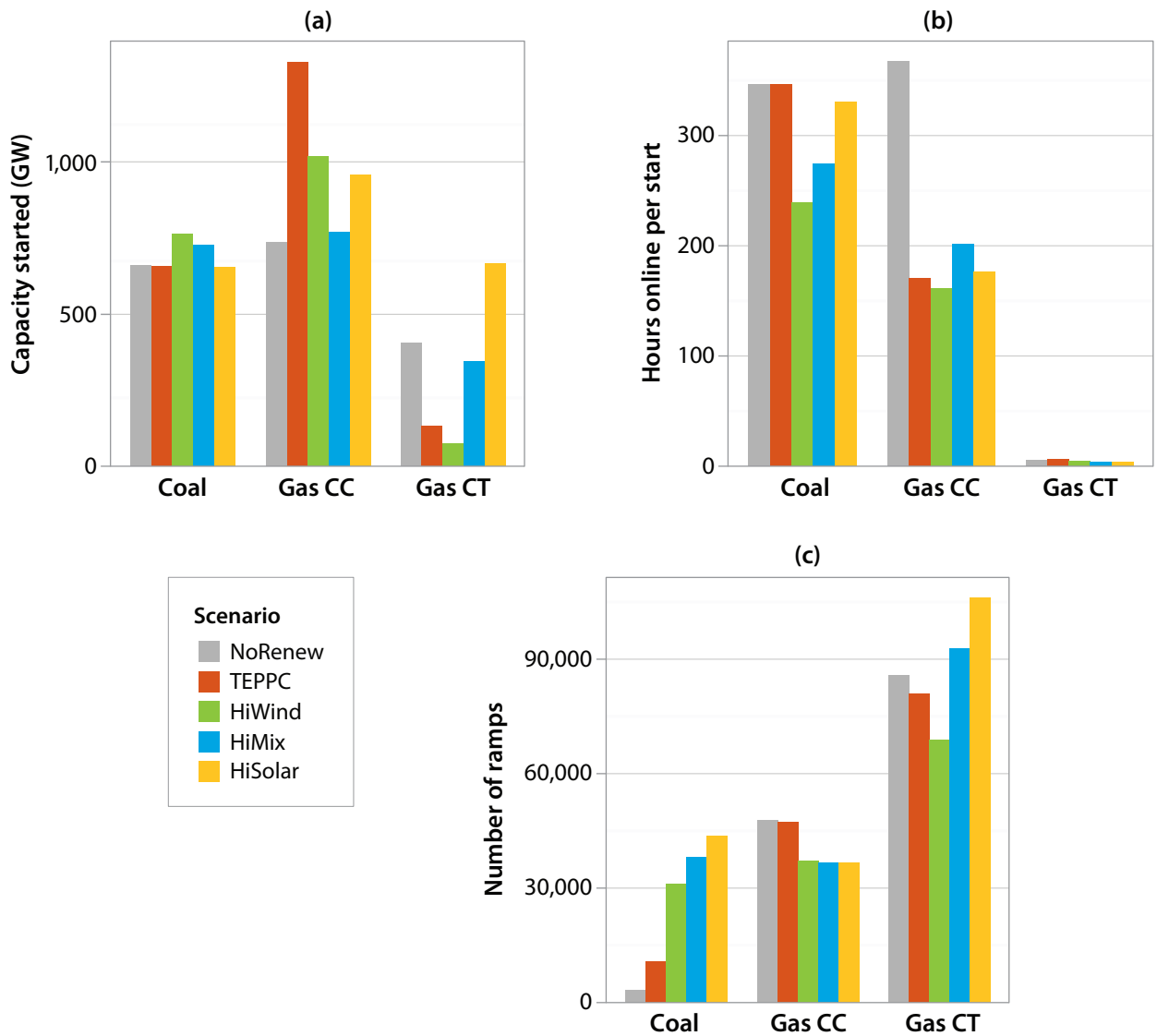
Figure ES-9. (a) Capacity started, (b) average number of hours online per start (must-run CTs have been excluded), and (c) total number of ramps for each plant type by scenario for 1 year

To determine the importance of considering wear-and-tear start costs during optimization, we ran the High Wind Scenario without including wear-and-tear start costs (but including start fuel costs) to compare to the original High Wind Scenario. Although this had almost no impact on annual generation from different unit types, it had a very significant impact on the number of starts at CC and CTs, which have very low start fuel costs. This demonstrates that it is important to consider wear-and-tear start costs during optimization.

Figure ES-10 gives a more detailed look into the starts and ramps. The solid line shows the committed coal capacity and the shaded area shows the dispatched capacity. The white area between the solid line and the shaded area illustrates how far the coal capacity has been backed down. In the No Renewables and TEPPC Scenarios, there is little change in coal commitments and the coal plants are typically running at or near full output, with an exception during the minimum net load day of March 29. In the high-penetration scenarios in the spring, coal capacity is shut down approximately each week, and the coal is ramped up and down each day, especially with high penetrations of solar. In the summer, coal is ramped very little except for some ramping in the High Solar Scenario during the day.
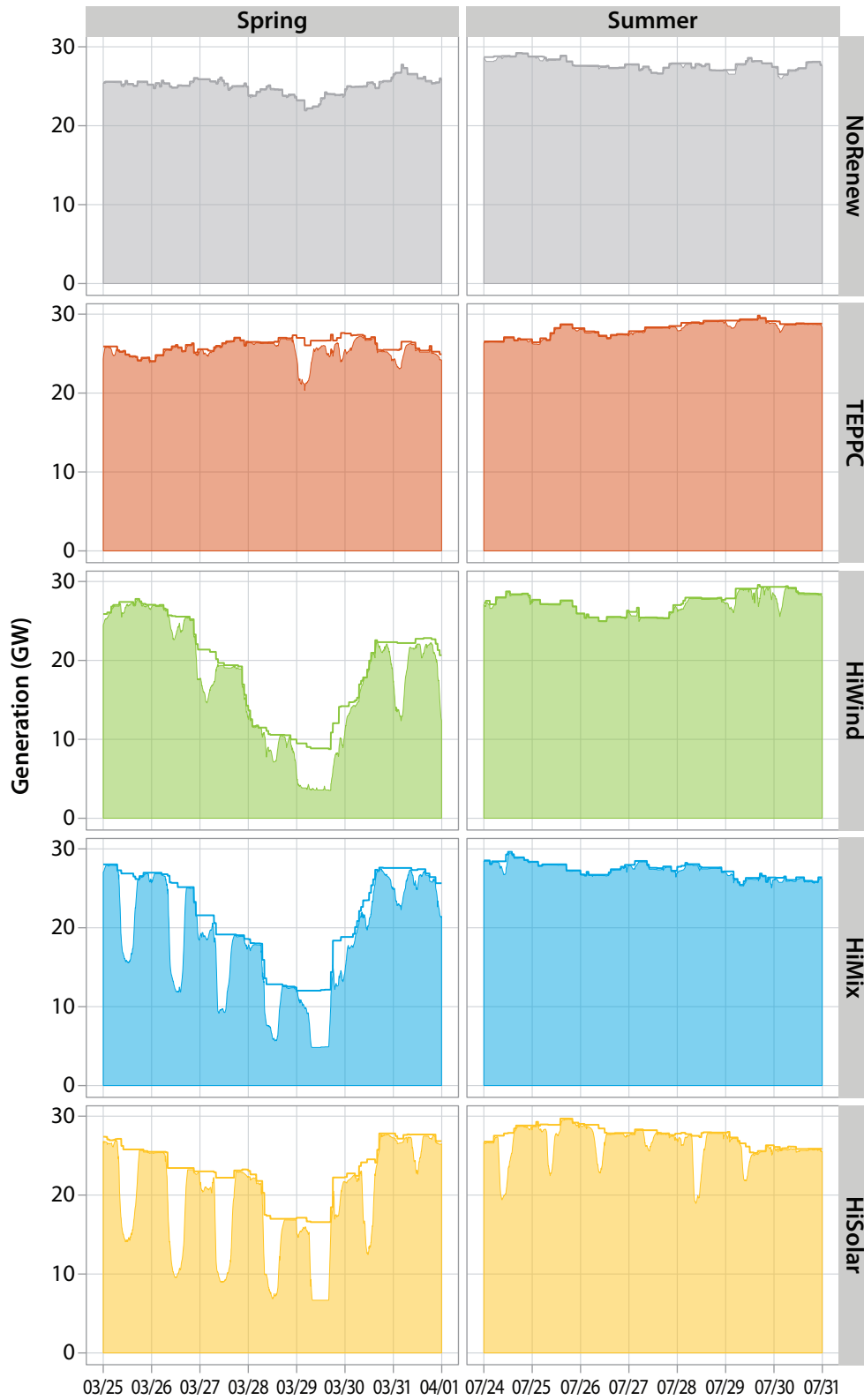
Figure ES-10. (Solid line) capacity committed and (shaded area) dispatched for coal units during March and July sample weeks

Wind- and Solar-Induced Cycling Affects Fossil-Fueled Plant Operations and Maintenance Costs

Figure ES-11 shows the production cost (operational cost of meeting load in the Western Interconnection in 2020) of each scenario. Production costs do not include any capital costs, except capitalized maintenance caused by cycling or noncyclic operation. The production cost was dominated by fuel costs, assuming an average natural gas price of $4.60/MMBtu and a zero carbon price. Noncyclic VOM costs comprise about a tenth of the total production cost. Cycling VOM costs (starts, start fuel, and ramping costs) were all a small percentage of the total production cost. They range from 1.5% of the total production cost in the No Renewables Scenario using lower-bound cycling costs to 7% in the High Solar Scenario using upper-bound cycling costs.
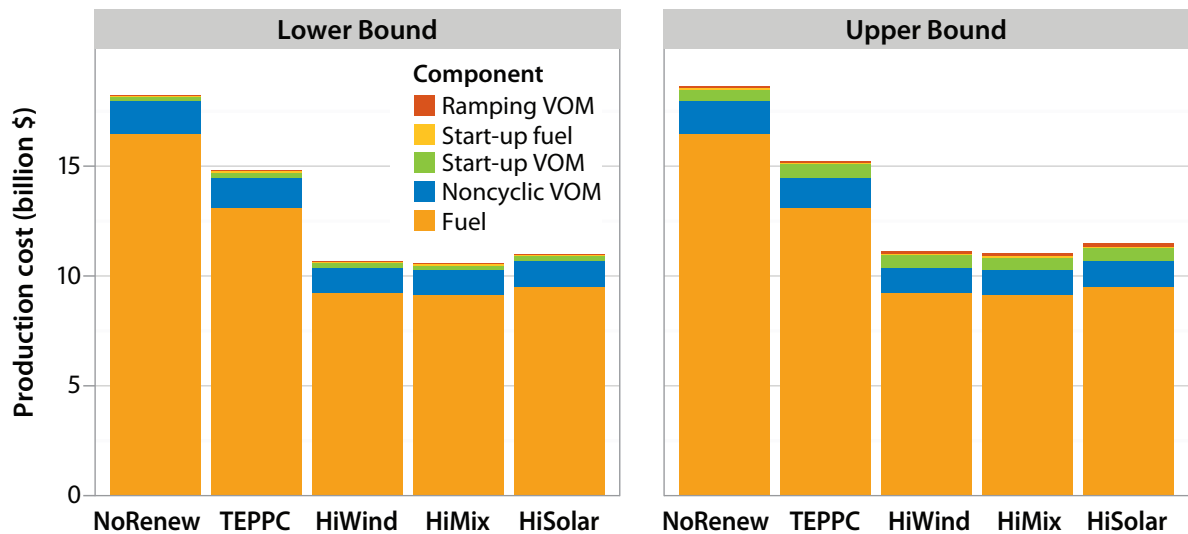
Figure ES-11. Production cost for each scenario showing the (left) lower and (right) upper bound for the cycling costs
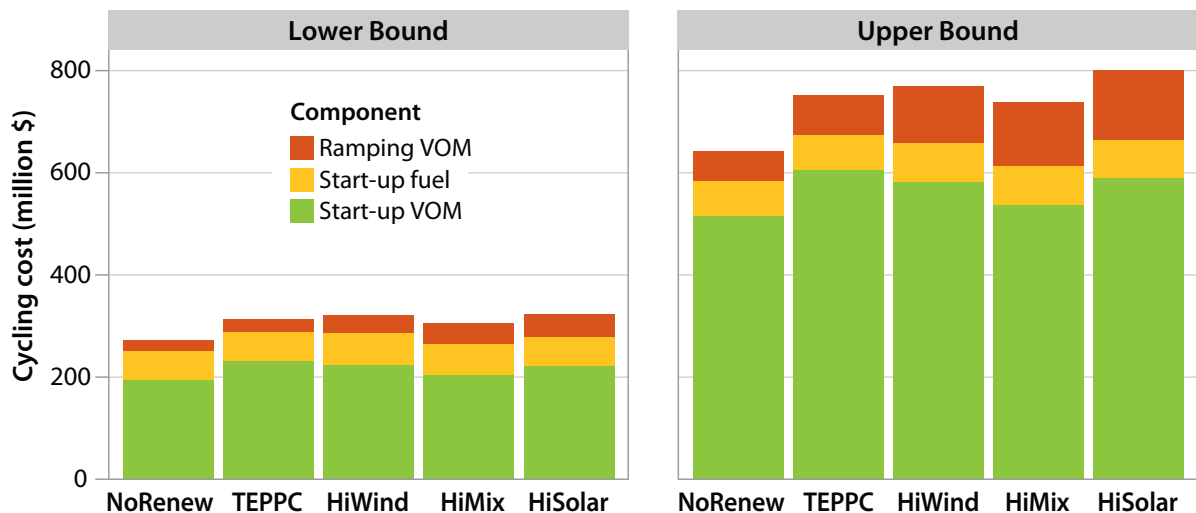
Figure ES-12. Production cost components resulting from cycling, showing the (left) lower and (right) upper-bound wear-and-tear costs for each scenario

Note: Cost components have been broken down into starts, start fuel, and ramping costs.

Figure ES-12 shows only the cycling portion of these same costs. The cycling costs range from about $270 million in the No Renewables Scenario using the lower-bound cycling costs to about $800 million in the High Solar Scenario using the upper-bound cycling costs. When wind and solar are added to the system, cycling costs increase by $35–$157 million, or 13%–24%. Interestingly, the High Mix Scenario has a higher wind/solar penetration but lower cycling costs than the TEPPC Scenario. There is not necessarily a monotonic increase in cycling costs with wind/solar penetration. In terms of cycling costs, there may be a big step in going from 0% to 13% wind/solar, but a much smaller step in going from 13% to 33%.

> **Wind- and solar-induced cycling increases average fossil-fueled plant O&M costs by $0.47–$1.28/MWh in the high-penetration scenarios. Gas CTs bear the highest wear-and-tear cycling costs.**

We first examine these costs from the perspective of the fossil-fueled plants. Figure ES-13 divides the cycling costs shown in Figure ES-12 by each MWh of fossil-fueled generation. These cycling O&M costs increase from $0.45–$1.07/MWh in the No Renewables Scenario to $0.63–$1.51/MWh in the TEPPC Scenario, where the ranges reflect the uncertainty in the wear-and-tear costs. This cycling wear and tear increases to $0.92–$2.36/MWh in the high-penetration scenarios. Table ES-2 shows the cycling cost impacts of wind and solar for each scenario.

Table ES-2. Increase in Cycling Cost (Compared to No Renewables Scenario)

Scenario	Total (Million $)	Per MWh Wind/Solar Generation	Per MWh of Fossil-Fueled Generation
TEPPC	42–108	$0.41–$1.05/MWh	$0.18–0.44/MWh
High Wind	50–127	$0.20–$0.50/MWh	$0.52–1.24/MWh
High Mix	35–95	$0.14–$0.38/MWh	$0.47–1.14/MWh
High Solar	52–157	$0.22–$0.67/MWh	$0.50–1.28/MWh
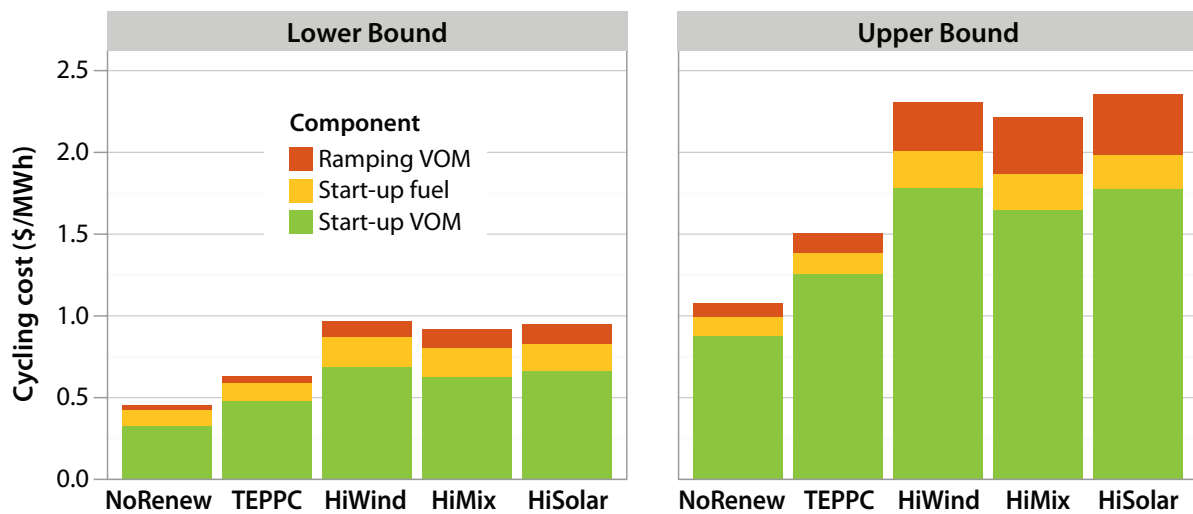
Figure ES-13. Cycling cost, showing the (left) lower- and (right) upper-bound wear-and-tear costs for each scenario

Note: These cycling costs are defined as the total system-wide cycling costs per MWh of fossil-fueled generation.

Figure ES-14 further disaggregates the cycling cost by plant type. For confidentiality reasons, only the lower bounds can be shown. Note, however, that although the absolute magnitudes of costs are higher with the upper bounds, the relative comparisons discussed here also hold true for the upper bounds. CTs (must-run CTs were excluded to delve into these impacts) bear the brunt of the wear-and-tear costs (Figure ES-14, right). Notably, these cycling costs actually decrease at low wind/solar penetrations (TEPPC Scenario) and do not change in the High Wind Scenario from the No Renewables Scenario. For the coal plants (Figure ES-14, left), cycling costs are only slightly affected. For the CC plants (Figure ES-14, center), cycling costs increase with increasing wind/solar penetrations.
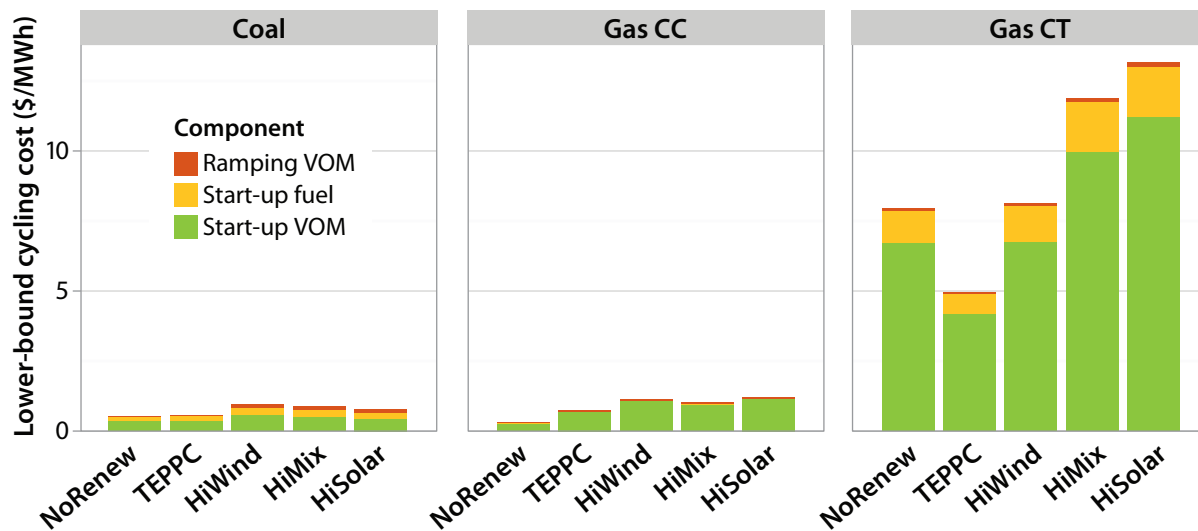
Figure ES-14. Lower-bound cycling cost for (left) coal,
(center) gas CC units, and (right) gas CTs (excluding the must-run CTs)

Note: Total, system-wide, lower-bound cycling costs were disaggregated by plant type and divided by MWh of generation of that plant type.

Cycling Increases Production Costs Slightly

We next examine these costs from a system perspective. When we compared the production cost of each scenario to the No Renewables Scenario, we saw a decrease of $3.34–$3.43 billion at low penetrations (TEPPC Scenario) and $7.12–$7.65 billion in the high-penetration scenarios (see Section 6). This change in production cost is dominated by displaced fuel costs.

Dividing this production cost reduction by the amount of wind and solar energy delivered yielded a production cost reduction of $32.6–$33.2/MWh in the TEPPC Scenario and $29.4–$30.6/MWh in the high-penetration scenarios (see Table ES-3 for details). Figure ES-15 breaks down the production cost reduction into cost components. Cycling costs (shown by the positive values) offset $0.14–$0.67 of the fuel and VOM reduction per MWh of wind and solar generated in the high-penetration scenarios. This production cost reduction does not reflect fixed capital costs or PPA costs. Utility planners conducting a cost-benefit analysis of wind and solar might want to weigh such fixed capital costs against production costs, but that analysis is not conducted here.

> Cycling costs increase by $0.14–$0.67 per MWh of wind and solar generated in the high-penetration scenarios, based on the specific system characteristics of the Western Interconnection.
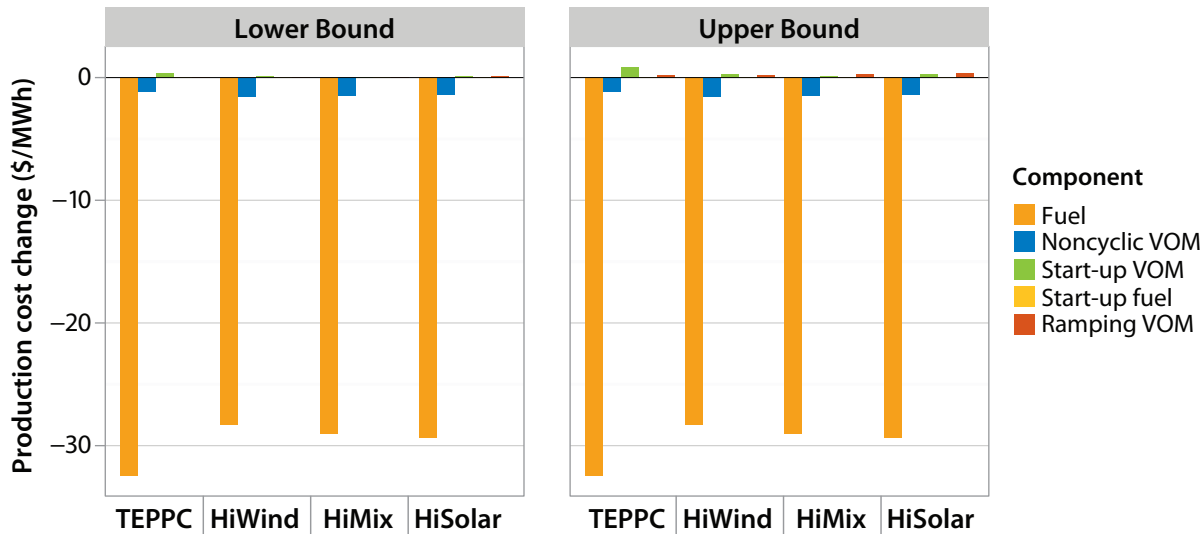
Figure ES-15. The change in production cost for each scenario relative to the No Renewables Scenario, per MWh of wind and solar generation, for the (left) lower-bound and (right) upper-bound wear-and-tear costs

Note: Production costs do not include any fixed capital or PPA costs.

**Table ES-3. Change in Production Cost, Compared to No Renewables Scenario**

Scenario	Production Cost Reduction (Billion $)	Production Cost Reduction ($ per MWh of Wind and Solar Generated)
TEPPC	3.34–3.43	32.6–33.2
High Wind	7.48–7.56	29.4–29.7
High Mix	7.59–7.65	30.2–30.4
High Solar	7.12–7.23	30.2–30.6

Note: Production costs do not include any fixed capital or PPA costs.

CO_2, NO_X, and SO_2 Emissions Reductions Are Significantly Greater Than Cycling Emissions

Figure ES-16 (left) shows the total CO_2 emissions for each scenario. Ramping had no significant impact on CO_2 emissions, so those estimates are not shown. The start-up CO_2 emissions (shown by the thin, dark green line at the top of each bar) were negligible in all cases. Figure ES-16 (right) shows the CO_2 emissions saved by each MWh of wind/solar. Avoided CO_2—considering part-load, ramping, and starts—was 1,100 lb/MWh to 1,190 lb/MWh of wind and solar produced in the high-penetration scenarios (see Table ES-4). CO_2 emissions from starts were negligible. We also calculated the part-load penalty—which was the incremental CO_2 emissions from part-loading—as negligible. This emissions analysis reflects aggregate emissions across the Western Interconnection. Any specific plant might have lower or higher emissions than shown here. Because wind tended to displace more coal compared to solar, and because coal emission rates of CO_2, NO_x, and SO_2 are higher than those of gas, higher penetrations of wind resulted in higher levels of avoided emissions.

Starts, ramps, and part-loading had a negligible impact on CO_2 emissions reductions of wind and solar.
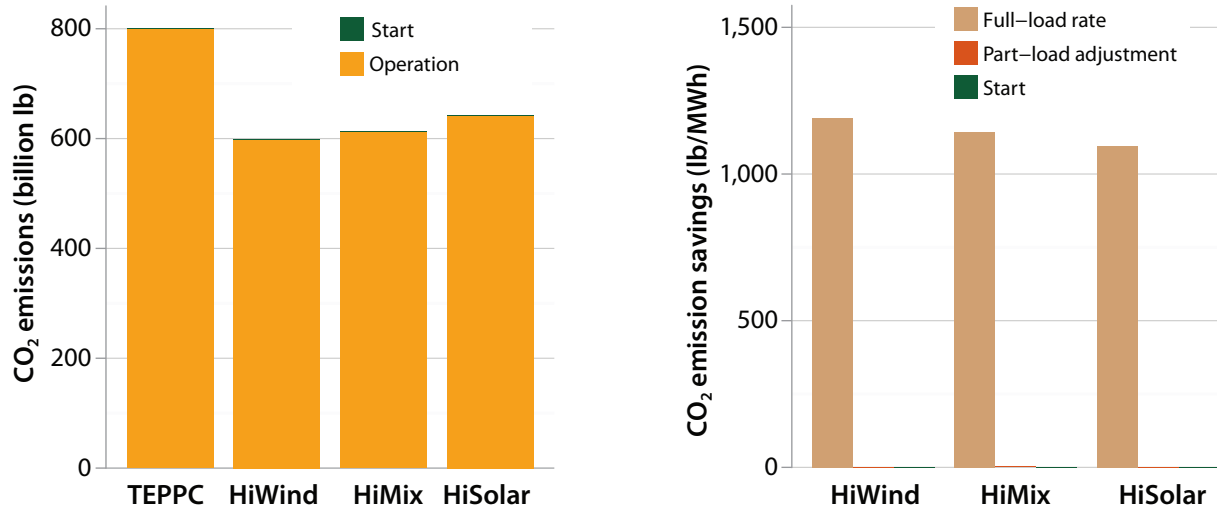
Figure ES-16. CO_2 emissions by scenario: (left) absolute CO_2 emissions for operation and starts and (right) CO_2 emission reductions compared to the No Renewables Scenario, separated into the constant emissions rate assumption and adjustments for part-load and starts

Note: Ramping emissions are excluded because they have no significant impact on CO_2 emissions.

Table ES-4. Emissions Avoided per MWh of Wind and Solar—Considering Part-Load, Ramping, and Start Impacts

Scenario	Avoided CO_2 (lb/MWh)	Avoided NO_x (lb/MWh)	Avoided SO_2 (lb/MWh)
High Wind	1,190	0.92	0.56
High Mix	1,150	0.80	0.44
High Solar	1,100	0.72	0.35

Note: Part-load impacts were not studied for SO_2 because of inadequate data.

From the fossil-fueled plant perspective, average CO_2 emission rates of coal, CCs, or CTs change only slightly with wind and solar as shown in Figure ES-17 (top). Figure ES-17 (bottom) shows that adding wind and solar can positively or negatively affect emissions rates, depending on plant type and scenario. Generally for coal and CCs, wind/solar improves emissions rates by up to 1%. The largest negative impact of wind- and solar-induced cycling is in the High Wind Scenario on the CTs where the emissions rate increases by 2%. This is on average; individual units might be more or less affected.

> **Wind- and solar-induced cycling can have a small positive or negative impact on NO_x and SO_2 emissions rates, and it depends on the pollutant and mix of wind and solar.**

Figure ES-18 shows the analysis for NO_x emissions. There was a negligible impact of starts on NO_x. Ramping reduced the avoided NO_x by 2% to 4%. This is shown in Figure ES-18 (right) as a small negative contribution. Part-loading impacts, on the other hand, increased avoided NO_x by 4% to 6%. On average, coal units in the West emit less NO_x per MWh of generation at part-load. The net impact of considering cycling improved avoided NO_x emissions from wind/solar by 1% to 2%.
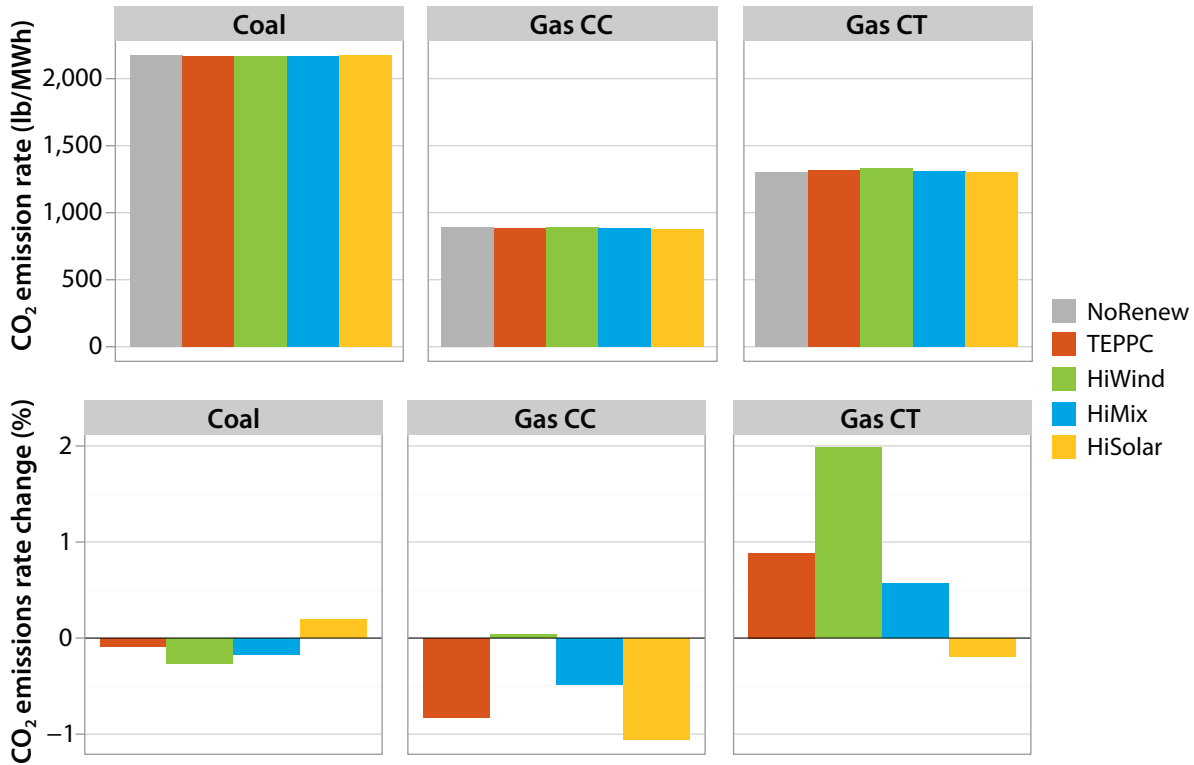
Figure ES-17. (Top) average CO_2 emission rates by plant type (defined as CO_2 emissions divided by MWh of coal, CC, or CT generation) for each scenario and (bottom) change in emissions rate compared to the No Renewables Scenario
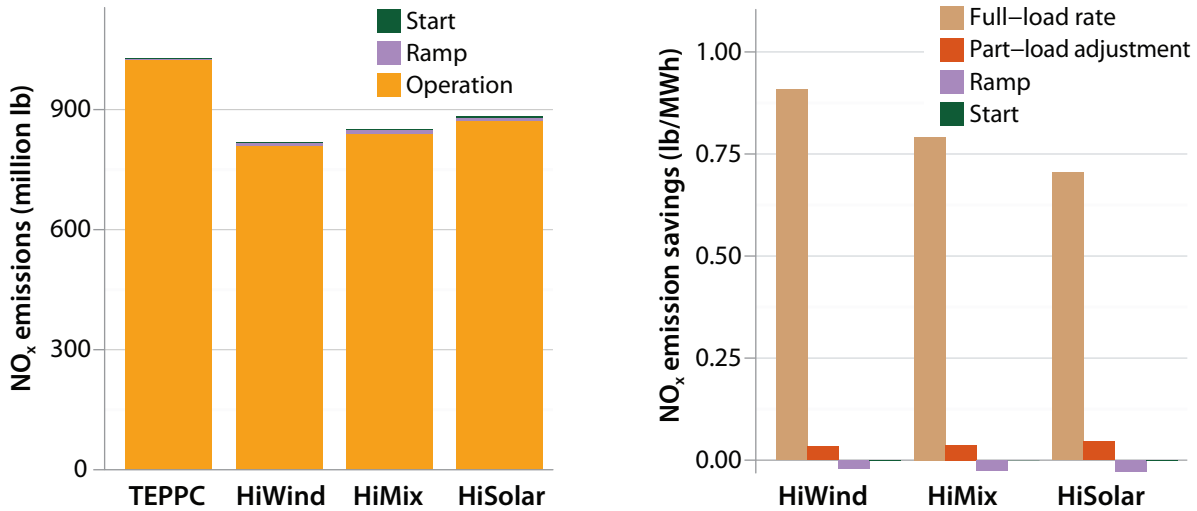

Figure ES-18. NO_x emissions by scenario: (left) absolute NO_x emissions for operation, ramps, and starts, and (right) NO_x emission reductions compared to the No Renewables Scenario, separated into the constant emissions rate assumption and adjustments for part-load, ramps, and starts

Figure ES-19 shows that average NO_x emission rates for different plants can also be positively or negatively affected by wind/solar. Wind- and solar-induced cycling impacts on NO_x emissions rates are relatively small. Impacts on coal units are negligible, but high-penetration scenarios increase overall CC NO_x emission rates by approximately 5%. CTs show the largest impacts. The scenarios with a high wind-to-solar ratio show reductions in CT emissions rates by approximately 10% and the scenario with a high solar-to-wind ratio shows increases in CT emissions rates by approximately 10%. This is on average; individual units might be more or less affected.

Figure ES-20 shows the emissions analysis for SO_2. Because there were inadequate data to create SO_2 emission part-load curves, part-load impacts were not studied for SO_2. Ramping impacts on avoided SO_2 were modest for the high-penetration scenarios, reducing avoided SO_2 by 2% to 5%. Start-up emissions affected the avoided emissions rates by significantly less than 1%. The net impact of considering starts and ramps lessened avoided SO_2 from wind/solar by 2% to 5%.

Figure ES-21 shows the SO_2 emissions rates for coal plants. The High Wind Scenario improves the SO_2 emission rate by 1%; the High Solar Scenario increases the SO_2 emission rate by 2%.
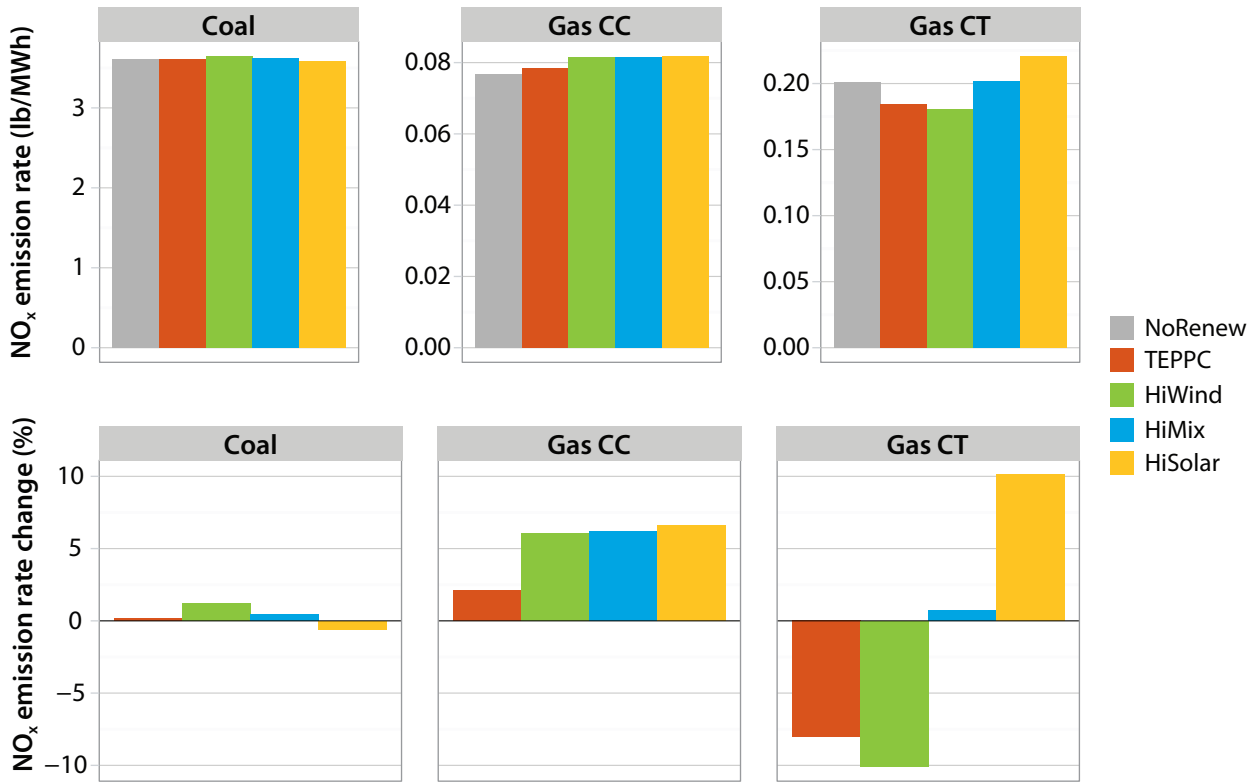
Figure ES-19. (Top) average NO_X emissions rates by plant type for each scenario and (bottom) change in NO_X emissions rate from the No Renewables Scenario

Note: Observe the difference in y-axes.
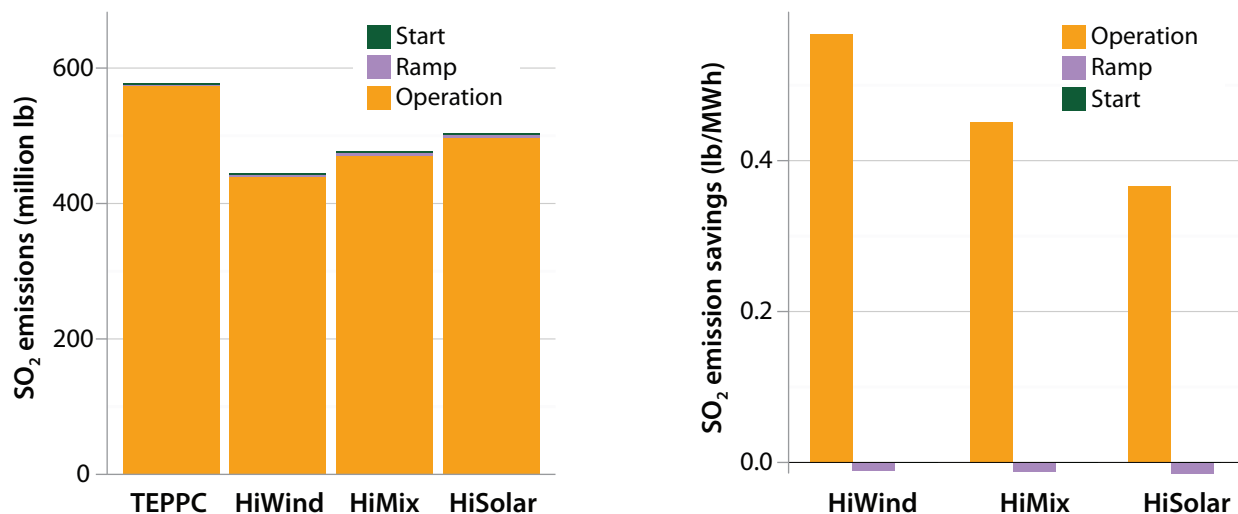
Figure ES-20. SO_2 emissions by scenario: (left) absolute SO_2 emissions for operation, ramping, and starts, and (right) SO_2 emission reductions compared to the No Renewables Scenario, separated into the constant emissions rate assumption and adjustments for ramps and starts.
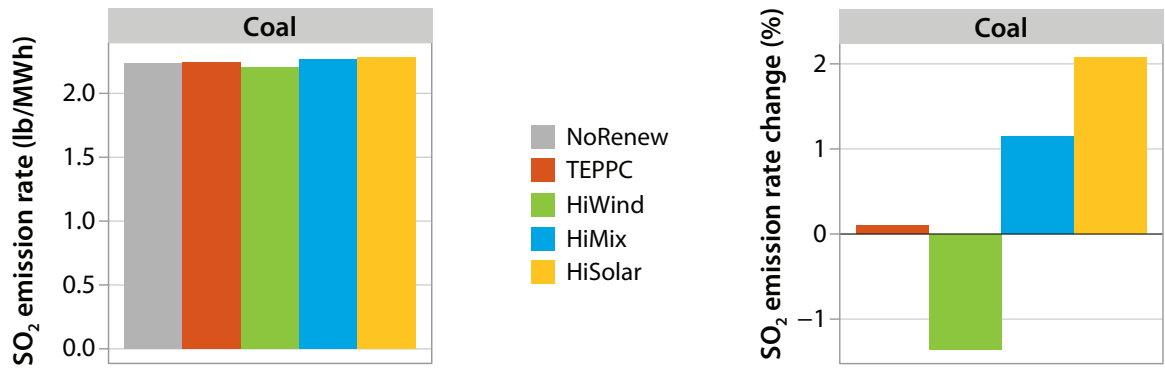
Figure ES-21. (Left) average SO$_2$ emission rate for each scenario and (right) change in SO$_2$ emission rate from No Renewables Scenario

Sometimes, transmission congestion or minimum generation levels of the thermal plants result in a need for curtailment. We curtailed wind and solar in these situations. Wind/solar curtailment was highest in the High Wind and High Solar Scenarios, and much reduced (to below 2%) in the High Mix Scenario (see Figure ES-22). High solar penetrations resulted in the highest curtailment, but curtailment was still modest (below 5%). High solar penetrations resulted in curtailment midday; high wind penetrations more frequently resulted in curtailment at night. We did not model take-or-pay contracts or production tax credits, which would result in a cost for wind/solar curtailment, and possibly reduced wind/solar curtailment at the expense of increased fossil-fueled plant cycling. Because wind/solar curtailment was low, however, we do not think a cost for wind/solar curtailment would change our results significantly.
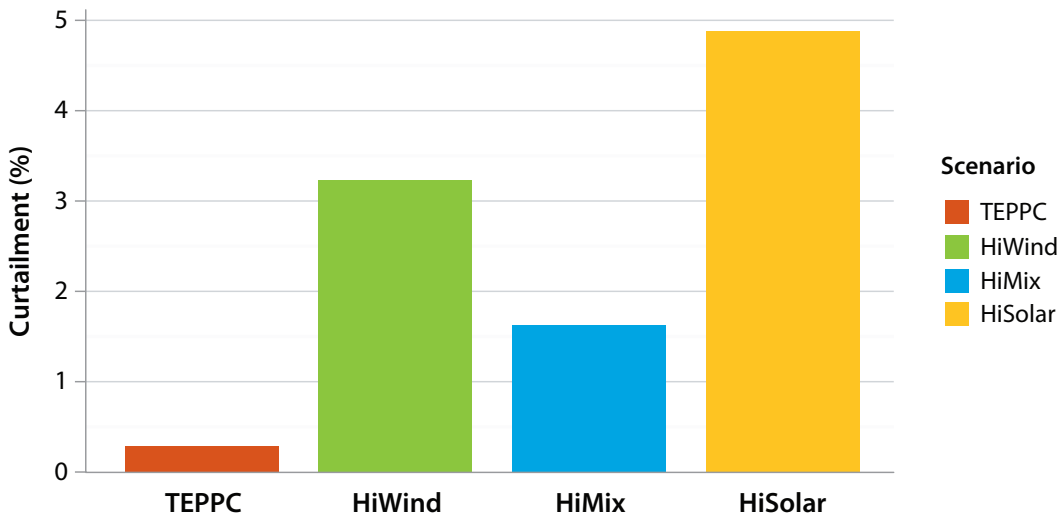
Figure ES-22. Curtailment as a percentage of potential wind and solar generation

The high-penetration scenarios saw the least curtailment with a balanced mix of wind and solar.

Gas Price Has a Greater Impact on Cycling Costs than Wind and Solar Penetration

To understand the impacts of gas prices on the results, we modeled the High Mix and No Renewables Scenarios with gas prices averaging $2.30/MMBtu, $4.60/MMBtu (the core assumption), and $9.20/MMBtu. In the $2.30 case, system operations changed significantly because gas CC units often became cheaper than coal units. As a result, the gas CC units were often operated as baseload and cycled less. Adding wind and solar in all cases, however, displaced approximately one-quarter coal and three-quarters gas CC generation. Figure ES-23 shows the annual generation for all unit types.
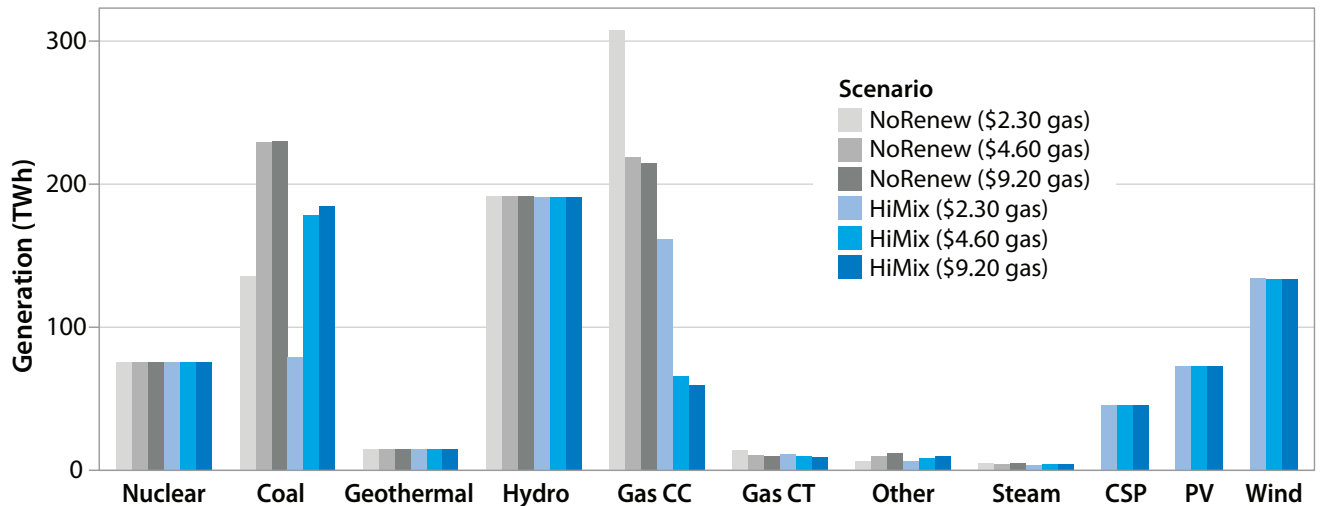
Figure ES-23. Annual generation by type in the gas price sensitivities

Figure ES-24 shows the capacity started in the gas price sensitivities. This plot also illustrates that gas CC units are operated as baseload units in the $2.30 No Renewables Scenario, and as "peakers" (meaning that they are run for a relatively short period each time they are turned on) in the $9.20 cases. Coal units are started less often (and generate less power) in the $2.30 cases because gas CC units are cheaper.
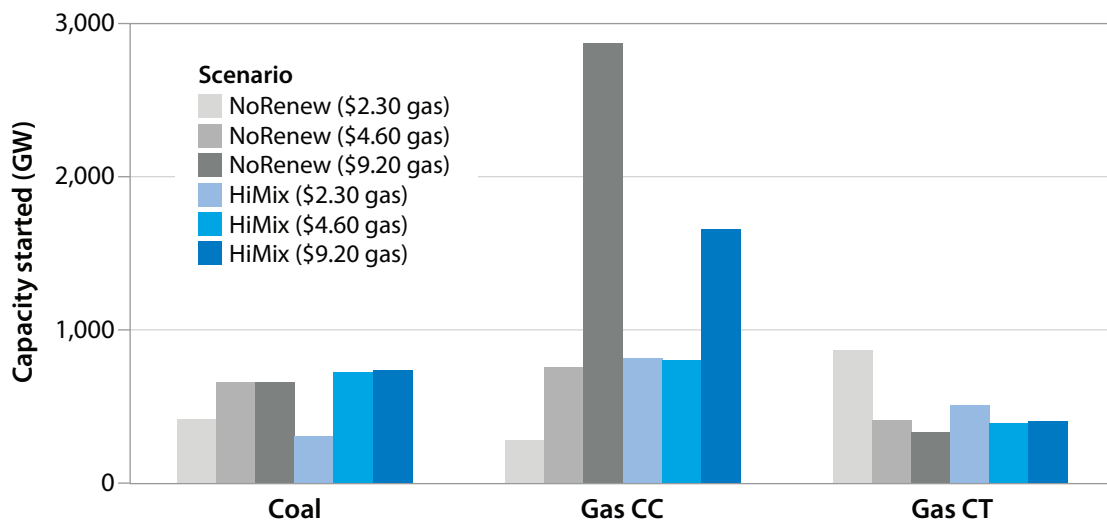
Figure ES-24. Capacity started in the gas price sensitivities

Figure ES-25 shows that cycling costs are affected much more by gas price assumptions than by wind and solar penetration. In the $2.30 and $9.20 gas price sensitivities, adding wind and solar actually reduces the overall cycling cost slightly because some of the starts are displaced at various unit types. Because fossil-fueled generation is displaced, though, adding wind and solar increases the cycling cost per MWh of fossil-fueled generation by $0.30–$1.16, a range that is relatively consistent regardless of gas price. Cycling costs increase at fossil-fuel units despite the reduction in overall cycling costs because fossil-fuel unit operation is significantly reduced in the High Mix Scenario.
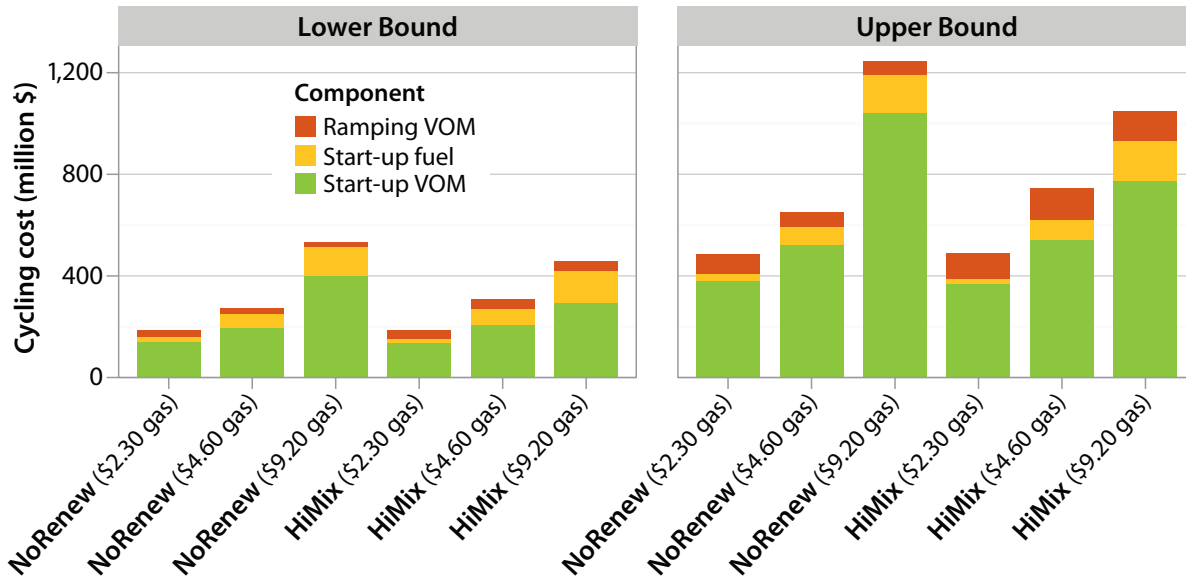
Figure ES-25. Cycling cost in the gas price sensitivities showing (left) lower and (right) upper bounds

> The price of gas has a much greater impact on system-wide cycling costs than the addition of wind and solar. Adding wind and solar affects the cycling cost per MWh at thermal units similarly under various gas price assumptions.

Solar Dominates Variability and Wind Dominates Uncertainty

Many integration studies have investigated high wind penetrations (EnerNex 2011; Charles River Associates 2010; New York Independent System Operator 2010; Intelligent Energy 2009; GE Energy 2008; United Kingdom Department of Enterprise, Trade, and Investment 2008; EnerNex 2006). Fewer studies have examined high penetrations of solar—in part because high solar penetrations have only recently become a concern and in part because of lack of data to model solar well (Orwig et al. 2012; Navigant Consulting et al. 2011).

Utilities have concerns about whether fast-moving clouds over PV plants might result in high variability. PV has two characteristics that affect this variability: (1) the size of the plant and (2) the number of plants. A small plant, such as a rooftop PV system, might see high variability from clouds, but the impact of a small system's variability on the bulk power system is minimal. Impacts could be seen on a distribution level, but WWSIS-2 focuses only on impacts at the transmission level. A large plant can have a higher impact on the bulk power system, but its larger area helps to smooth out the variability. With additional PV plants, the geographic diversity of the plants and the improbability of cloud fronts obscuring all PV plants at the same time result in further smoothing of this variability, as shown in Figure ES-26.
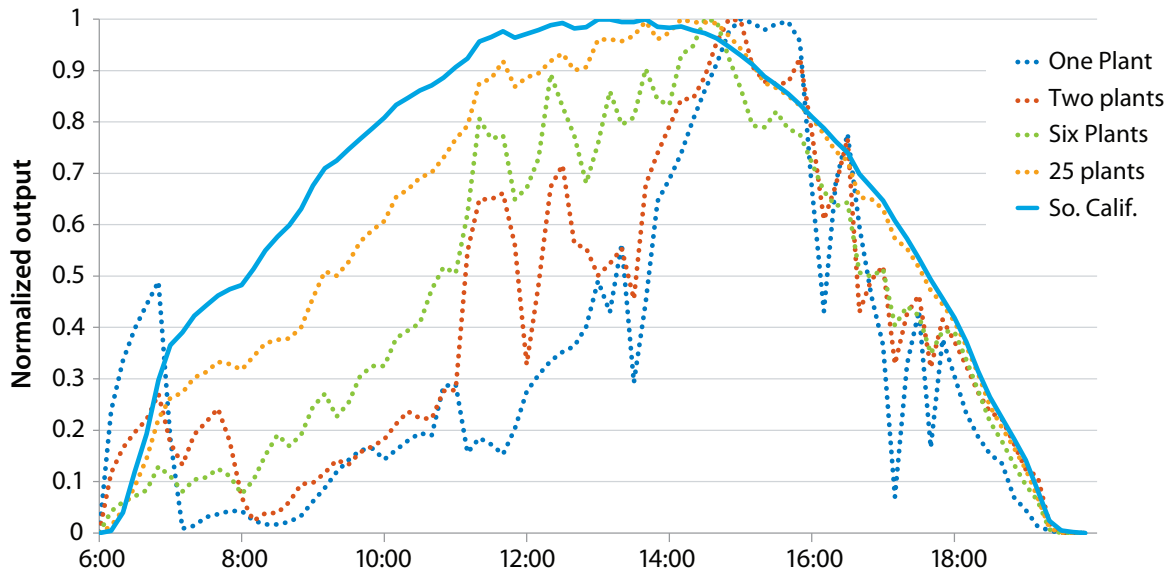
Figure ES-26. Normalized power output for increasing aggregation of PV in Southern California for a partly cloudy day

> **Solar dominates variability extreme events. At a system level, however, most of this variability comes from the known path of the sun through the sky, instead of from fast-moving clouds.**

The sunrise and sunset *do,* however, affect variability significantly with high penetrations of solar. High penetrations of solar dominate variability on a 5-minute and an hourly basis, and extreme events are because of sunrise and sunset (see Figure ES-27). Although extreme variability events increase, they can also be relatively easily mitigated because we know when the sun sets and rises every day. In fact, because we know the path of the sun through the sky for every hour of the year, system operators can accommodate much of this diurnal variability. We removed this known diurnal variability when we calculated reserves for solar (see Section 5).
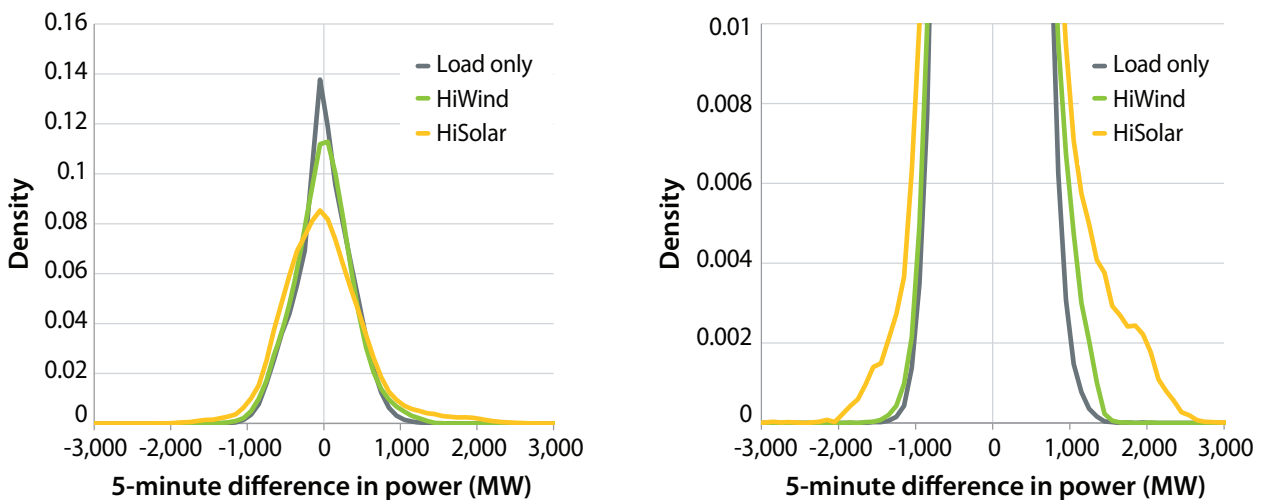
Figure ES-27. (Left) distributions of 5-minute changes in power output for load only and the net load for the High Wind and High Solar Scenarios and (right) an enlargement of the tails of the distribution

Wind, on the other hand, led to greater uncertainty. The high penetrations of wind led to greater extremes in the DA forecast error, as shown in Figure ES-28. Because the 4HA wind forecasts are much more accurate, shown by the tighter distribution in Figure ES-29, this uncertainty in the DA time frame can be mitigated with a 4HA unit commitment of CCs and CTs. Similarly, higher penetrations of wind led to higher reserve requirements (Ibanez et al. 2013) than those with high penetrations of solar because reserve requirements for wind/solar are driven by short-term uncertainty.

> **Wind dominated the uncertainty extreme events in the DA forecast. We can mitigate this by committing gas CCs and CTs in the 4HA time frame, in which forecasts are more accurate.**
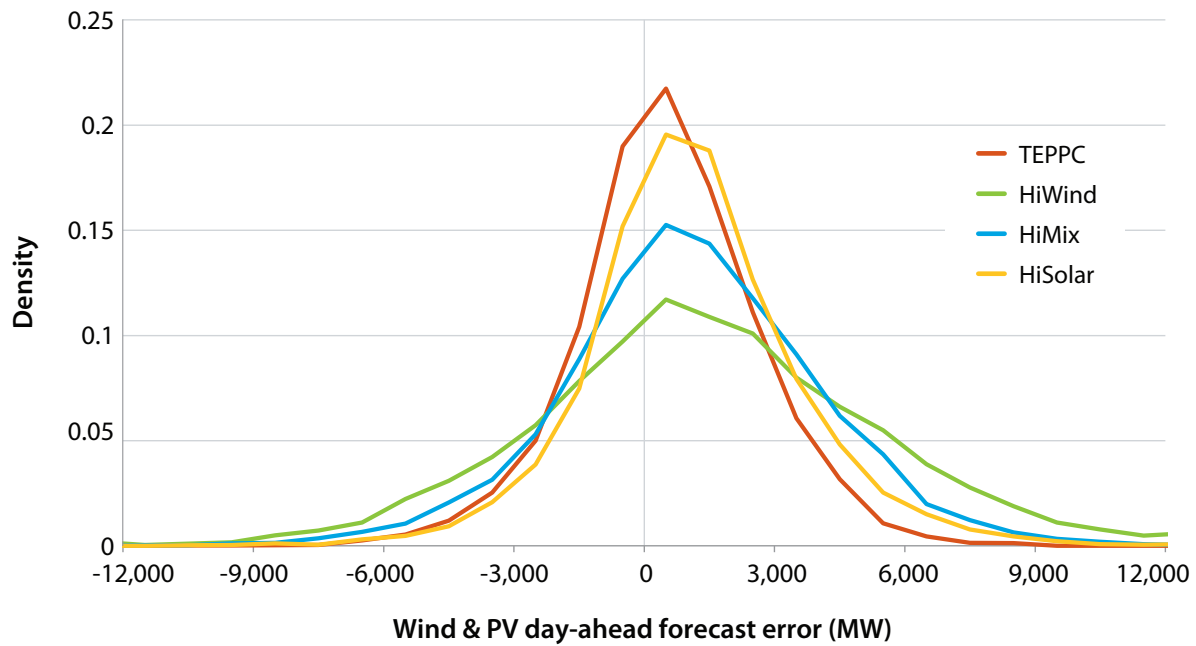
Figure ES-28. DA wind and PV forecast error for the TEPPC, High Wind, High Mix, and High Solar Scenarios
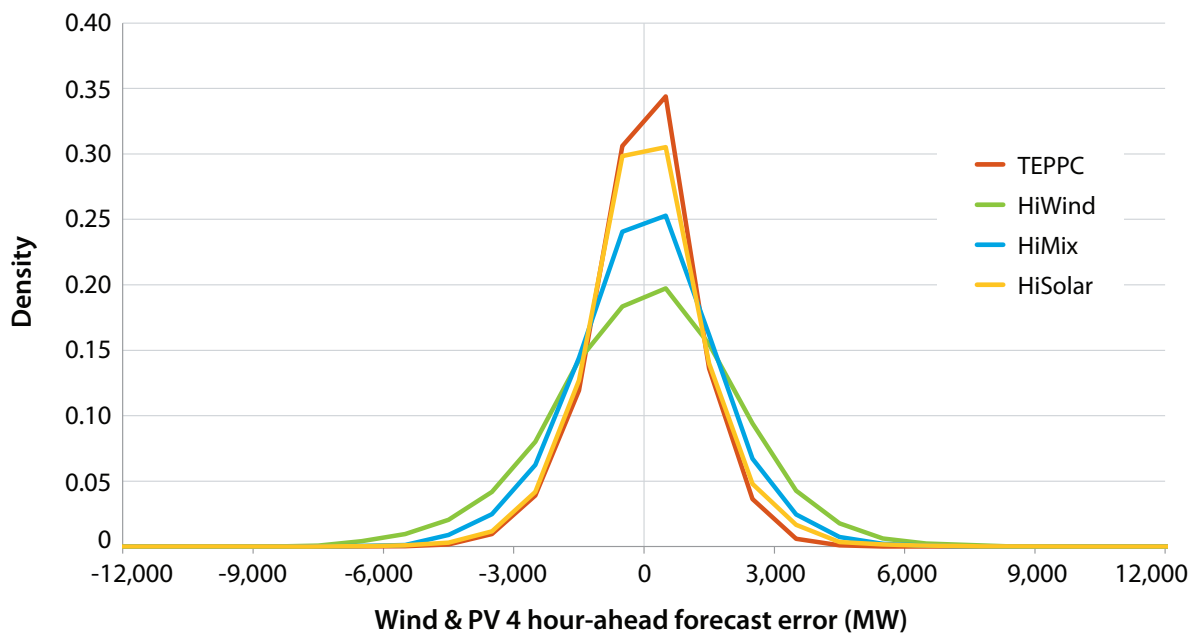
Figure ES-29. 4HA wind and PV forecast error for the TEPPC, High Wind, High Mix, and High Solar Scenarios

Conclusions

We conducted a detailed operational analysis of the Western Interconnection, focusing on the wear-and-tear costs and emissions impacts from cycling of fossil-fueled plants. Detailed wear-and-tear costs and forced outage rate impacts were determined for seven categories of plants for starts, ramps, and noncyclic operation. Emissions impacts were obtained for every power plant for starts, ramps, and part-load operation. Subhourly impacts were examined using a unit commitment and an economic dispatch model with 5-minute dispatch resolution.

In this study, we found that wind and solar increase annual cycling costs by $35–$157 million, or 13%–24%, across the Western Interconnection. Cycling costs for the average fossil-fueled plant increase from $0.45–$1.07/MWh to $0.63–$2.36/MWh, compared to total fuel and VOM costs of $27–$28/MWh. Any specific unit could see more or less cycling and associated costs. Starts, not ramps, drive total cycling costs. CTs bear the brunt of the cycling costs, although CT cycling costs do not increase in the High Wind Scenario and are actually decreased in the TEPPC Scenario. Wind and solar lead to markedly increased ramping for coal generators, and coal runs fewer hours per start with high wind penetrations. Coal units ramp daily instead of weekly as wind/solar, especially solar, penetrations increase. Wind and solar have a relatively small impact on the number of starts for coal units. Wind and solar mostly displace gas CC generation and cut CC unit runtime per start in half. Gas CTs start and ramp less often in scenarios with high ratios of wind to solar penetration. High solar penetrations, on the other hand, lead to more starts, shorter run times, more ramping, and more generation for CTs.

From a system perspective, the $35–$157 million cycling cost increase is a small percentage of the annual fuel displaced by wind and solar of approximately $7 billion. Each MWh of wind and solar generation displaces $29.90–$33.60 of fuel and VOM costs. Wind- and solar-induced cycling offsets $0.14–$0.67/MWh of this reduction in the high-penetration scenarios and $0.41–$1.05/MWh in the low-penetration scenario, based on the specific generator and system characteristics modeled for the Western Interconnection.

We found that cycling impacts on CO_2 emissions are negligible. Emissions reductions of NOx are 1%–2% more than expected when considering cycling and part-load in detail because, on average, coal plants in the West have lower NO_x emissions rates at part-load. Emissions reductions of SO_2 are 2%–5% less than expected because of cycling.

We also compared the impacts of wind and solar, using new data sets that illuminated the subhourly variability of utility-scale PV. Wind and solar generation affect the system in different ways. They both mostly displace gas CC generation, but wind also tends to displace more coal. Solar tends to dominate variability extremes, but it can be mitigated because most of this variability is known and can be anticipated in the unit commitment. Wind tends to dominate uncertainty extremes because of tail events in the DA wind forecast error. This can be mitigated by committing gas CC units in the 4HA time frame and gas CTs in shorter time frames. High wind/solar penetrations result in modest curtailment—up to 5%. WWSIS-2 finds that a balanced mix of wind and solar reduces curtailment to less than 2%.

Future Work

Even though system-wide impacts of cycling are modest, an individual unit could suffer higher than average cycling. Plant owners in this situation will want to know whether they should retrofit their unit or change their operations to better manage cycling at a lower overall cost. Ongoing work includes research on potential retrofits or operational strategies to increase the flexibility of fossil-fueled generators. This includes analysis of the costs and benefits of retrofitting existing plants for options such as lower minimum generation levels or faster ramp rates.

Additional analysis work that would illuminate the impacts of cycling and further compare wind and solar includes the following:

- Market impacts on fossil-fueled plants: How do increased O&M costs and reduced capacity factors affect cost recovery for fossil-fueled plants? What market structures might need revision in a high wind and solar paradigm? How do the economics look for those plants that were most affected?

- Fuel-price sensitivities: How are operations and results affected by different fuel prices for coal and gas?

- Different retirement scenarios: How are operations and results affected if significant coal capacity is retired or if the balance of plants is flexible versus inflexible?

- Storage: Does storage mitigate cycling and is it cost effective?

- Impacts of dispersed versus centralized PV: How does rooftop versus utility-scale PV affect the grid?

- Reserves requirement testing to fine tune flexibility reserves: What confidence levels of flexibility reserves are most cost effective and still retain reliable grid operation?

- Scenarios with constrained transmission build-outs: If transmission is constrained, what is grid performance and how is cycling affected?

- Reserve-sharing options: How do different reserve-sharing options affect grid operations?

- Increased hydro flexibility and modeling assumptions: How does flexibility in the hydro fleet affect grid operations and what is the impact on cycling?

- Hurdle rates to represent market friction: With higher hurdle rates to mimic less BA cooperation, how are grid operations and cycling affected?

- Comparison of the detailed 5-minute production simulation modeling with cycling costs to hourly production simulation modeling without cycling costs: How much more accurate is the detailed modeling?

- Gas supply: Is additional gas storage needed? How does increased wind/solar affect gas scheduling and supply issues?

- Market sequence: How much does the system benefit from the 4HA market?

Table of Contents

List of Figures

List of Tables

1 Introduction

This section presents an overview of the project, including the study's objectives and major tasks; covers the technical review process used to develop the study; describes how this study improves on previous work; and outlines the report's organization.

1.1 Background and Objectives

The Western Wind and Solar Integration Study is a landmark analysis of the operational impacts of high penetrations of wind and solar power on the Western Interconnection power system of the United States. The goal is to understand the effects of and investigate mitigation options for the variability and uncertainty of wind, photovoltaic (PV), and concentrating solar power (CSP). In Phase 1 of the Western Wind and Solar Integration Study (WWSIS-1), we found no technical barriers to integrating 35% wind and solar energy in the subregions of Colorado Coordinated Planning Group, Sierra, and Southwest Area Transmission (shown in Figure 1), and up to 27% across the Western Interconnection, if operational changes could be made (GE Energy 2010). The two most significant operational changes suggested by the study were increased balancing authority (BA) cooperation and increased use of subhourly scheduling between BAs for generation and interchanges.
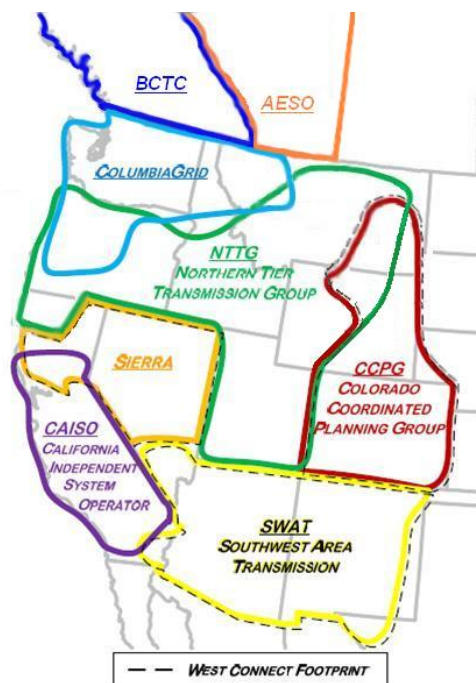
Figure 1. Map of the Western Interconnection subregions

High wind and solar output can cause coal and other generators to cycle more frequently (see Figure 2). In this report, cycling is a broad term meaning shutting down and restarting, ramping up and down, and operating at part-load. In this report, a *start* is defined as "restarting a unit that is offline." *Ramping* is defined as "load-following operation in which a unit goes from full output to some minimum level and back to full output." *Cycling* encompasses both starts and ramps and also refers to operation of a unit at less than full output.

1

Limited data have been available, however, to demonstrate the cost and emissions impacts of this type of operation. The increased cycling (see examples in Figure 2) prompted utility operators and policy makers to request quantification of the impacts of cycling on wear-and-tear costs and emissions impacts. To that end, we initiated Phase 2 of the WWSIS (WWSIS-2) in 2011, with a primary objective of quantifying wear-and-tear impacts and emissions effects created by cycling on the fossil-fuel–based generation fleet.

Additionally, in WWSIS-1 solar penetrations were capped at 5%, and only CSP and rooftop PV were modeled because of limited capabilities to model utility-scale PV output on a subhourly timescale. Subsequent advances in synthesizing subhourly PV plant output allowed WWSIS-2 to model higher levels of solar penetration, including utility-scale PV, while maintaining technical rigor and credibility.

Finally, because wind and solar generation varies on a subhourly basis, a new modeling method with subhourly capability was required. To meet the subhourly requirements, WWSIS-2 used Energy Exemplar's commercial production simulation tool (PLEXOS) for the modeling work. PLEXOS can model a 5-minute dispatch, which allows subhourly impacts of wind and solar to be investigated in detail.
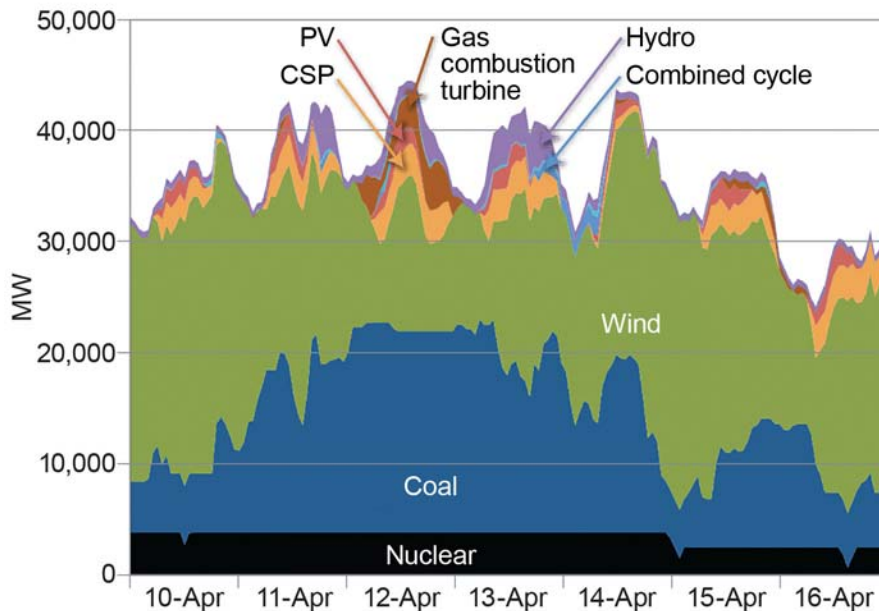
**Figure 2. WWSIS-1 system dispatch
for the most challenging week of 3 years of data analyzed**

Note: This is the most challenging week due to the high wind
penetration, low load, and significant variability in wind output
throughout the week

1.1.1 Wear-and-Tear Cost and Impact Data for Cycling

Cycling of thermal plants causes temperature swings that can lead to creep, fatigue, and fatigue-creep interaction in components and equipment. This in turn can lead to increased operations and maintenance (O&M) costs, more frequent repairs, reduced component life, and more frequent forced outages. Furthermore, some plants were designed for baseload operation and have limited ramping capability. We recognize that fossil-fueled units have varying capabilities, and in this study, industry-accepted ramp limits were used for each unit.

In WWSIS-2, we divided the fossil-fuel–based fleet into seven categories, three for coal-fired plants, and four for gas-fired plants:

- Coal-fired
    - Small, subcritical steam (35 MW–299 MW)
    - Large, subcritical steam (300 MW–900 MW)
    - Large, supercritical steam (500 MW–1,300 MW)
- Gas-fired
    - Combined cycle (CC)—combustion turbine (CT)/steam turbine (ST), heat recovery steam generator (HRSG)
    - Simple-cycle, large-frame CT
    - Simple-cycle, aero-derivative CT
    - Steam (50 MW–700 MW).

For each of these categories, the following input data were developed:

- Start costs for hot, warm, and cold starts
- Ramping costs for load-following from maximum output to minimum generation to maximum output
- Noncyclic variable operations and maintenance (VOM) costs, defined as the variable O&M costs for when the plant is operating at steady state
- Forced outage rate impacts of hot, warm, and cold starts
- Long-term heat-rate degradation
- Start fuel use
- Start costs, excluding fuel costs but including auxiliary power, chemical, and water costs.

Detailed discussions of the input data related to wear and tear, including definitions for each of the preceding terms (e.g., warm start) can be found in Section 2.1.

It is important to note that high-impact, low-probability events such as a generator failure were not included in these wear-and-tear costs because there were not enough data to assess the impact of cycling on those events. This is an area that requires further research.

1.1.2 Emissions Impacts From Cycling

In WWSIS-2, we developed a unit-specific database of emissions of carbon dioxide (CO_2), nitrogen oxides (NO_x), and sulfur dioxide (SO_2) for fossil-fueled generators, including starts, ramping, and part-load operation. The development of these emissions rates and impacts is discussed in Section 2.

1.1.3 Operational Impact Analysis

In WWSIS-2, we used these newly developed input data to analyze operational impacts. This included statistical analysis of net load (net load is load minus wind minus solar) and extreme events, along with unit commitment and economic dispatch.

WWSIS-2 modeled up to 33% wind and solar energy penetration in the U.S. portion of the Western Interconnection. Five primary scenarios were created to study the impacts of wind and solar penetration and compare wind and solar:

- No Renewables (0% wind, 0% solar)
- TEPPC[1] Scenario (9.4% wind, 3.6% solar)
- High Wind Scenario (25% wind, 8% solar)
- High Solar Scenario (8% wind, 25% solar)
- High Mix Scenario (16.5% wind, 16.5% solar).

Transmission was expanded to bring the new wind and solar resources to load. The Western Interconnection was simulated using a 5-minute production simulation model (PLEXOS) to study scenarios in 2020. TEPPC's 2020 Portfolio Case 1 (PC1) was used as a basis for the modeling. Metrics such as production cost, generation displacement, emissions, starts, hours run, ramps, and reserve violations were used to assess performance of the scenarios.

When we conducted WWSIS-1, utilities asked us to consider wear-and-tear costs from cycling. When we asked utilities for cycling costs for their generators, however, we found that most did not know their cycling costs, which may be because historically, many of their generators have not performed significant cycling. Those that did have cycling costs (Connolly et al. 2011) held that information as confidential. WWSIS-2 is one of the few studies (Connolly et al. 2011; GE Energy 2011) that explicitly considers wear-and-tear costs and is the only study we know of that incorporates wear-and-tear costs into the unit commitment and dispatch optimization process.

1.2 Technical Review

A Technical Review Committee (TRC) for WWSIS-2 was established to review input data, assumptions, methodologies, and results. The TRC included relevant utility and transmission planning staff in the Western Interconnection. Because the focus of Phase 2 was on emissions and wear and tear, the project team specifically incorporated coal and gas plant operation and wear-and-tear industry expertise in the TRC. The TRC met approximately every other month. Smaller working groups were established to review details, including solar data, wear-and-tear

---

[1] TEPPC stands for Transmission Expansion Planning Policy Committee, a committee of the Western Electricity Coordinating Committee (WECC). WECC is the regional reliability organization for the Western Interconnection.

impacts, hydropower (hydro) assumptions, and reserves. These smaller groups met on an as-needed basis. In addition, other utility industry experts, such as WECC working group leaders or reserve sharing group administrators, were consulted as appropriate.

1.3 Study Improvements and Constraints

Although the driver for WWSIS-2 was industry's concern about the impact of cycling on their plants, emissions, and cost recovery, we were also able to capitalize on improvements and refinements in many aspects of the data inputs and modeling that had been developed since WWSIS-1. In addition, we addressed stakeholder feedback from WWSIS-1.

To help answer questions related to cycling, we created two new data sets for WWSIS-2 (see Section 2):

- The National Renewable Energy Laboratory (NREL), jointly with WECC, contracted with Intertek-APTECH to develop wear-and-tear costs and forced outage rate impact data for seven plant types based on their cycling cost studies of 400 plants around the world (Kumar et al. 2012). This improves on WWSIS-1, where we were only able to use standard planning inputs for start costs with no specific consideration for wear and tear because data were lacking.

- NREL developed unit-specific emissions data for emissions rates as a function of generator output and for starts and ramps. In WWSIS-1, we used block emission rates for various levels of output for each generator with no specific consideration for starts or ramping. The production simulation analysis was conducted throughout the entire interconnection to capture all emissions impacts from wind and solar.

To help assess the contribution from wind and solar, the wind and solar data sets were refined as follows:

- Solar data: When we conducted WWSIS-1, the capability to model utility-scale solar plant output on a fast time frame was not yet available. This limited the study to a 5% solar energy penetration of distributed generation (DG) rooftop PV and CSP. WWSIS-2 helped to create a capability to model utility-scale PV, and all solar plant outputs were revised accordingly. This allowed us to credibly model 25% solar energy penetrations. We synthesized 1-minute PV and CSP plant output in WWSIS-2.

- Wind data: In WWSIS-1, an artifact of the modeling process left increased variability in the wind plant output data on a 3-day interval. As a result, WWSIS-1 was forced to exclude every third day of data in the statistical analysis. This 3-day seam was corrected for WWSIS-2 (see Appendix A).

- The original wind forecasts for WWSIS-1 did not have a statistical correction, resulting in a positive bias in forecasts compared to plant output. Actual wind forecast error distributions from three BAs were used to refine the wind forecast errors in WWSIS-2, resulting in a much smaller bias and forecast error distributions that better represent today's forecasting capabilities.

- Four-hour-ahead (4HA) wind and solar forecasts were developed for WWSIS-2 to allow for commitment of gas CC and gas steam units.

WWSIS-1 modeled Western Interconnection operations on an hourly time frame. In WWSIS-2, the Western Interconnection was modeled using PLEXOS, which can dispatch down to a 5-minute interval and optimize dispatch of CSP storage. It can also optimize security-constrained unit commitment and economic dispatch with a large number of constraints, including penalties for ramping of fossil-fueled generators to reflect wear-and-tear costs. WWSIS-1 used a day-ahead (DA) commitment and real-time dispatch every hour. WWSIS-2 used a DA and 4HA commitment and a real-time dispatch every 5 minutes.

In WWSIS-1, no additional reserves were held in the core cases for wind and solar. Demand response was found to be a cost-effective alternative to increasing reserve requirements. In WWSIS-2, a new methodology was developed to determine regulation and flexibility reserve requirements for wind and PV. This methodology assesses the fast- and medium-term variability of wind and PV and holds reserves to meet a fixed confidence interval of that variability. We found that sun movement, not cloud movement, dominates PV variability and removed the known diurnal PV variability from our reserves calculation.

Conceptual transmission build-outs were generated using expert judgment for WWSIS-1 to bring resources to load. In WWSIS-2, iterative PLEXOS runs were conducted for each scenario for a year to bring shadow prices across interfaces down to a consistent cutoff level. The shadow price is the marginal value of relaxing the interface limit constraint. It defines the potential value of new transmission along each interface (but not the cost). WWSIS-2 used an optimal DC power flow (with static power transfer distribution factors) respecting transmission constraints instead of the pipeline model used in WWSIS-1.

WWSIS-1 scenarios compared the use of local versus remote resources and varying levels of wind and solar penetration. WWSIS-2 scenarios compared wind versus solar on the power system. The high-penetration case of WWSIS-1 modeled 35% wind/solar energy in some subregions with 27% across all of the Western Interconnection. WWSIS-2 modeled 33% wind/solar energy across the U.S. portion of the Western Interconnection. The 33% value was arbitrary but chosen because it matches the California Independent System Operator (CAISO) 2020 renewable portfolio standard (RPS) requirement. Both studies, WWSIS-1 and WWSIS-2, modeled the entire Western Interconnection and excluded wind/solar resources in Mexico and Canada because of limited data from those countries.

There were limitations to what modeling was feasible during the time frame of this project. Examples are given in the following list:

- The Western Interconnection currently operates with nearly 40 BAs, and only two of these are independent system operators (ISOs). WWSIS-2 did not model confidential information about bilateral contracts that supply power to the BAs. Instead, the Western Interconnection was modeled as 20 zones with interface constraints between them but without hurdle rates. As a consequence, the economic interchange between BAs was optimized by the program without any penalties or costs for such transfers between BAs. A 5-minute economic dispatch was used between zones.

- WWSIS-2 was not intended as a transmission planning study. To reduce impacts of transmission-related effects, transmission was expanded at a zonal level to bring resources to load in a consistent manner across scenarios.

6

- WWSIS-2 modeled wear-and-tear impacts with nominal values for each plant type. This is a simplification in that wear-and-tear impacts are specific to each plant and vary with age, vintage (plants from different eras have different capabilities), design, and operating history.

- WWSIS-2 was conducted as a snapshot in time of a future wind and solar penetration. It did not study the interim steps required to reach that future snapshot. Although 33% wind and solar penetration across the U.S. portion of the Western Interconnection in 2020 is not likely, we wanted to use a stakeholder-vetted model, so we built our model on the WECC TEPPC 2020 PC1 case.

- WWSIS-2 did not address dynamic response and reliability of the power system with high penetrations of wind and PV. Frequency response and transient stability were not considered here but are being addressed in Phase 3 of WWSIS.

- The amount of conventional generation that is installed in the Western Interconnection is the same for all scenarios. It is not reduced with increasing wind and solar penetration.

1.4 Organization of This Report

The rest of this report is organized as follows:

- Section 2 describes the input data used in the study. This includes the wear-and-tear costs and impacts as well as emissions impacts from cycling of fossil-fueled generators. The section also discusses refinements to the wind and solar output and forecast data sets.

- Section 3 presents the scenarios and operational assumptions, including the siting of the five scenarios and the transmission expansion for each scenario. The section also discusses the production simulation methodology and assumptions.

- Section 4 reviews the statistical analysis for the five scenarios.

- Section 5 discusses regulation, flexibility, and contingency reserves for each scenario. WWSIS-2 developed new methodologies for holding reserves based on the characteristics of wind and solar variability and uncertainty.

- Section 6 presents the operational impact results from the production simulation modeling.

- Section 7 assesses findings and conclusions from the study and presents recommendations for future work.

2 Input Data

Input data sets for WWSIS-2 included wear-and-tear costs, emissions impacts, wind plant forecasts and output, and solar plant forecasts and output.

2.1 Wear-and-Tear Costs and Impacts

Cycling, or varying the load level of a fossil unit—including starts, ramping or load-following, and operation at minimum load—can create thermal and pressure stresses in the boilers, steam lines, turbines, and auxiliary components, and these stresses can accelerate wear in various systems. This wear and tear may result in increased capital and maintenance costs and/or reduced life expectancies for components that may increase equivalent forced outage rates (EFOR; Connolly et al. 2011; Electric Power Research Institute [EPRI] 2001). Additionally, varying the load level over prolonged periods typically degrades a fossil unit's fuel conversion efficiency (i.e., heat rate; see Lefton and Besuner 2001).

Although the effects of cycling are understood in qualitative terms, most integration studies to date have not quantified these values, nor have they examined whether the effects are significant in comparison to other items (e.g., initial capital costs, fuel costs, and wear and tear associated with running a unit at design capacity, among others). Consequently, to more accurately assess impacts of wind and solar, WWSIS-2 needed the wear-and-tear costs and impacts for cycling of the fossil-fueled fleet.

Cycling-related wear mechanisms are complex and often involve multiyear time lagging. Because these effects are difficult to assess, utilities often have not quantified the costs or impacts related to cycling. NREL, jointly with WECC, retained Intertek-APTECH (APTECH) to develop this data. This section describes the wear-and-tear cost data set but for more details, please see APTECH's report (Kumar et al. 2012).

APTECH has conducted 400 in-depth cycling studies for coal and gas plants around the world using a combined bottom-up and top-down approach (Kumar et al. 2012). Bottom-up, component-level studies used real-time monitoring data, previous engineering assessments of critical components, and a survey of plant personnel. The bottom-up accounting techniques broke down component-specific costs. Top-down studies used lightly screened annual maintenance, capital and forced outage costs, unit composite damage accumulation models, and statistical regression methods. The top-down analysis can capture major direct effects and even operator error and other indirect effects to estimate cycling costs. High-impact, low-probability events such as a generator failure were not included in these wear-and-tear costs because there were not enough data to assess the impact of cycling on those events. This is a topic for future study.

For each plant, a best-fit estimate for cycling costs was created through linear regression between annual O&M costs and operational data (including the number of hot, warm, and cold starts; ramping; and total generation). Uncertainty in this regression resulted from the limited sample size, the noise inherent in variations of annual cost and cycling characteristics, and the standard and heuristic numerical procedures; the upper and lower bounds describe the uncertainty range. These were determined by re-running the regression analysis while forcing the cycling cost estimates to deviate from the best estimate. The range of solutions was assessed visually and by goodness of fit statistics.

APTECH provided both lower- and upper-bound data for WWSIS-2 but requested that the raw upper-bound data (or analyses using the upper-bound data that would allow readers to back out the raw upper-bound data) be kept confidential. Raw lower-bound data are presented here. Both the lower- and upper-bound data are used in the WWSIS-2 production simulation analyses and aggregate results are presented here. These wear-and-tear results, then, represent "bookend" costs.

From these 400 studies, APTECH extracted data from 170 plants located in North America that used a consistent assessment methodology. The data from these units were statistically analyzed to derive cycling costs and impacts. Next, the data were used to develop operating data for seven categories of plants, with each category including between 11 and 39 plants. Here are the categories, followed by a description of the data developed for each category:

- Large, coal-fired, subcritical steam (300 MW–900 MW)
- Small, coal-fired, subcritical steam (35 MW–299 MW)
- Large, coal-fired, supercritical steam (500 MW–1,300 MW)
- Gas-fired CC, which consists of CT/ST and HRSG
- Gas-fired, simple-cycle, large-frame CT
- Gas-fired, simple-cycle, aero-derivative CT
- Gas-fired steam (50 MW–700 MW).

In this analysis, the following wear-and-tear parameters were estimated for each of the seven categories:

- Cost of a hot start
- Cost of a warm start
- Cost of a cold start
- Cost of ramping
- VOM costs for noncyclic operation
- Increased EFOR because of a cold start
- Increased EFOR because of a warm start
- Increased EFOR because of a hot start
- Long-term heat-rate degradation.

Each plant category consisted of a variety of plants with different operating histories, ages, and designs. It is likely that a newer plant that was designed for cycling would have lower cycling wear-and-tear costs and an older plant that was not designed for cycling but was heavily cycled would have higher costs. APTECH conducted statistical analysis of the costs for these various plants, thereby showing the costs of the average plant in its sample as well as the range of costs. We applied the median of the lower bounds and the median of the upper bounds to each plant category in WWSIS-2. Therefore, WWSIS-2 does not capture detailed cycling costs specific to any individual plant's age, design, vintage, or operating history. The increased EFOR rates and long-term heat degradation were not used in the WWSIS-2 analysis. In the future, these data could help understand some of the long-term impacts of increased cycling.

2.1.1 Start Costs

This section describes the various components that are included in the start costs and shows the lower-bound hot, warm, and cold start cost distributions for the seven unit types.

In this study, the start costs were divided into four categories:

- Maintenance and capital expenditures
- Operational heat-rate impacts
- Start fuel
- Start auxiliary power, chemicals, and labor (costs not captured in the preceding categories).

Although some of these costs are directly observable (e.g., the cost of fuel), others must be inferred (e.g., start-related maintenance and heat-rate degradation costs are not known until years after the event), with some uncertainty. To help characterize this uncertainty, upper and lower bounds were developed for each of the 170 plants in the APTECH study. This information was then used to develop the cost distributions shown in Figure 3.

Figure 3 illustrates the distribution of estimated lower-bound hot-, warm-, and cold-start costs for the various unit types per start for each MW of capacity. The definition of hot, warm, and cold starts is based on the number of hours the unit was offline and varies with the type of unit (Kumar et al. 2012). The figure illustrates a statistically significant difference between the start costs of the various unit types and shows that cost within a category can vary significantly.

The study found that most coal units cost more to start than gas units; however, the distributions overlap for most unit types, and some coal units cost less to cycle than some gas units. Small coal units have the highest cost per MW for starts. This is partly because of the historical operation at these units with extensive cycling.
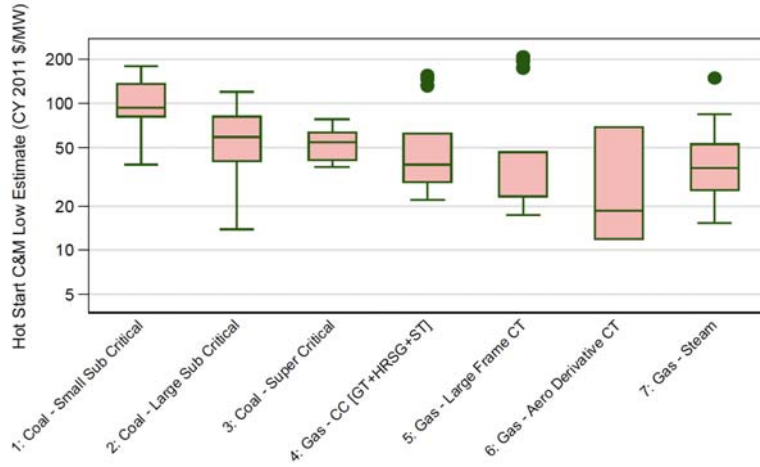
(a)
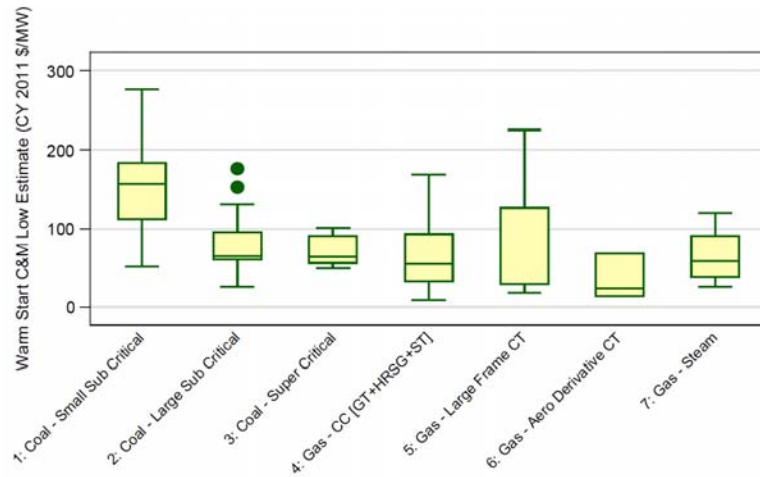
(b)
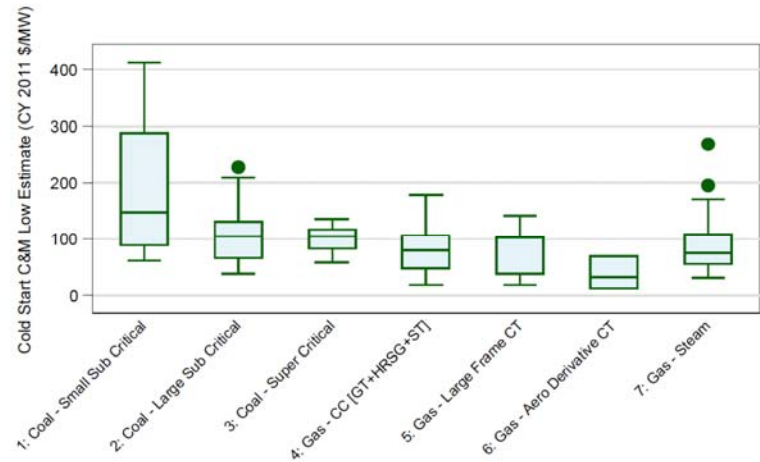
(c)

Figure 3. (a) Hot-, (b) warm-, and (c) cold-start lower-bound costs per start per MW of capacity

Notes: The range shows the 25th to 75th percentile; the median is shown within that range.
Nonoutlier extrema are depicted by the whiskers in the plots. Outliers are represented as dots.

11

For most unit types, cold starts at the lower-bound cost approximately double the lower-bound cost of hot starts, with warm starts somewhere in between. Starts for aero-derivative CT generators were found to be the same for hot, warm, and cold starts at the lower bound, because the units cool so quickly that all starts are classified as cold starts.

Note that only lower-bound costs are shown because the upper-bound data are confidential. Although not shown, the upper-bound costs were used in the analysis and results are presented in Section 6.

2.1.2 Ramping (Load-Following) Costs

Figure 4 shows the cost (per MW of capacity) of ramping the unit by approximately 30% of its maximum capacity (e.g., from 90% of capacity to 60% and back to 90%). Cycling damage and therefore cycling cost is driven by thermal and pressure stresses. Because these stresses are not as large during ramping as they are during starts, the cost per ramping event is typically two orders of magnitude lower than cold starts. Consequently, ramping costs are very unlikely to affect the commitment or dispatch of generators. Ramping, however, is much more common than starts for many unit types, so the costs can still be important to consider when calculating the impacts of wind and solar penetration on the electric power system. To simplify modeling, then, we did not use the ramping costs in the unit commitment and dispatch modeling but instead applied them to the dispatch results to determine aggregate system ramping costs.
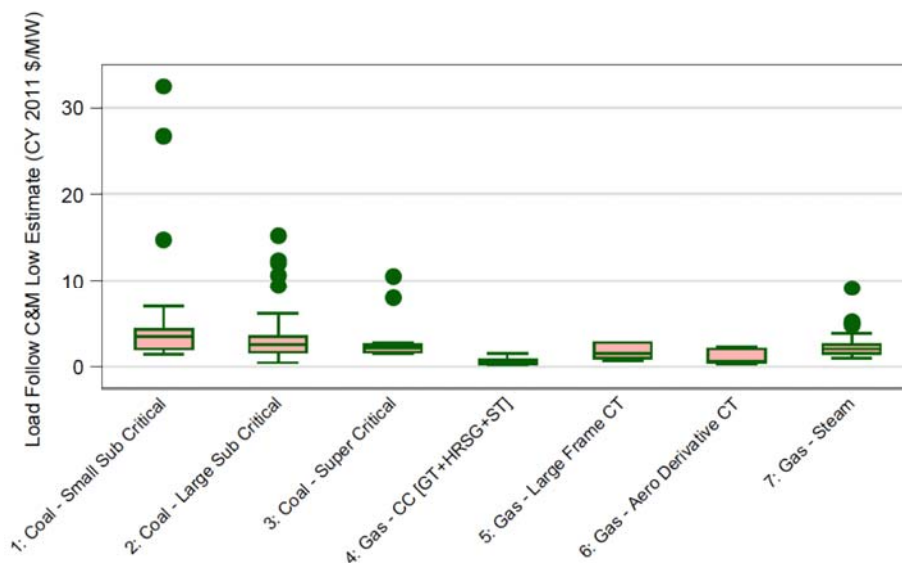
Figure 4. Lower-bound ramping costs per ramp per MW of capacity

Notes: The range shows the 25th to 75th percentile; the median is shown within that range. Nonoutlier extrema are depicted by the whiskers in the plots. Outliers are represented as dots.

2.1.3 Noncyclic Variable Operation and Maintenance Costs

Previous studies typically used a single VOM cost per MWh of generation in production cost modeling to represent VOM costs regardless of whether the unit was started, ramped, or in noncyclic operation. In this study, we explicitly disaggregated VOM into start costs, ramping costs, and noncyclic VOM. APTECH provided these three cost data sets so that the sum of these

12

yielded the entire VOM cost for a plant, thus covering all types of operation consistently. Figure 5 shows the distribution of the lower-bound estimates for noncyclic VOM costs for the seven categories. Steam units (including coal-fired and gas-fired) tend to have higher noncyclic VOM costs than CCs and CTs.

Low-load operation can also increase costs. For example, cycling can increase wear-and-tear damage because of process changes such as wet steam conditions in the low-pressure turbine and feedwater heaters.
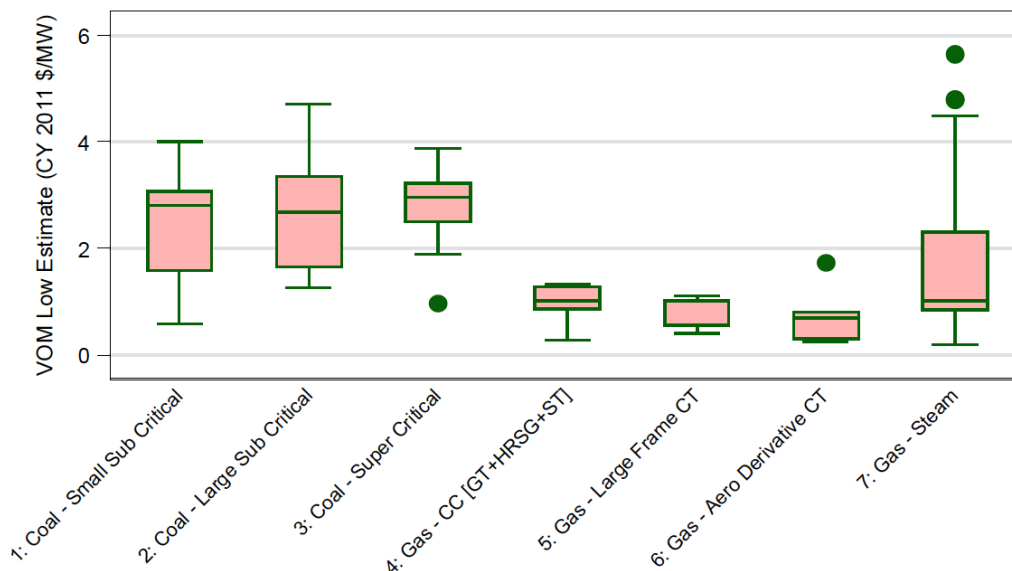
Figure 5. Lower-bound noncyclic VOM costs per MW of capacity

Notes: The range shows the 25th to 75th percentile; the median is shown within that range. Nonoutlier extrema are depicted by the whiskers in the plots. Outliers are represented by dots.

2.2 Emissions

Typical integration studies use average emissions rates for ranges of output levels for each unit. Cycling a fossil-fueled unit, however, can affect emission rates. In WWSIS-2, we more accurately determined total CO_2, SO_2, and NO_x emissions by calculating emissions for noncyclic operation at various output levels and also for starts and ramps.

The impact of cycling on avoided emissions from wind and solar is an area of controversy. Some studies claim wind-induced cycling significantly impacts or even completely negates emissions reductions (Bentek Energy 2010; Katzenstein and Apt 2009). Other analyses suggest otherwise (Fripp 2011; Pehnt et al. 2008). Some studies use regression models to correlate wind output with emissions. It is difficult for those methods to capture the interchanges between BAs or the intertemporal impacts of hydro redispatch or changing unit commitments. Other studies balance the variability from a single wind plant with a single fossil-fueled unit. It is difficult for those methods to capture the smoothing impact from the geographic diversity of wind/solar plants in that BA, the fact that wind may be moving in the same direction as load and thus helping the system balance, or the depth of the dispatch stack of fossil-fueled and hydro plants that balance

the system. WWSIS-2 used unit-specific emission rates (based on starts, ramps, and noncyclic operation), modeled many wind/solar plants in detail including their geographic diversity, and ran a production simulation analysis of the entire interconnection to determine emission impacts.

We analyzed the measured CO_2, SO_2, and NO_x emissions and generation from nearly all fossil units in the United States using the 2008 U.S. Environmental Protection Agency (EPA) Continuous Emissions Monitoring (CEM) data set (EPA 2009). Emissions monitoring is required on all sulfur-emitting units and all other units above 25-MW capacity. The EPA reports hourly generation and heat input (fuel usage in MMBtu), along with CO_2 and NO_x emissions. Based on U.S. Energy Information Administration (EIA) Form 923 data (EIA 2009), 94% of all generation from fossil-fueled units came from units with CEM. We developed a methodology to determine the additional emissions because of starts and ramps and characterized emission rates for part-load operation. Results were categorized for coal units and for gas CC, CT, and steam units.

Heat rate, part-load emissions, and start-up emissions are discussed in the following sections.

2.2.1 Heat Rate

Emissions and heat-rate curves were fit for each unit using hourly data points for generation, heat input, and NO_x. Heat input and NO_x emissions were fit with generation as the independent variable. CO_2 emissions were calculated directly based on heat input and carbon content of the fuel. A nonparametric local linear fit with tri-cube weighting was used so that no predefined functional form was set to the units (see Figure 6). Hours immediately following starts were not considered in the fit. The units with correlation coefficients below 0.7 between the actual emissions and predicted emissions (based on the local linear fit to generation) were not included in the analysis. Combined cycle units with average heat rates larger than 9.2 MMBtu/MWh were replaced with average CC properties. This results from the way the data are reported; CC units are not required to report generation from the steam generator. In the Western United States, a small number of CC units do not report generation from the steam generator (this is more common in the Eastern United States).
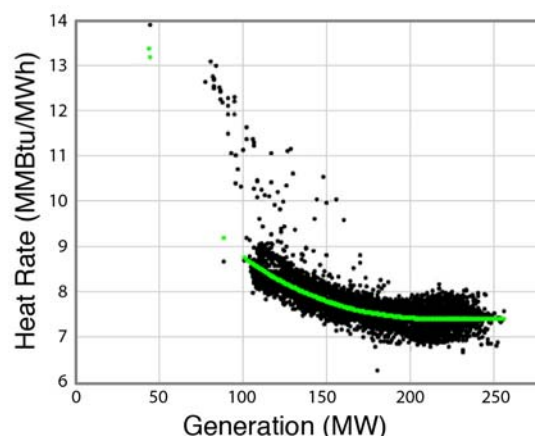
Figure 6. Typical heat-rate curve for a gas CC unit from a measured EPA CEM data set

Notes: The green line shows local linear fit. Residuals are defined as the difference between the measured emissions and the fit.

14

2.2.2 Part-Load Emissions

Heat rates were compared for CCs, CTs, coal, and gas steam units. Table 1 shows the resulting penalties for operating at part-load. This penalty is defined as the percentage increase in emissions rate (lb/MWh) when the average unit is operating at 50% maximum capacity. CC units are the most efficient at full load and part-load. CCs and CTs, though, have the most significant penalties for operating at 50% compared to 100% maximum generation. Coal, CTs, and gas steam units have similar heat rates when operating at full load, but at 50% the coal and gas steam units have heat rates only 5%–6% higher than at full loading. In general, typical CTs are less efficient (e.g., heat rates are 18% higher) at part-load.

The average NO_x emissions as a function of load were compared for the different unit types. Steam units (coal and gas) emit approximately an order of magnitude more NO_x per MWh than gas CC units and CTs. Although part-load operation leads to a NO_x penalty for the CCs and CTs, this was found to benefit the coal-fired steam units. For example, coal units operating at 50% were found to emit 14% less NO_x per MWh compared with full-loading operation; gas CC units were found to emit 22% more NO_x per MWh at 50% load compared with full load. Most of the NO_x from all units is created from nitrogen in the combustion air ("thermal" NO_x), as opposed to in the fuel, so flame temperature is likely a primary driver of NO_x emissions. Because of the significant part-time usage of pollution control equipment for SO_2, it was impossible to create part-load emission curves.

Table 1. Emissions Penalty for Part-Load Operation

Type of Unit	CO_2 (%)	NO_X (%)
Coal	5	−14
Gas CC	9	22
Gas CT	18	15
Gas Steam	6	−14

2.2.3 Start-Up Emissions

Starting an offline fossil-fueled unit increases emissions for several reasons. It takes fuel to bring the unit online, and that fuel adds emissions without adding energy to the grid. Starts can increase emissions rates because most pollution-control equipment does not become fully effective until the exit flue gas temperatures are high enough to support the chemical reactions needed to remove the pollutants. Pre-combustion techniques tend to work when flame temperatures are in the normal operating range (after start-up).

To estimate start-up emissions, each start was analyzed for deviation between actual and predicted emissions. The difference between actual and predicted emissions during the time period until the generator reached its typical minimum generation level was classified as start-up emissions. These emissions were then averaged for all the starts in 2008 for each unit. If emissions occurred before the unit started to generate power, these emissions were also counted.

The production simulation modeling used the actual unit-specific emissions rates; however, for presentation purposes, generation-weighted averages are used here. As a result, units that produced large amounts of electricity had more influence than units that did not produce much electricity.

15

Table 2 shows the start penalties for different types of units and different emissions. They are expressed in MMBtu or lb/MW of unit capacity. For example, a coal unit emits 1.98 lb/MW capacity of excess NO_x during start-up. This is equivalent to operating the unit at full load for approximately 30 minutes. Although coal units emit the most NO_x during starts, CCs and CTs emit more as a fraction of full-load emissions. During starts, CCs emit the same NO_x as approximately 7 hours of full-load operation. For the purposes of this study, starts were not segregated among cold, warm, and hot because many units did not have enough data to justify the split. Coal units emit the same amount of SO_2 during start-up as approximately 30 minutes of full-load operation.

Table 2. Start-Up Emissions per MW Capacity

Type of Unit	Heat Input (MMBtu/MW)	NO$_X$ (lb/MW)	SO$_2$ (lb/MW)
Coal	16.5	1.98	3.9
Gas CC	2.0	0.53	n/a
Gas CT	3.5	0.79	n/a
Gas Steam	13.7	0.84	n/a

Most coal units are started using oil or gas, so the heat input penalty and the CO_2 emissions penalty will likely differ because the carbon content of the start fuel is different from that of the operating fuel.

2.2.4 Ramping Emissions

Ramping emissions were estimated in a similar way to the start-up emissions. Deviations from predicted emissions after ramping events were analyzed to understand how emissions change during and after ramping events. We analyzed several sensitivities for the definition of a ramp. The definition that included the most number of ramps but still had potentially significant emissions impacts was a ramp that covered 30% of the unit's capacity within 4 hours. To account for any residual impacts of the ramp, any deviation from predicted emissions within 12 hours of the ramp is counted toward ramping emissions. The total ramping emissions are divided by the number of ramps for each unit to calculate the average ramping emissions for each unit. Table 3 presents generation-weighted averages for the units in the Western Interconnection. Ramping emissions are much lower than start-up emissions. The most significant ramping emission impact is the NO_x emissions from coal units (equivalent to 10–15 minutes of full-load operation). CO_2 ramping emission impacts are equivalent to less than 3 minutes of full-load operation.

Table 3. Ramping Emissions per MW Capacity

Type of Unit	Heat Input (MMBtu/MW)	NO$_X$ (lb/MW)	SO$_2$ (lb/MW)
Coal	0.57	0.73	0.82
Gas CC	0.08	0.00	n/a
Gas CT	0.28	0.02	n/a
Gas Steam	–0.09	0.05	n/a

2.3 Load Data

It is important to use time-synchronized load and weather data because there are correlations between load, wind, and solar irradiance. The load and weather patterns from the historical year 2006 were used in this study, projected out to the year 2020. One-minute load data were obtained from the WECC Variable Generation Subcommittee.

2.4 Wind Data

This section discusses the type of wind data used in the study as well as the methods used to develop the data. Data were developed for wind plant output and wind forecasts.

2.4.1 Wind Plant Output Data

Integration studies typically model hypothetical wind plants for which limited measured data exist. As a result, a consistent data set of wind outputs must be generated synthetically. In WWSIS-1, 3TIER used a numerical weather prediction (NWP) model to synthesize wind speeds on a 10-minute, 2-km interval in the U.S. portion of the Western Interconnection. 3TIER generated 960 GW of hypothetical wind plant output for 2004 to 2006 (3TIER 2010; Potter et al. 2008; Potter et al. 2007). Those original wind output data ("actuals") had increased variability every 3 days because the modeling process included 3-day restarts of the NWP model (Lew et al. 2011; 3TIER 2010; GE Energy 2010). Although the wind output for each site respected realistic 10-minute maximum changes in output, unrealistic 10-minute variability resulted when sites were aggregated.

WWSIS-2 evaluated various approaches to yield realistic variability when sites were aggregated, along with realistic spatial correlation between sites. Figure 7 shows the method that worked best, which included random splicing of data from unaffected days to the affected seams. This method, which is detailed in Appendix A, was used to correct the wind data for WWSIS-2.

2.4.2 One-Minute Wind Plant Output Data

For the subhourly production simulation modeling, WWSIS-2 required higher time-resolution data, so the 10-minute data set was converted to 1-minute output. This task, which is detailed in Appendix B and summarized here, was accomplished using statistical down-sampling based on measured 1-minute output from wind plants in the Western Interconnection. The high-frequency range of actual data was used to simulate the high-frequency variability between the 10-minute intervals of wind power data provided by 3TIER. A fast Fourier transform (FFT), which has previously been used for power spectrums of wind data (Edwards 2009), was applied to measured wind plant output from the Cedar Creek Wind Farm in Colorado.

First, a cubic spline interpolation was applied to the 10-minute data to obtain power estimates at 1-minute intervals. Then high-frequency data from the measured Cedar Creek wind plant were applied to generate the noise component of the wind power data.
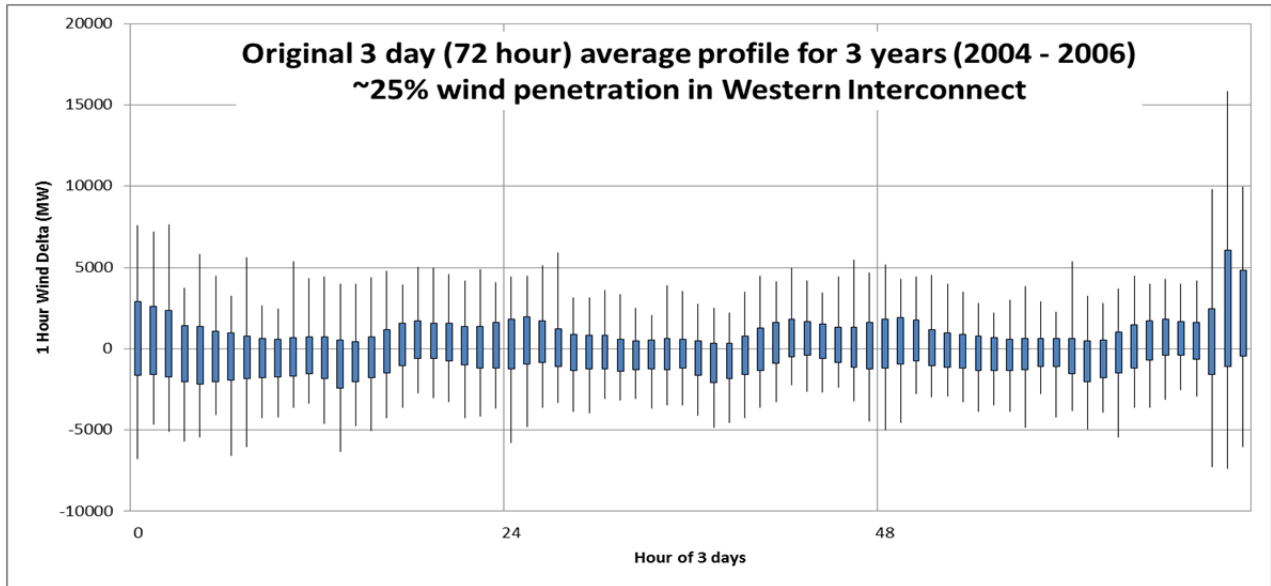
(a)
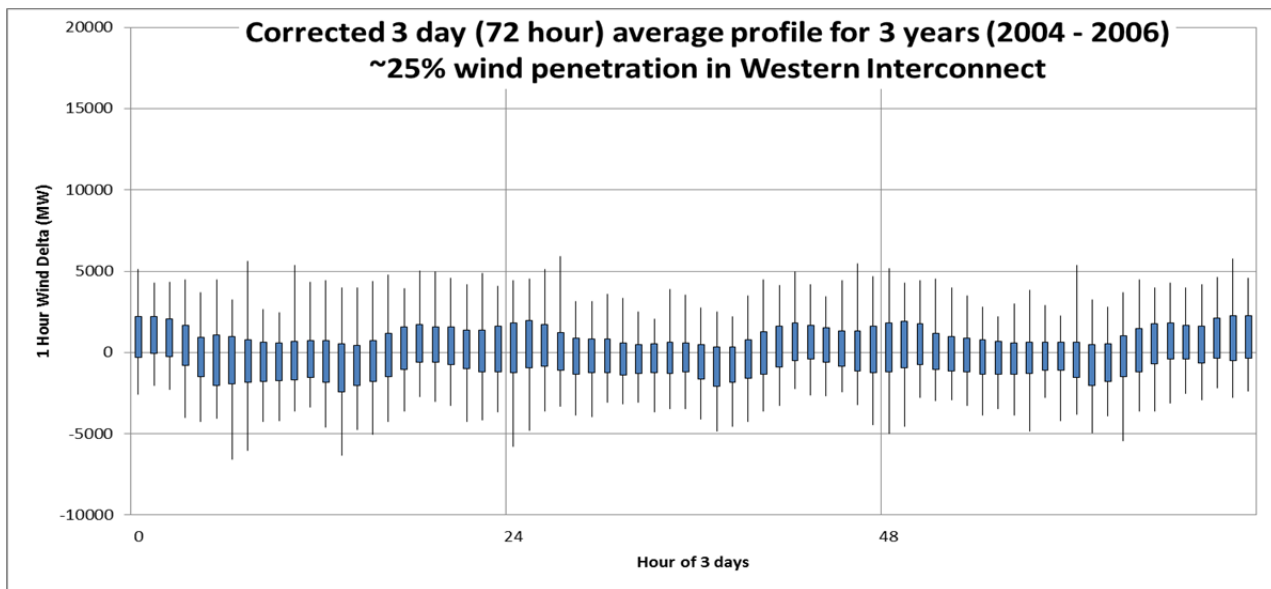
(b)

Figure 7. One-hour change in wind output for the (a) original and (b) corrected data

Notes: The years from 2004 to 2006 were parsed into 3-day intervals to illuminate the 3-day seam that is shown by increased variability at the end of the third day in the original data. The whiskers are the minimum and maximum values for each hour of the 3-day intervals. The bars show the mean value plus and minus one standard deviation.

Figure 8 compares the simulated interpolated data to actual data for a short segment of time between August 2011 and December 2011. Also plotted is actual noise, which is the actual data minus the cubic spline fit and the simulated noise. Although the noise of the simulated data was more uniform and less in magnitude than that of the actual data, in general the simulated data did resemble the actual data.

18
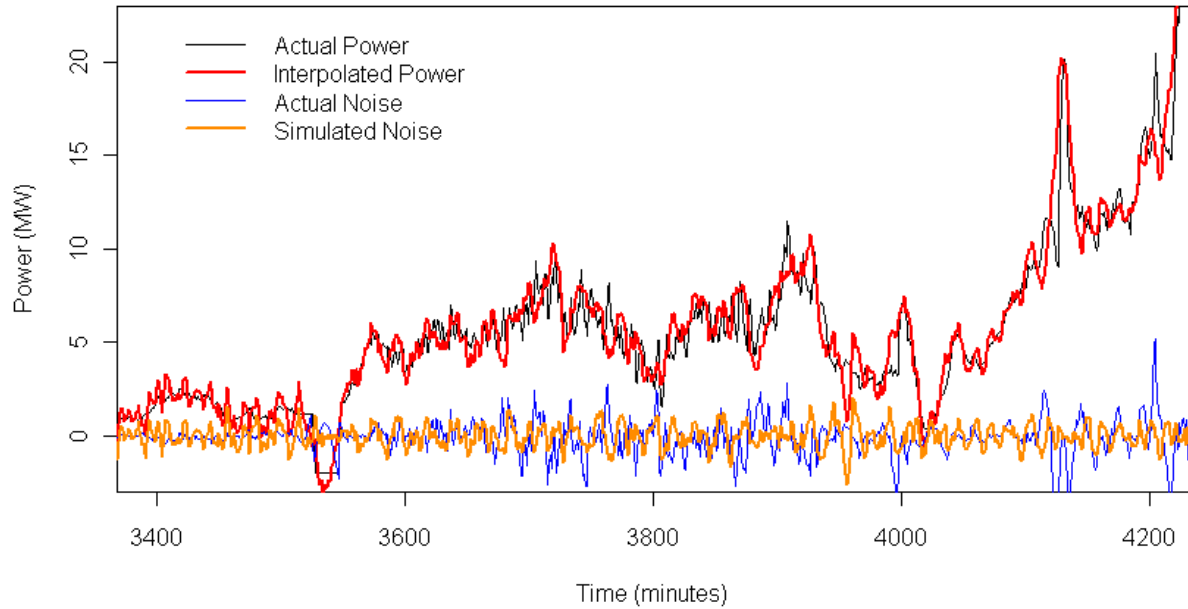
(a)
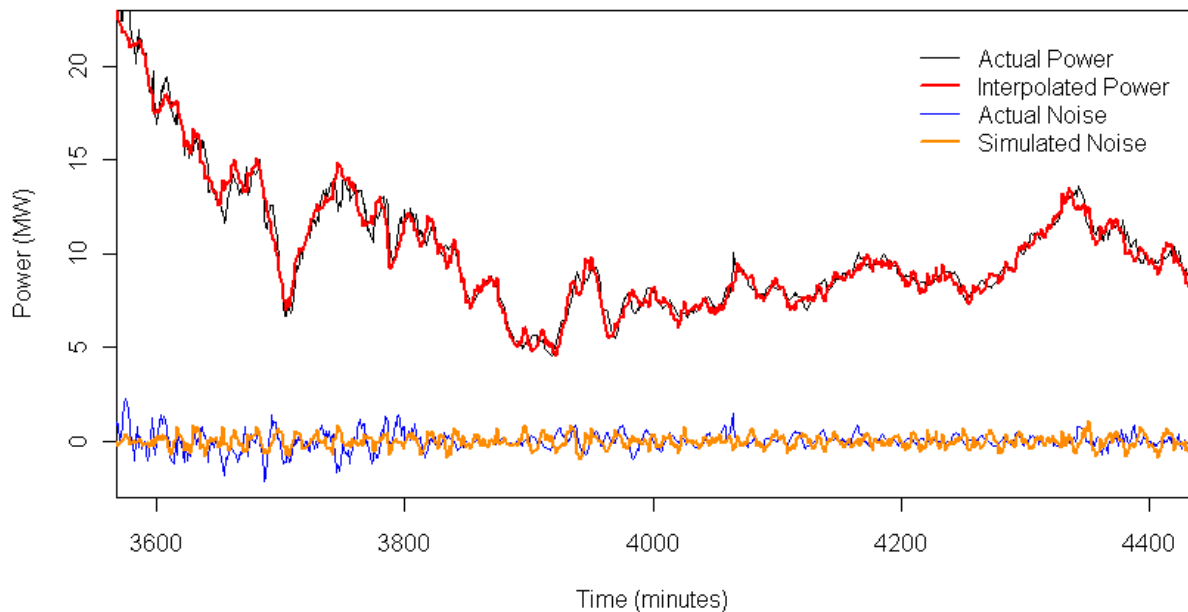
(b)

Figure 8. Comparison of interpolated 1-minute wind power data to actual data for
(a) August 2011 (time between 3,400 and 4,200 minutes) and
(b) December 2011 (time between 3,600 and 4,400 minutes)

2.4.3 Wind Power Forecasts

Wind forecasts were developed for DA, 4HA, and 1-hour-ahead time horizons. The following sections describe the methods used to develop the forecasts as well as how the current forecasts differ from those used in WWSIS-1.

2.4.3.1 Day-Ahead Forecasts

In addition to wind power actuals, wind power forecasts for hypothetical wind plants had to be synthesized. The original wind forecasts in WWSIS-1 were synthesized using the same NWP model as the actuals but with a different input data set. Because these forecasts did not receive a statistical correction, some bias issues arose, resulting in forecasts that tended to be 10% to 15% higher than actuals on average. Additionally, forecasting techniques have improved since those original data sets were created.

To best reflect realism in forecasts, we analyzed measured DA wind forecast errors from the Public Service Company of Colorado, CAISO, and the Electric Reliability Council of Texas (ERCOT). We then adjusted the forecast error distributions of our forecasts from WWSIS-1 to match the measured wind forecast error distributions. This process is detailed in Hodge et al. (2012) and described in the following paragraphs. Hodge et al. (2011a, 2011b) show more examples of statistical distributions of wind forecasts.

We analyzed the first four statistical moments of the measured wind forecast error distributions: the mean, variance, skewness (which measures symmetry of the distribution), and kurtosis (which measures the relationship between the peak and the tails of the distribution). Inadequate data prevented us from adjusting the mean and skewness, and the variance and kurtosis were the main statistical features from an error frequency viewpoint, so the revisions focused on these measures. Although some of the bias was adjusted out through this process, some bias remained in the year-to-year error distribution as a remnant of the original forecasts.

It is important to retain realistic temporal and spatial correlations in wind forecasts for these data sets (Lew et al. 2011) for accuracy in operational modeling. If, for example, one plant misses its forecast significantly, it is likely that a nearby plant will also miss its forecast significantly. Similarly, if a plant misses its forecast significantly in one hour, it is likely to do so again in the subsequent hour. Spatial correlations were inherent in the original forecast data set because of the NWP generation process. In this adjustment process, we focused on getting the BA-level forecast error distributions correct, because the forecasts were used in WWSIS-2 to commit units in each of 20 zones where each zone was roughly equivalent to a BA. This means that on an individual plant or interconnection level, the forecast error distributions might not have been as realistic.

Figure 9 gives a visual representation of the modification process. The first step was to hyperbolically fit the BA-level data. Using the operational data, the second step was to interpolate what the moments should be (empirically) as a function of a given BA's capacity. Analysis of the data revealed that the variance and kurtosis values of both the operational and original forecast data were strongly correlated with the wind capacity considered, an indirect measure of the geographic diversity.

The third step involved in determining the values of the hyperbolic parameters was ensuring that the moments were matched in an optimal fashion. The optimization process involved a particle swarm routine that evaluated the moment-matching subroutine until convergence on the optimal hyperbolic parameters. As a result of this process, the character of the original forecast errors was maintained, minus the statistical anomalies, and the empirical information about moments was imparted on the updated forecasts.

The fourth step involved determining the error at each hour of the year according to its quantile. This was achieved by stepping through the original forecasts, determining its quantile at that hour, and mapping that to the quantile of the theoretical distribution to allow the determination of the updated error at each hour.

The fifth and final step was to take the 8,760 hourly errors and partition them to the site level to produce the updated forecasts. This was accomplished by uniformly distributing the error to each site, respecting physical boundary conditions. The sign of the error was always maintained from the original to the updated forecasts.
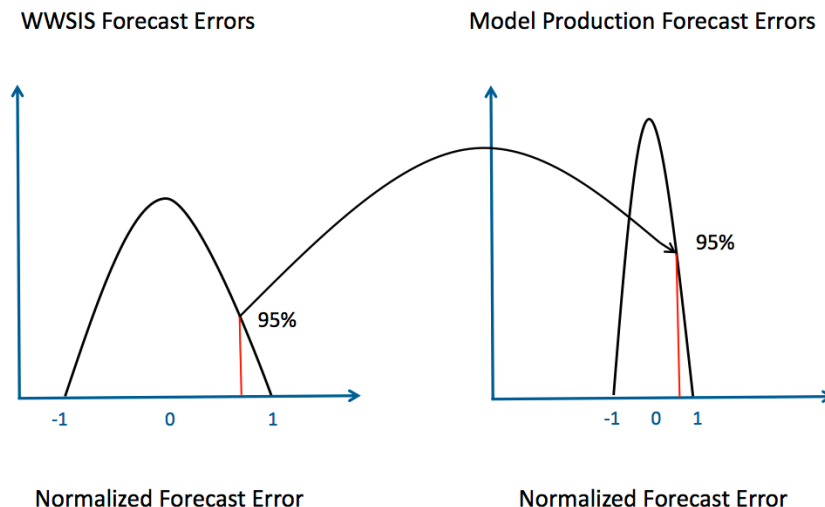
Figure 9. Depiction of the matching process between BA level errors in the WWSIS data set and the adjusted forecast errors

2.4.3.2 Four-Hour-Ahead Forecasts

The persistence model, which is often used in short-term forecasting, follows the simple assumption that the power output in a future time frame will be the same as it is in the current time frame. Although the forecasts produced by operational forecasting systems generally outperform the persistence forecast at the 4HA time frame, these data were not available from the original WWSIS-1 forecasting model runs, and additional NWP runs were not possible. For these reasons, we tried to find the persistence time frame that best matched the forecast error distribution shape from operational 4HA forecasts. The reference data came from an approximately 300-MW wind plant in the Xcel Energy service territory. A collection of ten 30-MW WWSIS-1 wind plants in a similar geographic location were aggregated to provide a comparable persistence forecast error data set. We examined 1-hour, 2-hour, 3-hour, and 4-hour persistence error distributions and found that the 2-hour-ahead persistence distribution matched the operational 4HA forecast the best, especially at the tails of the distribution, which are the critical operational impact events (see Figure 10). As a result, we used a 2-hour-ahead persistence to synthesize our 4HA forecasts.
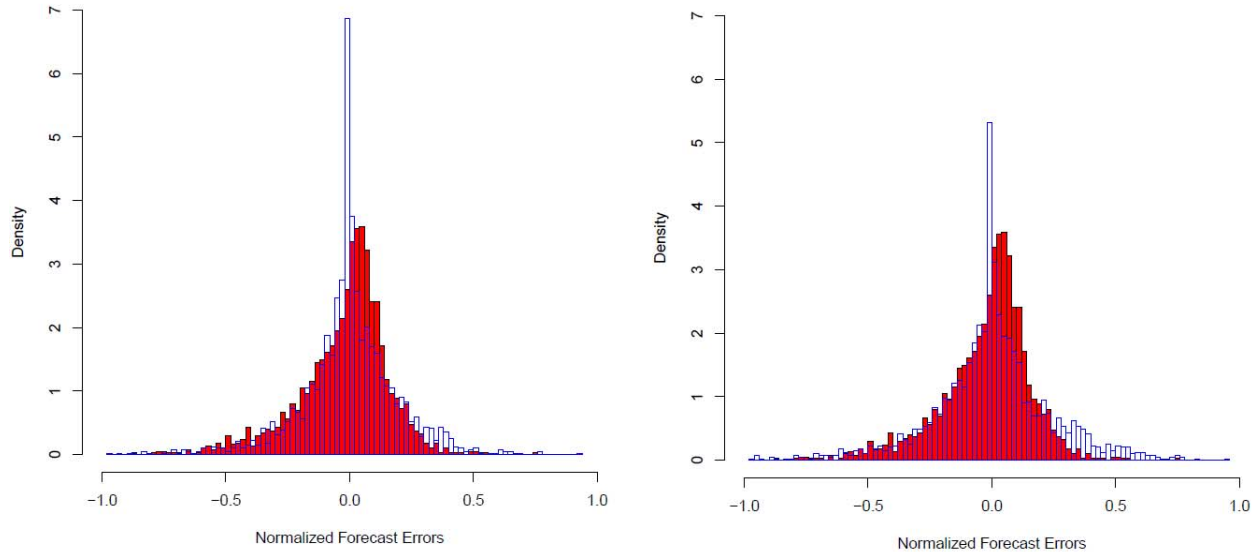
Figure 10. Comparison between the observed 4HA forecasts from an (red) operational system and the (blue) persistence forecasts with a (left) 2-hour time lag and a (right) 3-hour time lag

2.4.3.3 One-Hour-Ahead Forecasts

One-hour-ahead forecasts were developed in WWSIS-1 using 1-hour-ahead persistence forecasts. The forecasts take an average output value of the previous 60 minutes and apply it as the forecast for the next 60 minutes. These forecasts were unchanged in WWSIS-2.

2.5 Solar Data

This section discusses the type of solar data used in the study as well as the methods used to develop the data. Data were developed for both solar plant output and solar forecasts.

2.5.1 Solar Power Output Data

The original solar data used in WWSIS-1 was based on limited knowledge of spatial-temporal correlations of PV output. For instance, as PV plant capacity increases, the relative variability should decrease because of spatial averaging of localized irradiance fluctuations. The characteristics of this effect were not well understood at that time and so only DG rooftop PV was modeled. Utility-scale PV was excluded. In WWSIS-2, new techniques were developed to characterize subhourly temporal variability based on spatial variability (Hummon et al. 2012). This allowed WWSIS-2 to include DG rooftop PV, utility-scale PV, and CSP with thermal storage.

Hummon and colleagues (2012) developed an algorithm to generate synthetic global horizontal irradiance (GHI) values on a 1-minute interval using satellite-derived, 10 km × 10 km gridded, hourly irradiance data. The satellite-derived irradiance data, from Clean Power Research's SolarAnywhere database, was based on a semi-empirical model developed by Perez (2002) and Perez and colleagues (2002). During each hour, the observed GHI value of the grid cell of interest and the surrounding grid cells was related, via probability distributions, to one of five temporal cloud-coverage classifications, shown in Figure 11.
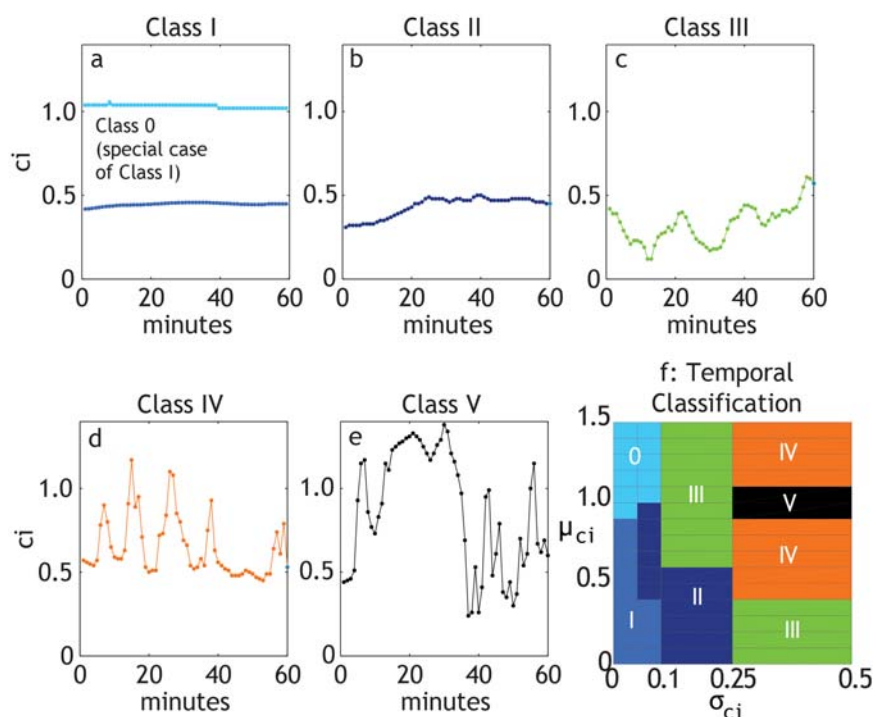
Figure 11. Examples of the five classes of temporal variability are shown in plots (a) through (e)

Notes: Classes I–III (a–c) are based on the width of the distribution of ramps. Classes IV–V (d and e) are characterized by a rapid change between two or more different cloud-cover densities (e.g., clear sky with small, dense clouds moving at a high altitude). Panel (f) shows how the temporal classes are defined in terms of the mean (σ_{ci}) and standard deviation of the clearness index (σ_{ci}) for 60 consecutive minutes.

Subhourly irradiance data was collected through NREL's Measurement and Instrumentation Data Center (www.nrel.gov/midc) for seven sites. Synthesis algorithms were used to select 1-minute interval GHI values based on the classification of the grid cell of interest in a particular hour.

Sandia National Laboratories (Hansen 2012) conducted an independent validation of the subhourly algorithm described here and found that the modeled data could reasonably be used for WWSIS-2. Most of the validation sites showed that the modeled data agreed reasonably with the measured data. The modeled data showed significant disagreement with two sites that may have microclimate conditions.
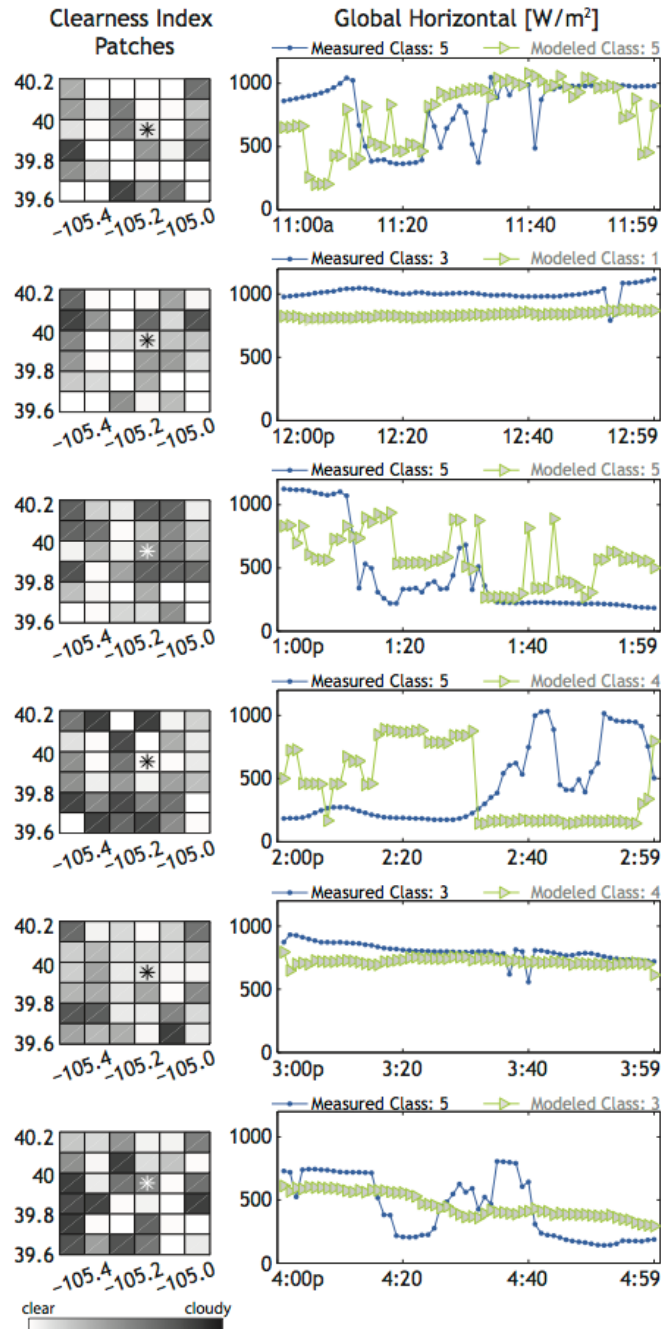
Figure 12. Snapshot satellite clearness index (left) and temporal GHI (right) from NREL on August 22, 2005

Notes: Satellite clearness index patches represent the snapshot at the end of the hour. Measured (black circle) and modeled (green triangle) time series GHI, located at 39.911 N, –105.235 W, with a time step of 1 minute, are shown on the right. The temporal variability class of the measured data (black) and modeled data (gray) are located above each time series plot.

24

2.5.2 Solar Forecast Data Synthesis

In addition to synthesizing hypothetical solar power plant outputs, we needed to synthesize solar uncertainty, or forecast error, for each plant.

DA solar forecasts made use of the WWSIS-1 solar forecasts conducted by 3TIER based on NWP simulations (3TIER 2010). No regional operational solar forecast error data were available to use to adjust these forecasts for current forecast methodologies, so these forecasts were unchanged from WWSIS-1.

Four-hour-ahead solar forecasts were modeled using 2-hour persistence of cloudiness because it was found that with wind forecast errors, 2-hour persistence matched 4-hour forecast errors reasonably well. One-hour-ahead forecasts were modeled using 1-hour persistence of cloudiness (based on average power the previous hour). A persistence forecast would have ignored the fact that the sun traces a known path through the sky. Because we wanted to incorporate this known diurnal solar variability into our synthesized forecasts, we used persistence of cloudiness.

3 Scenarios and Operational Assumptions

WWSIS-2 modeled up to 33% wind and solar energy penetration in the U.S. portion of the Western Interconnection. Five scenarios were created to study the impacts of wind and solar penetration on cycling and compare the effects of wind and solar:

- No Renewables (0% wind, 0% solar)
- TEPPC Scenario (9.4% wind, 3.6% solar)
- High Wind Scenario (25% wind, 8% solar)
- High Solar Scenario (8% wind, 25% solar)
- High Mix Scenario (16.5% wind, 16.5% solar).

Because the Western Interconnection already has a small percentage of wind and solar, the No Renewables Scenario is somewhat artificial. However, the No Renewables Scenario typically was used as a reference, though, to capture the effect of all wind and solar in the system and not only the incremental changes between the TEPPC and the high-penetration scenarios. The No Renewables Scenario is the equivalent of the TEPPC Scenario with all wind and solar removed. All the high-penetration scenarios also include all of conventional generation from the TEPPC data set. In other words, no additional retirements resulted from adding wind and solar. That is a topic for future study.

This section describes the methods used to site the variable generation in the scenarios, model the scenarios, and build out the transmission to accommodate the new wind and solar.

3.1 Siting

NREL's Regional Energy Deployment System (ReEDS) model (Short et al. 2011) was used to site the wind and solar plants for each scenario. The TEPPC Scenario (9.4% wind, 3.6% solar) was based on the WECC TEPPC 2020 PC1 base-case scenario. The TEPPC Scenario was designed by WECC to include the amount of wind and solar that western states would need to meet their 2020 RPS targets. The high-penetration scenarios (High Wind, High Solar, and High Mix) were designed so that wind and solar provided a nominal 33% of electricity in the U.S. portion of the Western Interconnection in 2004, 2005, and 2006. Note that the 33% penetration is by energy, not capacity. The penetration levels would be higher if measured by capacity because CFs of wind and solar are less than those of conventional plants. The 33% penetration level was chosen to be consistent with CAISO's 2020 RPS requirements, which are the strictest in the Western Interconnection. The No Renewables Scenario did not have any wind or solar, so no siting work was required.

Table 4 shows the penetration levels for each scenario. Wind and solar are nominally built to 33% energy penetration considering the historical weather patterns of 2004, 2005, and 2006. The analysis in this report is for the year 2006, which had typical solar but better wind than the average of the years 2004–2006. After curtailment,[2] the 2006 penetration levels are 30%–33% of U.S. load in the Western Interconnection and 24%–26% of total load in the Western Interconnection.

---

[2] In this case, curtailment includes CSP storage curtailment. Some of this curtailment is built into the design of the generator.

Within the Western Interconnection, the interties from the United States to Canada and Mexico are relatively small, compared with the U.S. system. Therefore, wind/solar variability primarily impacts the U.S. generators, where the nominal penetration levels are 33%. More than 85% of total cycling costs and more than 90% of the incremental cycling costs because of renewable penetration are incurred by U.S. generators in all scenarios. However, because the addition of wind/solar can change how these interties are operated and result in displacement of generation across the border, total cost and emissions results should be assessed across the entire Western Interconnection, in which nominal penetration levels are 26%.

Table 4. Renewable Energy Penetration Levels

	2006 Penetration Level Across U.S. WECC After All Curtailment*	2006 Penetration Level Across All WECC After All Curtailment*
TEPPC	13.2	10.5
High Wind	32.6	26.0
High Mix	32.2	25.6
High Solar	30.2	24.1

* "All Curtailment" includes CSP storage curtailment, some of which is built into the design of the CSP generators.

For all the scenarios, solar was defined as 60% PV and 40% CSP. This CSP included 6 hours of thermal storage. The solar plants modeled for WWSIS-2 were as follows:

- Rooftop PV—aggregated, DG PV on residential and commercial rooftops. This represents 40% of installed PV in all scenarios.

- Population-weighted PV—utility-scale PV plants in urban and suburban areas (e.g., airport installations and other MW-scale installations). This represents 20% of the installed PV.

- Best-resource-located PV—utility-scale PV plants in desert and remote locations where the resource is exceptional. This represents 40% of the installed PV.

- CSP—utility-scale power plants with 6 hours of thermal storage. The storage was dispatched using the PLEXOS model.

Additional information about each scenario is given in Table 5 and shown in Figure 13.

**Table 5. Installed Solar and Wind Capacity
and Average Capacity Factor for Each State for Each Scenario**

TEPPC

State	Rooftop PV		Utility Scale PV		CSP		Wind		Total	
	Capacity (MW)	CF	Capacity (MW)	CF	Capacity (MW)	CF	Capacity (MW)	CF	Capacity (MW)	CF
Arizona			1,171	22%	472	43%	3,681	30%	5,324	30%
California			3,545	25%	3,221	44%	7,299	30%	14,065	32%
Colorado			1,342	20%	169	37%	3,256	29%	4,767	27%
Idaho							523	27%	523	27%
Montana							838	34%	838	34%
Nevada			304	22%	334	42%	150	25%	788	31%
New Mexico			140	27%	156	39%	494	28%	790	30%
Oregon							4,903	26%	4,903	26%
South Dakota										
Texas										
Utah			571	20%			323	31%	894	24%
Washington							4,652	27%	4,652	27%
Wyoming							1,784	42%	1,784	42%
Total			7,074	23%	4,352	43%	27,900	29%	39,326	30%

High Solar

State	Rooftop PV		Utility Scale PV		CSP		Wind		Total	
	Capacity (MW)	CF	Capacity (MW)	CF	Capacity (MW)	CF	Capacity (MW)	CF	Capacity (MW)	CF
Arizona	4,498	19%	9,570	23%	9,644	42%	270	33%	23,982	30%
California	9,006	18%	14,258	23%	9,197	43%	5,203	33%	37,663	28%
Colorado	1,127	18%	4,437	22%	1,440	35%	3,617	31%	10,620	27%
Idaho	3	15%	2	16%			583	28%	588	28%
Montana	25	15%	34	17%			988	35%	1,047	34%
Nevada	772	19%	6,503	24%	672	40%	150	25%	8,098	25%
New Mexico	943	20%	2,874	24%	574	38%	644	32%	5,034	26%
Oregon	101	14%	126	21%			4,665	26%	4,892	26%
South Dakota	4	17%	6	19%			330	37%	340	37%
Texas	233	20%	335	23%					568	22%
Utah	2,132	17%	3,759	21%			323	31%	6,214	20%
Washington	405	13%	759	19%			4,952	27%	6,116	25%
Wyoming	10	18%	18	21%			1,634	43%	1,662	42%
Total	19,261	18%	42,680	23%	21,526	42%	23,357	31%	106,824	27%

28

High Wind

State	Rooftop PV Capacity (MW)	CF	Utility Scale PV Capacity (MW)	CF	CSP Capacity (MW)	CF	Wind Capacity (MW)	CF	Total Capacity (MW)	CF
Arizona	1,975	19%	2,330	25%	3,303	43%	4,941	30%	12,548	31%
California	4,875	18%	5,372	25%	2,469	45%	11,109	30%	23,824	28%
Colorado	1,059	18%	1,128	22%	169	37%	6,226	35%	8,581	31%
Idaho	3	15%	2	16%			1,333	29%	1,338	29%
Montana	22	15%	34	17%			6,658	36%	6,714	36%
Nevada	398	19%	344	22%	439	42%	3,270	31%	4,452	30%
New Mexico	172	20%	209	27%	156	39%	4,784	38%	5,321	37%
Oregon	91	14%	101	22%			5,473	26%	5,665	26%
South Dakota	4	17%	6	19%			2,640	36%	2,650	36%
Texas	76	20%	122	27%					198	24%
Utah	361	17%	489	21%			1,343	32%	2,193	27%
Washington	371	13%	492	20%			5,882	27%	6,745	26%
Wyoming	9	18%	18	21%			10,184	43%	10,211	43%
Total	9,417	18%	10,647	24%	6,536	43%	63,840	34%	90,439	32%

High Mix

State	Rooftop PV Capacity (MW)	CF	Utility Scale PV Capacity (MW)	CF	CSP Capacity (MW)	CF	Wind Capacity (MW)	CF	Total Capacity (MW)	CF
Arizona	3,655	19%	5,394	25%	9,374	42%	1,440	32%	19,863	33%
California	8,412	18%	9,592	23%	3,594	44%	6,157	31%	27,754	26%
Colorado	1,127	18%	1,653	22%	169	37%	4,396	33%	7,344	29%
Idaho	3	15%	2	16%			1,093	29%	1,098	29%
Montana	25	15%	34	17%			4,288	36%	4,347	36%
Nevada	772	19%	3,282	26%	562	40%	1,560	32%	6,177	28%
New Mexico	943	20%	1,280	27%	298	40%	3,134	38%	5,654	33%
Oregon	101	14%	126	21%			5,413	26%	5,640	26%
South Dakota	4	17%	6	19%			1,950	36%	1,960	36%
Texas	208	20%	193	25%					401	22%
Utah	1,204	17%	1,216	22%			683	33%	3,102	22%
Washington	405	13%	709	19%			5,762	27%	6,876	26%
Wyoming	10	18%	18	21%			7,244	44%	7,272	44%
Total	16,870	18%	23,504	24%	13,997	42%	43,118	34%	97,489	30%

(a)

(b)

(c)

(d)

**Figure 13. Siting of PV, CSP, and wind plants for the
(a) TEPPC, (b) High Solar, (c) High Mix, and (d) High Wind Scenarios**

Notes: Wind, PV, and CSP plants are shown in green, yellow, and red,
respectively; larger plants are depicted with larger circles.

3.2 Production Simulation Methodology and Operational Assumptions

Modeling a power system as large and complex as the Western Interconnection requires
balancing detail (to ensure that important inputs are properly characterized) with simplifying
assumptions (to create a manageable model that can be run within a reasonable amount of time).
We based our inputs and assumptions as much as possible on the WECC TEPPC model, which
has been thoroughly vetted through a public stakeholder process.

With the exception of the large ISO in California and Alberta, the Western Interconnection
consists of nearly 40 vertically integrated utilities that balance their systems with their own
generation and confidential bilateral transactions with neighboring utilities—creating a system that
is difficult to model because much of the information about the system's operation is confidential.
WECC TEPPC, the subregional transmission planning groups, and others who model the Western
Interconnection face this same constraint. Consequently, simplifying assumptions were used to
model the Western Interconnection. In a manner similar to that used for the WECC TEPPC 2020

PC1 model, we modeled the Western Interconnection assuming least-cost economic dispatch, without consideration of the confidential bilateral contracts. The Western Interconnection was modeled zonally, using the 20 WECC Loads and Resources Subcommittee (LRS) zones. By working at the zonal level, we obviated the need to design transmission collector systems for each wind and solar plant and instead assigned each plant to a high-voltage bus.

We modeled the future year 2020 using historical weather patterns and loads from 2006. To account for the variance in start day between the two years (i.e., 2006 started on a Sunday, and 2020 will start on a Wednesday), we time shifted the load and weather data. WWSIS-2 used the WECC TEPPC 2020 PC1 case as the basis for the Western Interconnection model. All data are given in Pacific Standard Time.

The WECC TEPPC 2020 PC1 case was procured from Energy Exemplar, the creators of the PLEXOS tool. The TEPPC Scenario was based on the WECC TEPPC 2020 PC1 case (WECC 2011). All wind and solar plants were removed from this scenario to create the No Renewables Scenario. The high-penetration scenarios used the wind and solar siting discussed in Section 3.1.

The WECC LRS provided NREL with estimated transmission capacity between the zones for 2010, and adjustments were made based on projects that have been added to the TEPPC 2020 case. Transmission capacity was added between zones for each scenario based on a methodology described in Section 3.3. An initial error in the transmission database had occurred when the WECC TEPPC database was converted into the PLEXOS format. This was later corrected to include only foundational and other transmission projects that were expected to be in service by 2020. This correction did not take place until after the transmission build-outs of Section 3.3 were completed. After the correction, the transmission build-out work was reexamined and found to be satisfactory.

We modeled regulation, flexibility, and contingency reserves. Regulation and flexibility reserves were modeled on the variability and short-term uncertainty of wind and solar output with the reserves for solar designed so that the known solar variability (e.g., sunrise and sunset) was removed from the reserve calculations. Section 5 discusses the reserve requirement calculation and methodology in detail.

It is unclear what reserve sharing will be in place in the near future. The study team developed reserve sharing assumptions through discussions with the subregional reserve sharing groups. These assumptions were then vetted through the TRC. Regulation reserves were held assuming sharing across the entire U.S. portion of the Western Interconnection. The choice was an attempt to model the reliability-based control (RBC) metric that is currently in field trials across the United States. RBC requires little regulating reserve control action when the interconnection frequency is near its target. Because frequency is the same across the interconnection, RBC essentially looks like a single regulating-reserve sharing group. Flexibility and contingency reserves were held by zone. Although contingency reserve sharing groups exist in the Western Interconnection, their rules differ. As a result, we used a conservative approach and required each zone to meet its own flexibility and contingency reserve requirements.

Although hurdle rates can be assigned between zones to reflect "friction" of interchanges and the differing levels of BA cooperation between zones (Jordan and Piwko 2013), no hurdle rates were

assigned in our scenarios. Essentially, this choice modeled the Western Interconnection as a single BA with flexibility and contingency reserves held on a zonal level. Future work could include the use of hurdle rates to model multiple BAs.

The unit commitment and economic dispatch modeling consisted of three separate market runs: DA, 4HA, and real-time markets. The three markets were used so that the unit commitment simulation could incorporate improving forecasts over the three time horizons. The DA run used DA forecasts for wind and solar generation. The optimization horizon for the unit commitment in the DA market was 48 hours. The unit commitment from the first 24 hours of each step was saved and input to the 4HA market for coal, nuclear, and biomass generators. These generators typically have long start times and need to be committed more than 4 hours ahead of time. The extra 24 hours in the unit commitment horizon (for a full 48-hour window) were necessary to properly commit the generators with high start costs and the dispatch of CSP with thermal storage. For hydro, the nominal hourly production was allowed to vary in the DA market; however, the flows calculated in the DA market were then used to fix energy production in the 4HA and real-time markets.

The 4HA market was used to commit the CC, oil, and gas steam units. The commitments for the coal, nuclear, and biomass generators were input from the DA unit commitment for these generators. The 4HA market was modeled in 24-hour windows. Results from only the first 4 hours from each run were saved for the real-time model, and the extra 20 hours in the unit commitment window helped optimally dispatch the CSP thermal storage. It was sometimes optimal for CSP units to store their energy and deliver it when prices were highest, which occasionally occurred during the load rise the following morning before PV generation began. This demonstrates the value of a 24-hour optimization window.

The unit commitment for all thermal units except CT and internal combustion units was passed from the 4HA market to the real-time market. It was assumed that all CT and internal combustion units could be started in the real-time market; they would not require any additional lead time for starts. The real-time market was a dispatch with 5-minute time steps and without any foresight of future 5-minute intervals.

Regulating and contingency reserves were held in the DA, 4HA, and real-time markets. Flexibility reserves were held in the DA and 4HA markets and released in the real-time market. Penalties for violating load and regulating, contingency, and flexibility reserve requirements are shown in Table 6. These penalties were chosen to be high enough that starting a new unit to provide reserves would typically lower system costs compared to allowing the reserves to go unserved.

Table 6. Penalties for Unserved Load and Reserves

Load and Reserves	Penalty for Violating Constraint ($/MWh)
Load	6,000
Regulating Reserves	4,100
Contingency Reserves	4,000
Flexibility Reserves	3,900

32

The hydro flexibility assumptions were similar to those used in the WECC Energy Imbalance Market study (Milligan et al. 2012) and based on discussions with Bonneville Power Administration and Western Area Power Administration. Approximately one-third of all hydro energy follows its profile from 2006 because of the extensive constraints (environmental, institutional, and—in some cases—physical) on operation. Two-thirds of all hydro energy was allowed some flexibility. These generators have monthly energy limits, along with maximum capacity and minimum generation levels that change monthly. The PLEXOS model optimized the usage of the hydro between these limits.

Start costs were based on the analysis described in Section 2.1. Because of a lack of wear-and-tear start cost data on nuclear, biomass, and internal combustion units, we applied the costs of small, subcritical coal units (the most expensive units to cycle) to nuclear units, the costs of large, subcritical coal units to biomass units, and the costs of aero-derivative CTs (the least expensive units to cycle) to internal combustion units. Start fuel requirements were also included in the database based on the analysis in Section 2.1. It was assumed that all coal units start with natural gas (or a fuel with equivalent cost); all other units started with their primary fuel. Although it is understood that start fuels do vary markedly in cost, the start fuel costs were small so this simplification was found to be adequate for modeling purposes.

We first ran the production simulation analysis with the median lower bounds for start costs so that commitment and dispatch was optimized with these wear-and-tear costs taken into account. Ramping costs were difficult to incorporate into the model and small, which made them unlikely to affect commitment and dispatch. Consequently, ramping costs were added to the model dispatch results after the optimization was performed. Next we ran the production simulation analysis with the median upper-bound start cost and fuel usage data, but found that properly committing large coal units and other units with large start costs using upper-bound start costs required a unit commitment horizon of significantly more than the 48-hour window used in this study. For the upper bound of each range, the upper-bound start costs were calculated after the optimization was done using lower-bound start costs. Although upper-bound start costs could lead to a slight change in unit commitment, we did not consider this in this study, so these results are a ceiling on the impact of upper-bound start costs. Future work could include an iteration on WWSIS-2 results, applying upper-bound costs to units that cycle frequently and lower-bound costs to units that cycle rarely.

Several important industry changes have occurred since the original TEPPC 2020 data set was created. The two most significant of these changes are the number of expected retirements and repowering of existing units, and fuel price assumptions.

Because of recent changes in air and water pollution legislation in the United States, system planners have projected that more units will retire in the near future (before 2020) than originally expected. Some of these units have retired and/or been replaced already. As part of updating their data set, TEPPC members solicited advice from WECC members on which units were planned to retire or be replaced or repowered. This new information (now part of WECC's updated TEPPC 2022 data set) was believed to more accurately represent the conditions that will exist in 2020 than the information in the WECC TEPPC 2020 data set, so the updated retirement schedule was integrated into the WWSIS-2 scenarios.

Similarly, recent gas price projections differ significantly from the higher projections in the WECC TEPPC 2020 data set. Consequently, gas price assumptions from the WECC TEPPC 2022 data set were incorporated into the study's TEPPC 2020 scenario. The average gas price for the Western Interconnection used in this study was $4.60/MMBtu.

Because the U.S. system in the Western Interconnection has connections with Canada and Mexico that are relatively small compared to the size of the full system, the analysis in this project focused on the U.S. portion of the Western Interconnection. New transmission to Canada and Mexico was not considered in the transmission build-out. Most results presented are focused on the generators and loads within the U.S. portion of the Western Interconnection; however, all of the Western Interconnection, including Canada and Mexico, was modeled to maintain consistency in assumptions about imports and exports with the United States. To avoid unserved load in Canada and Mexico, natural gas CC generation was added to these regions until they had sufficient capacity to provide electricity locally. This was necessary because of extensive load growth and lack of information on Canada and Mexico generation capacity growth for the TEPPC 2020 cases.

An additional change was that unit heat-rate curves from the WECC TEPPC 2020 PC1 data set were replaced with observations from the EPA CEM data analysis (see Section 2.2). To speed up model runtime, the new heat-rate curves were limited to two-part piece-wise linear heat-rate curves. This produced similar results compared to using more divisions in the piece-wise linear curve. Fuel usage from starts, based on findings and assumptions from Kumar and colleagues (2012), was also included within the optimization. CO_2 emissions were calculated using the modeled fuel usage. NO_x and SO_2 emissions were calculated after the optimization based on six-part piece-wise linear NO_x and SO_2 curves for each unit. If no matching units were found in the CEM data set—or if a good fit could not be performed—the average heat-rate and emission curves were used for each unit type.

Table 7 shows the key assumptions for the thermal (fossil-fueled and nuclear) units in the PLEXOS optimization. Heat rates and start costs were created specifically for this study. Ramp rates and minimum generation levels were based on standard TEPPC assumptions (except for nuclear minimum generation levels). Note that nonfuel start costs are much higher for the WWSIS-2 study compared to TEPPC assumptions, except for the gas CT units. These units are typically smaller than the coal or gas CC units, and the TEPPC assumptions were based on per-unit start costs. This led to artificially high start costs per MW for the typical gas CT units.

Table 7. Average Characteristics Used for Thermal Units in PLEXOS Optimization

Type of Unit	Minimum Generation (as a % of maximum capacity)	Ramp Rate (%/min)	Heat Rate (at full load)	WWSIS-2 Nonfuel Start Cost ($/MW)	TEPPC Nonfuel Start Cost ($/MW)
Coal	40[a]	1.1[a]	10.5	124	11[a]
CC	52[a]	0.9[a]	7.6	81	47[a]
CT	38[a]	4.5[a]	10.7	67	93[a]
Steam	12[a]	1.7[a]	10.7	86	12[a]
Nuclear	95	0.3[a]	11.0	155	-[a]

[a] Denotes an original assumption from the TEPPC database (aggregated for all units of each type). Other information in this table was created for this study as described in Section 2. The TEPPC start costs were not used for this study.

34

3.3 Transmission

The transmission expansion methodology and results are summarized in this section. Appendix C contains additional graphs and tables of the details. We ran iterative PLEXOS runs for the system for a year to bring shadow prices across interfaces down to a consistent cutoff level. The timing of the transmission builds was not modeled. WWSIS-2 used an optimal DC power flow respecting transmission constraints instead of a simplified pipeline model. We used static power transfer distribution factors based on the WECC TEPPC 2020 PC1 case. To simplify the transmission expansion, these power transfer distribution factors were assumed to be unchanged with the addition of new transmission.

Forty-four transmission paths were considered at a zonal level. Nodal transmission build-outs might need to be considered in future analyses to examine details of congestion and flows, but that will require design of collector systems for the new wind and solar resources. Because WWSIS-2 was not meant to be a transmission planning study, transmission expansion was limited to increasing capabilities on existing paths instead of adding new source and sink pathways.

It is important to note that in much of the Western Interconnection, utilities have physical, rather than financial, rights to transmission (i.e., a transmission path may be fully contracted during some period of time yet not fully utilized during that period). Because those transmission contracts are confidential, we were unable to model them; instead, we assumed that all transmission was used optimally.

Although parts of Canada and Mexico are in the Western Interconnection, we did not build additional transmission to those zones; instead, we built in enough conventional generation in those zones to meet load so that paths to those zones were not congested. This is consistent with WECC TEPPC practice, which is based on the fact that actual flows between Canada's Alberta Electric System Operator and the United States, for example, are very limited.

We developed a methodology to expand capabilities on existing transmission paths by running the scenarios in PLEXOS for a full year and examining shadow prices across interfaces. We built 500 MW of additional transmission across interfaces where shadow price exceeded a fixed cutoff value. We then iterated and re-ran the revised scenario with the additional transmission in PLEXOS and added more transmission as appropriate until shadow prices no longer exceeded the cutoff.

We tested cutoff values from $5/MWh to $20/MWh. These were consistent with the approximate transmission costs of $1,600/MW-mile for 250 miles of new transmission with an 11% fixed-charge rate. Figure 14 shows successive transmission build-outs for decreasing cutoff values for the High Wind Scenario, compared to the initial capacity (in gray). As described subsequently, $10/MWh was selected as the best cutoff value.

Transmission build-outs were evaluated considering transmission costs, production cost, and curtailment. For a fixed cutoff value, as the wind and solar penetration—especially wind—increased, the transmission built also increased. Curtailment decreased with expanded transmission.

Table 8 gives the transmission build-out metrics for the different cutoff values shown in Figure 14.

Table 8. Transmission Build-Out for the High Wind Scenario

Metric	Initial	$20 Cutoff	$15 Cutoff	$10 Cutoff	$5 Cutoff
Cumulative Additional Transmission Capacity (MW)	0	5,500	7,500	10,500	18,000
Cumulative Transmission Annualized Cost (million $/yr)	0	242	330	462	792
Production Cost (billion $/yr)	11.8	11.3	11.1	10.9	10.6
Cumulative Production Cost Change from Initial Build-Out (million $/yr)		546	721	923	1,220
Average Benefit/Cost Ratio		2.26	2.18	2.00	1.54
Curtailment (TWh)	24.8	16.7	13.4	9.2	3/5
Curtailment as Fraction of Potential Wind and Solar Production	0.096	0.065	0.052	0.035	0.014
Transmission Cost per MWh Curtailment Savings ($/MWh)		30.1	29.0	29.7	37.3

Figure 15 depicts some of the metrics used to evaluate the transmission build-outs.

Figure 15 (a) shows the change in production cost for each scenario as a function of cutoff shadow price and transmission MW built. The transmission built in the High Solar Scenario at the $5/MWh cutoff shadow price was 10,000 MW, which was comparable to the transmission built in the High Wind Scenario at the $10/MWh cutoff shadow price. That 10,000 MW of transmission in the High Wind Scenario saves $923 million/year, however, which is about 50% higher than the $638 million/year saved in the High Solar Scenario.
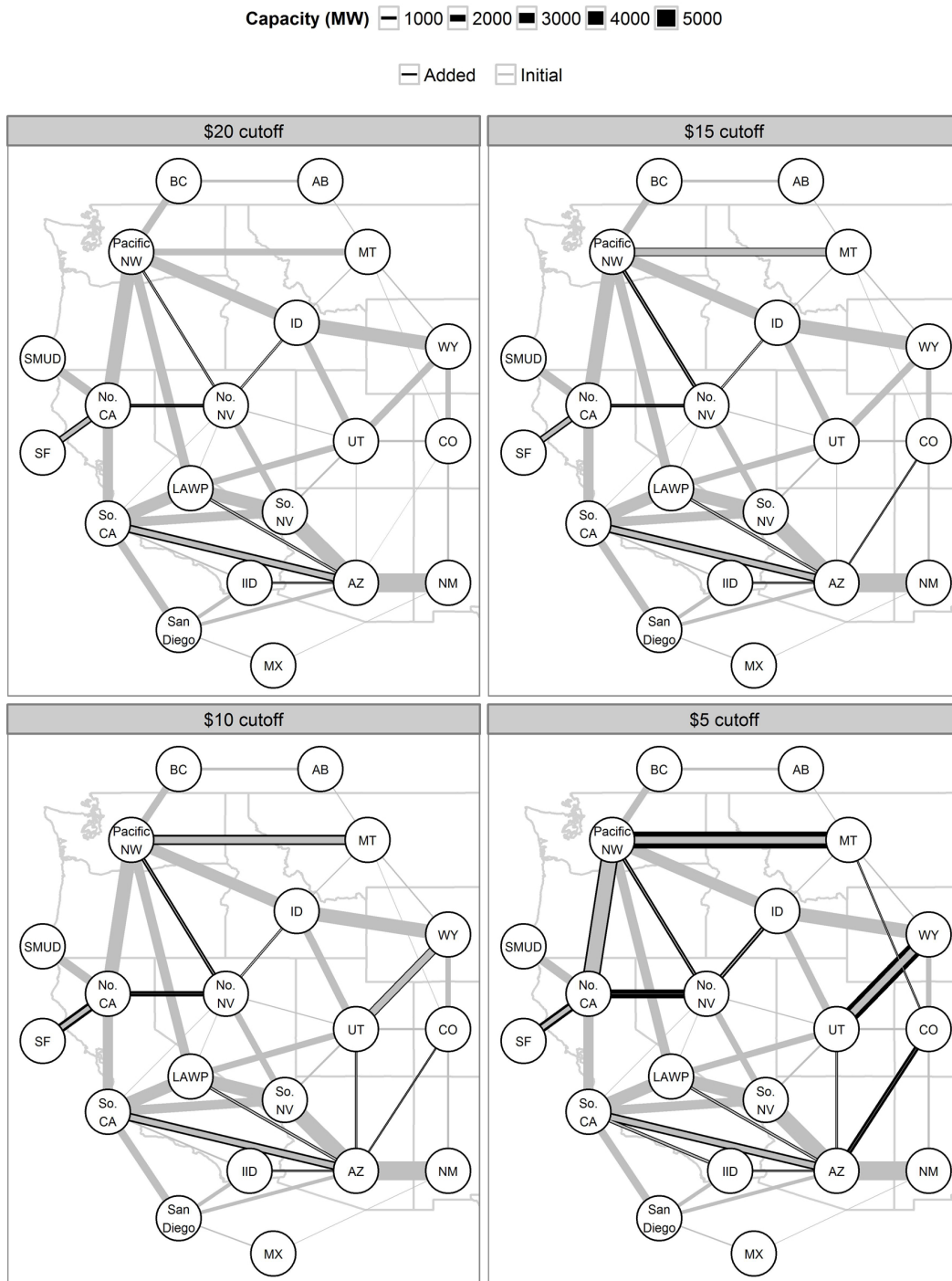
Figure 14. Iterative transmission build-out for the High Wind Scenario showing the different cutoff shadow prices

Notes: SMUD, Sacramento Municipal Utility District; LAWP, Los Angeles Department of Water and Power; IID, Imperial Irrigation District. The initial transmission capacity for major interfaces is shown by the width of the gray lines. New transmission capacity is shown by the width of the black lines.

Figure 15 (b) shows the net benefit of the transmission expansion, defined as the change in production cost minus the approximate transmission cost. As the cutoff value decreased and transmission was expanded, the net benefit increased, topped out, and then decreased. The cutoff value where this net benefit topped out varied but was generally $10/MWh. As a result, we selected the $10/MWh cutoff value to define the transmission build-out for each scenario. Curtailment decreased with expanded transmission.

Figure 15 (c) shows the curtailment as a function of cutoff shadow price and transmission MW built. Because solar peaks midday and wind is often stronger at night, wind curtailment is much greater than solar curtailment, even as transmission was built out for the High Wind Scenario. These results reflect only the DA model, so forecast error is not considered and curtailment is lower compared with the final runs presented in Section 6.
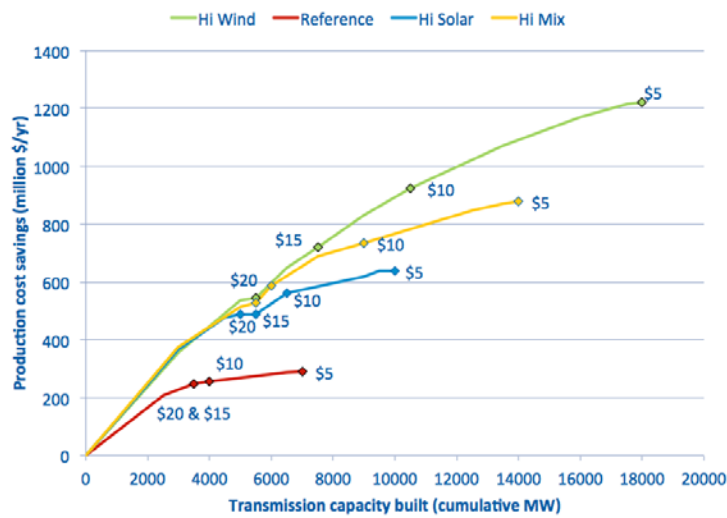
(a)
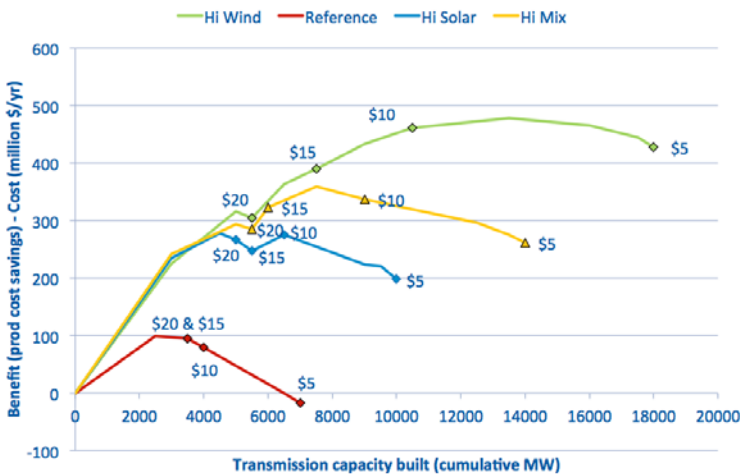
(b)
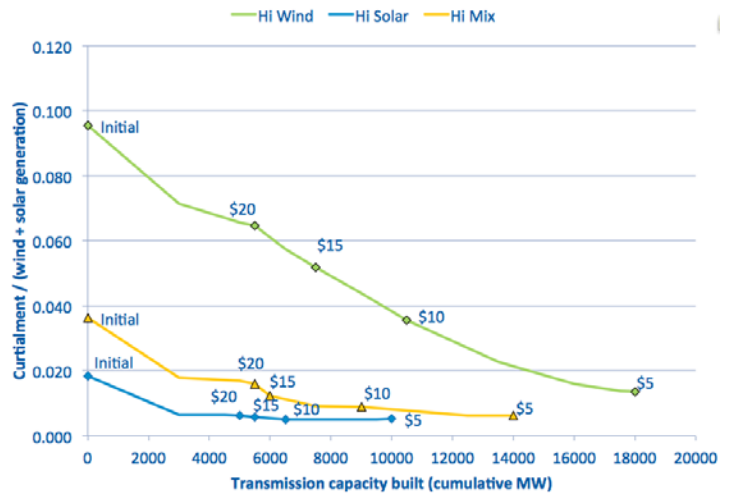
(c)

Figure 15. Comparison of transmission build-out metrics for the TEPPC, High Solar, High Wind, and High Mix Scenarios, showing (a) change in production cost versus MW built, (b) net benefit of transmission expansion versus MW built, and (c) curtailment versus MW built

Table 9 and Figure 16 summarize the transmission build-outs at the $10/MWh cutoff value for the scenarios. Note that transmission capacity was added to all scenarios, including the No Renewables and TEPPC case.

Table 9. Transmission Build-Outs for Four Scenarios With $10/MWh Cutoff

Metric	TEPPC	High Wind	High Mix	High Solar
Cumulative Additional Transmission Capacity (MW)	4,000	10,500	9,000	6,500
Cumulative Transmission Annualized Cost (million $/yr)	176	462	396	586
Production Cost (billion $/yr)	15.2	10.9	10.6	10.9
Cumulative Change in Production Cost (M$/yr)	255	923	733	561
Average Benefit/Cost Ratio	1.45	2.00	1.85	1.96
Incremental Benefit/Cost Ratio	0.27	1.54	1.11	1.65
Curtailment (TWh)	0.2	9.2	2.3	1.3
Curtailment as Fraction of Potential Wind and Solar Production	0.002	0.035	0.009	0.005
Transmission Cost per MWh Curtailment Savings ($/MWh)	122	29.7	55.7	129.5
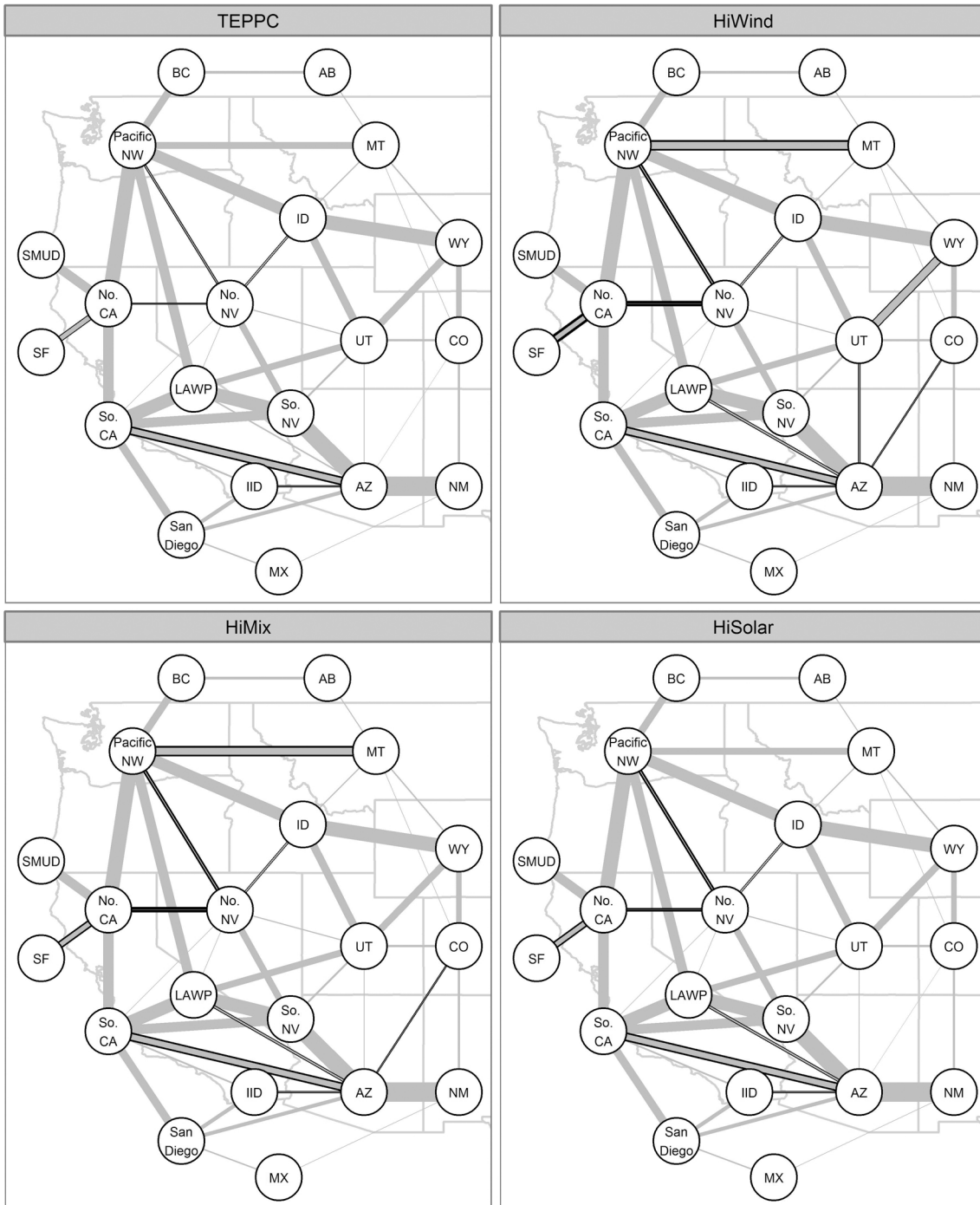
Figure 16. Final transmission build-out by scenario (using the $10 cutoff shadow price)

Notes: Initial transmission capacity for major interfaces is shown by the width of the gray lines. New transmission capacity is shown by the width of the black lines.

40

4 Statistical Analysis

We conducted statistical analysis on the scenarios, examining variability and uncertainty on various timescales, investigating penetration levels on various timescales, determining impacts of aggregation and geographic diversity, and comparing the impacts of wind and solar (Lew et al. 2012). We also investigated solar variability in detail, finding that most of it is known because of the path of the sun through the sky. Additional plots can be found in Appendix D.

Statistical and extreme event analysis was undertaken to examine the variability of solar, wind, and net load (defined as load minus solar minus wind) on a subregional and regional basis. All results in this section focus on and within the U.S. portion of the Western Interconnection. The subregional entities considered for detailed analysis were Columbia Grid (CG), Northern Tier Transmission Group (NTTG), WestConnect (WC), and CAISO.

Figure 17 (a)–(b) shows the hourly duration curves for wind and PV. The figure shows available wind and PV output, prior to the production simulation runs when curtailment is determined. The High Wind Scenario and the High Solar Scenario both produced similar peak output during the top wind and PV output hours. PV output was zero for half of the year during nighttime hours. CSP with 6 hours thermal storage can be considered dispatchable. The dispatch of the storage was optimized in the production simulation runs (see Section 5) and the resulting CSP duration curve is shown in Figure 17 (c). Because the CSP in this study is dispatchable, we include CSP in the statistical analysis only when it is appropriate. Much of the variability and uncertainty analysis focuses on wind and PV.

Figure 18 shows the net load duration curve, including CSP (wind, PV, and CSP output have all been subtracted from the load). Net loads are depressed consistently with high penetrations. The minimum net load is 30,000 MW lower in the High Solar than in the TEPPC Scenario.
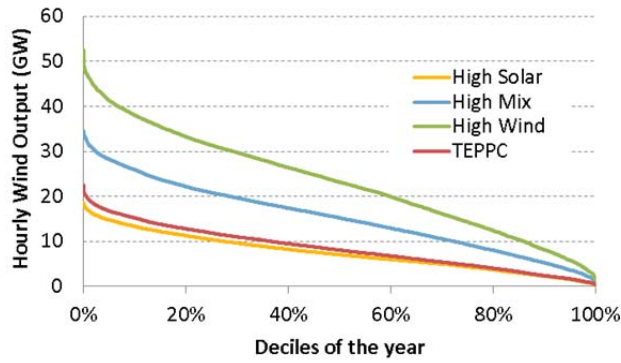
(a)
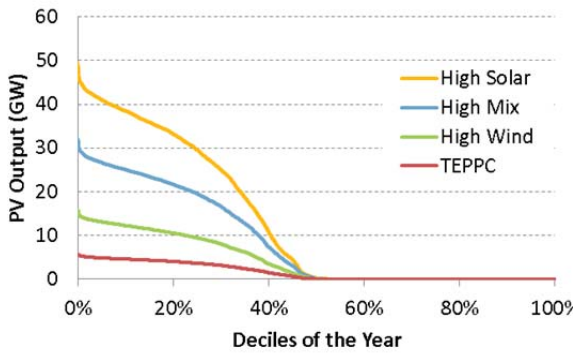
(b)
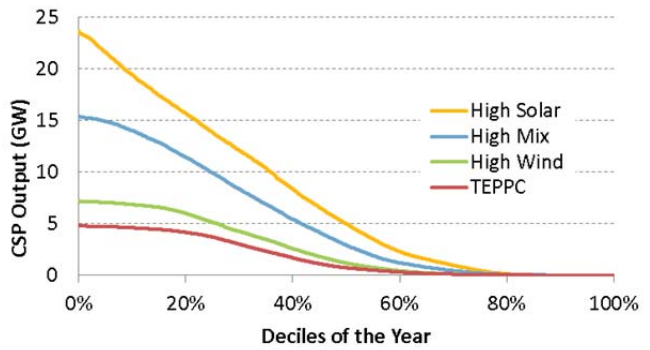
(c)

**Figure 17. Hourly (a) wind, (b) PV, and (c) CSP duration curves
for the (blue) High Solar, (red) High Mix, (green) High Wind, and (red) TEPPC Scenarios**
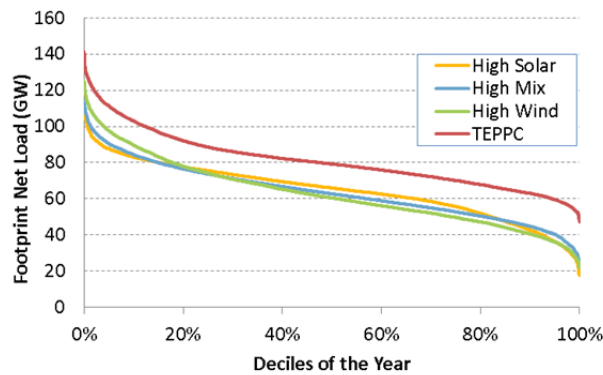
**Figure 18. Net load duration curve including CSP
for the (blue) High Solar, (red) High Mix, (green) High Wind, and (red) TEPPC Scenarios**

Table 10 shows the wind and solar penetration for selected subregions for each scenario. Note that wind and solar penetrations could be higher than the target penetration level because the penetration targets were designed for 2004–2006 and these data show 2006 only.

Table 10. Wind and Solar Penetration by Subregion

Penetrations for Selected Subregions	High Solar		High Mix		High Wind		TEPPC	
	Energy (TWh)	Penetration (%)	Energy (TWh)	Penetration (%)	Energy (TWh)	Penetration (%)	Energy (TWh)	Penetration (%)
Wind								
CAISO	12.7	5	13.6	5	21.7	8	15.2	6
CG	16.9	15	22.4	19	25.7	22	15.6	13
NTTG	16.7	14	39.2	32	53.4	44	17.2	14
WC	19.1	7	59.1	21	102.0	36	26.2	9
U.S. Western Interconnection	65.5	8	134.3	17	202.8	26	74.2	9
Solar								
CAISO	60.2	23	37.1	14	22.7	9	14.2	5
CG	1.9	2	1.8	2	1.5	1	0.6	1
NTTG	9.5	8	3.8	3	1.3	1	7.8	6
WC	124.7	44	86.6	31	37.0	13	8.1	3
U.S. Western Interconnection	196.3	25	129.4	17	62.5	8	30.7	4
Total								
CAISO	72.9	28	50.7	19	44.4	17	29.4	11
CG	18.9	16	24.2	21	27.2	23	16.2	14
NTTG	26.3	22	43.0	35	54.7	45	25.0	21
WC	143.8	51	145.7	51	139.0	49	34.3	12
U.S. Western Interconnection	261.8	33	263.7	34	265.3	34	104.9	13

Figure 19 shows the contour plots for the net load, excluding CSP (wind and PV output have been subtracted from the load) for each scenario. The TEPPC Scenario, with 13% wind/solar, showed high summer peaks in the afternoon and early evening in the U.S. portion of the Western Interconnection. The High Wind Scenario depressed much of this peak and also exacerbated the net load minimums during the night in the winter. Decreasing minimum generation levels of fossil-fueled plants through retrofits and design of new generation will be helpful for high wind penetrations.
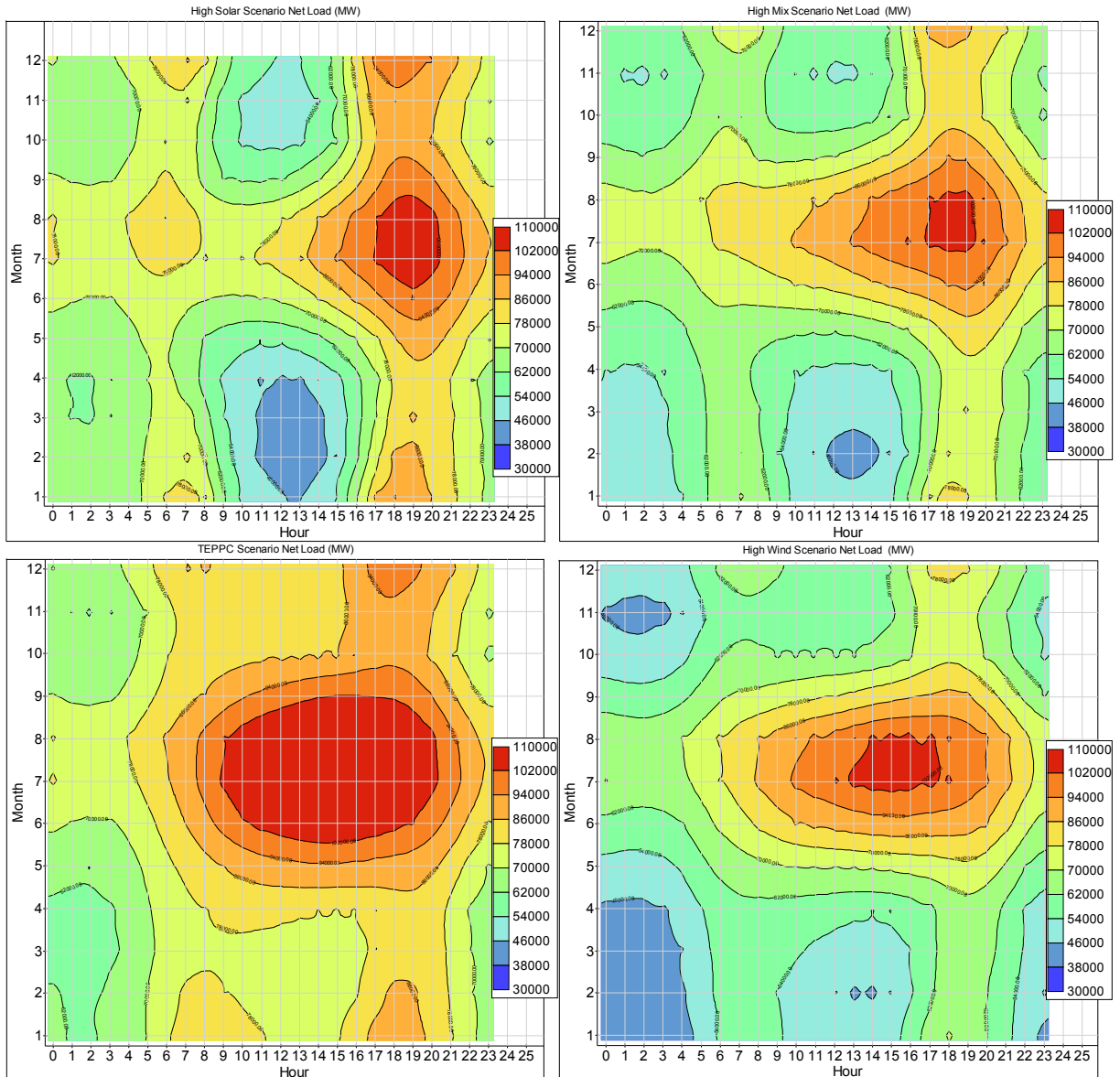
Figure 19. Contour plots of monthly average net load for each hour of the day for each scenario (clockwise from upper left): High Solar, High Mix, High Wind, and TEPPC

Note: CSP is not included in these plots, so net load here is load minus wind minus PV.

The High Solar Scenario clearly showed the diurnal double peak caused by the depression of net load at midday when solar output is highest. Contour lines that are close together, such as those in the nonsummer months after the morning net load peak and again before the evening net load peak, indicated steep net load ramps. Increasing ramping capabilities or reducing start times of fossil-fueled generation might be helpful in this scenario. Decreasing minimum generation levels through retrofits and new design of future plants could help manage winter midday net load minimums.

44

4.1 Geographic Diversity

Utilities have concerns about whether fast-moving clouds over PV plants could result in high variability. Two characteristics of PV plants affect this variability: (1) the size of the plant and (2) the number of plants. Clouds over a small plant, such as a rooftop PV system, can cause high variability, but the impact of a small system's variability on the bulk power system is minimal. There can be impacts on a distribution level, but WWSIS-2 focuses only on impacts at the transmission level. A large plant can have a higher impact on the bulk power system, but its larger area helps to smooth out the variability. With additional PV plants, the geographic diversity of the plants and the unlikelihood of cloud fronts obscuring all PV plants at the same time result in further smoothing of this variability.

Figure 20 shows the smoothing of solar output with increasing aggregation of solar sites throughout Southern California. At the individual plant level, cloud events were seen with the fast ramps in the PV plant output. These events smoothed out as output from 6 and then 25 plants were aggregated.

At the subregional level, individual cloud events could not be discerned.
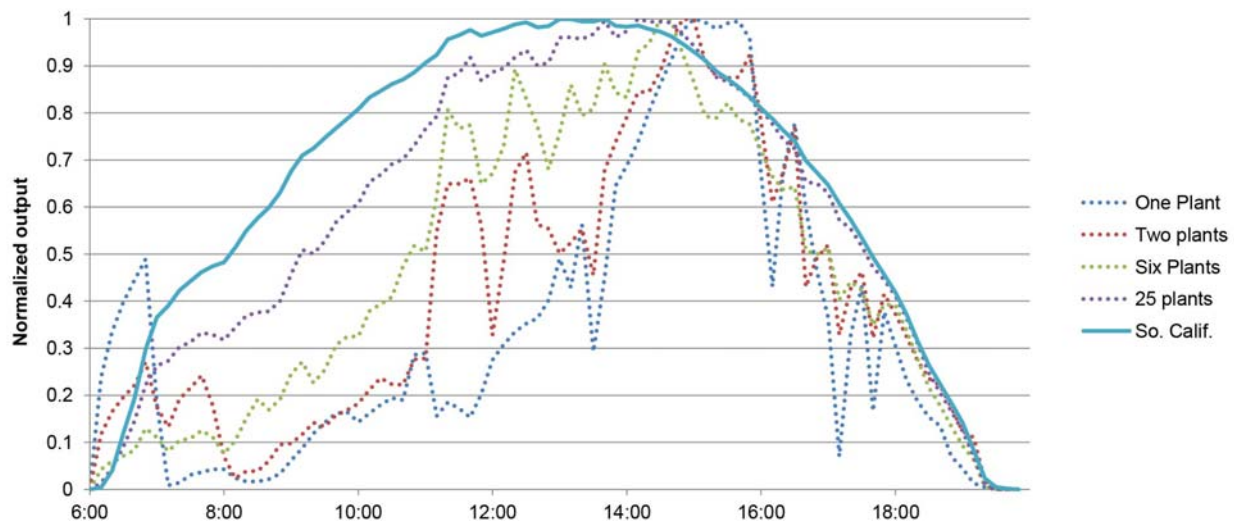
**Figure 20. Normalized PV output for increasing aggregation
of PV plants in Southern California for a partly cloudy day**

We used this same approach to compare rooftop PV, utility-scale PV, and wind in Figure 21. Total aggregate capacity was defined by increasing concentric circles that included larger areas and higher capacity. The analysis was performed on solar sites in Southern California. Variability was defined here as one standard deviation of the hourly change in output, or $\Delta\sigma$ (delta-sigma). The utility-scale PV and wind profiles started with relatively high variability when a few plants were examined. Wind variability dropped off rapidly as plants were aggregated, with the normalized variability leveling off at about 1%. Utility-scale PV variability leveled off at slightly less than 4%. Rooftop PV, already an aggregation of many small plants, and therefore starting with low variability, showed relatively little benefit as increasing amounts were aggregated throughout larger areas. The residual variability results mainly from the highly correlated change in position of the sun.

Wind shows the greatest benefit from geographic diversity. Rooftop PV has modest variability even at small aggregate levels.

(a)

(b)

(c)
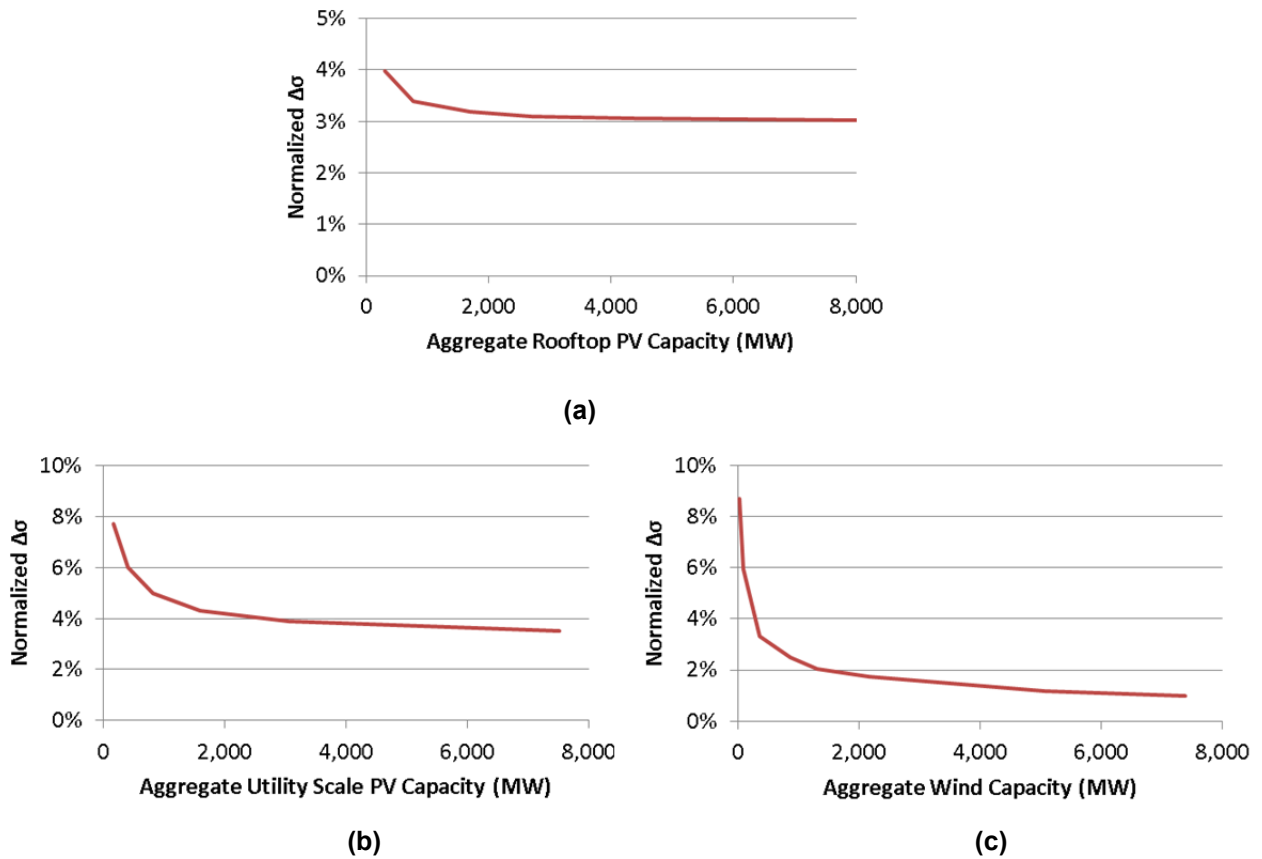
Figure 21. Normalized variability as a function of aggregate capacity for (a) rooftop PV, (b) utility-scale PV, and (c) wind

Notes: Observe the difference in y-axis scales. Δσ is one standard deviation of the hourly change in output.

4.2 Monthly Penetration

Figure 22 shows the monthly energy penetration for three of the scenarios. The High Solar Scenario is shown in Figure 22 (a), where the total penetration peaks in May. Solar dropped some in the summer months compared to May, with a slight drop in PV and a more pronounced drop in CSP. This appeared to be a characteristic of the 2006 solar data chosen for the study. In addition, higher temperatures lead to lower PV panel efficiency. Wind peaked in January, with the minimum appearing in the summer months.

Figure 22 (b) shows the penetration for the High Mix Scenario, with peak energy in April and minimum energy in the summer months, when wind was lowest. The monthly energy penetration for the High Wind Scenario is shown in Figure 22 (c). The overall profile closely followed the wind component, with peak energy in the winter and minimum energy in the summer.
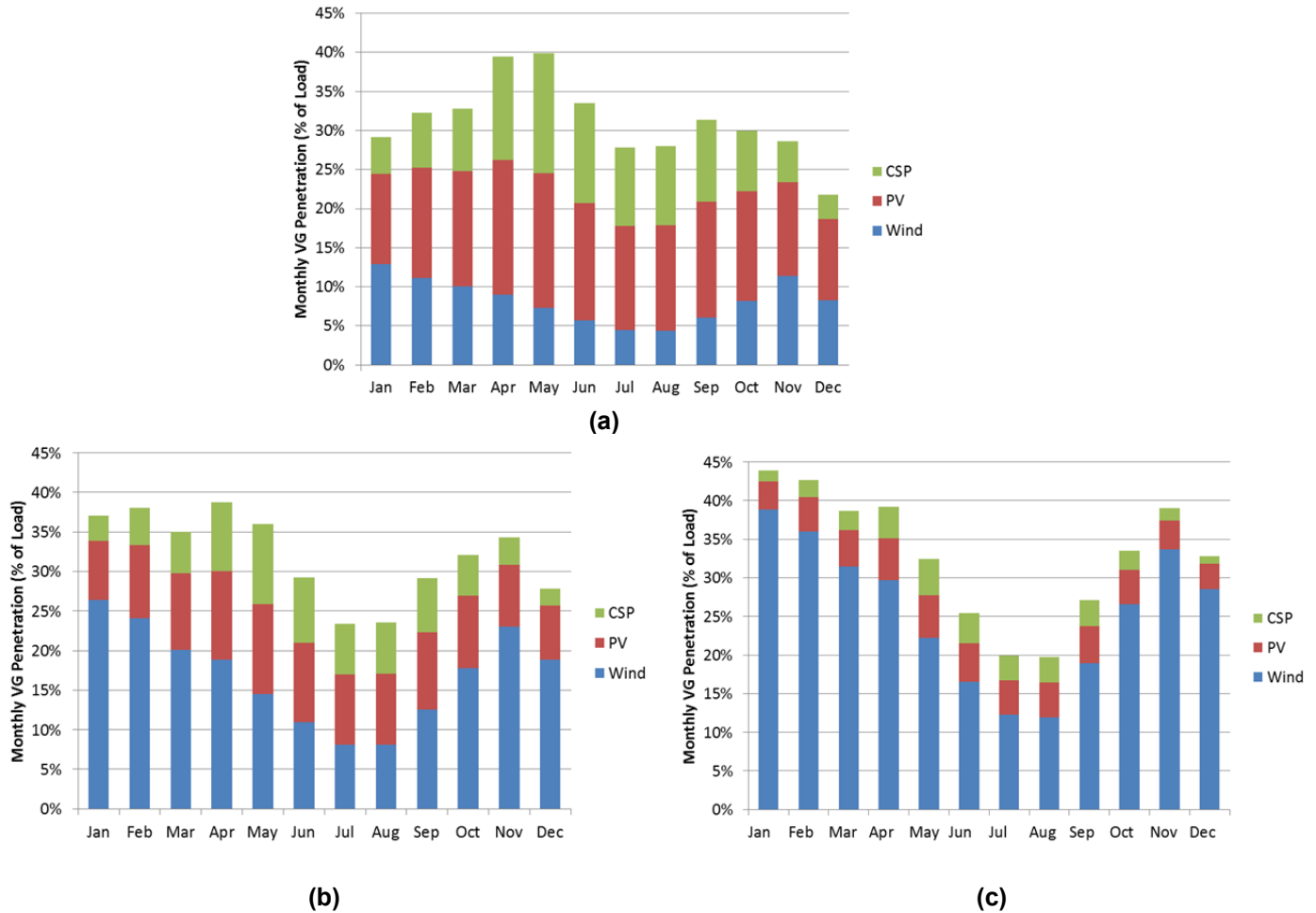
**Figure 22. Monthly penetration of wind, PV, and CSP
for the (a) High Solar, (b) High Mix, and (c) High Wind Scenarios**

4.3 Diurnal Variability

Figure 23 (a) shows the diurnal variability of the U.S. portion of the Western Interconnection load. On average, the morning load pickup was followed by a gradual rise to an evening peak, with a nighttime minimum. The hourly change in load, which experienced significant variability in the late afternoon, is also depicted.

Figure 23 (b)–(d) shows the net load (including CSP) variability of the high-penetration scenarios. In the High Solar Scenario, the high solar output at midday led to a double peak in net load, once in the morning and again in the evening. The hourly net load delta shows that the variability increased considerably at sunrise and sunset. For the High Mix and High Wind Scenarios, as the solar penetration decreased and the wind increased, the double peak in net load disappeared, with the net load shape being similar to the load shape, depressed by about 10,000 MW to 15,000 MW.
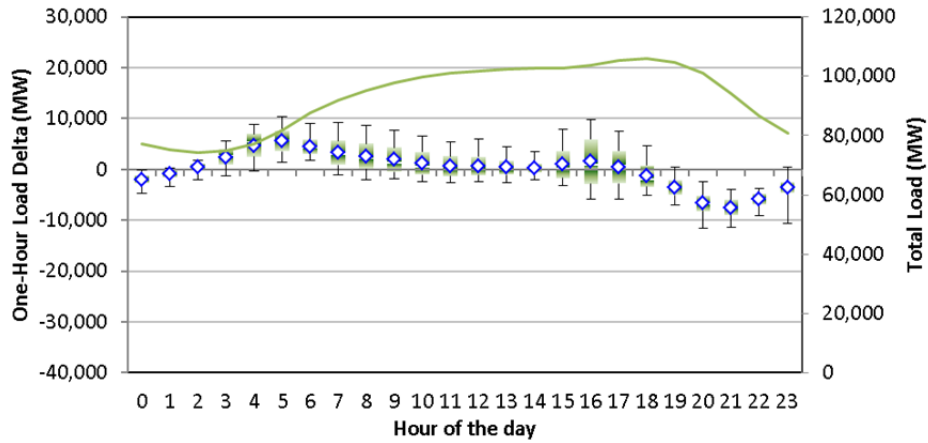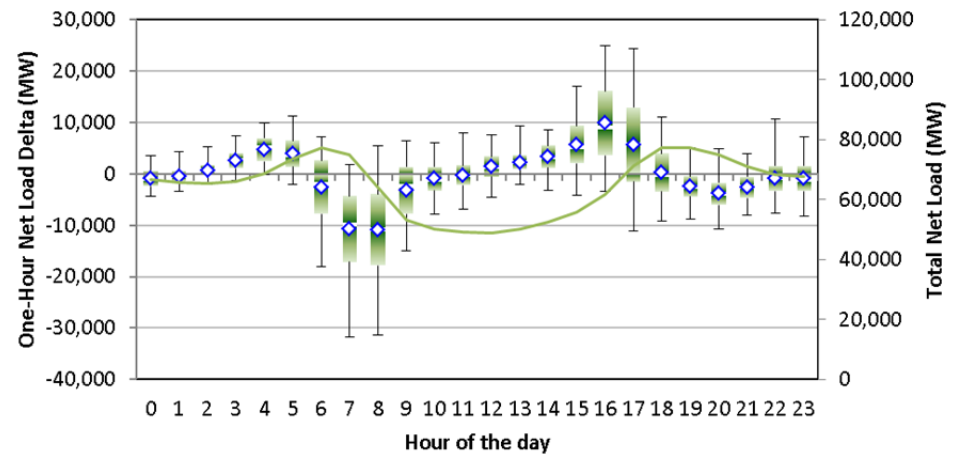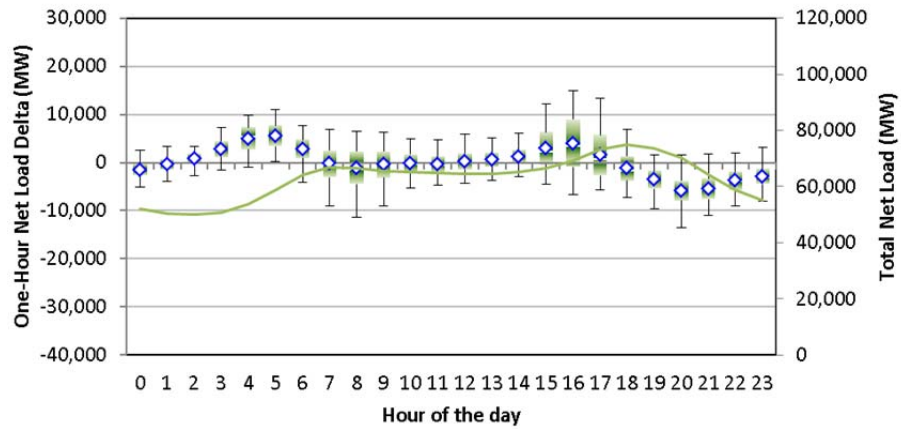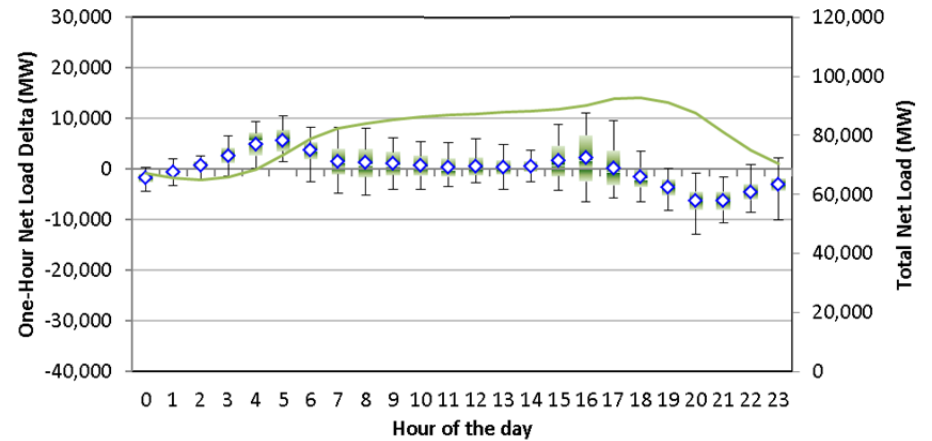
Figure 23. (a) Diurnal variability of the load (green line) and the hourly change in load (white line—median; diamond—mean; bar—standard deviation; whiskers—minimum and maximum); diurnal variability of net load and hourly change in net load for the (b) High Solar, (c) High Mix, and (d) High Wind Scenarios

Note: CSP dispatch is included in these plots, so net load is load minus wind minus solar.

4.4 Hourly Variability

The hourly variability was also examined.

Figure 24 (a) shows the hourly wind change versus the hourly load change for the High Wind Scenario (25% wind). Figure 24 (b) shows the hourly PV change versus the hourly load change for the High Solar Scenario (15% PV; CSP is not shown) for 8,760 hours of 2006. For these hourly variability plots, it is important to note that the top right and bottom left quadrants show the hours when solar and wind moved in the same direction as the load, helping the power system meet load.

Variability is not always undesirable. Wind and solar often help meet load.

The top left quadrant shows solar and wind increasing as load decreases. Operators may be able to curtail solar and wind production to balance load. The bottom right quadrant depicts the difficult hours for an operator, when solar and wind decreased while load increased. The bottom right quadrant extrema are particularly challenging. Ensuring enough up-reserves during these hours is critical.

The variability in solar resources needs to be interpreted a bit differently from the wind variability. The solar variability has two components: one that is caused by atmospheric conditions like clouds and one that is known because of the motion of the sun. Much of the solar variability results from the latter, which causes it to be much higher than wind variability.

Figure 24 (a) shows that wind variability was generally uncorrelated with both load variability and season. In contrast, Figure 24 (b) shows that PV helped the load during a significant number of hours, during sunrise and morning load rise. In the winter, however, load was increasing while PV output was decreasing during many hours. This is because the evening load peak occurs during the sunset hours (partly because of lighting). Figure 24 (b) also shows a large number of nighttime hours where the PV change was zero.
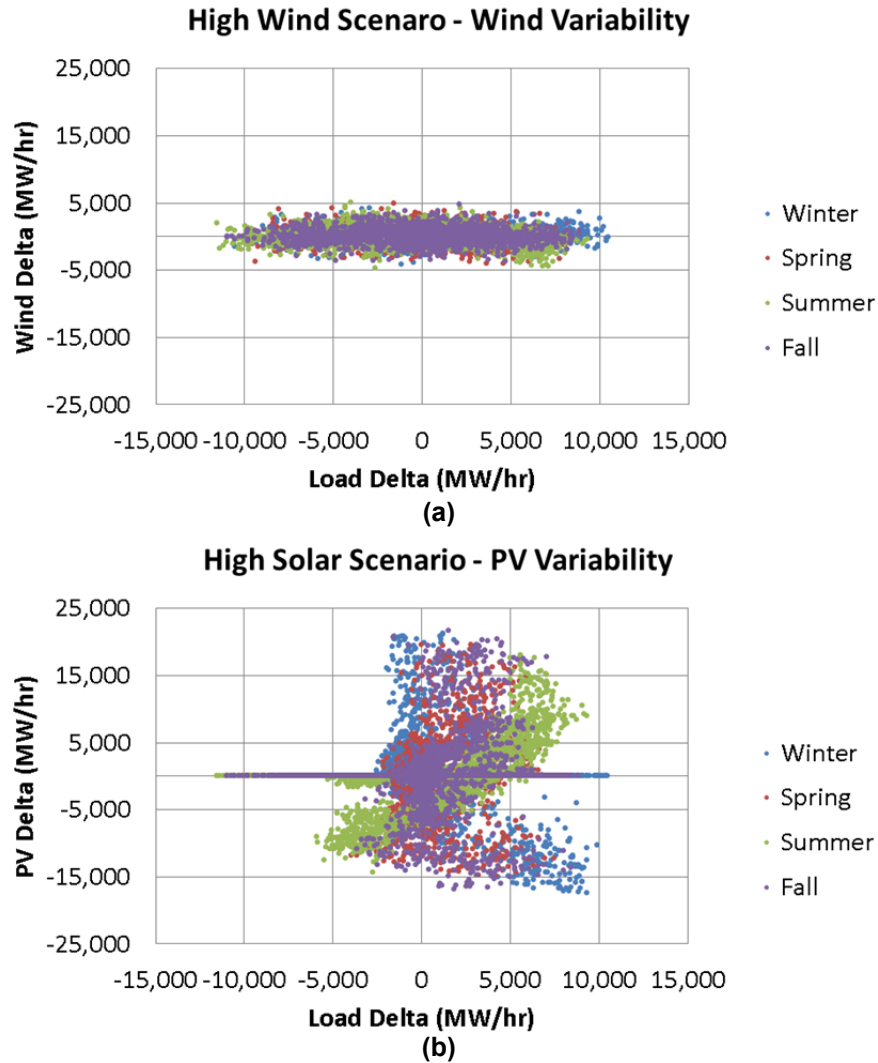
**Figure 24. (a) Hourly wind production change versus hourly load change
for the High Wind Scenario and (b) hourly PV production change
versus hourly load change for the High Solar Scenario**

Note: The colors depict different seasons.

Figure 25 (a)–(c) shows the hourly load change versus the hourly variability of the wind and PV output for the three high-penetration scenarios for 8,760 hours of 2006. They are plotted on the same y-axis scale, showing that the wind and PV variability in the High Solar Scenario was much greater than that of the High Mix Scenario and far greater than that of the High Wind Scenario. This disparity is entirely the result of the perfectly known solar variability from the motion of the sun, as the next section shows.
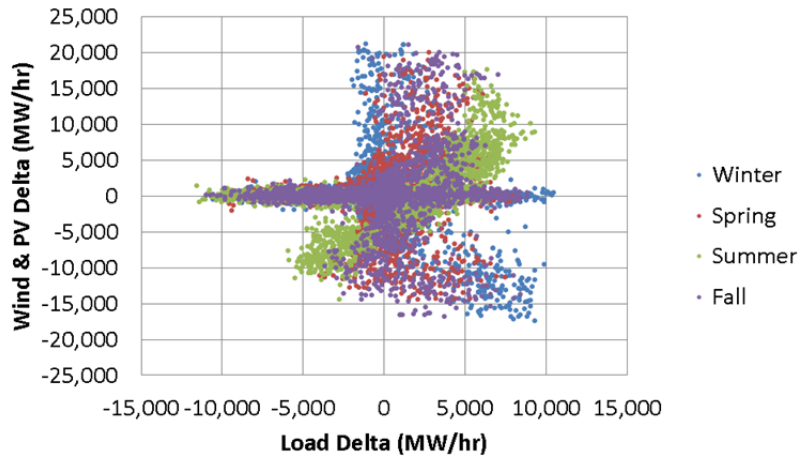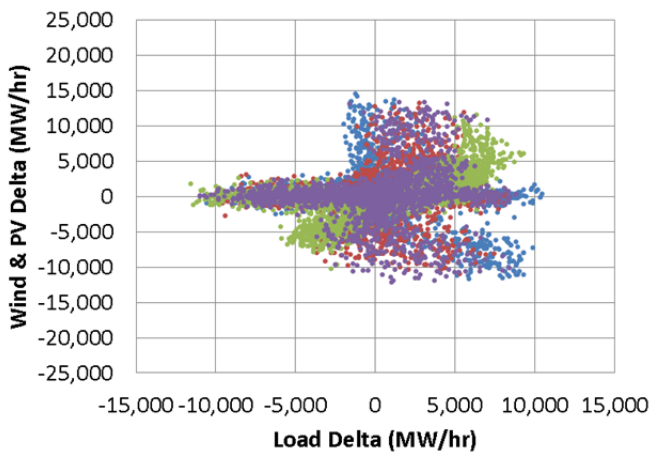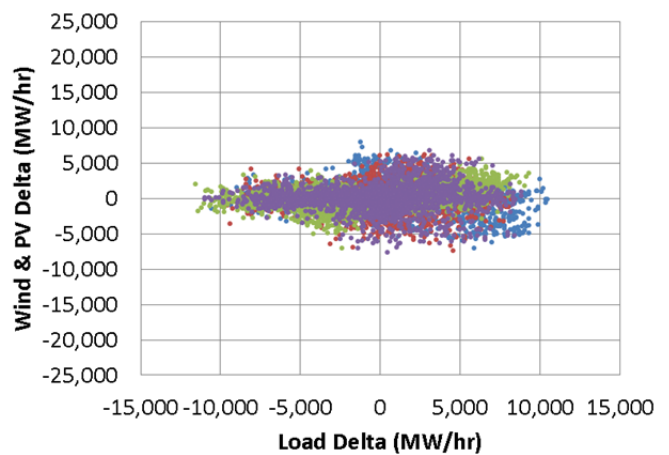
Figure 25. Hourly load change versus hourly wind and PV production change for the (a) High Solar, (b) High Mix, and (c) High Wind Scenarios for 2006

Note: The colors depict different seasons.

The maximum hourly wind and PV change in the High Solar Scenario was +22,000 MW/h and –17,000 MW/h, which was significantly higher than the +8,000 MW/h and –7,900 MW/h of the High Wind Scenario. This illustrates the significant variability that the system must accommodate for high solar penetrations. Section 6 will show how CTs start and ramp more frequently and how coal ramps more frequently to manage this variability.

Table 11 gives statistics for the 1-hour changes in net load for selected subregions. Subregions in the north, such as CG and the NTTG, had relatively less solar capacity and showed relatively modest changes in the standard deviation of 1-hour changes in net load and the minimum and maximum changes for both the High Solar and High Wind Scenarios. Subregions in the south, such as CAISO and WC, have much higher solar capacities. WC has a particularly high solar penetration level. As a result the 1-hour changes in net load were significantly affected in the High Solar Scenario.

51

Table 11. Statistics for 1-Hour Changes in Net Load for the High Solar Scenario for the U.S. Portion of the Western Interconnection Footprint and Selected Subregions

	CG	NTTG	WC	CAISO	Footprint
Sigma (MW)					
Load Alone	672	593	1,492	1,527	3,929
Reference Scenario	720	649	1,513	1,514	3,983
High Solar Scenario	735	777	3,505	1,985	6,279
High Mix Scenario	744	699	2,412	1,767	4,954
High Wind Scenario	747	728	1,773	1,547	4,189
Maximum Negative Delta (MW)					
Load Alone	−2,545	−1,842	−4,613	−5,182	−11,534
Reference Scenario	−3,422	−2,418	−4,802	−5,135	−12,827
High Solar Scenario	−3,437	−2,580	−13,197	−6,663	−22,257
High Mix Scenario	−3,590	−2,615	−8,695	−5,183	−15,661
High Wind Scenario	−3,544	−2,834	−6,395	−5,107	−13,478
Maximum Positive Delta (MW)					
Load Alone	2,971	2,096	3,774	4,721	10,451
Reference Scenario	3,180	2,112	4,327	5,553	11,194
High Solar Scenario	3,175	3,145	14,037	9,874	26,671
High Mix Scenario	3,256	2,491	10,220	8,736	20,391
High Wind Scenario	3,254	2,838	6,923	7,163	14,166
No. of Drops Less than 3 * Load Sigma					
Load Alone	1	3	2	13	0
Reference Scenario	14	24	6	9	1
High Solar Scenario	14	104	519	86	222
High Mix Scenario	20	38	249	17	31
High Wind Scenario	22	71	45	9	6
No. of Drops Greater than 3 * Load Sigma					
Load Alone	74	14	0	3	0
Reference Scenario	103	24	0	22	0
High Solar Scenario	110	127	707	197	371
High Mix Scenario	117	63	400	131	217
High Wind Scenario	120	69	109	75	39

4.4.1 Hourly Weather Variability of Solar

Solar variability consists of two components: diurnal variability (the perfectly known variability from sun movement) and weather variability (the variability from cloud movement and other atmospheric conditions). Because system operators can plan for the diurnal variability, we removed this component to assess the magnitude of the weather variability.

Figure 26 shows the weather variability component of solar variability for the High Solar Scenario. This figure can be directly compared to Figure 24 (b) to show that *solar variability is dominated by diurnal variability*. The weather variability component is similar to the wind variability in the High Wind Scenario as shown in Figure 24 (a).
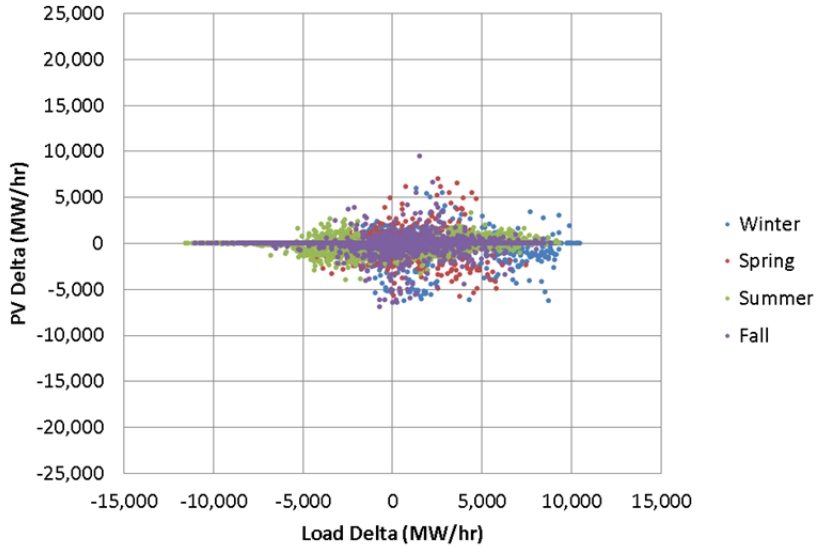
Figure 26. Weather variability component of PV variability for the High Solar Scenario

The total wind and PV variability, excluding the diurnal solar variability, is depicted in Figure 27. This can be compared directly to Figure 25 (a), which shows more than double the variability.
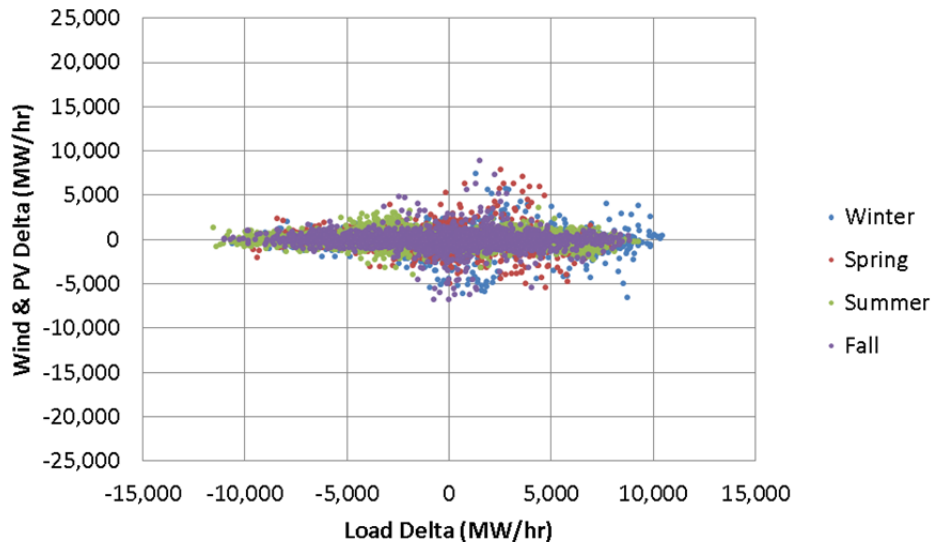
**Figure 27. Total wind and PV variability
excluding the diurnal solar variability for the High Solar Scenario**

53

4.5 Subhourly Variability

At the 5-minute level, correlations between changes in load and changes in wind and PV output were similar to those at the hourly timescale, as shown in Figure 28.

Again, significantly more 5-minute variability occurred in the High Solar Scenario.

(a)

(b)
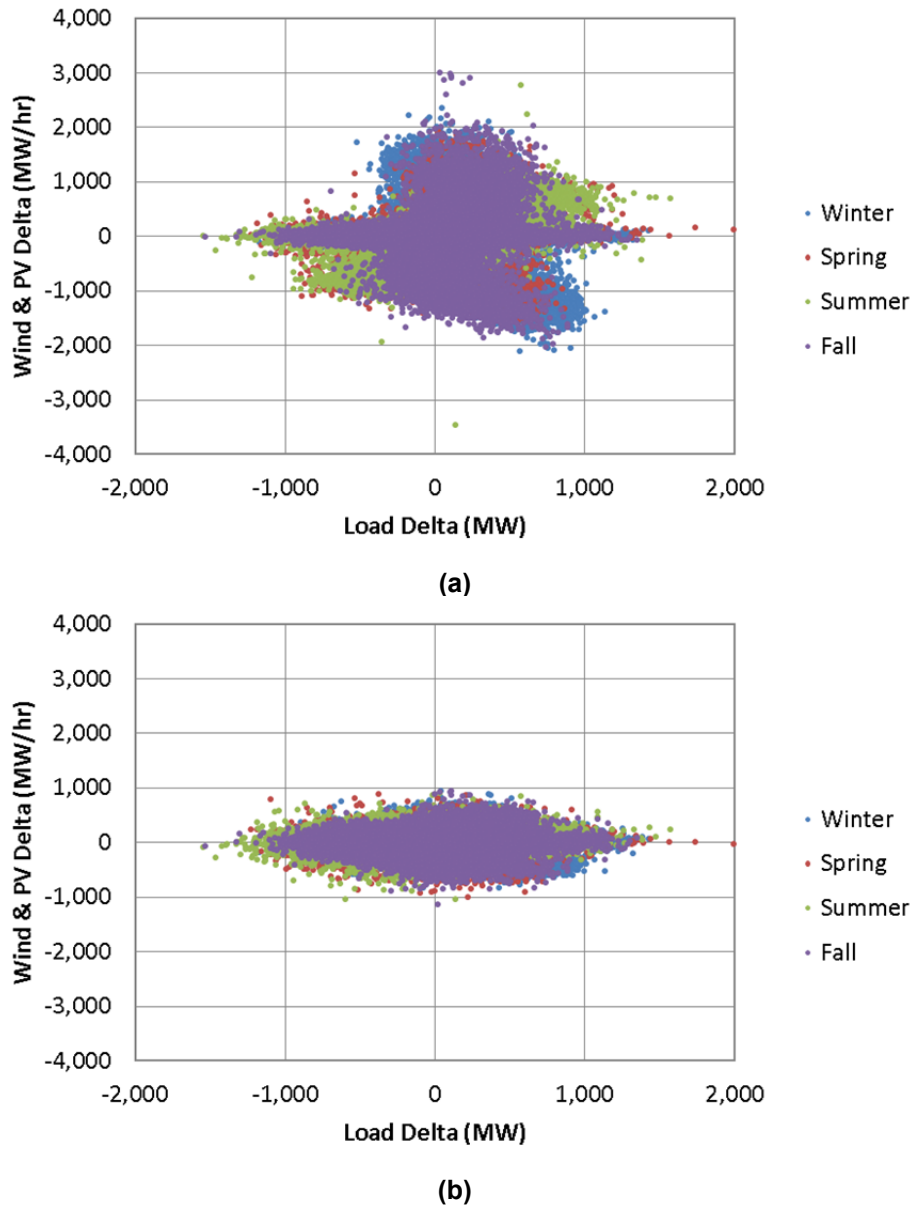
**Figure 28. Five-minute changes in load versus 5-minute changes
in wind and PV output for the (a) High Solar and (b) High Wind Scenarios**

Table 12 gives statistics for the 5-minute changes in net load for selected subregions. As with the hourly changes in Table 11, the subregions with lower solar capacities, such as CG and NTTG, showed relatively modest impacts in the subhourly time frame across scenarios. Subregions with higher solar penetrations, such as CAISO and WC, have much greater impacts, especially in the High Solar Scenario.

54

Table 12. Statistics for 5-Minute Changes in Net Load for the High Solar Scenario for the U.S. Portion of the Western Interconnection Footprint and Selected Subregions

	CG	NTTG	WC	CAISO	Footprint
Sigma (MW)					
Load Alone	65	59	153	145	358
Reference Scenario	74	68	158	146	366
High Solar Scenario	76	80	312	183	548
High Mix Scenario	77	77	231	166	447
High Wind Scenario	78	82	187	150	390
Maximum Negative Delta (MW)					
Load Alone	−712	−885	−1,084	−916	−1,541
Reference Scenario	−741	−872	−1,128	−911	−1,551
High Solar Scenario	−739	−882	−1,771	−961	−2,966
High Mix Scenario	−730	−861	−1,164	−913	−2,015
High Wind Scenario	−739	−858	−1,289	−901	−1,879
Maximum Positive Delta (MW)					
Load Alone	538	722	1,401	957	1,991
Reference Scenario	577	722	1,396	941	2,001
High Solar Scenario	576	726	2,090	1,290	3,611
High Mix Scenario	575	750	1,358	1,113	2,355
High Wind Scenario	633	760	1,388	902	2,020
No. Drops < 3 * Load Sigma					
Load Alone	103	146	471	177	97
Reference Scenario	541	655	500	190	137
High Solar Scenario	590	1,238	5,081	575	1,596
High Mix Scenario	669	1,296	2,040	327	431
High Wind Scenario	736	1,859	875	204	219
No. Rises > 3* Load Sigma					
Load Alone	1,011	394	260	244	174
Reference Scenario	1,402	768	293	450	209
High Solar Scenario	1,499	2,066	7,296	2,015	3,973
High Mix Scenario	1,602	1,463	4,129	1,586	2,340
High Wind Scenario	1,632	1,816	1,352	915	791

The tail events of the distribution are shown more clearly in Figure 29. The High Wind Scenario had little impact on the maximum and minimum 5-minute changes in net load but did increase the number of extreme events from load alone. The High Solar Scenario further increased the number of extreme events and caused them to be more extreme.
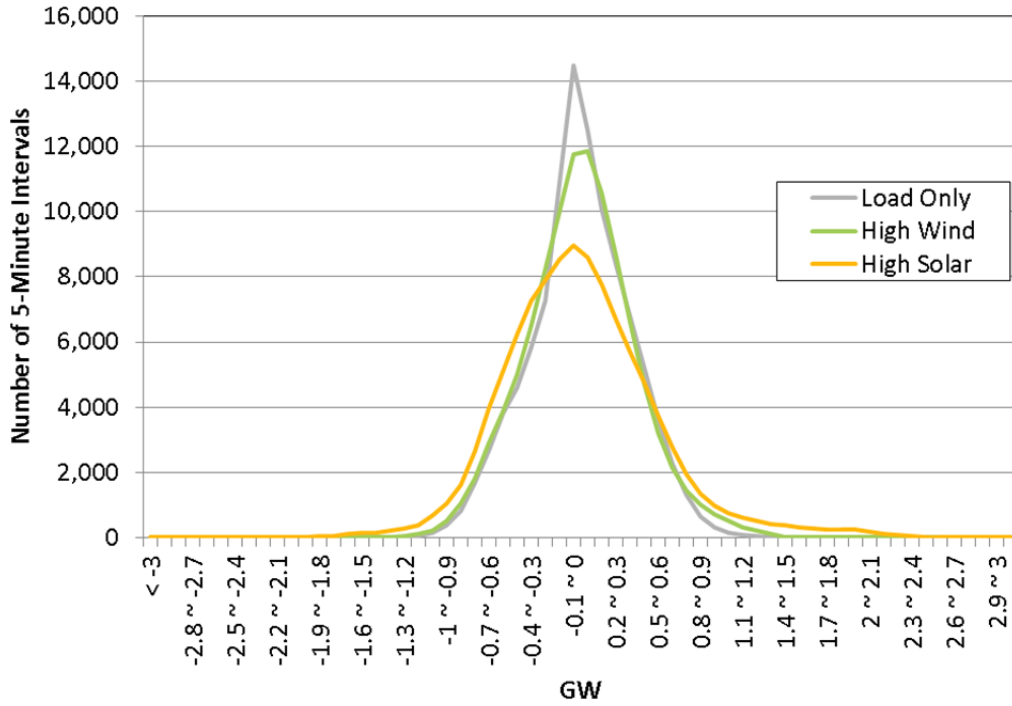
(a)
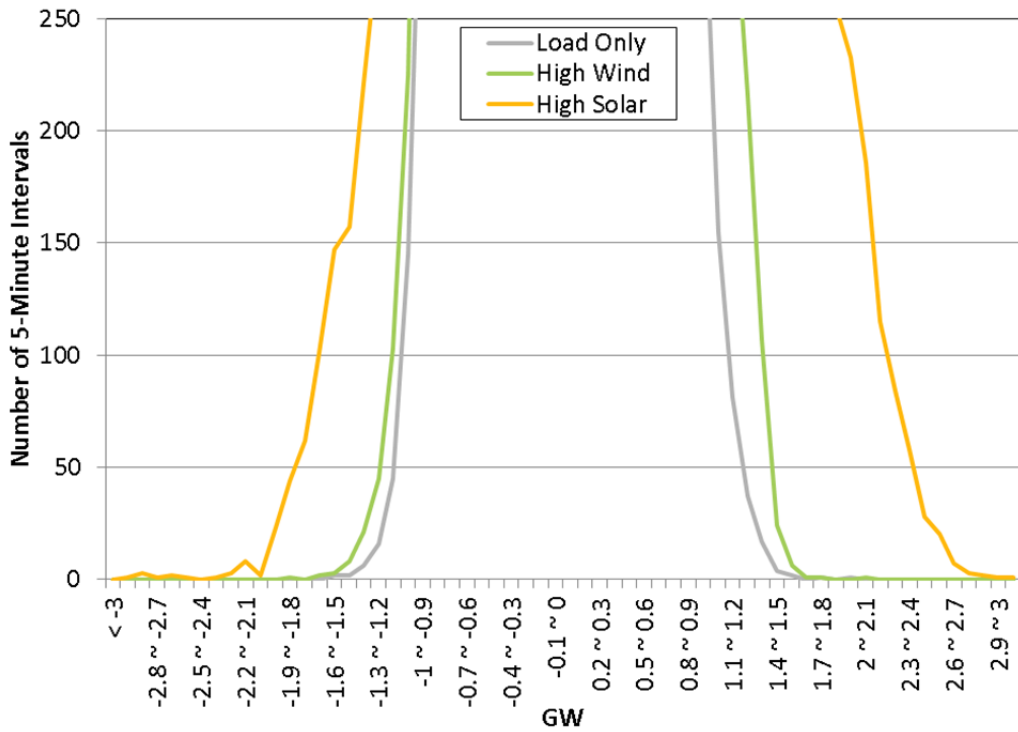
(b)

Figure 29. (a) Histogram of 5-minute changes in net load for the (grey) load-only, (green) High Wind, and (orange) High Solar Scenarios and (b) an expanded view of the distribution tails

56

4.5.1 Subhourly Weather Component of Solar Variability

We removed the diurnal component of the PV variability as we did for the hourly variability and compared the result to Figure 28 (a). Again, the weather component of subhourly solar variability is much smaller than the diurnal component of solar variability.
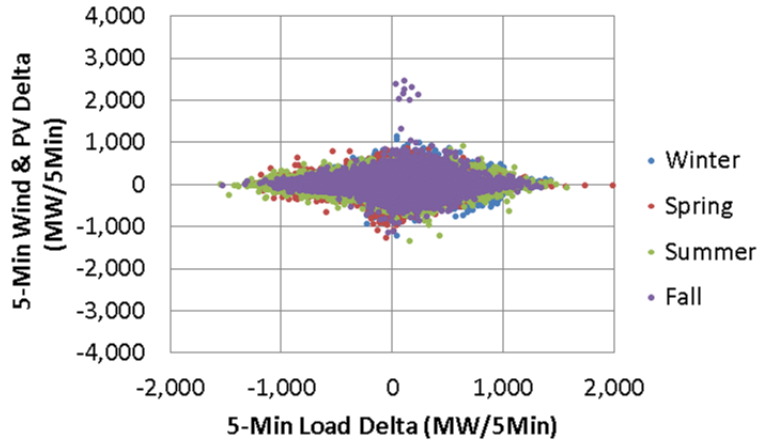
**Figure 30. Five-minute total wind and PV variability
excluding diurnal solar variability for the High Solar Scenario**

An interesting effect of removing the diurnal solar variability is that events are more prominent. For instance, the cluster of events in the fall from 2,000 to 2,500 MW/5-minute stands out as unique. These points are caused by a single event where there is cloud cover until mid-morning with a very fast up-ramp occurring at around 9 a.m. This ramp goes from near 0 output to near clear sky value in 45 minutes.

Figure 31 shows the distribution of the 5-minute changes shown in Figure 29 (a) with the diurnal component of solar variability removed. Comparing Figure 31 to Figure 29 shows a substantial reduction in the 5-minute changes associated with the weather portion of the PV resources seen in the scenarios.
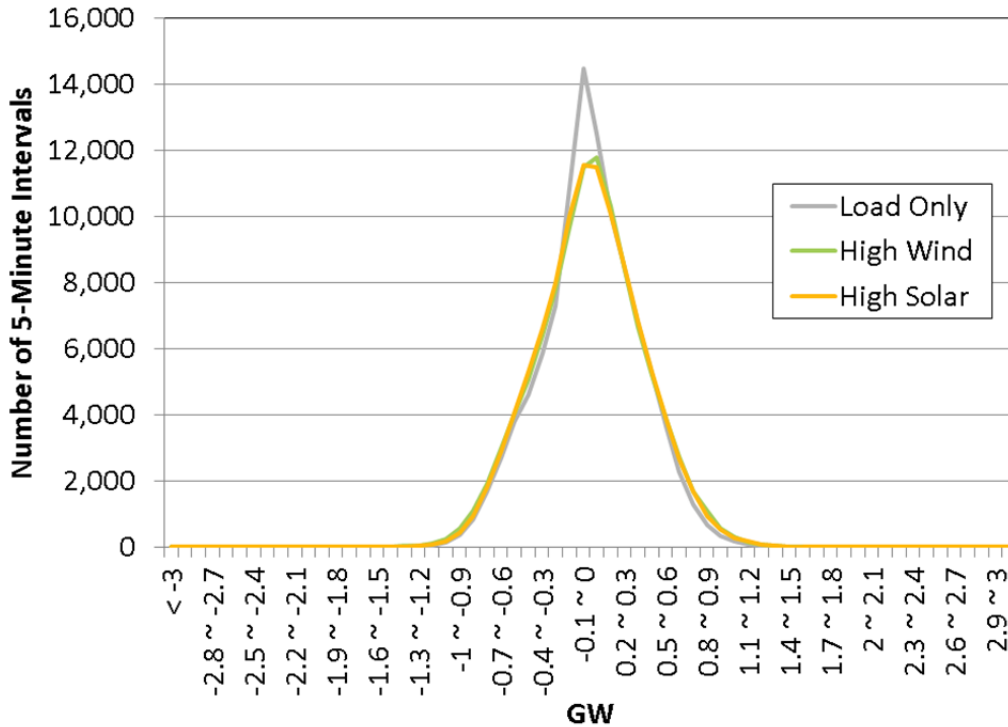
**Figure 31. Distribution of 5-minute changes
in load and net load for High Wind and High Solar Scenarios**

System operators can hold additional reserves to handle the increased variability from wind and PV. Wind flexibility reserve requirements are typically based on analysis of wind variability (EnerNex 2011; Milligan et al. 2011). Applying the same analytical techniques to solar would result in holding too much reserves because solar variability is dominated by the known diurnal variability. Therefore, we calculate flexibility reserve requirements based on the weather component of solar variability (Ibanez et al. 2013) as discussed in Section 5.

4.6 Weekly Time Series

Wind and solar tend to have a beneficial impact on the system in the summer months, when solar contributes to high summer peaks and winds tend to be moderate and complement the solar production. This can be seen in Figure 32, which shows the load, wind, PV, CSP, and resulting net load during a week in July. Additionally, because of the large number of generators online in the summer, significant resources are available to accommodate the variability and uncertainty of wind and solar.
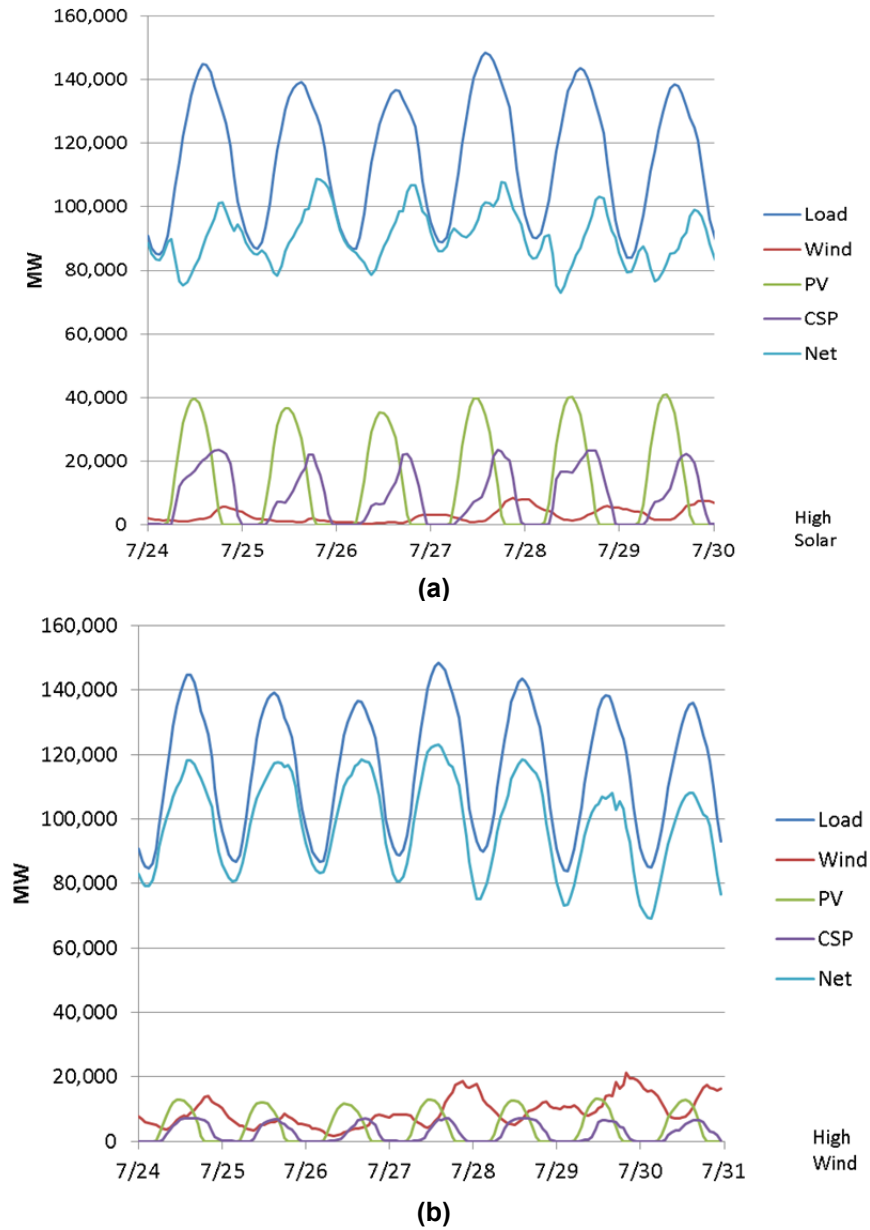
Figure 32. Profiles for the (a) High Solar and (b) High Wind Scenario for a week in July

In the spring, however, wind and solar tend to have a significant impact on the rest of the system. Both wind and solar output is high and loads are low in the spring in the Western Interconnection. Figure 33 shows the most challenging week of the year of data studied. Here most challenging is defined by the minimum net load condition (curtailment is not taken into account, so this is defined as load minus available wind and solar) that occurs on March 29. Note that the high solar production midday exacerbates the diurnal net load cycle, whereas wind production ramps more slowly over the course of several days. Because loads are low, fewer generators are online to help manage this variability, making this a challenging period for operators.
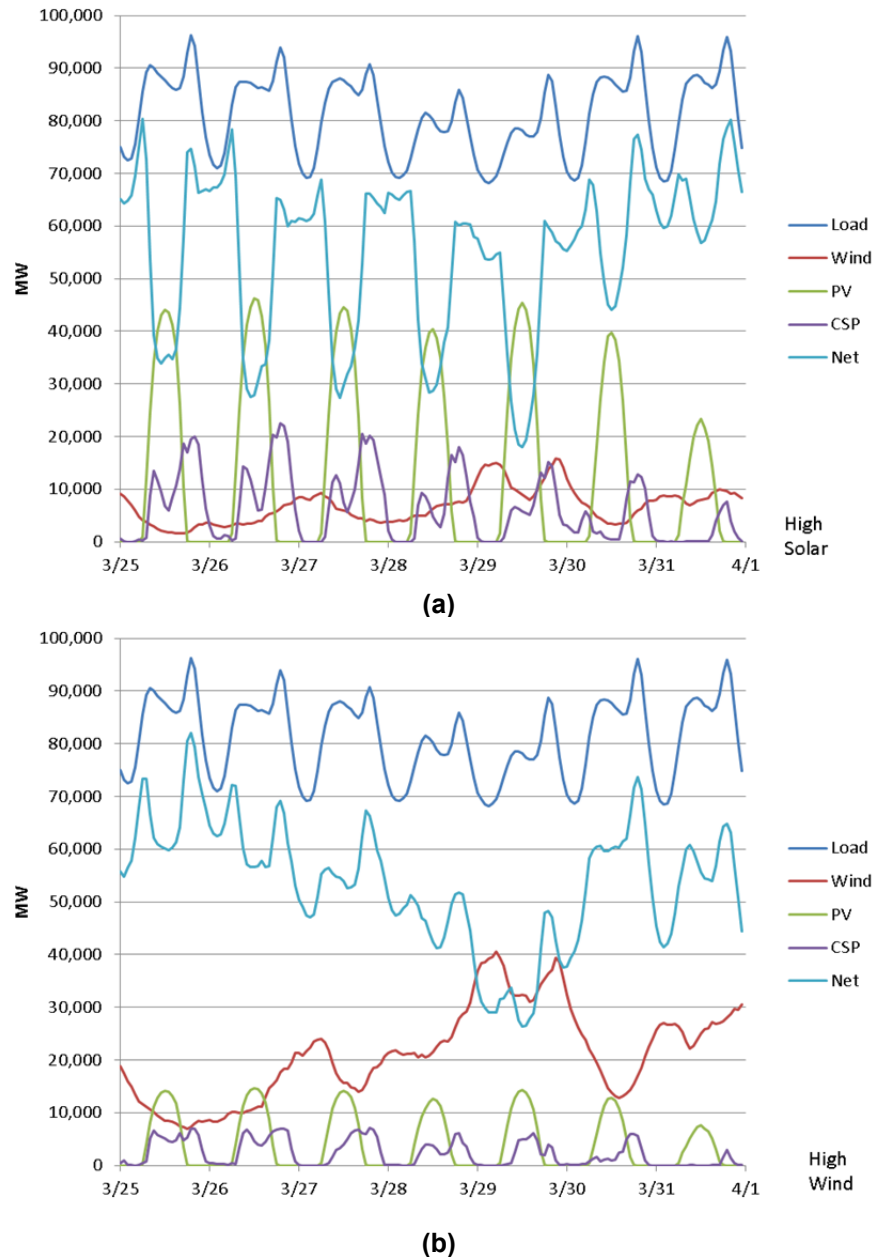
Figure 33. Profiles for the (a) High Solar and (b) High Wind Scenario for a week in March

4.7 Extreme Events

Most of the time, the power system can accommodate the variability and uncertainty of wind and solar, but extreme events can seriously challenge the system. Utility operators need to understand the nature of these extremes so they can plan accordingly. Extreme events can include the steepest ramps, the minimum net load, or the biggest forecast errors.

Figure 34 shows the hour with the highest net load up-ramp in the High Solar Scenario. A combination of the evening load ramp with sunset decreasing the solar output results in an up-ramp of 26,878 MW on February 2 at 16:00. System operators will need to have sufficient up-ramping capability to meet this up-ramp. Interestingly, the CSP thermal storage is not dispatched

60

by the production cost model to help meet that large up-ramp. Instead it is held until the next morning load rise when prices are higher. There was adequate up-ramp capability available during the net load up-ramp to keep prices reasonable so that the CSP storage was saved for the next morning, when prices were higher.
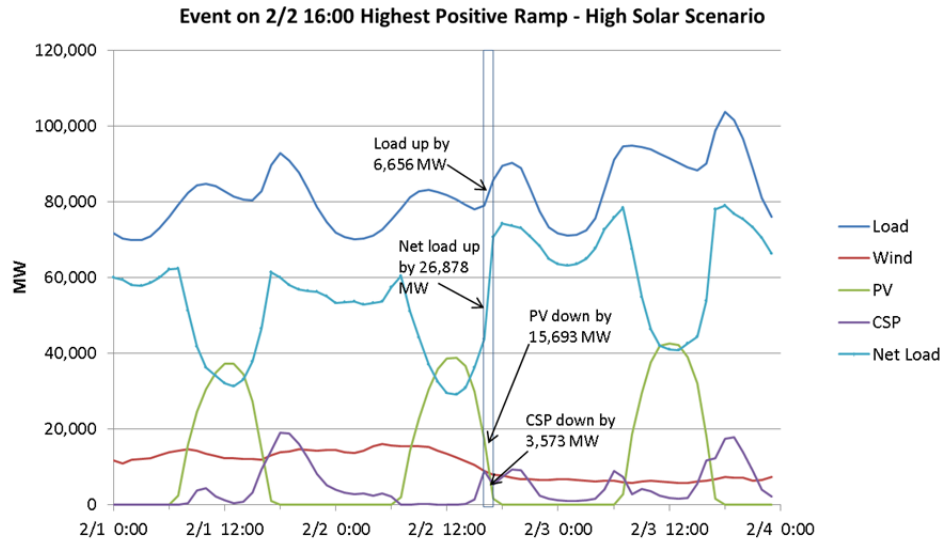
Figure 34. Highest hourly positive ramp (up-ramp) of 26,878 MW in the High Solar Scenario occurs on February 2 at 16:00

Figure 35 shows the largest down-ramp in the High Solar Scenario. Here sunrise causes a steep PV and CSP up-ramp, so that even though the load is increasing, the net load decreases sharply. If this ramp represents a potential problem to the system, a possible approach to mitigating sunrise ramps is to use solar as a resource for down reserves. This would be done by curtailing solar during the steep sunrise ramp.
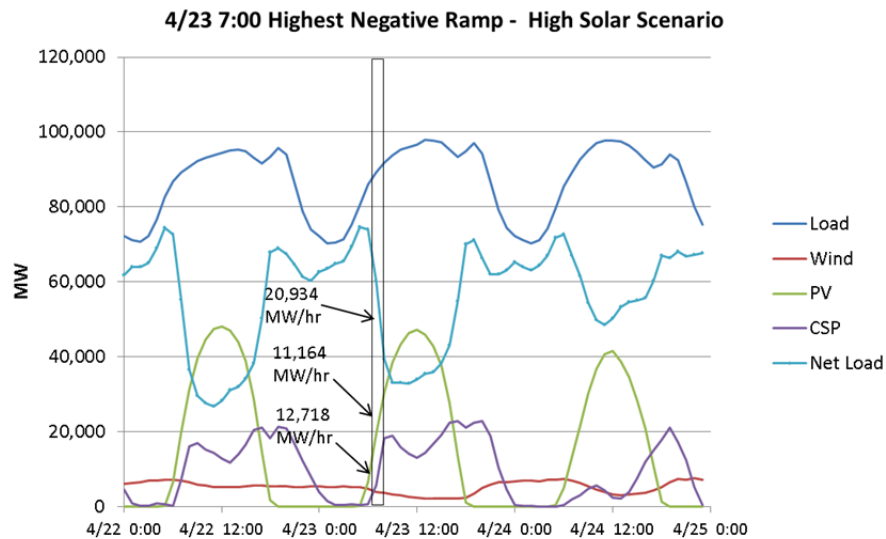
Figure 35. Highest hourly negative ramp (down-ramp) of 20,934 MW in the High Solar Scenario occurs on April 23 at 7:00

Figure 36 shows that the highest up-ramp occurs during the same hour for both the High Wind and High Solar Scenarios. Because the High Wind Scenario has less solar capacity, the up-ramp in this case is reduced to 13,533 MW.
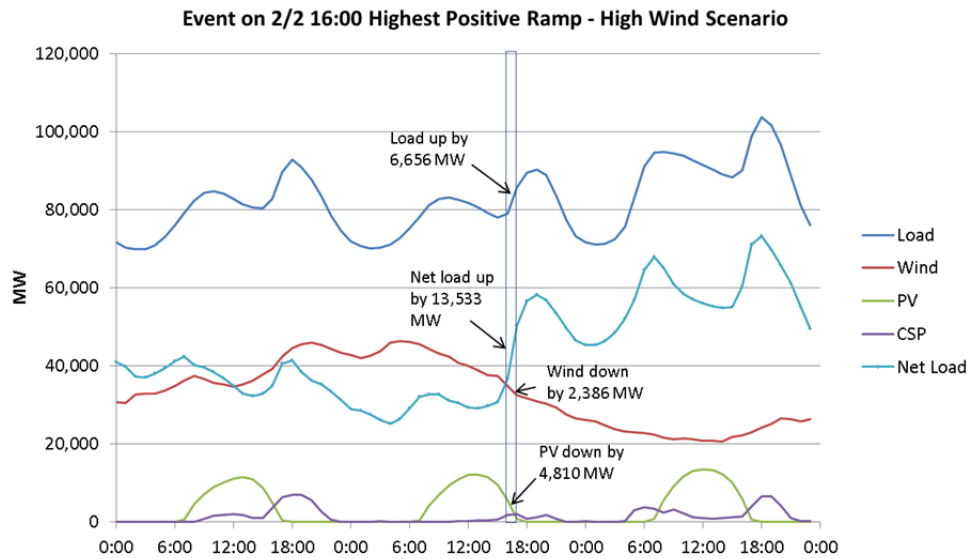
**Figure 36. The highest hourly up-ramp of 13,533 MW
in the High Wind Scenario occurred on February 2 at 16:00**

Figure 37 shows the biggest down-ramp in the High Wind Scenario. This occurred at night when the load was dropping off and wind output was increasing, resulting in a 1-hour 12,323-MW down-ramp. Interestingly, CSP storage was dispatched during this time, indicating that the ramp was manageable and did not lead to excessively low prices or curtailment.
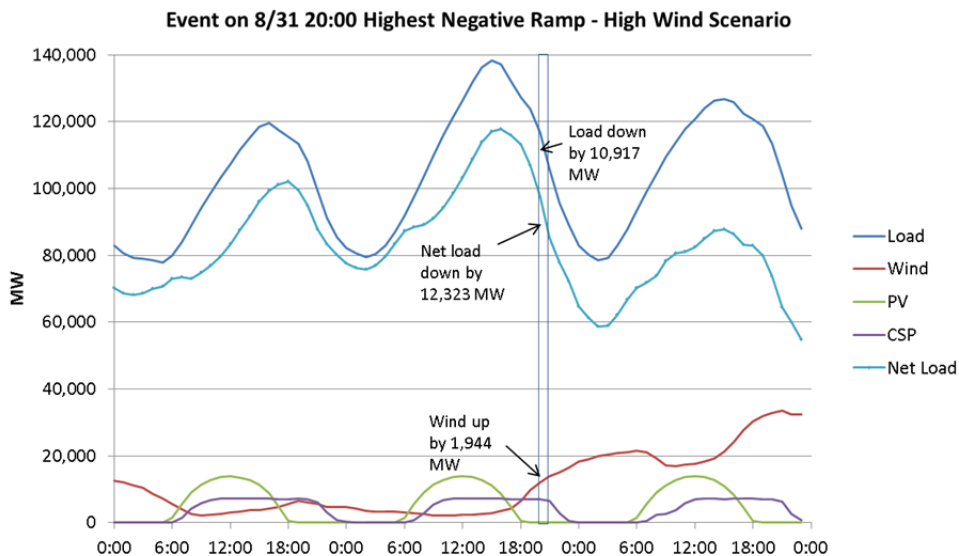
**Figure 37. The largest hourly down-ramp of 12,323 MW
in the High Wind Scenario occurred on August 31 at 20:00**

Minimum net loads are of concern, especially in this study, where we consider the impact of running fossil-fueled generators down to their minimums. System operators are currently accustomed to low net loads at night, especially if they have wind on their system. High solar penetrations change that. Figure 38 shows that the minimum net load condition in the High Solar Scenario occurs on March 29 at noon, caused primarily by high PV output and low springtime loads. CSP output is backed down and saved for the evening peak but some CSP output plus some wind output contributes to this condition.
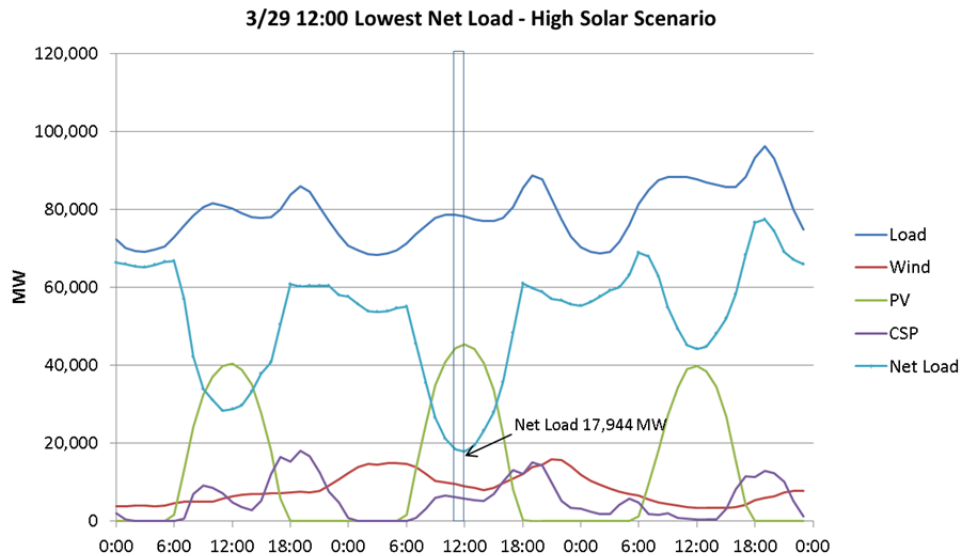
Figure 38. Minimum net load is 17,944 MW at noon on March 29 in the High Solar Scenario

Figure 39 shows that in the High Wind Scenario, the minimum net load condition occurs in the middle of the night, when loads are low and winter winds are high.
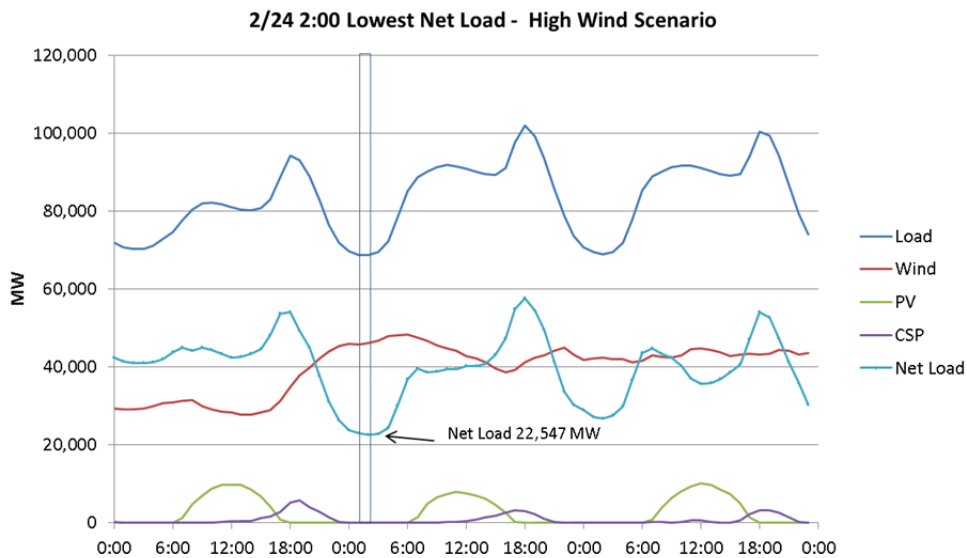
Figure 39. Minimum net load is 22,547 MW at 2:00 on February 24 in the High Wind Scenario

4.8 Day-Ahead Forecast Error Analysis

The accuracy of the DA forecasts for wind and solar strongly influence system operation, and especially system economics. Studies show that using DA forecasts in operations saves significant money in fuel costs (GE Energy 2010; GE Energy 2008; GE Energy 2007) by allowing conventional units to be decommitted if sufficient wind and solar production is forecast. This section addresses the DA forecast error statistics for this study.

The forecast error was calculated by subtracting the actual value realized from the DA forecasted value, so that positive forecast errors are over-forecasts and negative errors are under-forecasts. Figure 40 shows the forecast error distribution for the DA wind forecast. Note that with higher wind penetration, the distribution of errors spread out with a higher standard deviation.
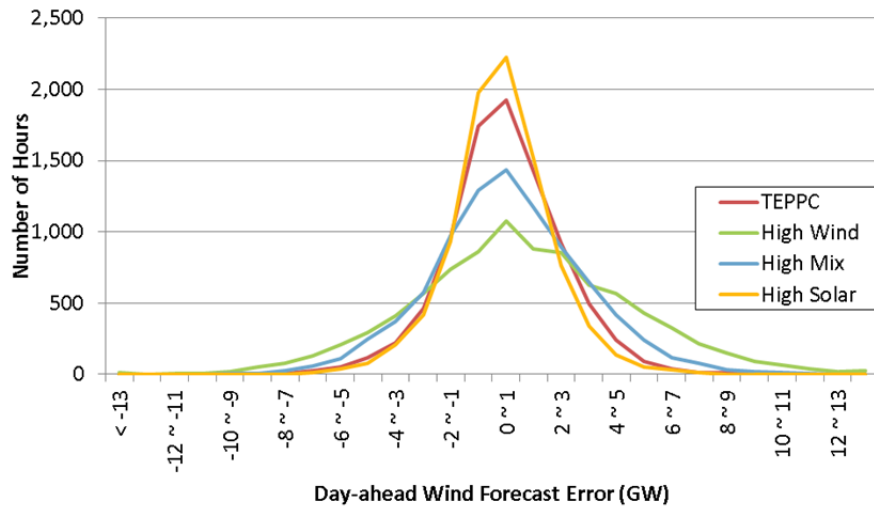
Figure 40. DA wind forecast error distribution for the U.S. Western Interconnection

Figure 41 shows the distribution of DA forecast error for PV. Nighttime hours were eliminated from this histogram calculation, so this represents about half as many hours as the wind distribution. This distribution is much tighter in general, with smaller tails showing that the solar forecasts seemed to be more accurate and had fewer extreme points. Note the difference in both x and y scales between the wind and PV error distribution plots.
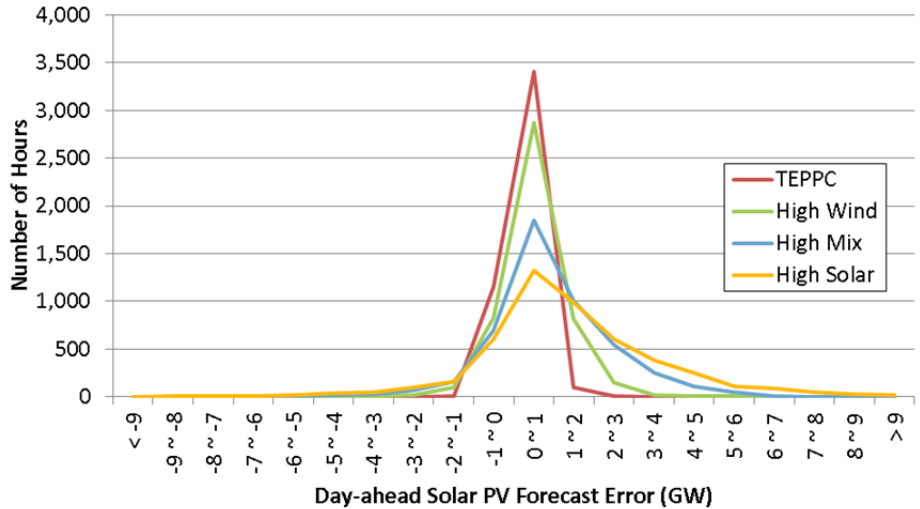
Figure 41. DA PV forecast error distribution for the U.S. Western Interconnection

Figure 42 shows the resulting distribution when the wind and PV data were combined and the total wind and PV forecast error was analyzed. The shape more closely resembles the wind distributions seen in Figure 40, but with even larger shoulders and tails.
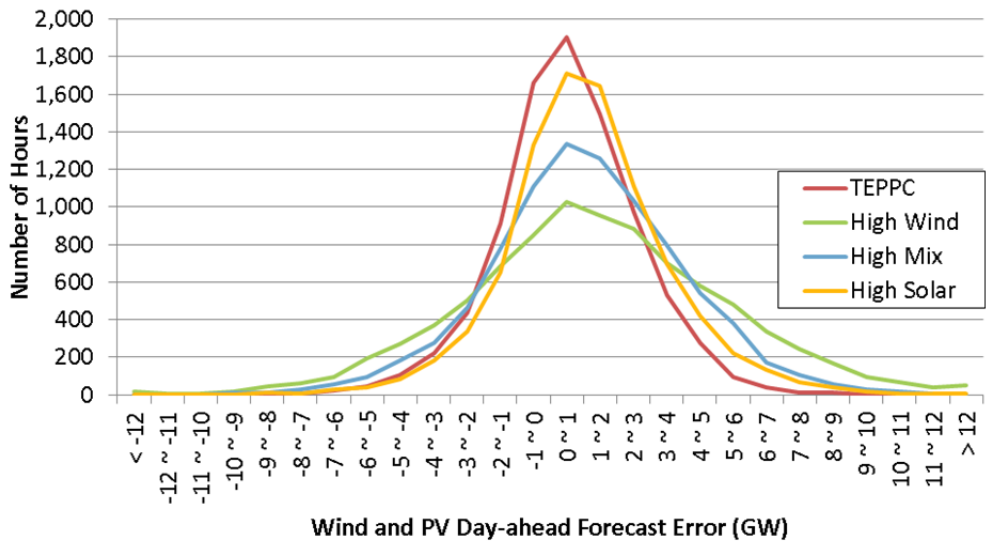
Figure 42. DA wind and PV forecast error distribution for the U.S. Western Interconnection

Figure 43 shows scatter plots of the total wind and PV forecast error plotted against net load for the entire U.S. Western Interconnection for the (a) High Solar and (b) High Wind Scenarios. In the High Solar Scenario, the highest forecast errors tended to occur with net load above the minimum of its range. This corresponded mainly to late morning to early afternoon hours, with which some of the highest uncertainty is associated. The most extreme errors seemed to occur in the winter and spring months.

High Solar Scenario – Total Forecast Error Versus Net Load

(a)

High Wind Scenario – Total Forecast Error Versus Net Load
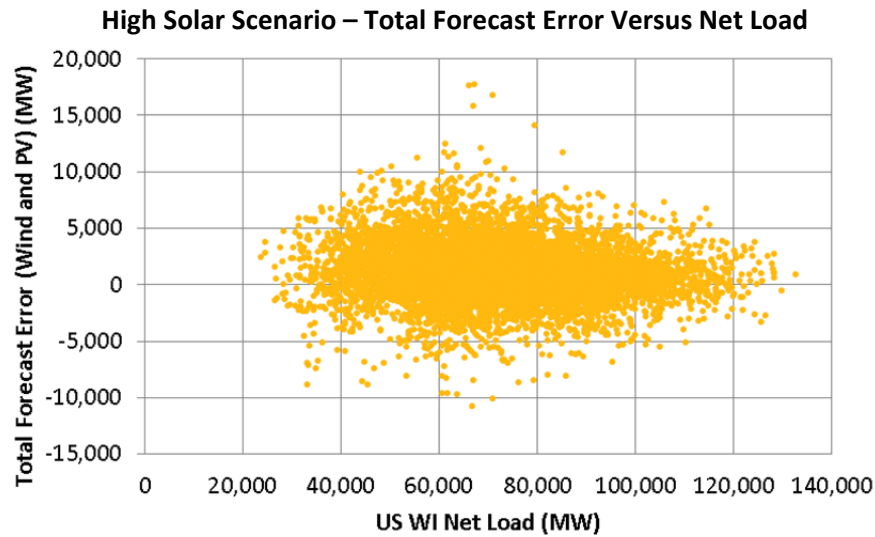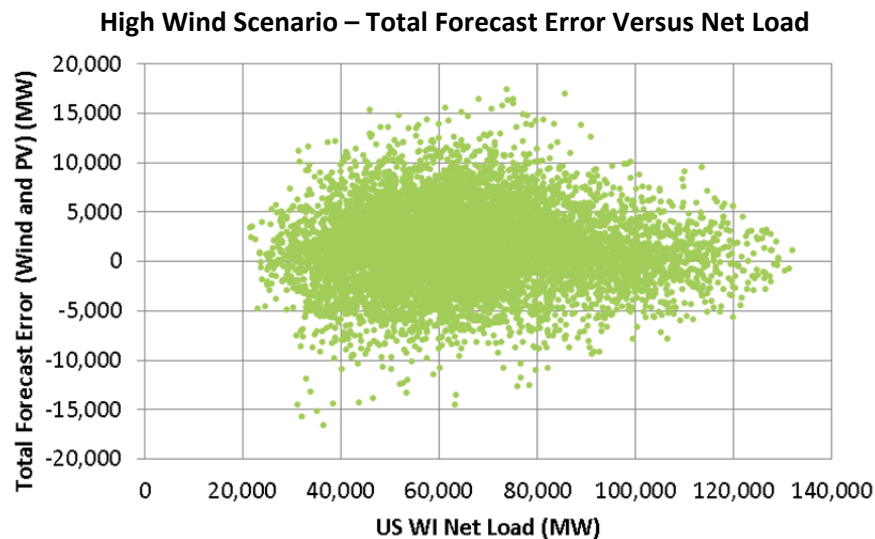
(b)

Figure 43. Total forecast error versus net load for the (a) High Solar and (b) High Wind Scenarios

Note: WI, Western Interconnection

The High Wind Scenario shows that the largest under-forecasts (negative values in Figure 43) seemed to occur at the low net load levels that would be associated with nighttime hours. Over-forecasts occurred most at mid-range net load levels, with the most extreme showing up in the late evening.

Table 13 gives the DA forecast error statistics for the High Solar Scenario. We measured the overall error characteristic using two values: the mean absolute error (MAE) and the root-mean-square error (RMSE). The table shows how these values changed for the various regions in the study as well as for the entire U.S. Western Interconnection.

Table 13. DA Forecast Error Statistics for the High Solar Scenario

Region	Capacity (MW)	MAE (MW)	MAE (%)	RMSE (MW)	RMSE (%)	Maximum Negative Error (MW)	Negative Error (%)	Maximum Positive Error (MW)	Maximum Positive Error (%)
Wind									
CAISO	4,406	451	10	649	15	−2,958	−67	2,384	54
CG	6,581	631	10	946	14	−5,101	−78	4,973	76
NTTG	5,787	495	9	711	12	−3,052	−53	3,807	66
WC	6,584	403	6	562	9	−2,726	−41	2,848	43
U.S. Western Interconnection	23,357	1,387	6	1,849	8	−8,458	−36	8,169	35
Solar (PV)									
CAISO	17,134	713	4	1,055	6	−5,310	−31	6,589	38
CG	1,211	105	9	156	13	−667	−55	619	51
NTTG	5,270	285	5	440	8	−2,103	−40	2,070	39
WC	36,526	1,248	3	1,771	5	−6,018	−16	9,189	25
U.S. Western Interconnection	60,141	1,882	3	2,628	4	−9,867	−16	16,974	28
Total									
CAISO	21,539	692	3	989	5	−5,243	−35	7,592	24
CG	7,792	639	8	947	12	−5,101	−64	4,973	65
NTTG	11,057	560	5	771	7	−3,169	−34	3,807	29
WC	43,110	936	2	1,435	3	−6,168	−22	9,576	14
U.S. Western Interconnection	83,498	2,004	2	2,676	3	−10,806	−21	17,714	13

Note that the error statistics (% MAE and % RMSE) were much higher for wind than for PV, but that the total errors tended to be closer for solar. The error statistics show that as the size of the regions increased, the error measures tended to decrease. This is because of the effects of aggregation of the error across large geographic areas. Table 14 shows these statistics for the High Wind Scenario.

67

Table 14. DA Forecast Error Statistics for the High Wind Scenario

Region	Capacity (MW)	MAE (MW)	MAE (%)	RMSE (MW)	RMSE (%)	Maximum Negative Error (MW)	Negative Error (%)	Maximum Positive Error (MW)	Maximum Positive Error (%)
Wind									
CAISO	7,970	693	9	977	12	−4,832	−61	3,756	47
CG	9,101	822	9	1,188	13	−6,587	−72	5,895	65
NTTG	16,854	1,179	7	1,582	9	−6,501	−39	7,584	45
WC	32,224	1,838	6	2,438	8	−9,558	−30	10,078	31
U.S. Western Interconnection	66,150	3,183	5	4,115	6	−16,574	−25	17,381	26
Solar (PV)									
CAISO	9,772	376	4	543	6	−2,776	−28	2,885	30
CG	969	82	8	121	12	−507	−52	491	51
NTTG	2,312	44	2	67	3	−377	−16	305	13
WC	14,979	369	2	520	3	−1,992	−13	2,356	16
U.S. Western Interconnection	28,032	660	2	909	3	−4,550	−16	5,340	19
Total									
CAISO	17,743	766	4	1,042	6	−4,879	−28	4,963	28
CG	10,070	825	8	1,188	12	−6,587	−59	5,895	65
NTTG	19,167	1,181	6	1,583	8	−6,501	−40	7,584	34
WC	47,203	1,875	4	2,477	5	−9,545	−21	10,078	20
U.S. Western Interconnection	94,183	3,229	3	4,161	4	−16,574	−18	17,381	18

Another view of the forecast errors shows when the errors are occurring. By averaging the total forecast error at each hour during each month and producing a contour plot of those data, we can see, on average, when the most severe errors occurred. Figure 44 shows this plot for the High Solar Scenario. The largest under-forecasts (blue colors) were most frequent on late summer afternoons and mid-evening in fall and early winter. The most severe over-forecasts (red color) occurred on winter afternoons. Generally there was a bias toward over-forecasting.

The High Wind Scenario presented a slightly different picture, as shown in Figure 45. The largest under-forecasts (blue color) occurred on late summer afternoons and evenings, with another peak in May around noon. The largest over-forecasts (red color) occurred at night in summer, with some occurring on the early spring mornings.
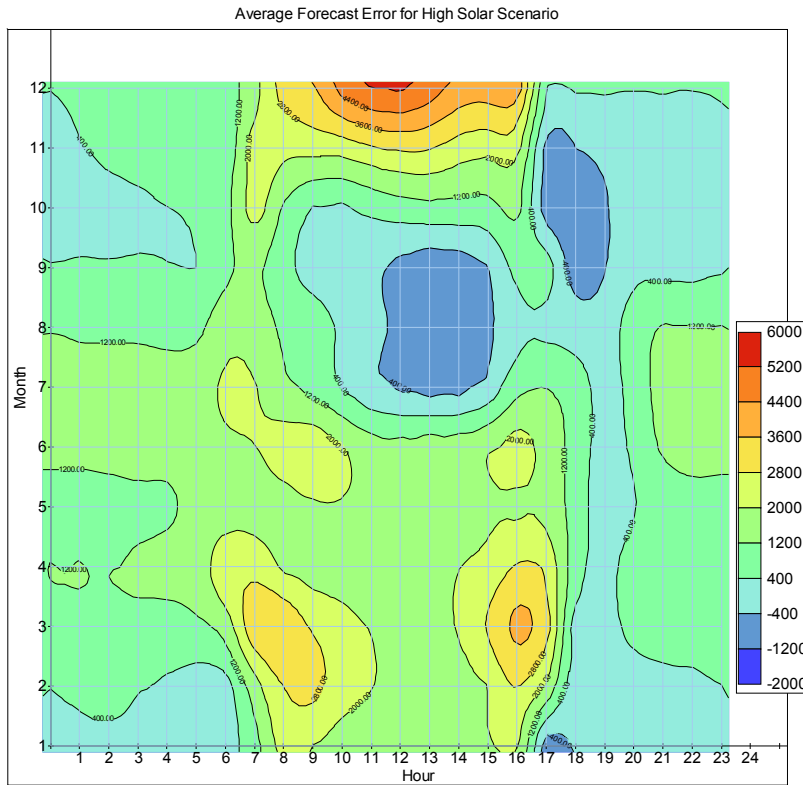
Figure 44. Contour plot of DA VG forecast errors for the High Solar Scenario
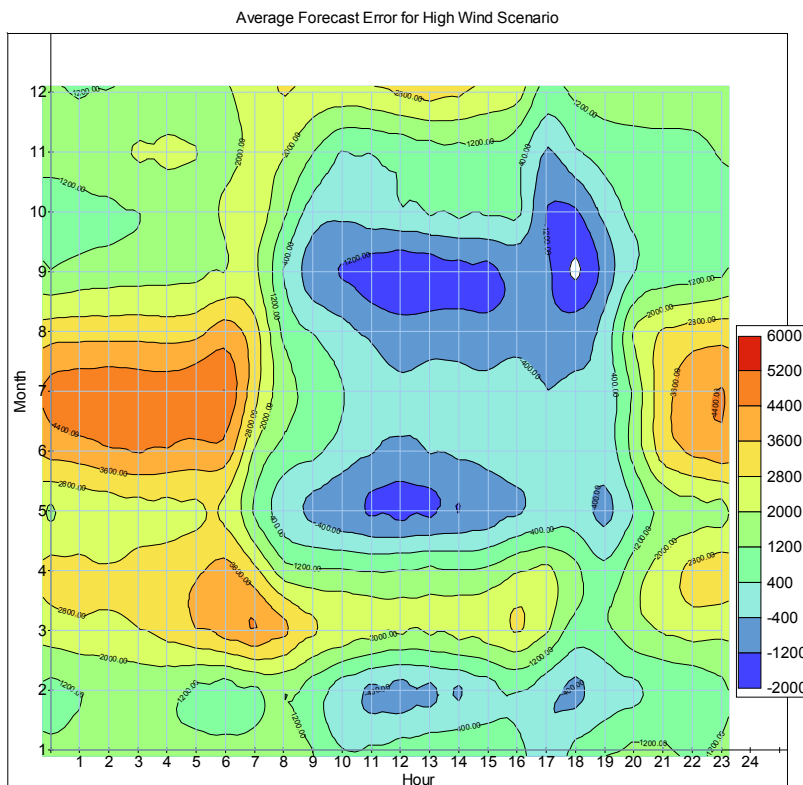
Figure 45. Contour plot of DA VG forecast errors for the High Wind Scenario

4.9 Four-Hour-Ahead Forecasts

Four-hour-ahead forecasts were used for a second unit commitment run performed with a 4-hour horizon. This run was able to commit units that could be started up within 4 hours, such as gas combined-cycle units. The 4HA forecasts that were developed for this purpose are described in Section 2.4.3.

As expected, the accuracy of the 4HA forecasts is considerably better than that of the DA forecasts. Comparing Figure 46 with Figure 40 shows a much narrower distribution of the wind forecast errors. Note the different scales on the two distributions. The standard deviation for the DA error for the High Wind Scenario is 3,972 MW; the standard deviation for the 4HA forecast error is 2,100 MW.
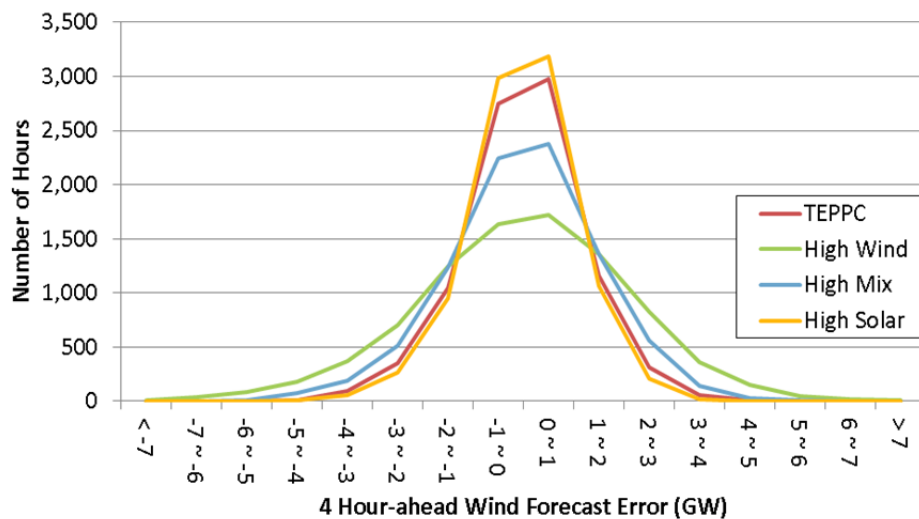
Figure 46. Four-hour-ahead wind forecast error distribution for the U.S. Western Interconnection

Figure 47 shows the distribution of forecast errors for the 4HA PV forecasts. Figure 47 can be compared to Figure 41, the equivalent plot for the DA forecasts. The standard deviation for the High Solar case is 1,038 MW; the same quantity for the DA forecast is 1,820 MW.
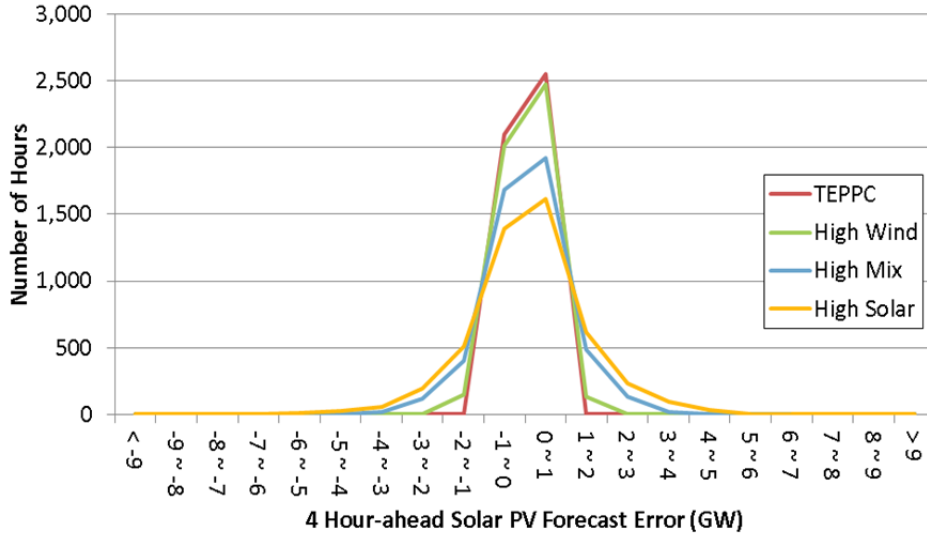
Figure 47. Four-hour-ahead PV forecast error distribution

Figure 48 shows the distribution for the 4HA wind plus PV forecast errors. Comparing this to Figure 42 again shows a large decrease in variability as measured by the width of the error distribution. The standard deviation of the error for the High Wind Scenario was decreased from 3,937 MW for the DA forecast to 2,115 MW for the 4HA forecast. *This illuminates the importance of the 4HA unit commitment. Recommitting plants to take advantage of significantly improved 4HA forecasts helps accommodate the uncertainty of wind and solar.*
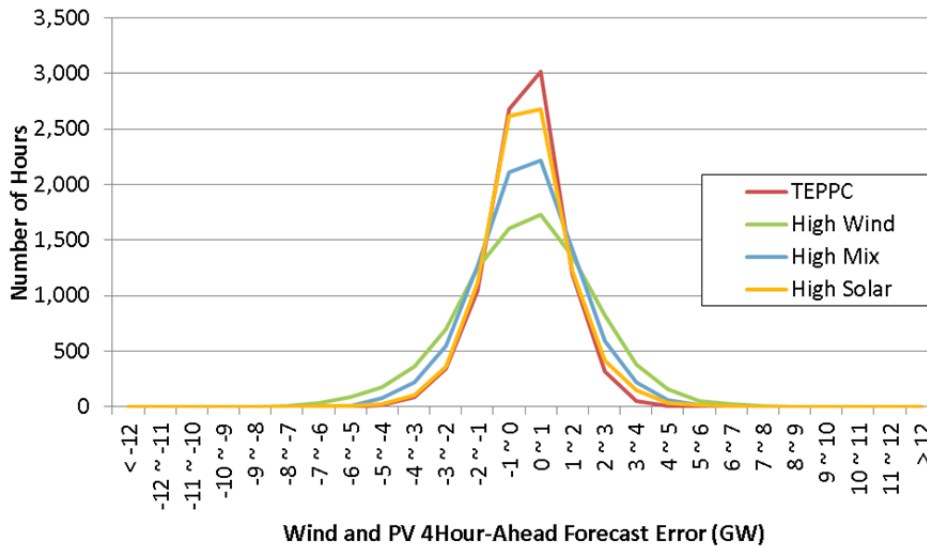
Figure 48. Four-hour-ahead wind plus PV forecast error distribution

Figure 49 shows a scatter plot of the 4HA total forecast errors compared to the system net load for the High Solar Scenario. Although the overall spread of the points was much narrower than the DA forecast error, several more extreme points were seen. These points are associated with 1 day in the data series.

71

High Solar Scenario – Total Forecast Error Versus Net Load
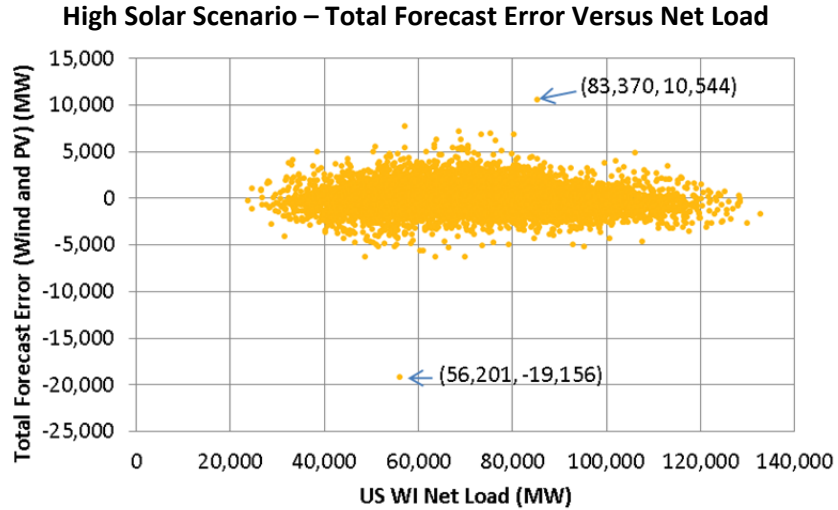
Figure 49. Four-hour-ahead wind plus PV forecast error scatter for the High Solar Scenario

The source of these extreme points is shown in Figure 50, which plots the two forecasts and the actual solar data for 1 day in October from the data set. The nearly 20,000-MW events appear to be legitimate misforecasts in hour 4 of the 4HA forecast that did not appear in the DA forecast. The 10,000 MW missed at hour 2 resulted from an unforecasted event that occurred in both forecasts. These misforecasts are caused by the methodology that we used to synthesize the 4HA forecasts (see Section 2). We used 2-hour persistence to synthesize the 4HA forecast but because there is no persistence to use in the first 2 hours as the sun rises, we had to use the DA forecast as a proxy. The very low actual output in solar hour 2, then, is picked up by the 2-hour persistence method and results in a significant misforecast. Commercial 4HA forecasts would not use such simplified methodologies and should result in more accurate forecasts.
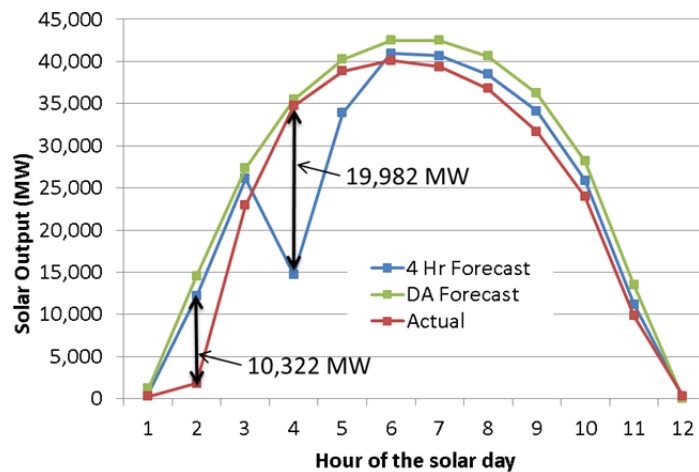
Figure 50. Detail of extreme 4HA solar forecast error caused by methodology used to generate 4HA forecasts

Figure 51 shows the scatter of 4HA total forecast errors for the High Wind Scenario. There is a range of roughly –8,000 MW to 8,000 MW in total forecast error compared to the ±17,000-MW range for the DA forecast shown in Figure 43 (b).

High Wind Scenario – Total Forecast Error Versus Net Load
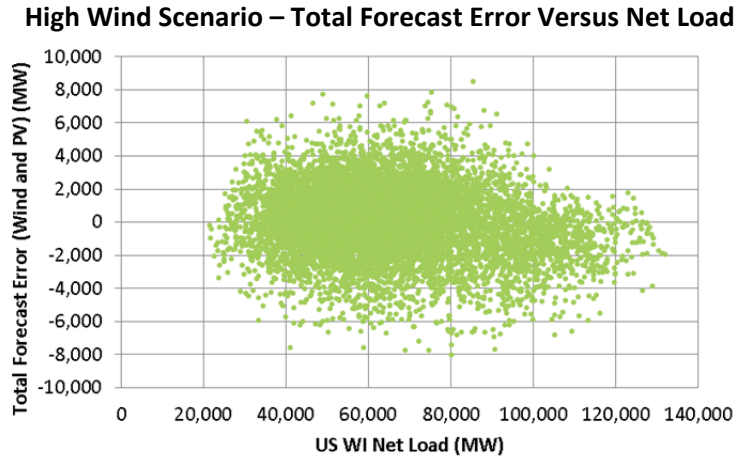
Figure 51. Four-hour-ahead forecast error scatter for the High Wind Scenario

Table 15 and Table 16 show the detailed statistics for the 4HA forecast errors for the High Solar and High Wind Scenarios. Comparing these tables to Table 13 and Table 14 further shows the reduction in error with the 4HA forecast.

Table 15. Four-Hour-Ahead Forecast Error Statistics for the High Solar Scenario

Region	Capacity (MW)	MAE (MW)	MAE (%)	RMSE (MW)	RMSE (%)	Maximum Negative Error (MW)	Negative Error (%)	Maximum Positive Error (MW)	Maximum Positive Error (%)
Wind									
CA	4,406	299	7	438	10	–2,306	–52	2,200	50
CG	6,581	312	5	454	7	–3,352	–51	2,485	38
NTTG	5,787	248	4	353	6	–2,102	–36	2,034	35
WC	6,584	269	4	356	5	–1,772	–27	1,688	26
U.S. Western Interconnection	23,357	785	3	1,038	4	–5,153	–22	4,280	18
Solar (PV)									
CA	17,134	418	2	597	3	–3,788	–22	2,658	16
CG	1,211	46	4	69	6	–339	–28	368	30
NTTG	5,270	157	3	249	5	–1,906	–36	1,573	30
WC	36,526	667	2	966	3	–14,380	-39	7,711	21
U.S. Western Interconnection	60,141	991	2	1,423	2	–19,982	–33	10,323	17
Total									
CA	21,539	424	2	596	3	–3,728	–17	3,247	15
CG	7,792	316	4	456	6	–3,352	–43	2,485	32
NTTG	11,057	282	3	392	4	–2,102	–19	2,040	18
WC	43,110	516	1	776	2	–13,643	–32	7,631	18
U.S. Western Interconnection	83,498	1,020	1	1,382	2	–19,156	–23	10,544	13

73

Table 16. Four-Hour-Ahead Forecast Error Statistics for the High Wind Scenario

Region	Capacity (MW)	MAE (MW)	MAE (%)	RMSE (MW)	RMSE (%)	Maximum Negative Error (MW)	Negative Error (%)	Maximum Positive Error (MW)	Maximum Positive Error (%)
Wind									
CA	7,970	441	6	619	8	−2,956	−37	3,052	38
CG	9,101	377	4	532	6	−3,464	−38	2,608	29
NTTG	16,854	550	3	725	4	−3,273	−19	3,878	23
WC	32,224	988	3	1,275	4	−5,691	−18	5,412	17
U.S. Western Interconnection	66,150	1,637	2	2,100	3	−7,864	−12	7,685	12
Solar (PV)									
CA	9,772	217	2	307	3	−1,596	−16	1,388	14
CG	969	37	4	55	6	−261	−27	300	31
NTTG	2,312	26	1	40	2	−232	−10	193	8
WC	14,979	201	1	289	2	−3,132	−21	1,880	13
U.S. Western Interconnection	28,032	352	1	496	2	−4,179	−15	2,617	9
Total									
CA	17,743	477	6	651	4	−2,853	−16	3,089	17
CG	10,070	378	4	533	5	−3,464	−34	2,608	26
NTTG	19,167	550	3	725	4	−3,273	−17	3,851	20
WC	47,203	990	3	1,281	3	−5,691	−12	5,412	11
U.S. Western Interconnection	94,183	1,650	2	2,115	2	−8,021	−9	8,499	9

5 Reserves

5.1 Operating Reserves

Operations of power systems occur at a range of timescales that can be summarized, from longer to shorter, as unit commitment, DA scheduling, load-following, and regulation (Ela et al. 2011). Unit commitment and scheduling are performed throughout days to economically commit the units in the system to meet forecasted load and other system requirements. During shorter periods of time (minutes to hours), the system redispatches its units to counteract deviations from the schedule through load-following. Similarly, traditional units are redispatched to perform regulation, which is the fast response of generators to changes that range from seconds to minutes.

The operator requires operating reserves so the system can positively respond to forecast errors and events that cannot be accounted for in the scheduling process. In the United States, the most common are regulation reserves, although load-following, or flexible, reserves are becoming more popular. Both are designed to account for the system's variability (expected changes in the system) and uncertainty (unexpected changes). Both load and conventional generators affect the variability and uncertainty through forecast errors and unexpected outages, respectively.

Wind and solar are variable and uncertain in nature because the unit output depends on ever-changing wind speeds and solar irradiance that cannot be perfectly predicted ahead of time. Consequently, high penetrations of these resources lead to an increase in reserves necessary in the system. These requirements are especially critical in long-term integration studies, such as the *Eastern Wind Integration and Transmission Study* (EnerNex 2011) or Phases 1 and 2 of the WWSIS, which simulate higher renewable energy penetrations than are seen in today's systems.

When treating reserves in this study, we determined the reserve requirements necessary to cover a significant level of uncertainty in wind and solar variability (Ibanez et al. 2013). The next part of our approach was adding these reserves appropriately to the requirements specified by TEPPC. The rest of this section follows this philosophy. Because the CSP plants have 6 hours of thermal storage that makes those plants dispatchable, albeit with constraints, we only increase reserves for the uncertainty and variability in the wind and PV output.

5.2 Wind Reserve Methodology

Previous work (Ela et al. 2011; EnerNex 2011) quantified the uncertainty of wind power. Because short-term variations in wind power output are small, persistence forecasts are a good predictor with which to calculate uncertainty. For instance, for an economic dispatch model run in 5-minute intervals (and assuming that 5 additional minutes are required to perform calculation and dispatch communication), 10-minute persistence forecasts would be used to estimate the uncertainty that the power system must be handle between dispatch points. The forecast errors can be calculated by comparing the forecasted and the actual power output.

Figure 52 shows that wind forecast errors are highest at moderate total wind production levels. Changes are expected to go up or down, and the wind turbine power curve is expected to be steepest at moderate wind speeds. In this study we only consider reserves caused by down-ramps from wind/solar because we assumed that excessive energy from wind and solar could be curtailed if the system was unable to accommodate it.

Confidence intervals (represented as red and blue lines) were used to determine up- and down-reserve requirements so that a certain percentage of occurrences were covered by the reserves. In Figure 52, the range of power (horizontal axis) was divided in 10 groups with the same number of points. For each group, the average power was calculated as well as the confidence intervals that covered 95% of forecast errors. The confidence intervals bands were then interpolated from the group averages. Beyond the first and last group mean point, the requirements were kept constant as a simplified conservative approach. A higher number of groups or a more sophisticated method (e.g., a moving window across the cloud of points) would yield a better fit around the lower and upper power regions.
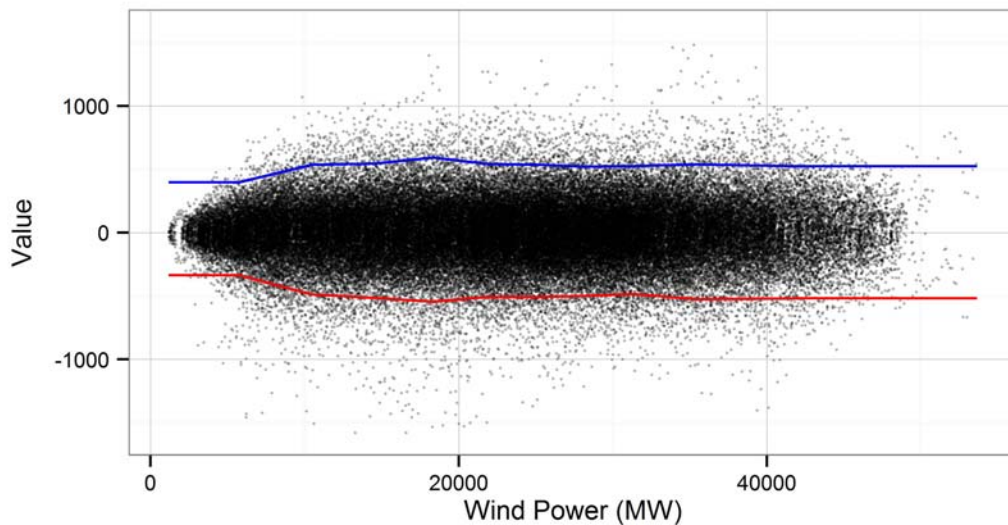
**Figure 52. Wind 10-minute forecast errors versus power output,
with 95% confidence interval bands for the High Solar Scenario**

The result was a dynamic determination of reserve requirements, as represented in Figure 53. The flexibility reserve requirements were based on 1-hour persistence forecasts. The confidence intervals covered 70% of events, which approximate levels of coverage used in past integration studies (EnerNex 2011).[3] Any remaining forecast error would be covered by online units not providing reserves or by offline quick-start units.

---

[3] The *Eastern Wind Integration and Transmission Study* (EnerNex 2011) assumed that spinning reserves covered 1 standard deviation of the 1-hour ramps. That coverage approximates to 70% under a normal distribution.
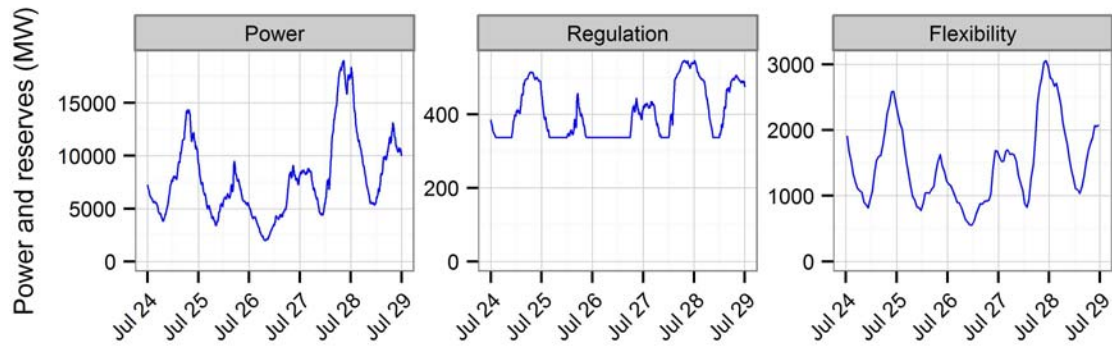
Figure 53. Wind power production and dynamic regulation and flexibility reserve requirement for the Western Interconnection in the High Wind Scenario

Note: Observe that the y-axis scales differ.

5.3 Solar Reserve Methodology

The proposed solar reserve methodology builds on the wind methods previously presented. Some adjustments were necessary to take into account solar daily patterns, but the process followed three distinct steps: (1) defining forecast error; (2) using explanatory variables to group similar patterns; and (3) applying the reserve requirements based on the explanatory variables.

As a reminder, the wind forecast errors were calculated based on persistence forecasts. Power output was used as an explanatory variable to find reserve requirements (Figure 52) and to create the dynamic reserve requirements (Figure 53). The following sections develop similar concepts for PV power.

5.3.1 Solar Forecast Errors

Solar-based generation presents clear patterns because of its dependency on the sun's path across the sky. These patterns are best captured with clear-sky simulations, which calculate the power output in the absence of clouds. The left panel in Figure 54 represents the actual and clear-sky power outputs in the Western Interconnection during three summer days in the High Solar Scenario. The right panel represents the 10-minute ramps in the same timescale.

77
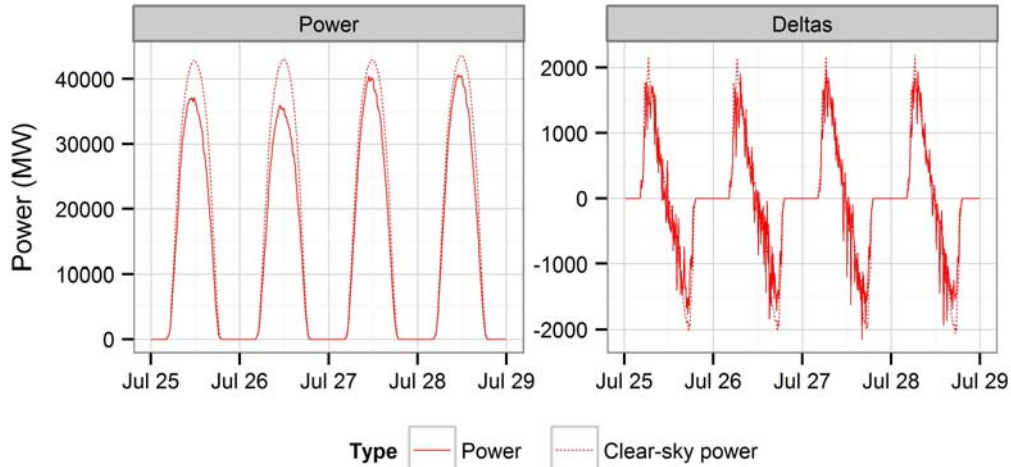
Figure 54. Power and clear-sky power output and ramps

If the same power-persistence forecast used for wind had been applied in this case, the largest demand for reserves would have occurred consistently around sunrise and sunset. However, reserves are not needed to cover known changes in power output because this is considered in the unit commitment. Figure 56 shows, however, that the power deltas could be decomposed into the contribution from the clear-sky power and a smaller, high-frequency variation because of weather. In other words, if the clear-sky trends (which are known) were removed from the power deltas, the reserve requirements would be smaller.

The first step in the creation of the short-term solar forecast was the definition of the solar power index (SPI), which represents the ratio between actual power, P, and clear-sky power, P_{CS}.

The forecast was based on the persistence of SPI. To obtain the forecast, we added the clear-sky ramp scaled by the SPI to the current power output. The forecast error could then be calculated as:

$$Error(t) = P(t+1) - \{P(t) + SPI(t) \times [P_{CS}(t+1) - P_{CS}(t)]\}$$
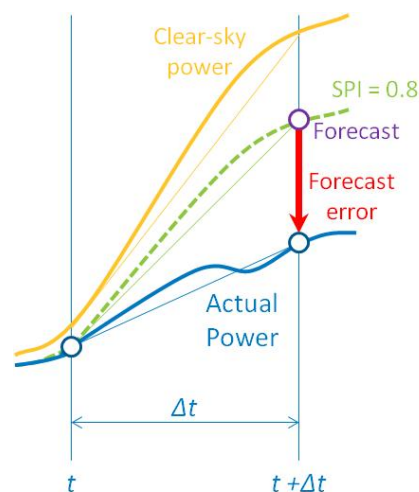
Figure 55. Graphical representation of short-term forecast for solar

78

Figure 56 shows the effect of using the clear-sky information to correct the short-term forecasts. The SPI persistence forecast has a much narrower distribution than the simpler power-persistence forecast and the standard deviation for both distributions are 274 and 1,273 MW, respectively. A more accurate short-term forecast ultimately leads to a significant reduction in reserve requirements. Clear-sky ramps will be met through the commitment of units with the remaining variability met through increased reserves, similar to the way that dispatch meets the forecasted load ramps and regulation is used only to meet load variations outside the forecasted ramps from one interval to the next.
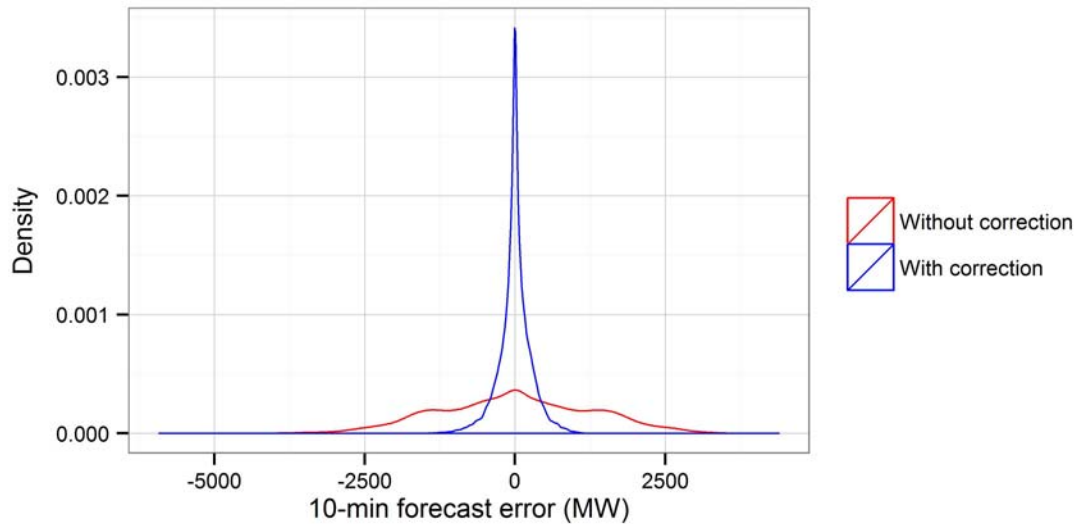
Figure 56. Ten-minute forecast error distribution with and without the clear-sky correction

5.3.2 Explanatory Variables

The challenge of determining suitable explanatory variables was finding the balance between the overall minimization of reserve requirements and simplicity. We found that the following two variables were especially effective at fulfilling this goal:

- SPI, as defined in the previous subsection, which effectively separated "cloudy" and "sunny" days

- Clear-sky ramps, which separated the different times of the day (positive in the morning, close to 0 at midday, and negative toward sunset).

For WWSIS-2, we calculated the reserves based on 5-minute time series. We first created 10 divisions; subsequently, we formed 100 groups by combining both variables. For each group, we calculated reserves by taking the appropriate percentiles (e.g., 2.5% and 97.5% to create 95% confidence intervals). To prevent outliers from dominating the reserves, we did not calculate reserves for a group if it presented less than 20 members. In that case, we used the reserves for the closest group instead.

We applied this method to all scenarios in WWSIS-2. We calculated regulation reserves using 10-minute time steps and 95% confidence intervals for the entire footprint. The results are represented in Figure 57, which suggests that reserve requirements depend on the combination of both explanatory variables, SPI and clear-sky ramps. The highest down-reserve requirements were usually located on the top right corner, which corresponded to sunrises where SPI was close to 1. On such occasions, the calculation of SPI was highly unstable given that the denominator (clear-sky power, P_{CS}) was very small. At times, the forecast called for a "sunny" sunrise, and the clear-sky correction was heavily weighted in the error calculation. The inability to produce a good forecast for these particular instances created the high reserve requirements. Figure 58 also shows that reserves were higher in the middle of days (clear-sky ramps close to 0) that were partly cloudy (SPI around 50%). For particularly sunny days (SPI close to 1), requirements were much smaller. Flexibility reserves were calculated for the different subregions using hourly time steps and 70% confidence intervals.
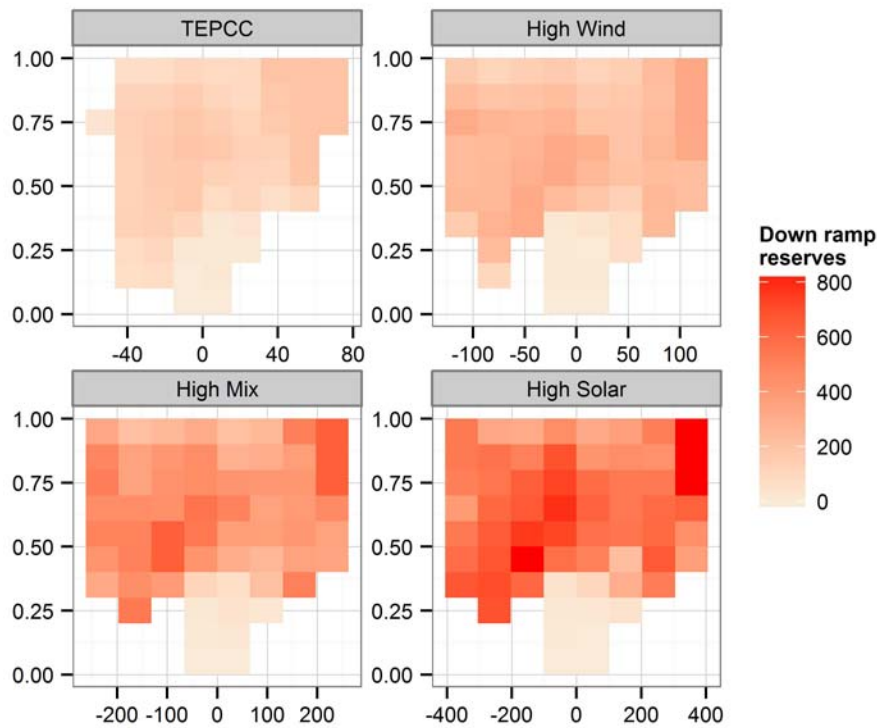
**Figure 57. Regulation reserve requirements by scenario
for the entire Western Interconnection**

5.3.3 Application of Reserve Requirements

After the reserve requirements were determined, they could be applied to the time series by finding the combination of the explanatory variables that best fit each point in time. For example, Figure 58 represents the resulting requirements for regulation and flexibility reserves in the Western Interconnection for selected days in July.
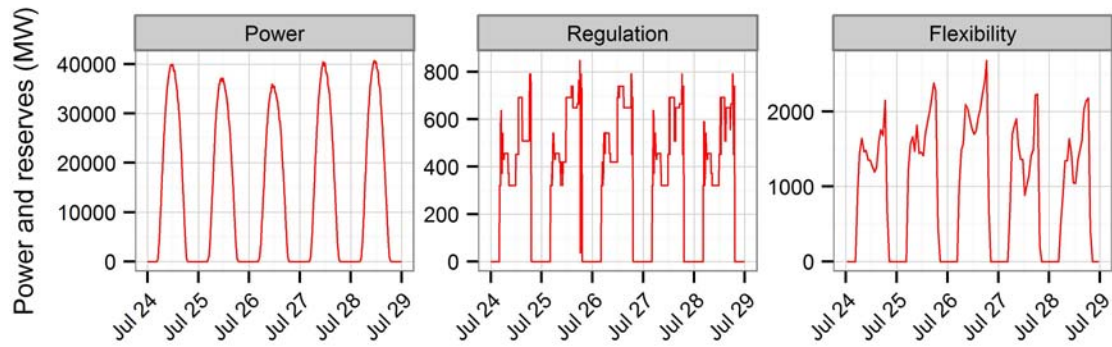
**Figure 58. Dynamic regulation and flexibility reserve requirements
for the Western Interconnection for the High Solar Scenario**

5.3.4 Total Reserve Requirements

The reserve methodologies for wind/solar were used, along with the base requirements for contingency and regulation reserves (as determined by WECC's TEPPC). Three types of spinning reserves were considered in this study and the total requirements were calculated as follows:

- Contingency reserves: 3% of the load with no consideration of wind/solar. The requirement was held for each zone independently.

- Regulation reserves: Geometric sum of base requirement (1% of load) and contribution of wind and PV (which cover 95% of 10-minute forecast errors). The requirement was held for the entire interconnection.

- Flexibility reserves: Geometric sum of wind and PV forecast errors (covering 70% of 1-hour errors). No load forecast was available, so load did not contribute to this requirement. The requirement was held for each zone independently.

The different requirements were added geometrically given that for short time steps, the forecast errors were considered to be uncorrelated. Table 17 summarizes the requirements for spinning reserve. Nonspinning reserves were not modeled in the study.

Table 17. Requirements for Spinning Reserves

Reserve	Calculation	Applied to
Contingency	$3\% \; load$	Zones
Regulation	$\sqrt{(1\% \; load)^2 + (Wind \; rqt)^2 + (PV \; rqt)^2}$	Interconnection
Flexibility	$\sqrt{(Wind \; rqt)^2 + (PV \; rqt)^2}$	Zones

Table 18 presents the total amounts of reserves required for each scenario. Contingency reserves remain unchanged. Total regulation reserves increase slightly and were higher with increasing penetration of wind. The distribution of reserves (Figure 59) shows that the High Solar Scenario presented the largest absolute requirement but, on average, requirements are lower.

81

Table 18. Total Amounts of Reserves

Scenario	Contingency (TW-h)	Regulation (TW-h)	Flexibility (TW-h)
No Renewables	29.44	9.81	0
TEPPC	29.44	10.14	10.45
High Wind	29.44	10.83	22.77
High Mix	29.44	10.61	17.83
High Solar	29.44	10.57	13.53
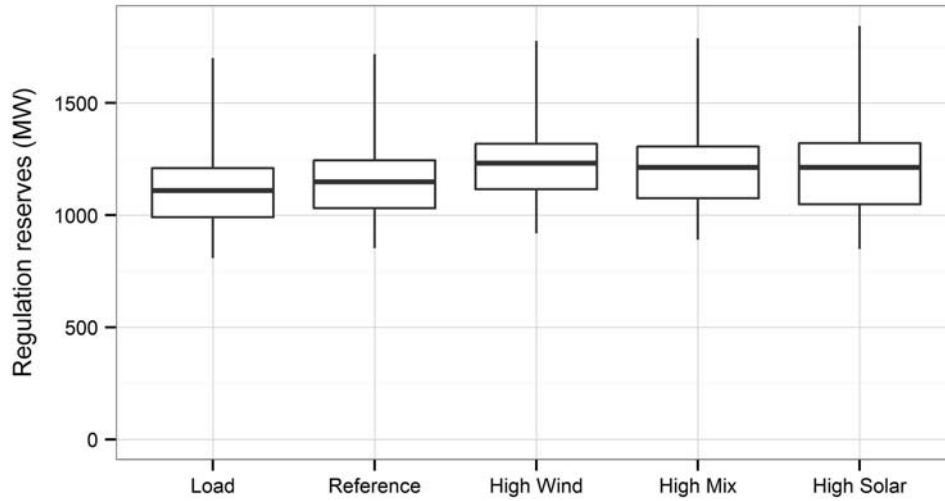
Figure 59. Distribution of regulation reserves by scenario

Note: The thick horizontal line is the median. The box shows the
25th to 75th percentile. The lines show the extent of the maximum and minimum.

Flexibility reserves only depend on wind/solar because of the absence of load forecasts. Table 18 and Figure 60 show that the larger uncertainty of wind drove the flexibility reserves.
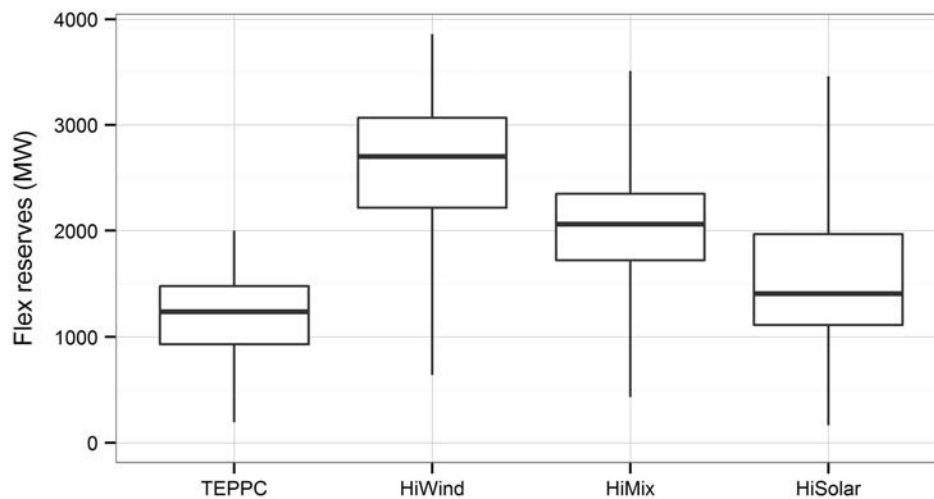
Figure 60. Distribution of flexibility reserve requirements by scenario
Note: The thick horizontal line is the median. The box shows the
25th to 75th percentile. The lines show the extent of the maximum and minimum.

Finally, Figure 61 combines the wind and PV power time series with regulation and reserve requirements for a few selected days in July. The total reserves are represented, along with the load, wind, and PV components. The geometric addition causes regulation requirements to be dominated by the load component. Wind components contribute more evenly, explaining the overall higher requirements. PV tends to fluctuate throughout the day.
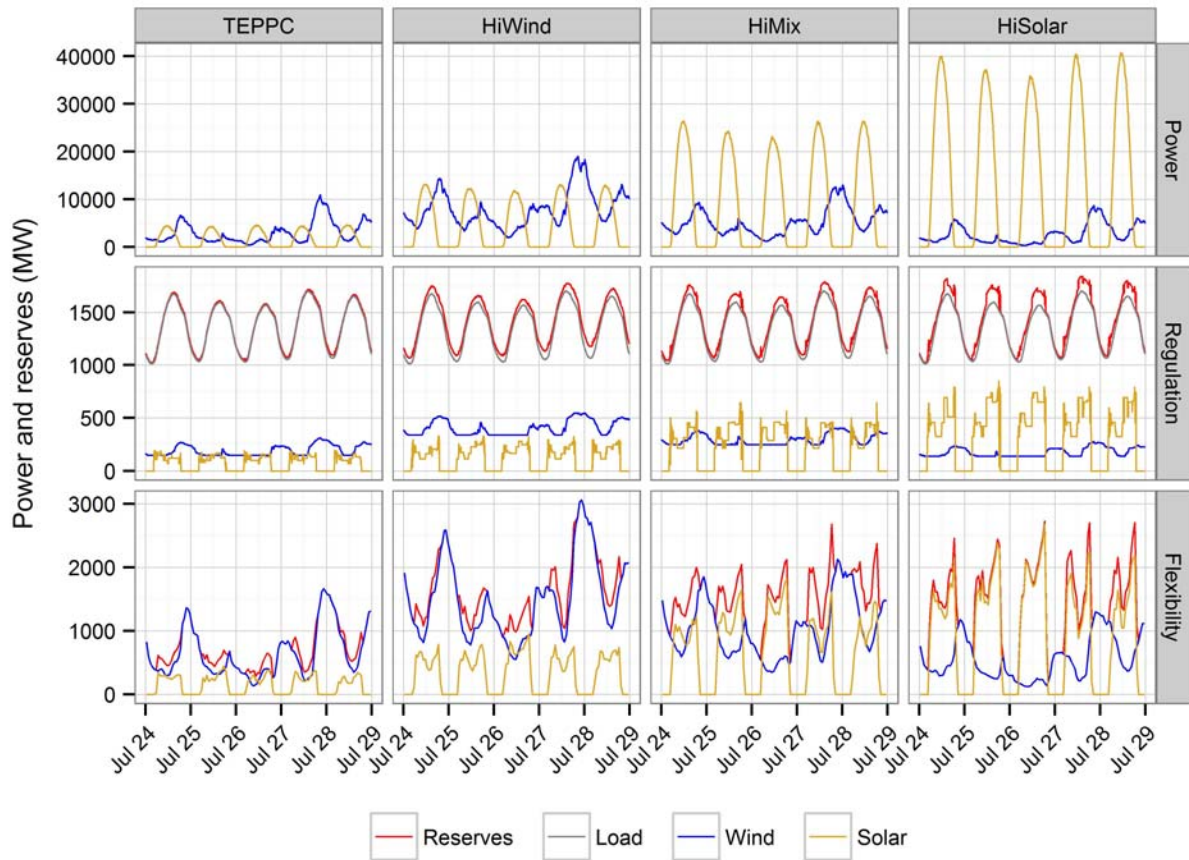
Figure 61. Power, regulation, and flexibility reserves for a few selected days in July, by scenario

6 Production Simulation Results

The results of running the unit commitment and economic dispatch modeling (using the PLEXOS model) are given in this section. All results are in 2011 nominal dollars.

6.1 System Dispatch

Dispatch stacks can be used to help understand how generators operate in various scenarios and how flexibility can be provided to handle variability and uncertainty in load and generation. System conditions vary greatly throughout the year, and Figure 62 through Figure 71 show 5-minute time-step dispatch stacks for the U.S. portion of the Western Interconnection for 2 significant weeks: the highest net load period of the year (during July) and the lowest net load period of the year (during March). Net load here was calculated *after* the system was dispatched, in contrast to in Section 4 where net load was calculated on the basis of total available wind/solar (before curtailment occurred). Table 19 shows weekly wind and solar penetration as a fraction of U.S. generation.

Table 19. Weekly Wind/Solar Energy Penetration During Sample Weeks

Scenario	Week of July 24 Penetration (%)	Week of March 25 Penetration (%)
No Renewables	0.0	0.0
TEPPC	7.9	16.2
High Wind	17.9	39.7
High Mix	21.8	38.1
High Solar	26.4	34.2

Figure 62 depicts dispatch for a week in July for the No Renewables Scenario. This shows essentially baseloaded operation of nuclear and coal units with mild load-following of the hydro units. The gas CC units pick up the bulk of the load-following duty with the gas CT units meeting the daily peak.
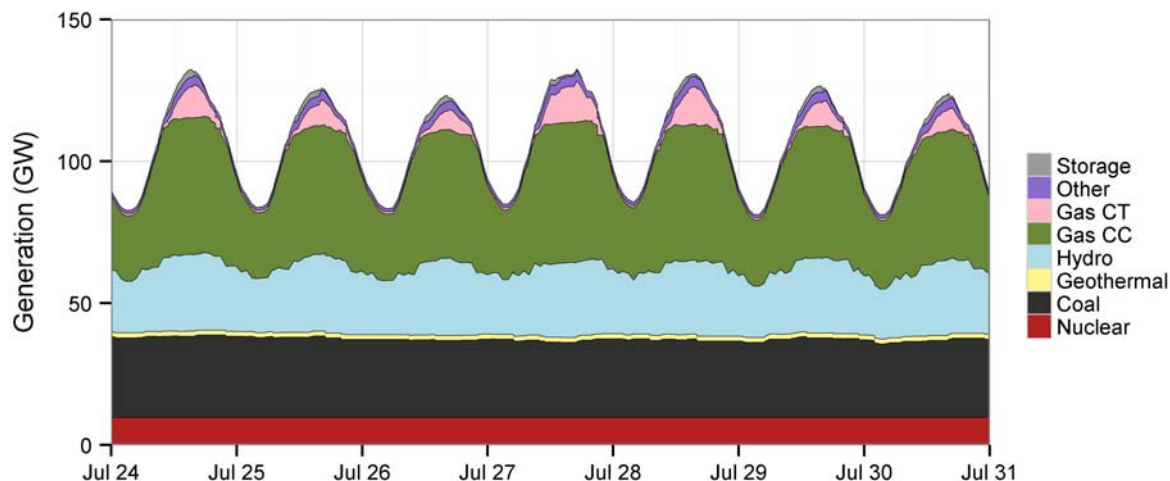
Figure 62. Summer dispatch stacks during the last week of July for the No Renewables Scenario

84

The TEPPC Scenario (shown in Figure 63) shows essentially the same operation of the existing units with renewable energy generation contributing a small amount to overall generation during this week with high load. Coal and hydro generation is unaffected by the additional wind/solar, which affect primarily the gas CC and CT units. Curtailment is negligible across scenarios for the week.
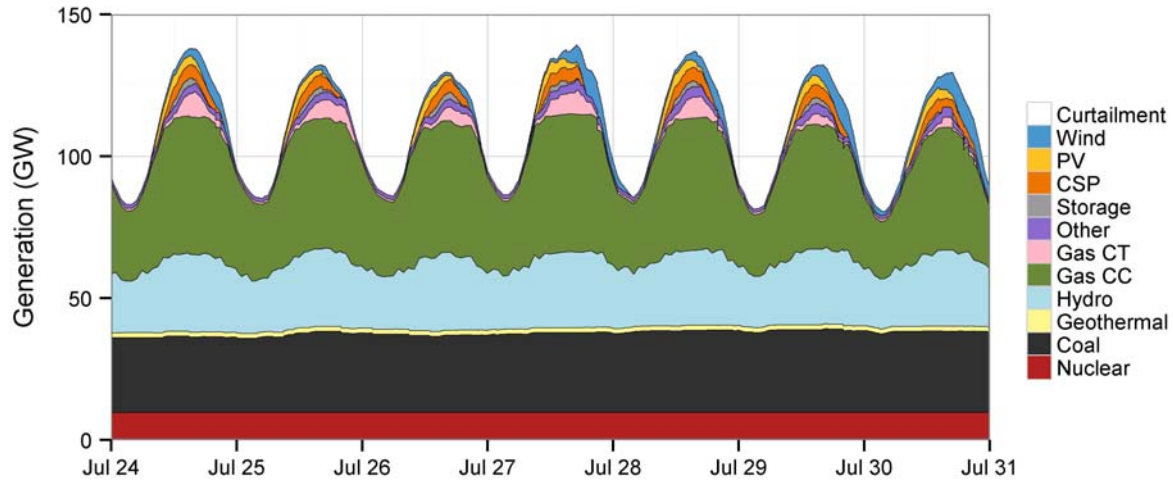
Figure 63. Summer dispatch stacks during the last week of July for the TEPPC Scenario

Figure 64 shows the same week in the High Wind Scenario. Impacts are modest, and the wind and solar mostly displace the CC and CT generation. Wind production picks up around the daily peak and drops off during the night and early morning.
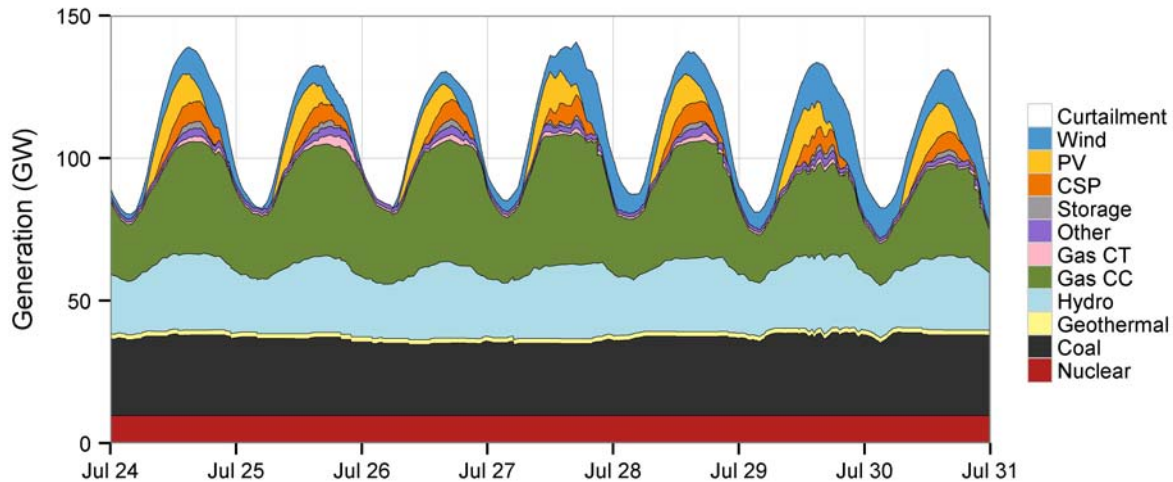
Figure 64. Summer dispatch stacks during the last week of July for the High Wind Scenario

Figure 65 shows the dispatch for the same week for the High Mix Scenario. Again, the CCs and CTs are mostly affected and displaced. The higher solar penetration in the summer helps to reduce the magnitude of the CC cycling.
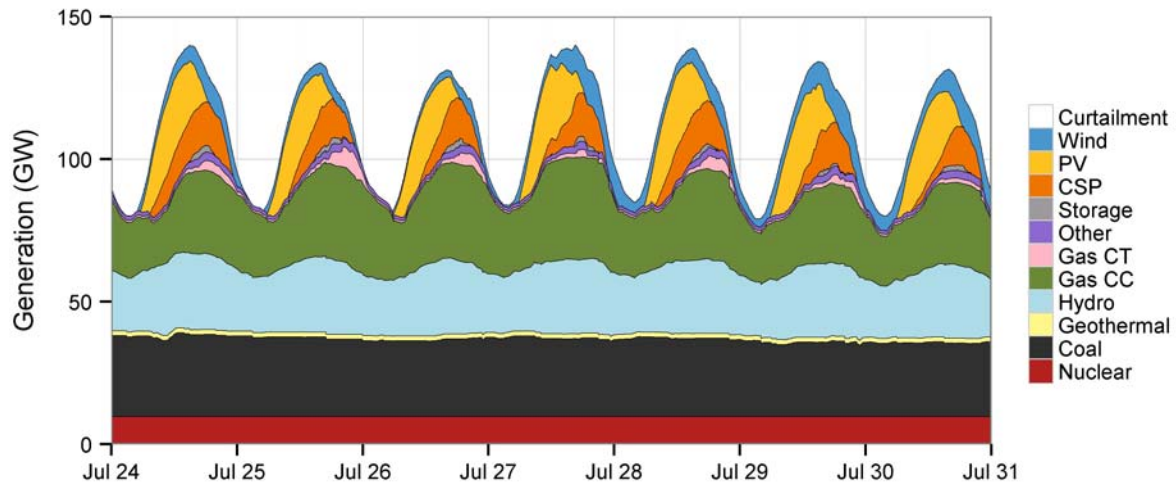
Figure 65. Summer dispatch stacks during the last week of July for the High Mix Scenario

Figure 66 shows the summer dispatch for the High Solar Scenario. In addition to the CCs and CTs, coal is also displaced by the solar generation. This occurs primarily in the late morning hours, when PV is generating near maximum capacity but load is still low compared to the peak. The coal units are not shut down in most cases; they are operated at lower generation levels.
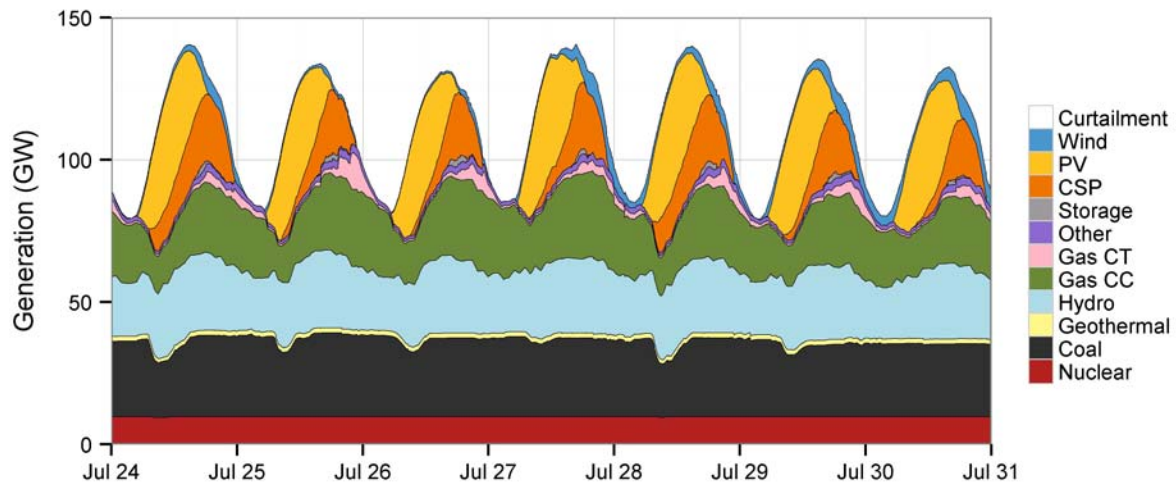
Figure 66. Summer dispatch stacks during the last week of July for the High Solar Scenario

As in WWSIS-1, spring is much more challenging for high-penetration scenarios than summer because the wind/solar output is high and the load is low. Figure 67 through Figure 71 show the dispatch stacks for a week in March. This week was selected for display because it represents the minimum net load condition, which occurs on March 29. The significant amount of wind on this day in the High Wind Scenario (Figure 69) displaces nearly all of the gas output and markedly cuts into the coal output, even starting to affect the nuclear units. The nuclear units were constrained to not run below 95%, so the impact on nuclear generation is small, although there are changes in the commitment of nuclear plants primarily because of the optimization of maintenance schedules for each scenario. On March 30, a significant DA wind forecast error occurs. Even though plenty of coal capacity is available, the coal units are not committed because of the DA forecast error (an over-forecast). Instead, the 4HA wind forecast foresees the reduction in wind and commits the CCs, which pick up the reduced wind output. The coal units do not get committed until later in the evening when load peaks.
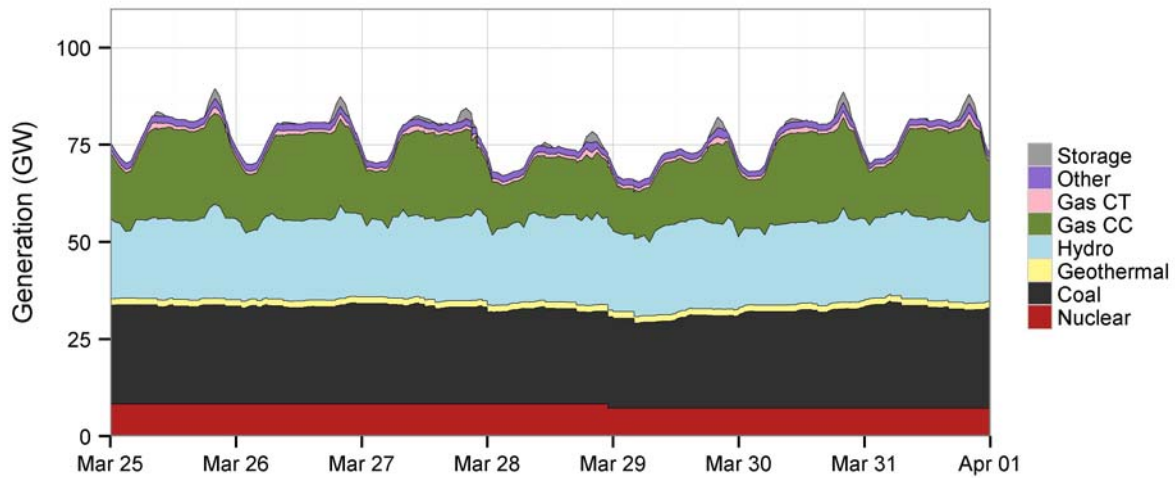
Figure 67. Spring dispatch stacks during the last week of March for the No Renewables Scenario
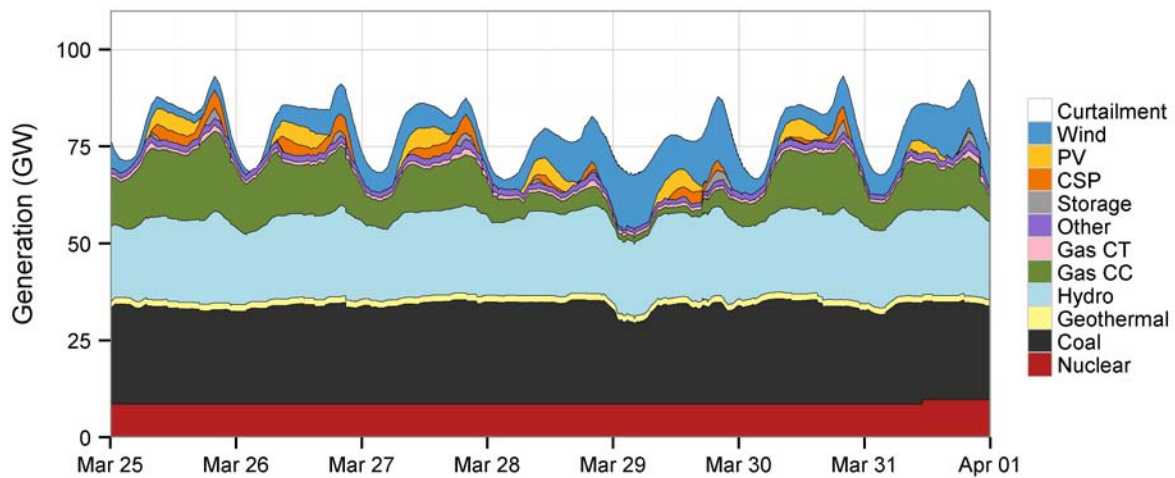
Figure 68. Spring dispatch stacks during the last week of March for the TEPPC Scenario
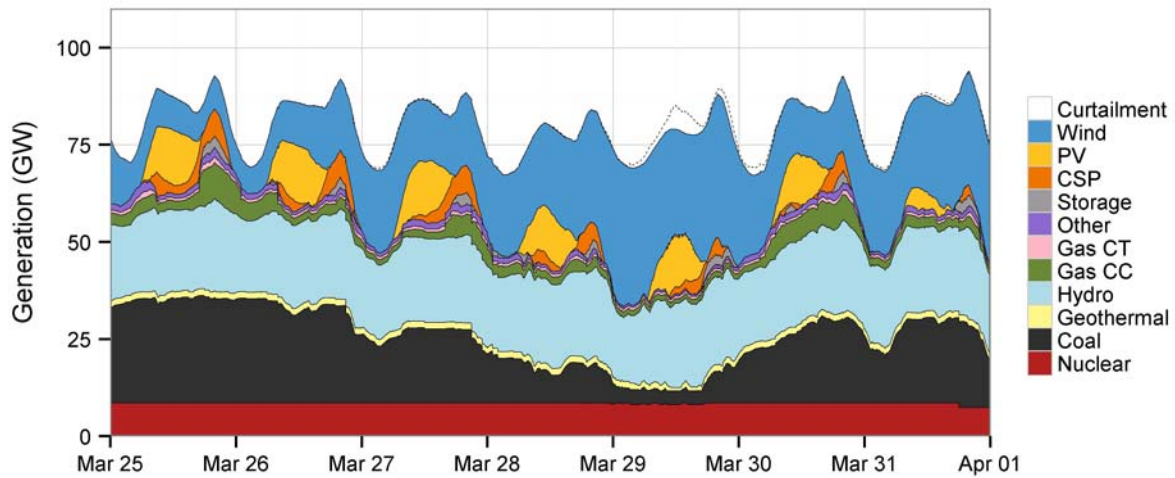
Figure 69. Spring dispatch stacks during the last week of March for the High Wind Scenario

Even the High Mix (Figure 70) and High Solar (Figure 71) Scenarios see low net loads during this time. The wind generation is high even at midday as the solar output is peaking, and this combination has a significant impact on the coal and gas units. In the High Solar Scenario, nearly all online coal generation is generating at minimum stable levels around noon each day, when PV output is the greatest but before load has peaked. Even with the coal at minimum stable levels, significant solar energy is still curtailed during the day as shown by the dotted line. This energy is curtailed partly because the start costs of coal generators do not justify turning them off in the morning and back on for the evening load peak.
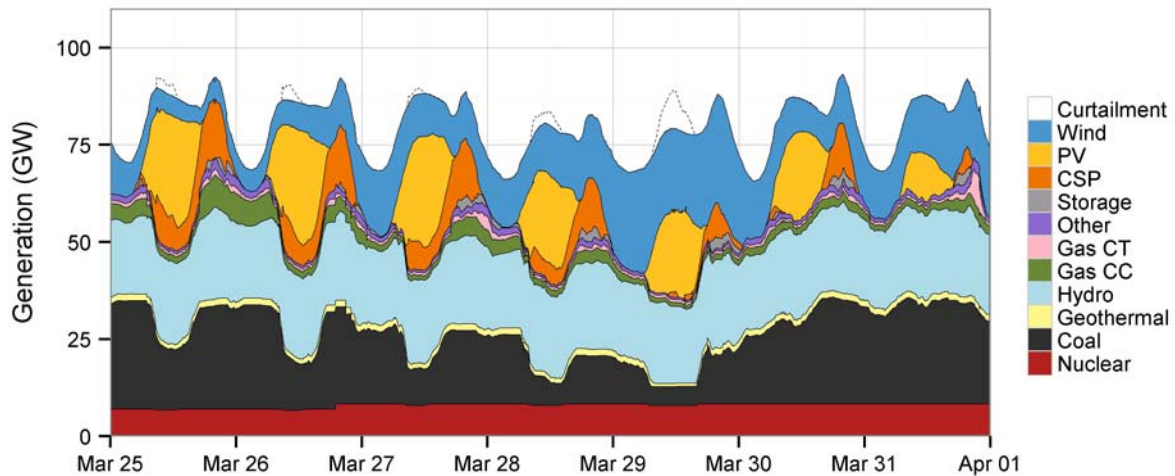
Figure 70. Spring dispatch stacks during the last week of March for the High Mix Scenario

88
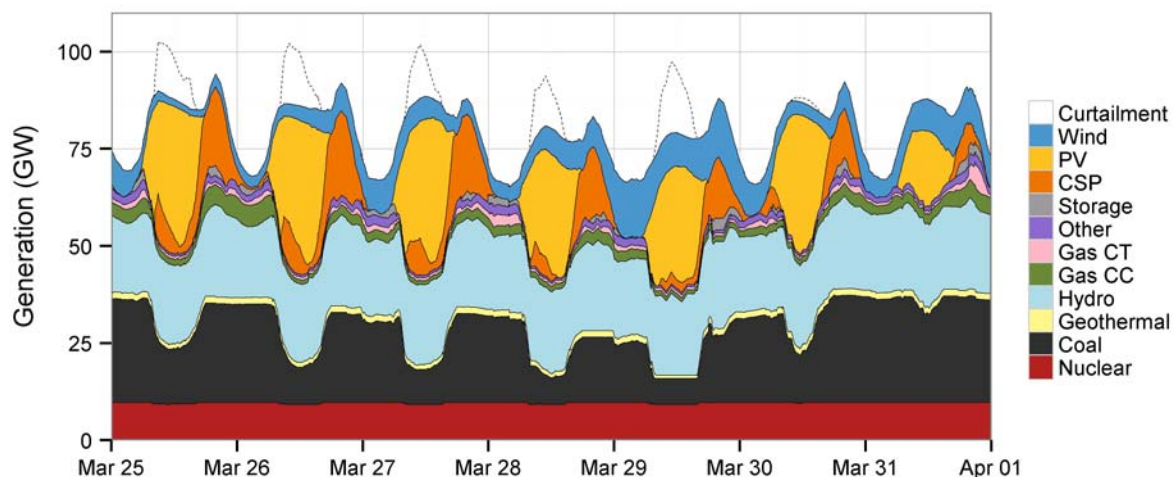
Figure 71. Spring dispatch stacks during the last week of March for the High Solar Scenario

The dispatch stacks show how the system uses the least expensive sources of supply-side flexibility to serve load and reserves in the presence of variability and uncertainty. System requirements in the spring differ greatly from those in the summer. In the summer, capacity is required more than flexibility, but in the spring, flexibility becomes more important. Flexibility can be provided to the system in a variety of ways:

- Cycling CTs—all scenarios
- Ramping and cycling CCs—TEPPC scenario
- Ramping coal on a daily basis—the High Solar Scenario
- Cycling coal on a weekly (or longer) basis[4]
- Curtailing renewable generators to avoid cycling coal generation—all high renewable scenarios
- Ramping hydro generation within its minimum and maximum generation constraints
- Utilizing storage (CSP thermal storage and pumped hydro storage) during high-load periods.

Figure 72 shows the dispatch of hydro, coal, CC, and CT generators during a spring and summer week. These plots help make direct comparisons between scenarios for different unit types.

---

[4] Many coal units were offline during the low net load event on March 29 in the High Wind Scenario.
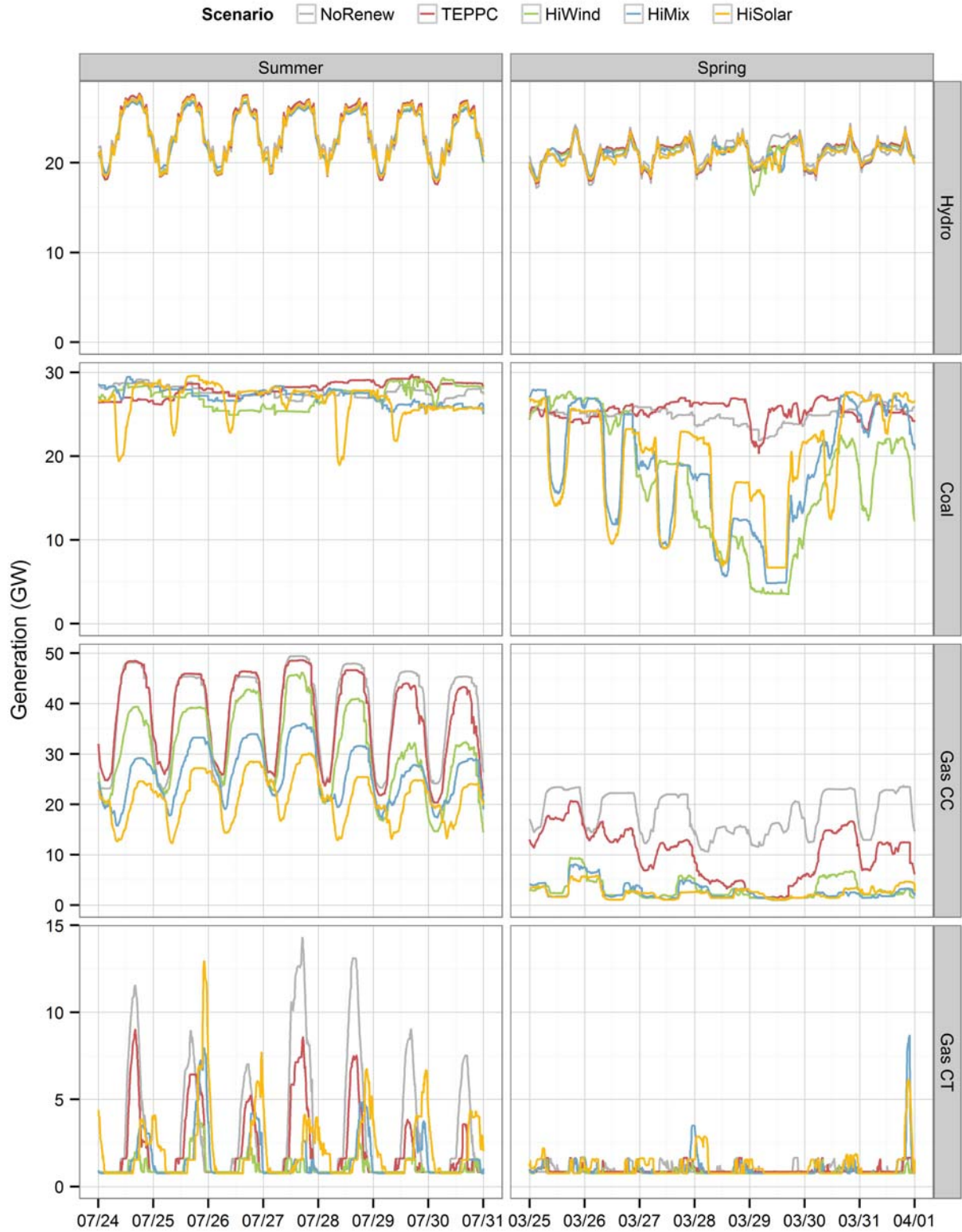
**Figure 72. Hydro, coal, gas CC, and gas CT dispatch
in the (left) summer and (right) spring for all scenarios**

90

The hydro units are used similarly in all scenarios. As explained in Section 4, the hydro dispatch is highly constrained. Compared to the week in March, the week in July sees higher maximum generation and similar minimum generation. The summer week shows very little variability between scenarios as net load peaks at similar times in all scenarios. The spring week has similar hydro dispatch in most scenarios, with the sharpest peaks and valleys occurring at slightly different times because the wind/solar varies between the scenarios.

Coal generation is dispatched similarly in the summer in most scenarios, although the High Solar Scenario does see some reduction just before noon most days that is not seen in the other scenarios. This reflects the net load reaching its minimum during those summer periods. In the spring, most coal units ramp on a diurnal basis down to minimum generation levels and back up to maximum capacity, especially in times of high wind/solar penetration. This cycling is most pronounced in the High Solar Scenario. Additionally, in all high renewable scenarios, there is some cycling of coal generators on an approximately weekly timescale. Although the coal units do not start much more in the high renewable scenarios, the units do ramp considerably more often. This ramping, described in more detail in this section, is the most significant change in how any generator type is operated with high renewable penetration.

Gas CC generators behave predictably in the summer. The dispatch of CCs in the No Renewables and TEPPC Scenarios is similar, and more solar penetration leads to increased displacement of CCs. The diurnal cycle of the generators ramping is similar in all scenarios, with the peak CC generation occurring later in the day with increasing solar penetration because the net load peaks after sunset in the scenarios with higher solar penetrations. In the spring, all scenarios show daily ramping of CC units. The high renewable scenarios show much less usage of the CC generators with less consistent patterns in the spring, however.

Gas CT generators are dispatched as peaker units in all scenarios, meaning that they are run for a relatively short period each time they are turned on, particularly in the spring. The CTs are used at a consistently later time of day in the High Solar Scenario because the PV reduces the net load until after sunset. About 1 GW of must-run CT generation is always online.

Figure 73 shows the CSP dispatch in the spring. This figure shows how the CSP thermal storage is used to minimize overall production costs. CSP often peaks once in the early morning hours, when prices are high before PV generation comes online. During the midday hours, CSP generates at a lower level because PV generation is high and net load and prices are low. The largest peak comes during evening hours when the PV generation is zero, load is still high, and prices are typically the highest.
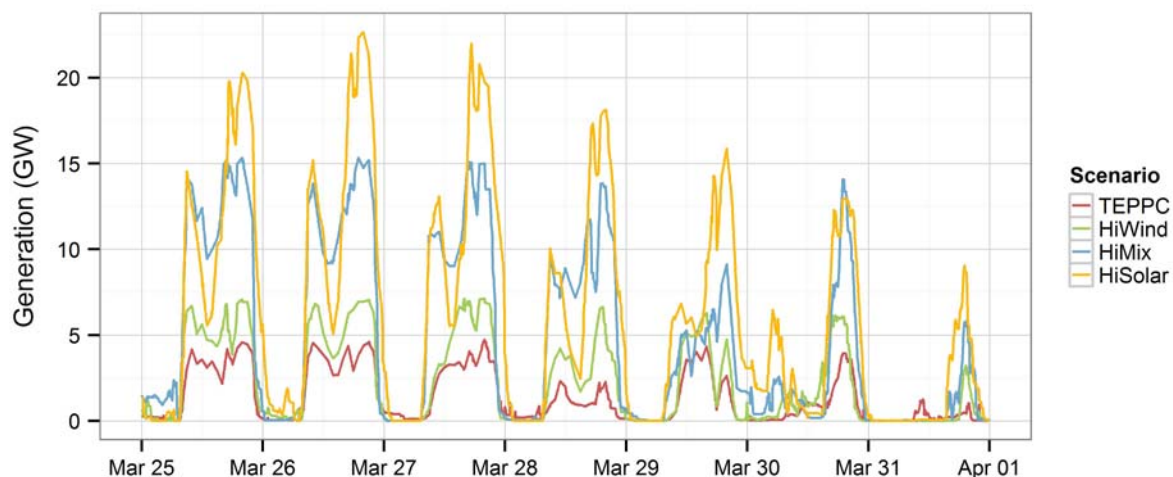
Figure 73. CSP dispatch in the spring for all scenarios

The electric power system provides supply-side flexibility in a number of ways. Cycling is one of those methods, along with hydro flexibility, storage dispatch, and curtailment of renewable resources.

6.2 Generation

This section examines the results of simulating the operation of the Western Interconnection for 2006. Figure 74 shows the wind/solar penetration for each scenario. Penetration targets of 33% were set based on the average wind and solar profiles over the 3 years: 2004, 2005, and 2006. Penetration does not total 33% because 2006 was a better wind year and a worse solar year than the 2004–2006 average. Also, CSP curtailment is not included on this plot because some of the curtailment is built into the design of the unit based on the ratio of storage size to turbine size. This explains the discrepancy between wind/solar penetrations in these high-penetration scenarios. Curtailment, which is modest, is described in detail in Section 6.7. All results in WWSIS-2 use hourly and 5-minute profiles for load, wind, PV, and CSP generation based on 2006 meteorological profiles. WWSIS-1 studied 2004 and 2005 as well and found no difference in the major results between the different years, but future work could examine the meteorological profiles of 2004 and 2005 using WWSIS-2 models and methodologies.
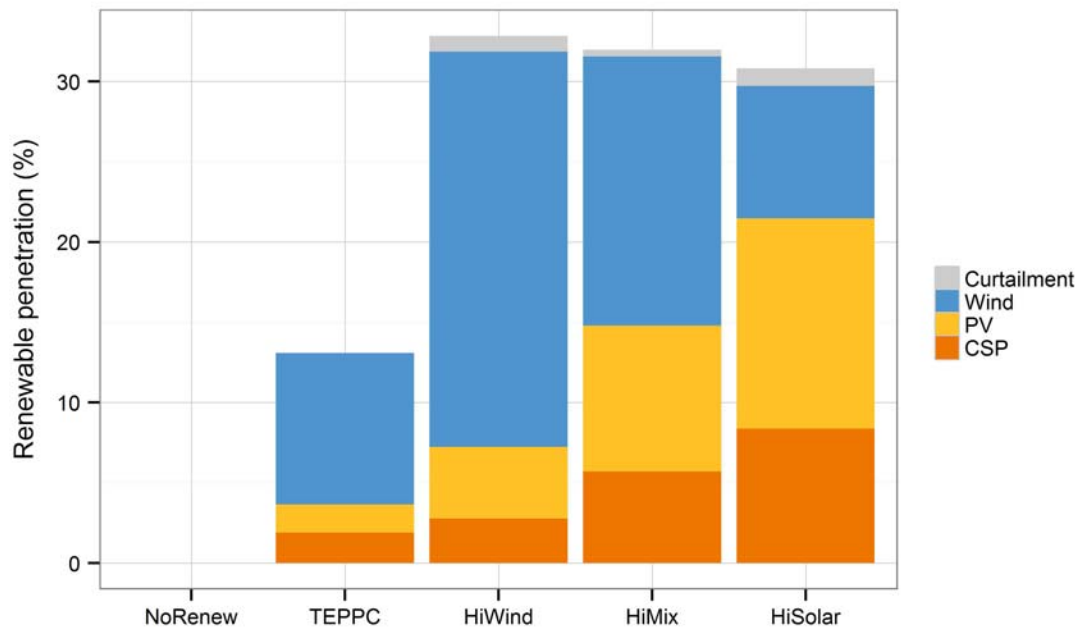
**Figure 74. Renewable energy penetration of CSP, PV, and wind
in the U.S. portion of the Western Interconnection for each scenario in 2006**

Figure 75 shows the generation for the scenarios by unit type. For reference, total generation for the U.S. portion of the Western Interconnection in most of the scenarios is approximately 800 TWh. Significant gas CC generation is displaced by renewable generation, as is some coal generation, especially in the High Wind Scenario. Gas CT use increases slightly with higher renewable penetrations in the High Solar Scenario.
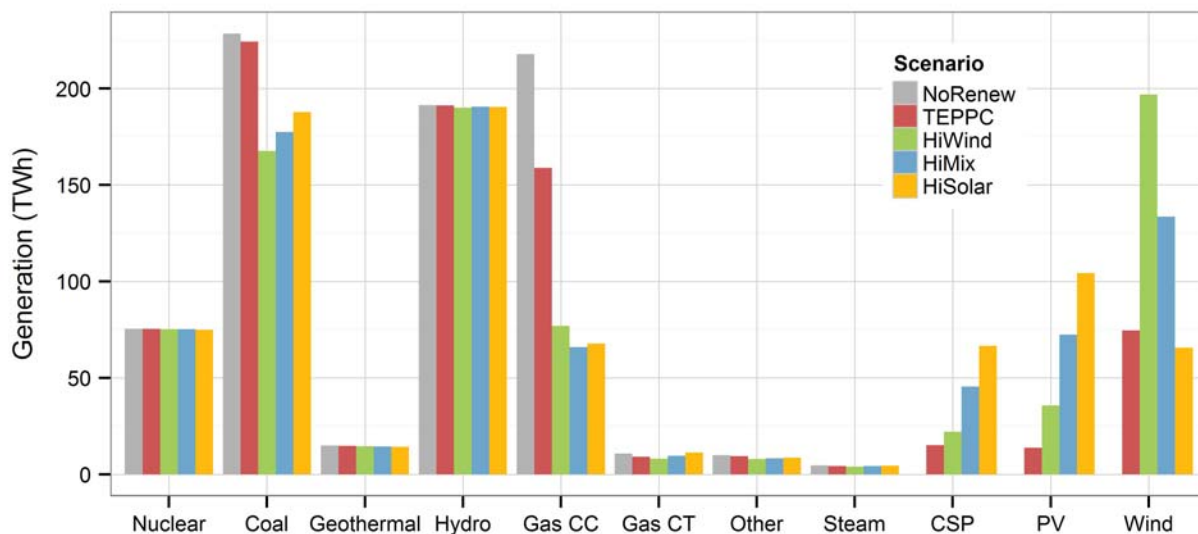
Figure 75. Generation from each type of generation unit by scenario

Figure 76 shows the amount of energy displaced for each unit type. In the TEPPC case, the 13% wind and solar mostly displaces gas units (primarily CCs) because these units have higher marginal costs than coal units. Coal makes up less than 7% of the displaced generation from the TEPPC wind and solar. In the high-penetration scenarios, coal makes up a larger fraction of the displaced generation because the online gas resources are almost fully displaced by wind and solar during some time periods. Among the high-penetration scenarios, the cases with more solar displace more gas and less coal because the solar generation is correlated with time periods where load is higher and more gas units are online. Section 6.9 discusses the impact of varying gas prices on displaced generation.
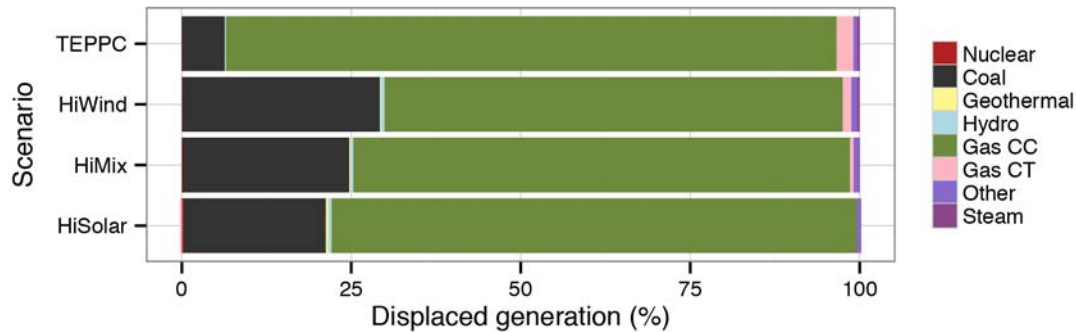
Figure 76. Generation displaced by wind and solar compared to No Renewables Scenario

Figure 77 shows the daily penetration of wind and solar on the power system, measured as total daily wind, PV, and CSP generation divided by total daily U.S. portion of the Western Interconnection load. The daily peak penetration is approximately 60% in the High Wind Scenario and is slightly lower in the High Mix and High Solar Scenarios. The High Wind Scenario has the most variability between days and between seasons. In all scenarios, the months of July through September have the lowest average penetration levels, which is partly the result of the higher load at that time of year and partly because of lower wind generation levels.
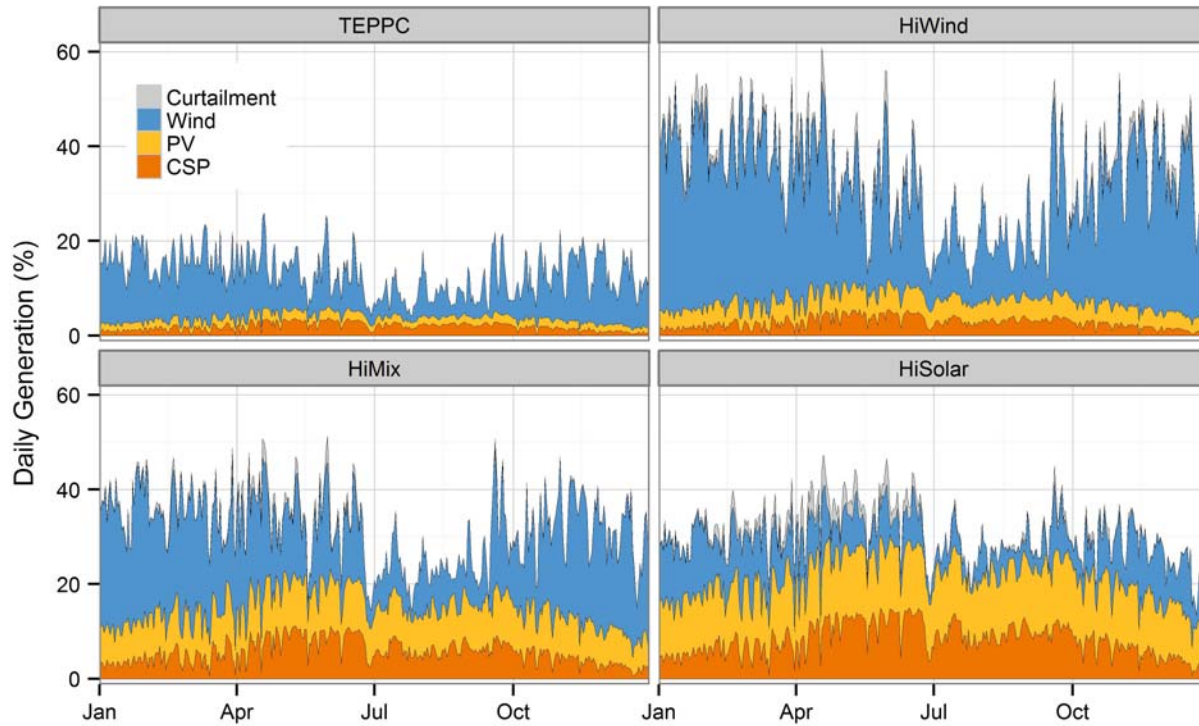
Figure 77. Daily wind and solar energy penetration for each scenario

Figure 78 shows a duration curve of the renewable penetration levels during every 5-minute interval. This is the actual penetration, after considering curtailment. Penetrations stay below 60%, partly because of the hydro, nuclear, and coal units that stay online and their downward constraints, which can result in wind/solar curtailment. The High Solar Scenario has more hours of very high penetration compared to the other high-penetration scenarios (these occur mostly at midday) and also more hours of very low penetration (these occur at night). In comparison, Xcel/Public Service Company of Colorado, SPP, ERCOT, and the Midwest Independent System Operator (MISO) have reached hourly instantaneous wind penetrations of 56%, 30%, 26%, and 25%, respectively (ERCOT 2012; Goggin 2012; MISO 2012; Jaffe 2011). Portugal, Spain, and Ireland have reached very high instantaneous penetrations of 85%, 60%, and 50% wind penetration, respectively (Estanqueiro et al. 2012). Remember that WWSIS-2 did not examine or account for frequency response and potential reliability issues that could arise if a fault were to occur simultaneously with high instantaneous wind and PV penetrations. That is being examined in Phase 3 of WWSIS.
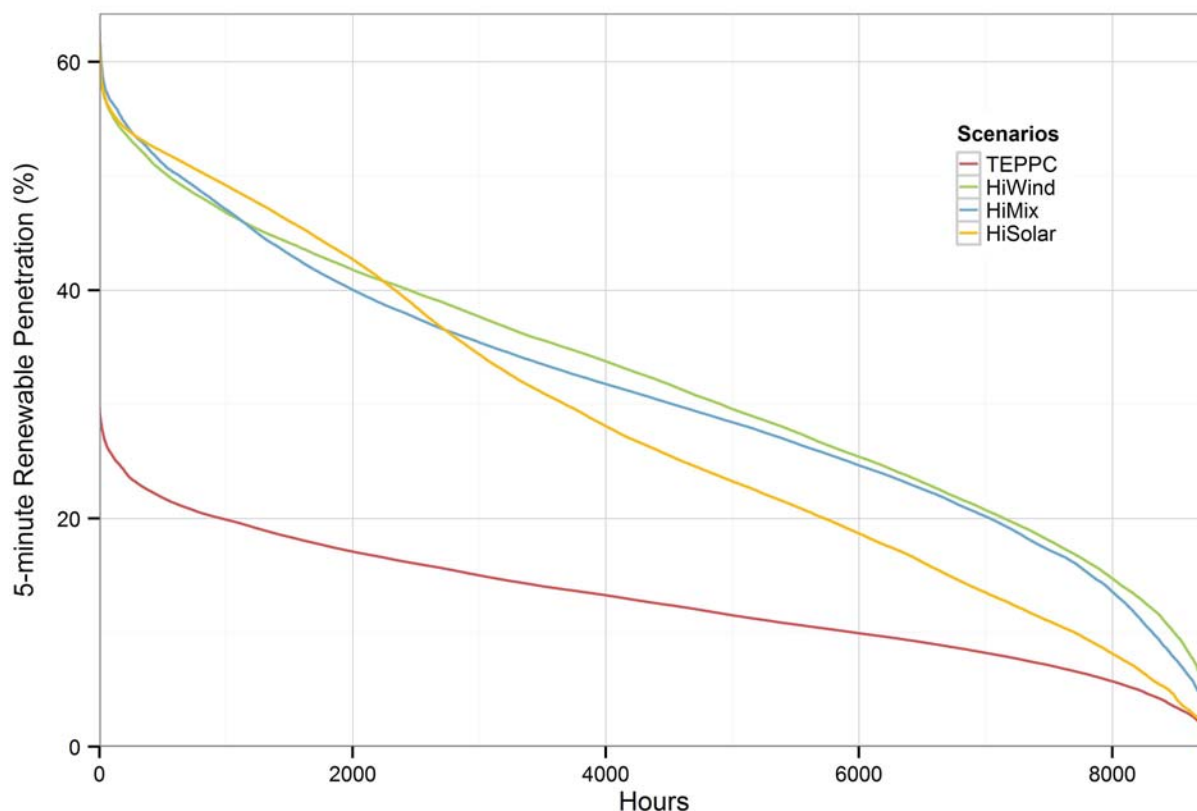
Figure 78. Duration curve of 5-minute wind/solar penetration for each scenario

Wind and solar in the U.S. portion of the Western Interconnection primarily displace generation from natural gas CC units. Low wind/solar penetrations displace very little coal, but higher penetrations displace up to 30% coal and 70% natural gas generation based on an assumed gas price that averages $4.60/MMBtu. Peak instantaneous renewable penetration rates stay below 60% in all scenarios.

6.3 Fossil-Fueled Unit Cycling

WWSIS-2 investigated the cycling of fossil-fueled generators, a major issue that includes starts, ramps, and part-load generation. Figure 79 (a) shows the generation capacity started (the sum of the number of starts times the capacity of each unit) for coal, gas CC, and gas CT units. Coal unit starts increase modestly in the High Mix and High Wind Scenarios and remain unchanged in the High Solar Scenario. Gas CC units start more in the TEPPC Scenario, but as more CC generation is displaced in the high-penetration scenarios, starts are more similar to the No Renewables Scenario. Gas CT units start less in the High Wind and TEPPC Scenarios, but more in the High Mix and the most in the High Solar Scenario. This is partly because of the sharper peak that occurs in net load in the hours after sunset in the scenario with more PV generation.
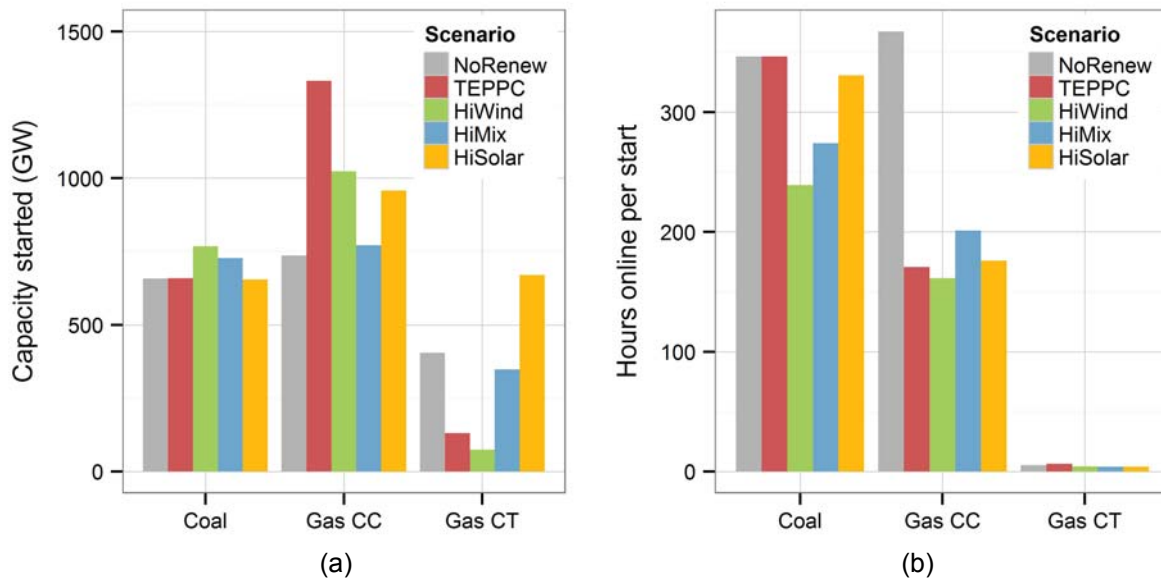
**Figure 79. (a) Capacity started and (b) number of hours online
per start by plant type for each scenario**

Figure 79 (b) shows the average number of hours online per start for each plant type. Must-run gas CT generators are not included in this chart because they have a major impact on the average number of hours CT generators are operated per start. More starts by a generator category are associated with fewer hours online per start. High wind penetration increases the coal starts, and coal units are run for shorter periods of time. The TEPPC Scenario has modest impacts on how the coal units are used; the 13% penetration affects mostly the gas units. High solar penetration does not have a significant impact on starts at coal units. The CCs are consistently generating less when they are started in all wind/solar scenarios. Wind penetration (in both the TEPPC Scenario and the High Wind Scenario) reduces the number of CT starts because it reduces the usage of CT generation. The scenarios with higher solar penetrations lead to similar or higher numbers of CT starts and similar numbers of hours online per start. In all scenarios, gas CT generators are peakers that average just 4–6 hours online per start.

Figure 80 shows (a) the total number of ramps and (b) the number of ramps per day of operation at coal and gas CC and CT units. Ramps are defined as a change in power output larger than 30% of maximum capacity. It is evident that wind and solar change coal operation. Coal units are ramped much more regularly in the wind/solar scenarios compared with the No Renewables Scenario, when coal units ramp an average of approximately once per week. In the high-penetration scenarios, ramping occurs approximately daily and the frequency is slightly higher in the scenarios with more solar. CC units ramp less in the wind/solar scenarios, but still ramp more per day of operation—more than two times per day in the high-penetration scenarios. CT operation is not very different across the scenarios—they are ramped regularly in all scenarios. Of all the cycling changes at fossil-fueled units, the most significant change in the way units are operated is that coal units are ramped much more in the wind/solar scenarios, especially the high-penetration scenarios.

97
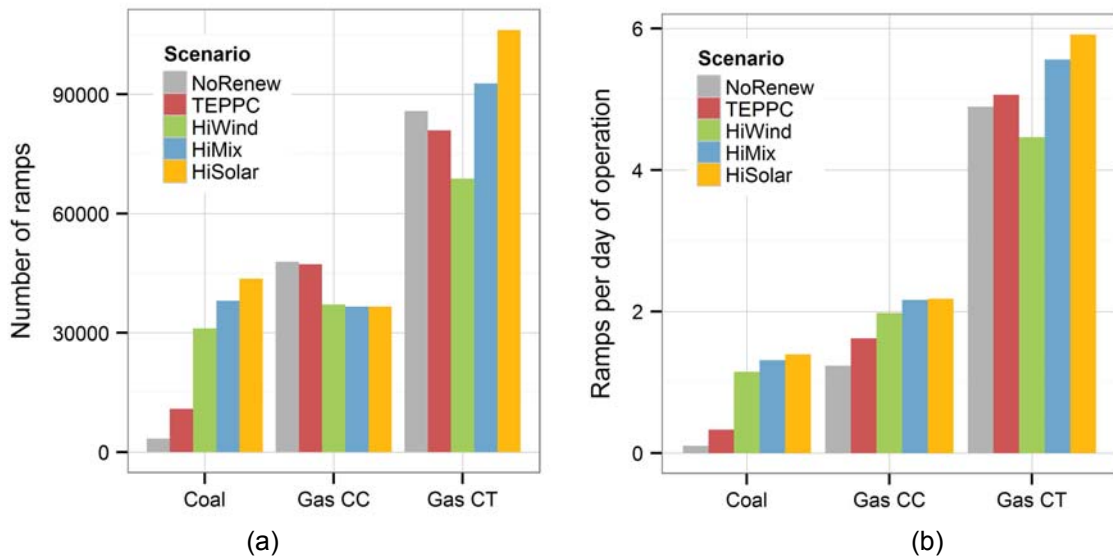
Figure 80. (a) Total number of ramps and (b) ramps per day by plant type for each scenario

Figure 81 shows the number of starts versus capacity for every unit, sorted by unit type and scenario. This plot shows (a) the number of starts and the distribution of starts for each unit type and (b) the relationship between size of the unit and the number of starts. Most coal units are started 20–30 times per year in all scenarios; most gas CC units are started 0–60 times in all scenarios. In the TEPPC and High Wind Scenarios, almost all CT units are started less than 50 times, but in the other scenarios some CTs are started up to 150 times per year. There is little relationship between the number of starts and unit size for the coal and gas CC units; however, for gas CT units, smaller units are started more often than larger units.
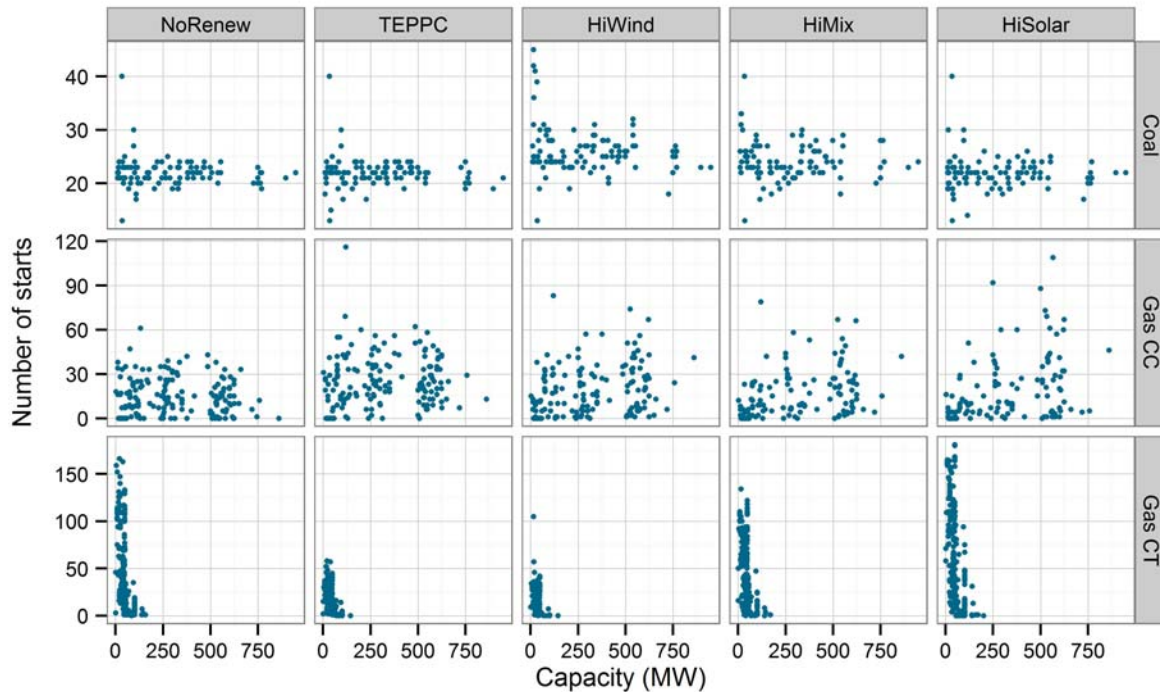
Figure 81. Number of starts versus capacity for every unit by unit type and scenario

Figure 82 shows the number of ramps versus unit capacity and illustrates the significant change in ramping by coal generators in the high-penetration scenarios. Very little ramping of coal generators occurs in the No Renewables Scenario, but most coal units ramp several hundred times per year in the high-penetration scenarios. A few small coal units ramp more than once per day on average. Gas CC units are operated similarly in all cases and it is evident that CTs are ramped less in the High Wind and TEPPC Scenarios; this is because they are online less and generating less in these scenarios.
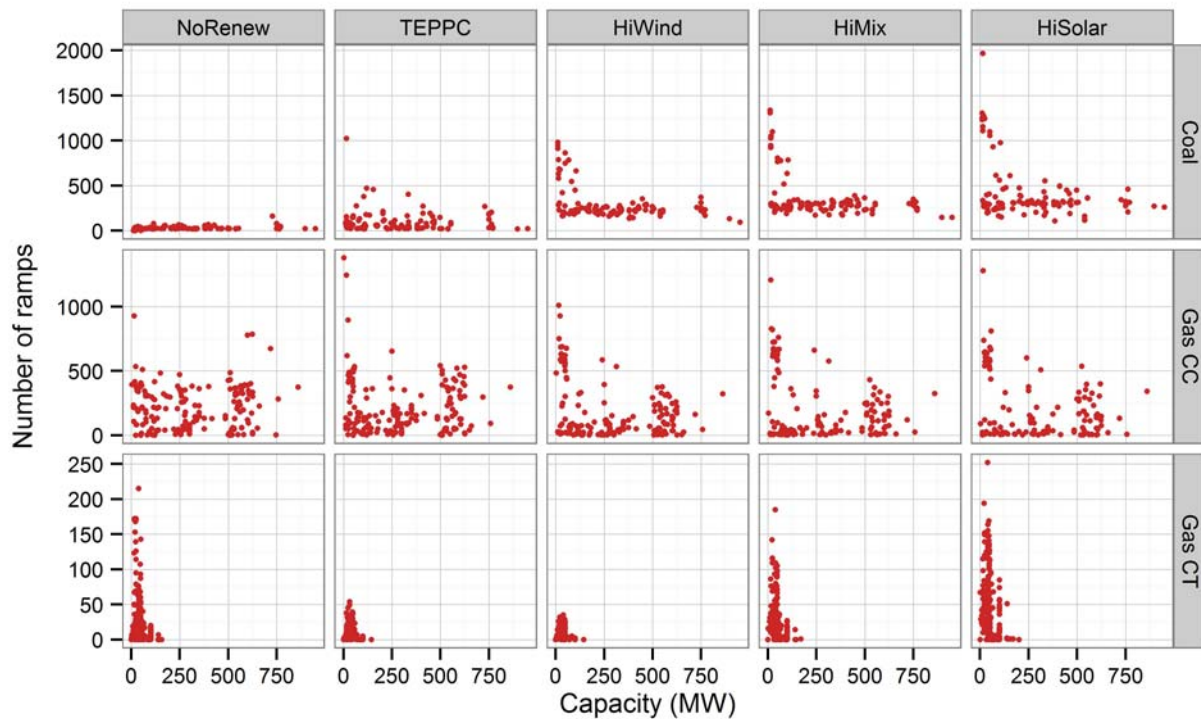
Figure 82. Number of ramps versus capacity for every unit by type and scenario

Figure 83 shows the committed capacity as a solid line and the actual dispatch as a shaded area for the coal generating units in all scenarios. This helps distinguish between starts, shutdowns, and part-loading of online generators when studying the dispatch. The online coal units are almost all operating at maximum capacity in the summer with the exception of some midday hours in the High Solar Scenario. In the spring in the high-penetration scenarios, the coal units show daily ramping (particularly the scenarios with more solar) and a weekly change in committed capacity because of a low load and high wind and solar output. Units are shut down between March 26 and 29 and started back up on March 30 and 31. More coal units are shut down in the High Wind Scenario compared to the High Solar Scenario, but more ramping occurs in the High Solar Scenario.
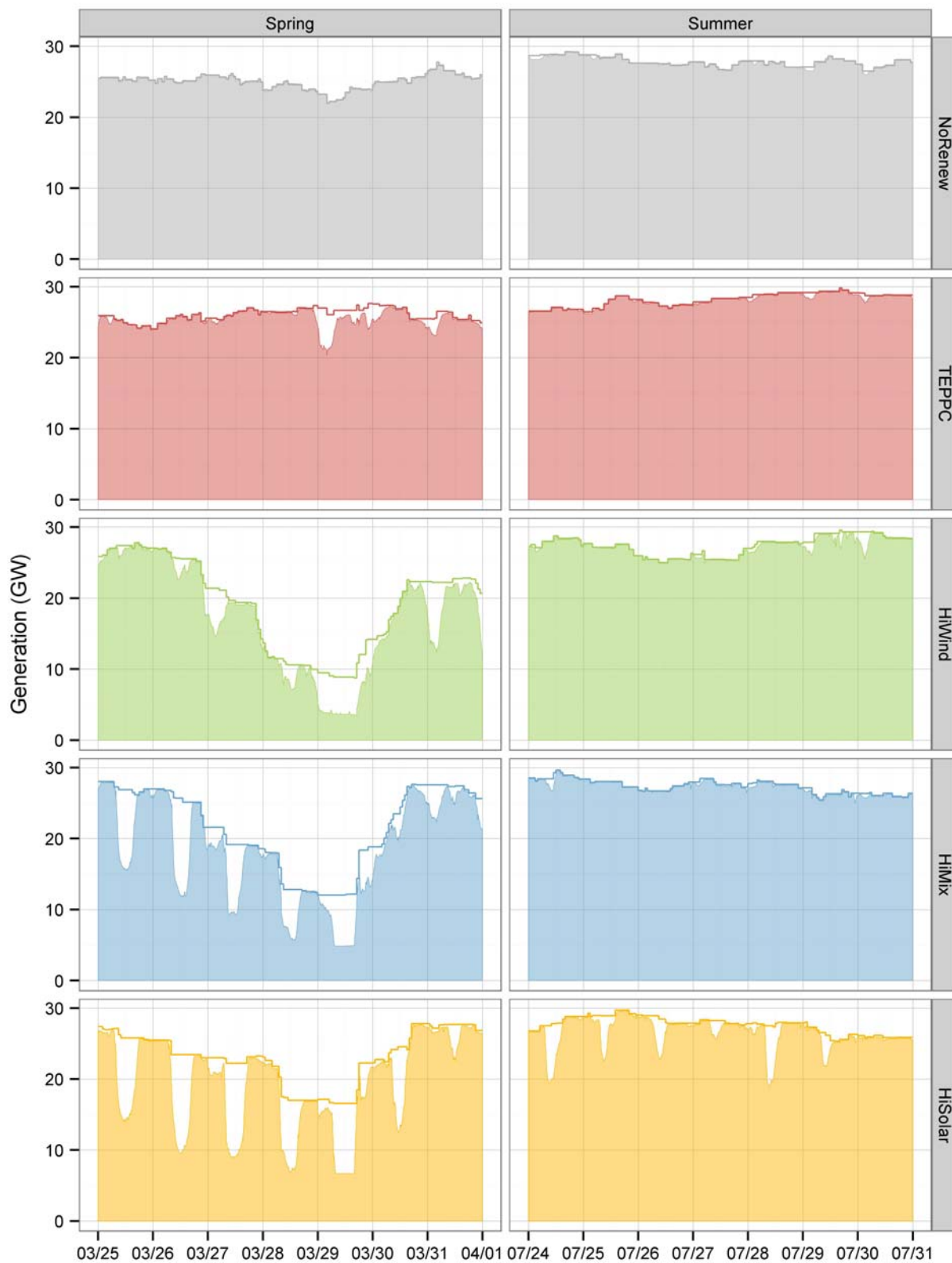
Figure 83. (Solid line) capacity committed and (shaded area) dispatched for coal units during March and July sample weeks for each scenario

100
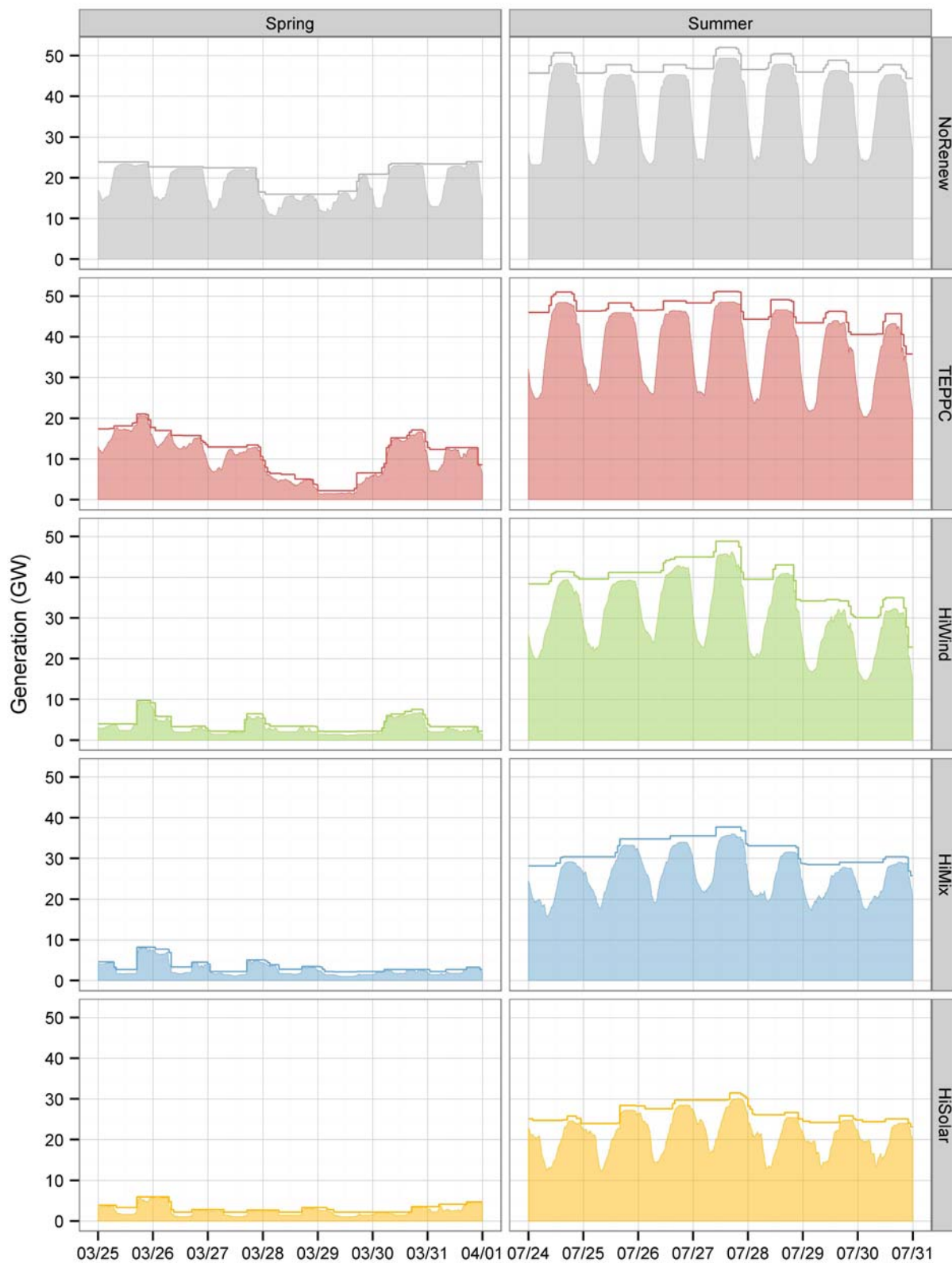
Figure 84. (Solid line) capacity committed and (shaded area) dispatched for gas CC units during March and July sample weeks for each scenario

Figure 84 shows the commitment and dispatch of gas CC units. In the summer, there is not much difference between scenarios in how these units are operated. Commitment changes slightly through the week and the units are ramped daily to near minimum generation levels. In the spring, these units are mostly displaced by the wind and solar generation in the high-penetration scenarios.

One of the questions that WWSIS-2 sought to answer was whether it was necessary to include wear-and-tear start costs (which are often unknown) within the system optimization or whether adding these costs after the optimization is sufficient. We ran a sensitivity analysis with zero wear-and-tear start costs. Figure 85 shows the generation by type for the case that included the lower-bound start costs (in blue) and the case that replaced the wear-and-tear start costs with zero (in orange). In both cases, start fuel costs (which are typically known) were included in the optimization. There is no significant change in annual generation for most generator types when wear-and-tear start costs are not included in the optimization. There is some trade-off between gas CC and CT generation. Interestingly, the CC generation is lower in the zero wear-and-tear start cost case. This is because the 4HA market sees the ability to shut down the CC generators for relatively short periods of time, yet if the actual wind and solar generation are lower than expected in real time, CTs need to be run to serve load that would have been served by a CC unit. Coal commitment and generation change very little in the zero wear-and-tear start cost case. This is partly because of the higher fuel cost for starting coal units, which means that the impact of the start VOM is not as significant.

Figure 86 shows the capacity started for the two start cost sensitivities. This shows a significant difference between the two cases. Eliminating wear-and-tear start costs leads to very different operation of the CC and CT units. They are both started and shut down much more often in response to variations in net load. Although examining the annual generation by type shows little advantage to using wear-and-tear start costs in the optimization, analysis of starts shows that including wear-and-tear start costs within the optimization is important for detailed analysis of high wind/solar penetration impacts.
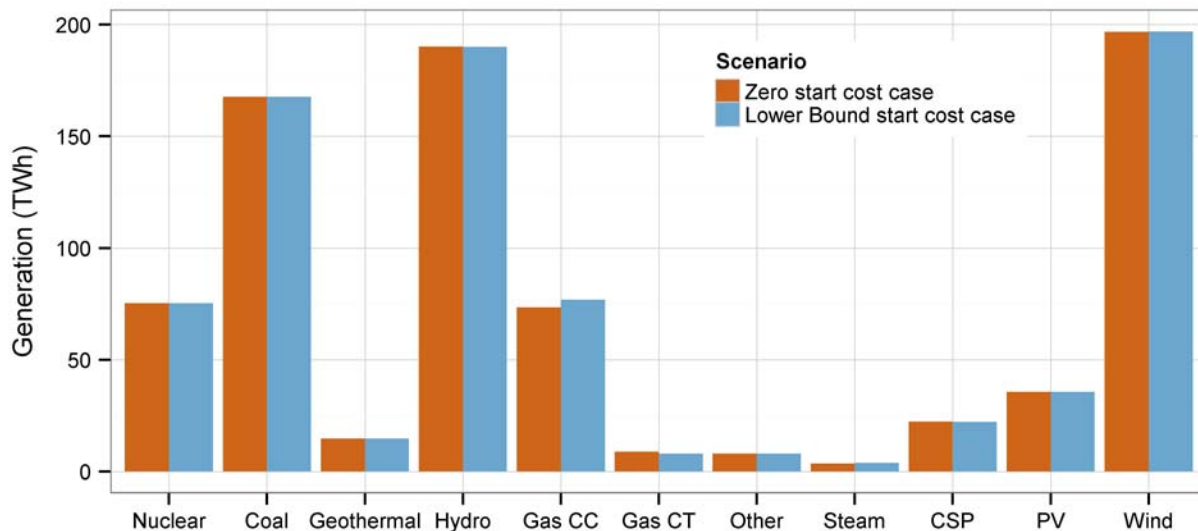
Figure 85. Generation by type for the High Wind Scenario with zero wear-and-tear start costs compared to lower-bound wear-and-tear start costs

Note: Start fuel costs were included in the optimization for both cases.
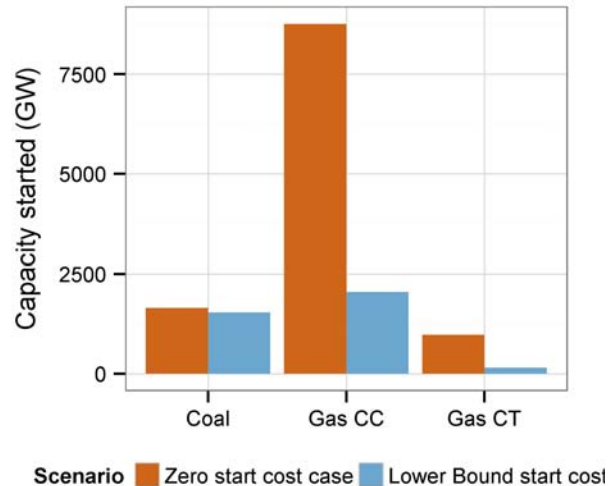
Figure 86. Starts by type for the High Wind Scenario with zero wear-and-tear start costs compared to lower-bound wear-and-tear start costs

Note: Start fuel costs were included in the optimization for both scenarios.

Coal units start a similar number of times in all of the scenarios. The largest difference in the way the coal units are operated in the high renewable scenarios is that they are ramped each day instead of each week. Gas CC units start more often and ramp more often per hour of operation in the high renewable scenarios. Gas CT units are used as peakers in all scenarios.

6.4 System Production Costs

Production cost changes from wind and solar generation are discussed in this section. Production cost changes comprise the change in fuel, noncyclic VOM, and start and ramping costs accruing from the presence of wind and solar. This section also shows the overall O&M cost impacts on the fossil-fueled units. Note that these are production simulation results and do not reflect capital costs of wind, solar, or transmission or the reduced capacity requirements throughout the system that result from the capacity value of renewable generation. The results also apply only to the Western Interconnection and are highly dependent on the existing generation mix in the region. Regions with significantly different generation mixes could see different production costs and emissions impacts. One of the main goals of this study was to understand how the costs of increased cycling by fossil-fueled generators might offset the production cost reduction from wind/solar generation. Although the system dispatch and generation starts showed only the U.S. portion of the Western Interconnection, the plots in this section include all of the Western Interconnection because the interchange between countries changes and the analysis must account for these cost (and emissions) impacts.

For cycling cost results in this section, we supply a range. The ranges are based on the lower- and upper-bound costs, which give an uncertainty range for cycling costs as described in Section 2. We ran the PLEXOS model using median lower-bound start costs to optimize unit commitment and dispatch to directly determine the system lower-bound cycling costs. We then applied median lower-bound ramp costs to the number of ramps.

We indirectly estimated the upper-bound cycling costs by applying the median upper-bound start and ramp costs to the number of starts and ramps. We did try to run PLEXOS using the upper-bound start costs to calculate the upper-bound cycling costs directly; however, after examining the results from several of these runs, we determined that properly committing large coal units and other units with large start costs required a unit commitment horizon of significantly more than the 2-day window used in this study. This would have led to unacceptable runtimes. The impact of this approach is that this method may underestimate curtailment and overestimate cycling costs (higher start costs would reduce the number of starts). As a result, we regard these system upper-bound cycling costs as a ceiling. Future work could include a sensitivity run of PLEXOS with the upper-bound start costs.

Figure 87 shows the total production cost (production costs do not reflect fixed capital or PPA costs) of each scenario. Cost components are broken down into fuel, noncyclic VOM, start costs (nonfuel and wear-and-tear start costs), start fuel costs, and ramping costs. Fuel costs dominate the production cost, and noncyclic VOM costs are also significant. Starts, start fuel, and ramping costs total between $271–$643 million (in the No Renewables Scenario) and $324–$800 million (in the High Solar Scenario; see Table 20). This represents a relatively small fraction (1.5%–7.0%, depending on the scenario) of total production costs. Although the three high-penetration scenarios have similar production costs, the High Solar Scenario is slightly higher because the renewable penetration level is slightly lower (See Figure 74). Figure 88 focuses on the wear-and-tear components of the production cost.
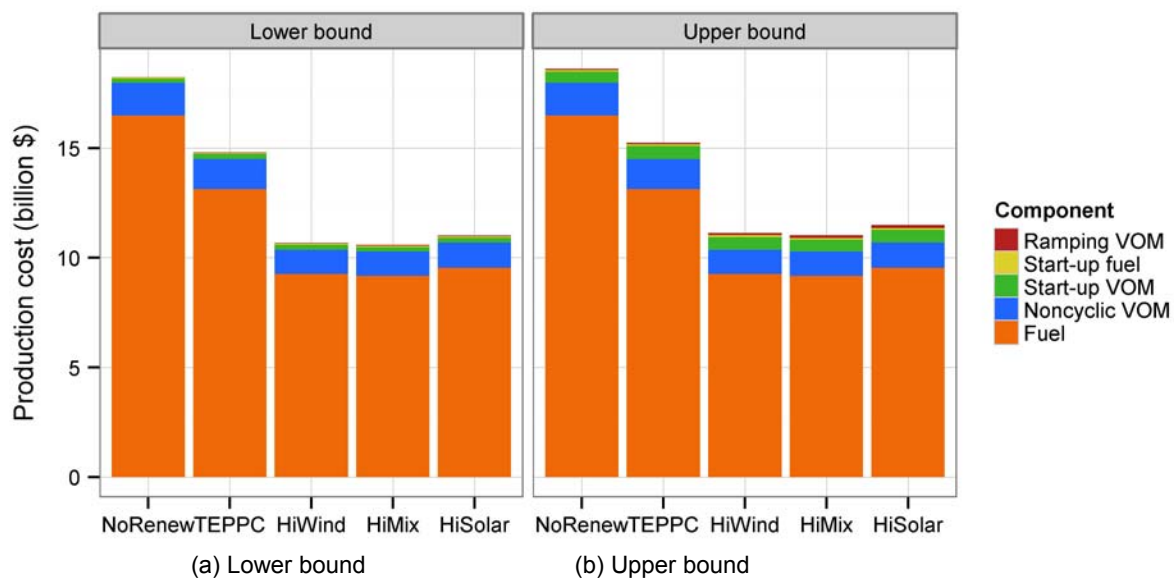
Figure 87. Total cost of each scenario broken down into fuel, noncyclic VOM, and lower- and upper-bound start wear-and-tear, start fuel, and ramping wear-and-tear costs
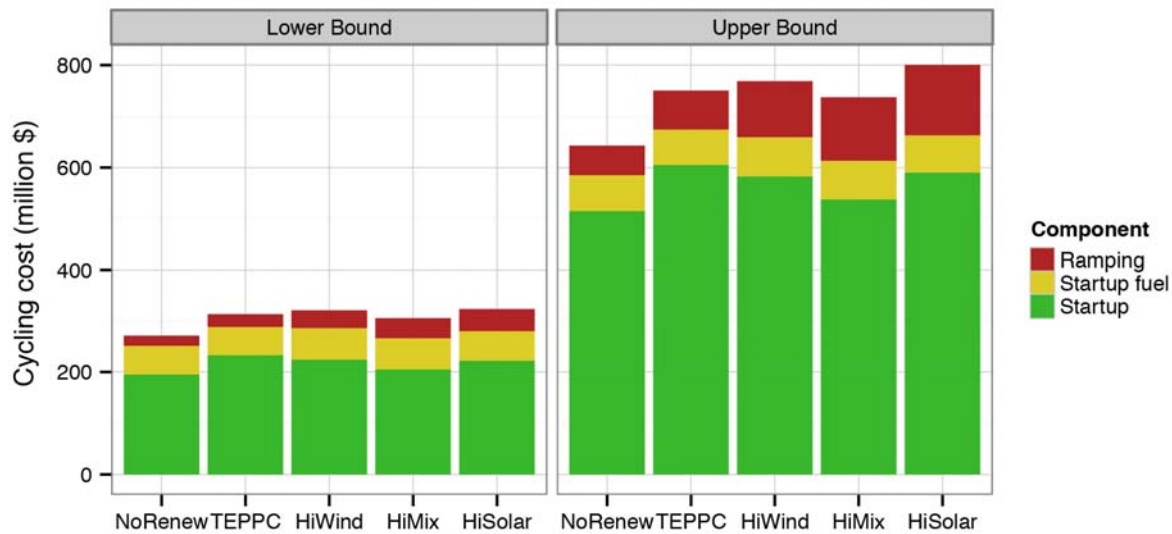
Figure 88. Cycling cost components, showing lower- and upper-bound costs from starts, start fuel, and ramping

Note: Production costs do not include any fixed capital or PPA costs.

Table 20. Cycling Costs (Starts, Start Fuel, and Ramping Costs) for All Scenarios

Scenario	Cycling Costs (million $)	Cycling Costs as a Fraction of Total Production Cost (%)
No Renewables	271–643	1.5–3.5
TEPPC	313–751	2.1–4.9
High Wind	321–769	3.0–6.9
High Mix	306–738	2.8–6.7
High Solar	324–800	2.9–7.0

The change in production cost from each wind/solar scenario to the No Renewables Scenario was examined. Production cost does not include any capital costs or PPAs for thermal units, renewable generators, or transmission. Figure 89 shows the total change in production cost per MWh of wind and solar produced. The reduction in production cost from wind and solar in the TEPPC case is $32.6–$33.2/MWh, considering upper- and lower-bound start costs, respectively. The reduction in production cost from wind and solar on a per MWh basis is lower in the high-penetration scenarios because more coal is displaced. The changes in production cost for the high-renewables scenarios are shown in Table 21. These values are highly dependent on gas price assumptions (see section 6.9), which average $4.60/MMBtu. These values are significantly less than the approximately $80/MWh value found in WWSIS-1, because the core scenarios in WWSIS-1 assumed a $9.50/MMBtu gas price and a $30/ton carbon tax, which led to displacing less coal and using more gas. We did not model a carbon tax in WWSIS-2.

Table 21. Production Cost Reductions Due to Wind and Solar for Each Scenario

Scenario	Change in Production Cost (billion $)	Change in Production Cost ($/MWh)
TEPPC	3.34–3.43	32.6–33.2
High Wind	7.48–7.56	29.4–29.7
High Mix	7.59–7.65	30.2–30.4
High Solar	7.12–7.23	30.2–30.6

Note: Production costs do not include any fixed capital or PPA costs. Change in production cost is shown as total change in production cost per MWh of wind and solar generated.

Start, start fuel, and ramping costs have a very small impact on the overall change in production cost from wind and solar. Fuel cost reductions account for the large majority of the production cost reductions. Noncyclic VOM also accounts for $340–$390 million of cost reductions between the high-penetration scenarios and the No Renewables Scenario. Wind and solar penetration does lead to increased starts for some plant types in some scenarios, but the increase in starts, particularly of coal (the most expensive units to start), is not large enough to significantly affect production cost. In the TEPPC Scenario, cycling costs offset the reduction in production cost of wind and solar by 1.2%–3.2%. In the high-penetration scenarios, the impact ranges from 0.5%–2.2% (see Table 22 for specific scenario results). These are system-wide changes in production cost; impacts on individual generators could be significantly different.

Figure 89 shows the fuel, noncyclic VOM, and cycling changes in production cost per MWh of wind and solar generation. Negative values (e.g., for fuel) indicate that the wind/solar scenarios save fuel over the No Renewables Scenario. Positive values (e.g., for ramping) indicate that ramping-related costs increase in the wind/solar scenarios.

Fuel cost reductions greatly outweigh any increase in ramping or start cost in the wind/solar scenarios, as shown by the size of the orange bars. Table 22 gives more detail on the impact of cycling on the change in production cost from wind and solar. Every MWh of wind and solar generation leads to $0.14–$1.05 in cycling costs, depending on scenario. The TEPPC Scenario shows the largest increase in cycling costs per MWh of wind and solar generation. The high-penetration scenarios show a $0.14–$0.67 increase in cycling cost per MWh of wind and solar generation.

(a) Lower bound   **(b) Upper bound**
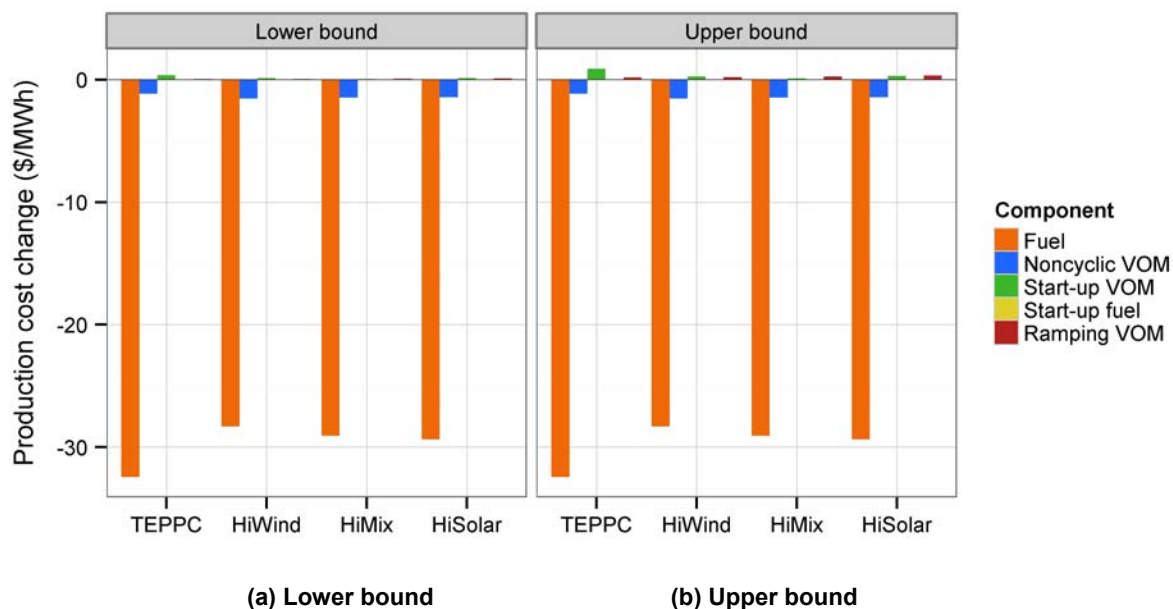
**Figure 89. Change in production cost (compared to No Renewables Scenario)
per MWh of wind and solar generation**

Note: Production costs do not include any fixed capital or PPA costs.

Table 22. Cycling Cost Impacts of Wind and Solar

Scenario	Total (million $)	Increase in Cycling Costs (compared to No Renewables Scenario)	
		Per MWh Wind and Solar Generation ($/MWh)	Per MWh of Fossil-Fueled Generation ($/MWh)
TEPPC	42–108	0.41–1.05	0.18–0.44
High Wind	50-127	0.20–0.50	0.52–1.24
High Mix	35-95	0.14–0.38	0.47–1.14
High Solar	52-157	0.22–0.67	0.50–1.28

We next consider the same cycling costs, but from the perspective of increased O&M of the fossil-fueled plants. Instead of dividing the cycling costs by each MWh of wind and solar generation, we now divide those same costs by each MWh of fossil-fueled generation. Figure 90 and Figure 91 show the cycling cost impacts to fossil-fueled generators. Figure 90 shows the lower-bound impacts of cycling on the nonfuel production costs from coal, gas CC, and gas CT generators. The upper-bound analysis for generator types is not shown because it is confidential. Note, however, that although the absolute magnitudes of costs are higher with the upper bounds, the relative comparisons discussed here also hold true for the upper bounds. Although wind- and solar-induced cycling has very little impact on O&M costs at the average coal unit, it has more impact on the average gas CC and gas CT generator. Figure 91 shows the lower- and upper-bound aggregate cycling costs per MWh of fossil-fueled generation. High-penetration levels of

wind and solar could add to the O&M of the average fossil-fueled generator by up to $1.28/MWh of fossil-fueled generation (see Table 22 for a range for each scenario). At 13% penetration, we find that the wind- and solar-induced cycling at the average fossil-fueled unit increases O&M by $0.18–$0.44/MWh. Note that Figure 88 shows that total cycling cost is more consistent between the scenarios compared to the cycling cost normalized by generation. Although cycling costs go up slightly in the renewable scenarios, the cycling costs per MWh of fossil-fueled generation go up more noticeably because the cycling costs are higher and the generation is lower in the high-renewable scenarios.
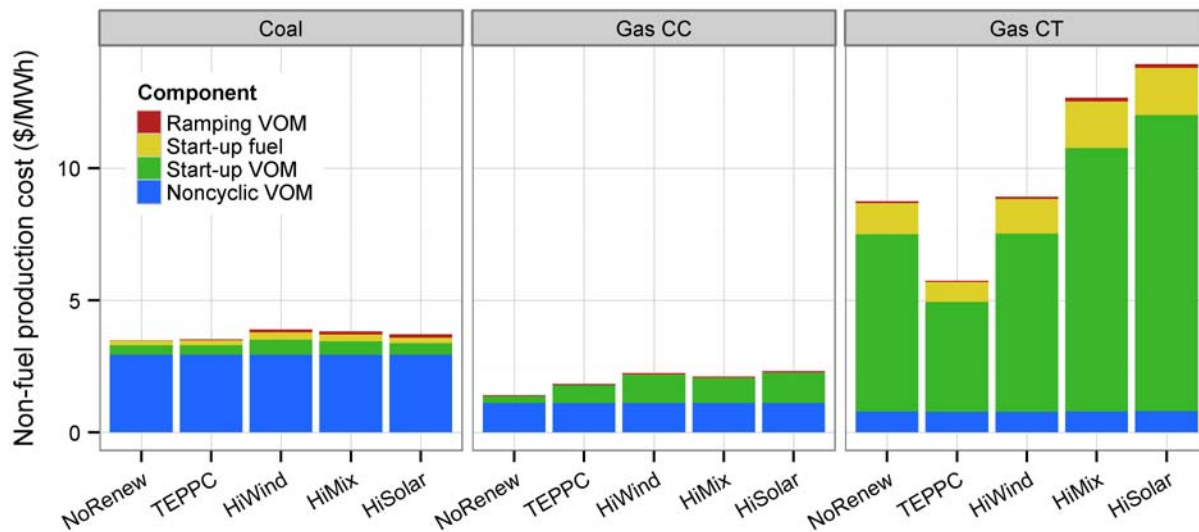
**Figure 90. Lower-bound cycling costs per MWh of (left) coal,
(middle) gas CC, and (right) gas CT generation**
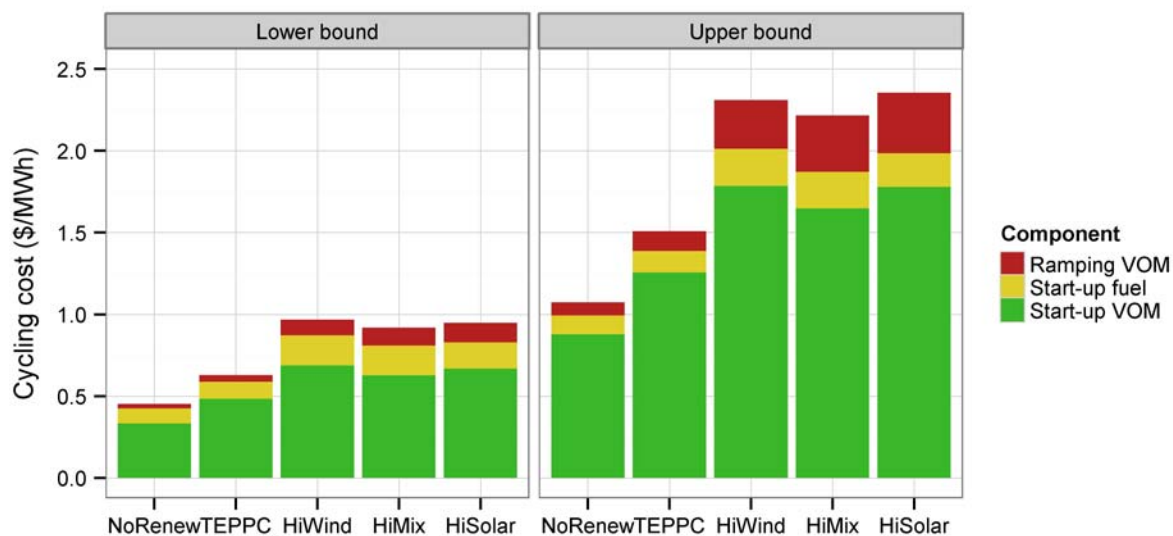
**Figure 91. Lower- and upper-bound cycling costs
per MWh of fossil-fueled generation for all scenarios**

Annual cycling costs across the West increase from $271–$643 million in the No Renewables Scenario to $306–$800 million when wind and solar are added. Wind and solar increase annual cycling costs by $35–$157 million, or 13%–24%. Cycling costs do not necessarily increase with wind and solar penetration: the High Mix Scenario has lower cycling costs than the TEPPC Scenario. The average fossil-fueled plant sees an increase in cycling costs of $0.18–$0.44/MWh generated in the TEPPC Scenario and $0.47–$1.28/MWh in the high-penetration scenarios. Regardless of wind and solar, gas CTs have the highest cycling O&M cost per MWh of generation because gas CTs perform the most cycling. Although the TEPPC Scenario resulted in decreased cycling costs for gas CTs and the High Wind Scenario did not affect cycling costs for CTs, the two scenarios with higher solar penetrations resulted in significantly increased CT cycling costs because CTs were often started to handle the evening peak. From a system perspective, wind and solar displace $3 billion in fuel and VOM annually in the TEPPC Scenario and $7–$8 billion in the high-penetration scenarios. In the TEPPC Scenario, wind- and solar-induced cycling costs offset the production cost reduction of wind and solar by $0.41–$1.05/MWh to $32.6–$33.2/MWh of wind and solar generated. In the high-penetration scenarios, wind- and solar-induced cycling costs offset the production cost reduction of wind and solar by $0.14–$0.67/MWh to $29.4–$30.6/MWh, based on the specific system characteristics modeled for the Western Interconnection. Production costs do not consider fixed capital or PPA costs.

6.5 Emissions

Wind and solar can displace energy and emissions that would otherwise be generated by fossil-fueled units. One of the main goals of this study was to understand how wind and solar affect CO_2, SO_2, and NO_x emissions. Emissions related to part-load operation, ramping, and starts were studied in detail, as described in Section 2. This section analyzes the emissions avoided by wind and solar penetration and also the changes in average emission rates from fossil-fueled units that result from the penetration of wind and solar generation.

Table 23 shows the avoided emissions per MWh of wind and solar in the high-penetration scenarios. This number is calculated as the change in total emissions (considering part-load, ramping, and start impacts) compared to the No Renewables Scenario divided by the wind and solar generation for each scenario.

Table 24 shows the reduction in emissions compared to the wind and solar penetration for each high-penetration scenario. These numbers include all generation and load in the Western Interconnection (including Canada and Mexico), which is why the penetration numbers are significantly lower than 33%. Emissions from all countries must be counted because the interchange between countries changes between the scenarios. CO_2 is reduced by 29%–34% throughout the Western Interconnection from the scenarios with 24%–26% wind and solar penetration. This shows that CO_2 is displaced at a higher fraction than the energy displacement from wind and solar. This occurs because the gas generation that is primarily displaced has a higher CO_2 emissions rate compared to the Western Interconnection average, which includes sources like nuclear and hydro generation that have no emissions. NO_x and SO_2 are reduced less than the penetration rates in the high renewable scenarios. This is because NO_x and SO_2 emission rates are orders of magnitude lower from gas units compared to coal, so these numbers are very sensitive to how much coal is displaced. Because the High Wind Scenario displaces the most coal generation, the avoided emissions rates and overall reductions are the highest in this scenario.

The emissions changes from the TEPPC Scenario compared to the No Renewables Scenario are not given in this section because the coal and gas portfolio in the No Renewables Scenario is partially based on the existing wind and solar capacity; this likely leads to the TEPPC Scenario displacing an unrealistically small amount of coal, resulting in smaller emission reductions than would be expected. The high-penetration scenarios include a mixture of coal and gas displacement, so the comparison with the No Renewables Scenario is appropriate.

Table 23. Emissions Avoided per MWh of Wind and Solar Generation—Considering Combined Part-Load, Ramping, and Start Impacts

Scenario	Avoided CO_2 (lb/MWh)	Avoided NO_X (lb/MWh)	Avoided SO_2 (lb/MWh)
High Wind	1,190	0.92	0.56
High Mix	1,150	0.80	0.44
High Solar	1,100	0.72	0.35

Table 24. Emissions Reductions Compared to Wind and Solar Penetration for All of the Western Interconnection (including Canada and Mexico)

Scenario	Interconnection-Wide Wind and Solar Penetration (%)	CO_2 Reduction (%)	NO_X Reduction (%)	SO_2 Reduction (%)
High Wind	26.0	33.5	22.3	24.1
High Mix	25.6	31.9	19.2	18.7
High Solar	24.1	28.8	16.2	14.1

Figure 92 through Figure 94 show the impacts of wind and solar penetration on CO_2, NO_x, and SO_2 emissions. Table 25 shows the impact of part-load, starts, and ramping on the overall avoided emissions rates. In general, impacts were relatively small and ranged from –4.5% (reducing the avoided emissions of wind and solar by 4.5%) to +6.3%. Start impacts were small in all cases (much less than 1%) because of the relatively modest change in the number of starts and the relatively small excess emissions caused by starting units for most pollutants.

Figure 92 shows the CO_2 emissions and changes for the wind and solar scenarios. The analysis described in Section 2 shows that ramping has no significant impact on CO_2 emissions, so those estimates are not calculated. The start-up CO_2 emissions are negligible (less than 0.1%) in all cases. The part-load CO_2 impact is also negligible (less than 1%) because the CO_2 penalty for part-load operation is relatively small.
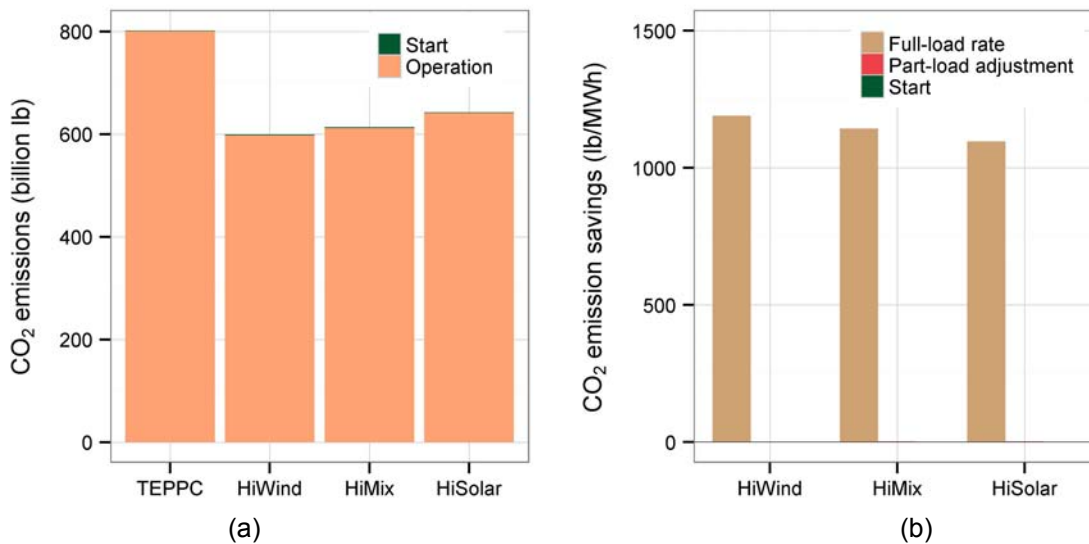
Figure 92. CO₂ emissions by scenario: (a) absolute CO₂ emissions for operation and starts and (b) CO₂ emission reductions per MWh of wind and solar generation compared to the No Renewables Scenario, separated into the constant emissions rate assumption and adjustments for part-load impacts and starts

The effects of cycling actually cause NO_x emissions reductions from wind and solar to be larger than expected, as shown in Figure 93. The effect of considering part-load emissions rates increases estimates of avoided emissions by 4%–6%. Part-loading increases the estimate of avoided emissions because coal units in the western United States typically emit less NO_x per MWh of generation at part-load compared to operating at maximum capacity (see Section 2). Ramping reduces avoided NO_x estimates by 2%–4%. Although the emissions penalty per ramp is very small, ramping increases dramatically at coal units in the high renewable cases (see Figure 80). Start-up emissions reduce the avoided NO_x estimates by less than 0.1% in all cases. In total, ramping, part-loading, and starts *improve* avoided NO_x emissions estimates by 1%–2%.
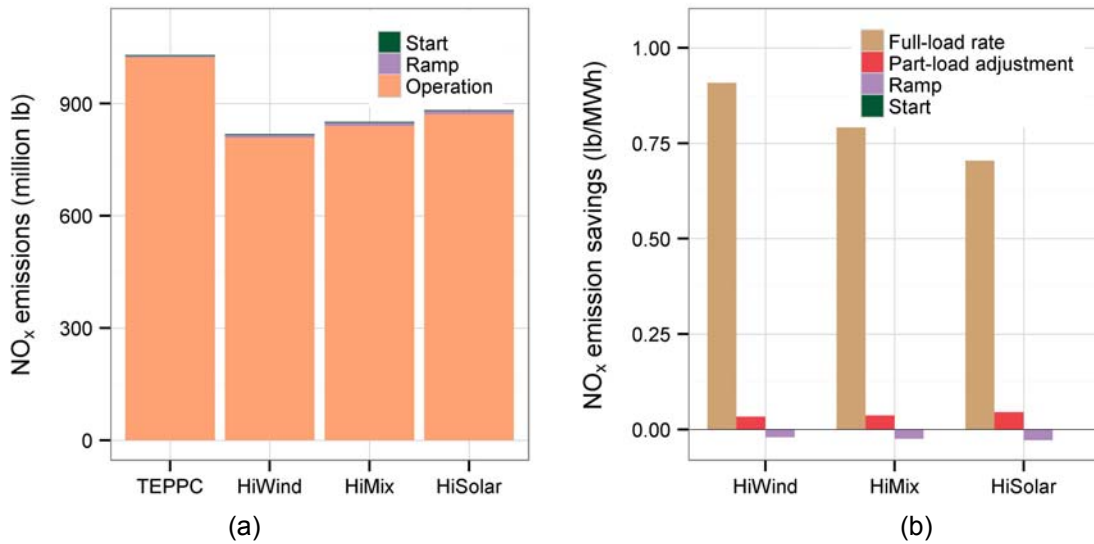
Figure 93. NO$_X$ emissions by scenario: (a) absolute NO$_X$ emissions for operation, ramping, and starts and (b) NO$_X$ emission reductions compared per MWh of wind and solar generation to the No Renewables Scenario, separated into the constant emissions rate assumption and adjustments for part-load impacts, ramping, and starts

Figure 94 shows the SO$_2$ emissions by scenario. Because there was not enough information to create SO$_2$ emission part-load curves, part-load impacts were not studied for SO$_2$. Ramping impacts on avoided SO$_2$ were modest for the high renewable scenarios, reducing avoided SO$_2$ by 2%–5%. This is also caused by extensive ramping at coal units. Start-up emissions impacts affected the avoided SO$_2$ emissions rates by significantly less than 1%.
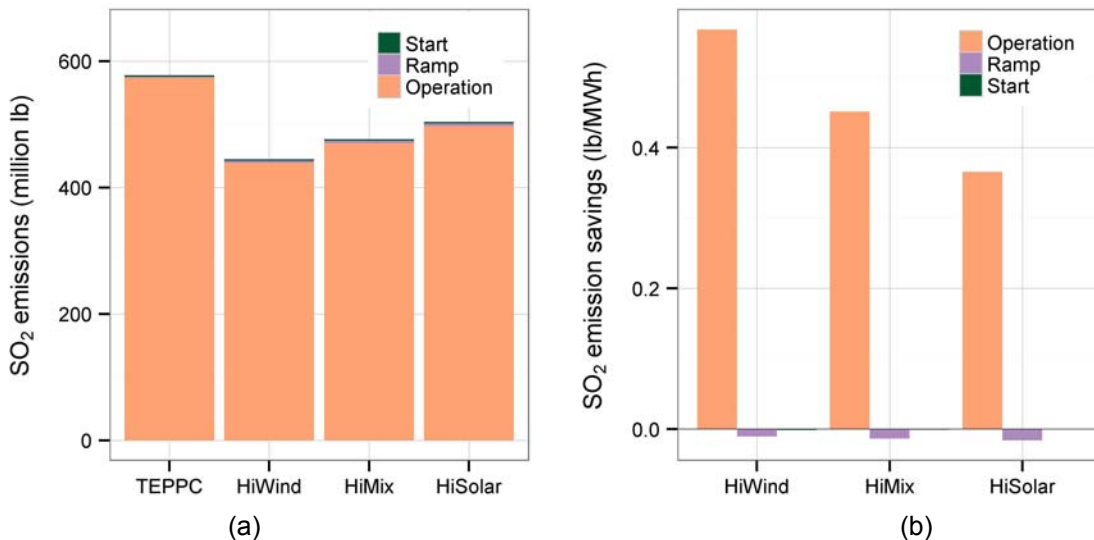

Figure 94. SO$_2$ emissions by scenario: (a) absolute SO$_2$ emissions for operation, ramping, and starts and (b) SO$_2$ emission reductions per MWh of wind and solar generation compared to the No Renewables Scenario, separated into the constant emissions rate assumption and adjustments for ramping and starts

112

**Table 25. Impacts of Part-Load, Ramping, and Starts on CO_2, NO_X, and SO_2
Avoided by Wind and Solar Generation**

Pollutant	Scenario	Part-Load Impact (%)	Ramping Impact (%)	Start Impact (%)
CO_2	High Wind	0.0	—	0.0
CO_2	High Mix	+0.2	—	0.0
CO_2	High Solar	+0.2	—	0.0
NO_X	High Wind	+3.6	–2.2	0.0
NO_X	High Mix	+4.6	–3.1	0.0
NO_X	High Solar	+6.3	–3.9	–0.1
SO_2	High Wind	—	–1.9	–0.2
SO_2	High Mix	—	–3.0	–0.2
SO_2	High Solar	—	–4.5	0.0

Notes: Negative numbers denote that avoided emissions are reduced; positive numbers mean that more emissions are avoided. Impacts are measured in the percent change in avoided emissions resulting from the category of impact. For example, if avoided emissions were 10 lb/MWh and start impacts reduced that by 1 lb/MWh, that would be a –10% impact.

We next view these same emissions from the perspective of a fossil-fueled generator that experiences emissions rate changes caused by cycling, instead of from the perspective of a wind/solar plant in which cycling changes avoided emissions. Figure 95 and Figure 96 show the CO_2 emissions rates and changes in CO_2 emissions rates for fossil-fueled generators for all scenarios. Although significant differences exist between the different technologies, very little difference in total emissions (including cycling-related emissions) per MWh of generation is seen between the scenarios for each technology. The largest difference between scenarios was a 2% increase in the emissions rate for the average gas CT in the High Wind Scenario. Solar actually reduces average gas CC unit emission rates slightly. These results are on average; individual units could be higher or lower.
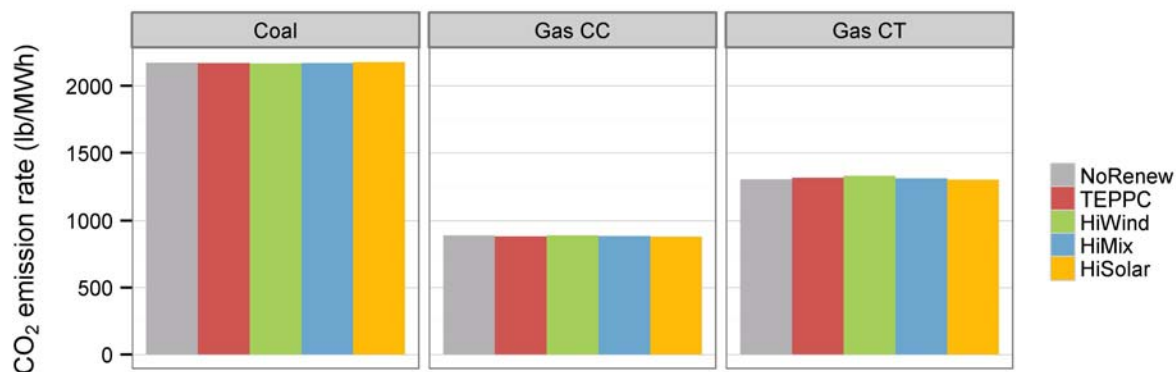
Figure 95. CO_2 emission rates from the average coal, gas CC, and gas CT unit
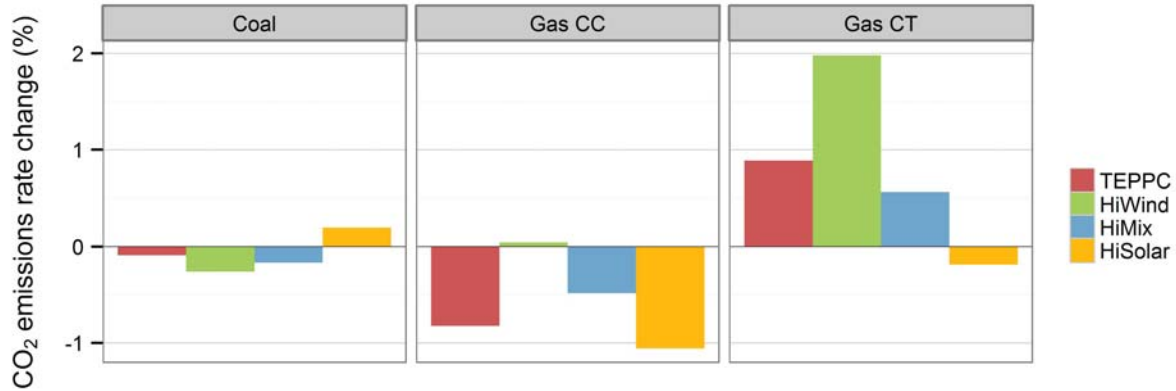
Figure 96. Change in CO$_2$ emission rates from the average coal, gas CC, and gas CT unit compared to the No Renewables Scenario

Figure 97 and Figure 98 show the NO$_x$ emission rates and changes between scenarios. Although NO$_x$ emissions differ between technologies by several orders of magnitude, wind/solar penetration has a modest impact on the emissions per MWh of generation from fossil-fueled units. For coal-fired units, the impact of wind and solar on emission rates is negligible. For CCs, high-penetration scenarios increase emission rates by approximately 5%. For CTs, wind tends to decrease emission rates and solar increases emission rates.
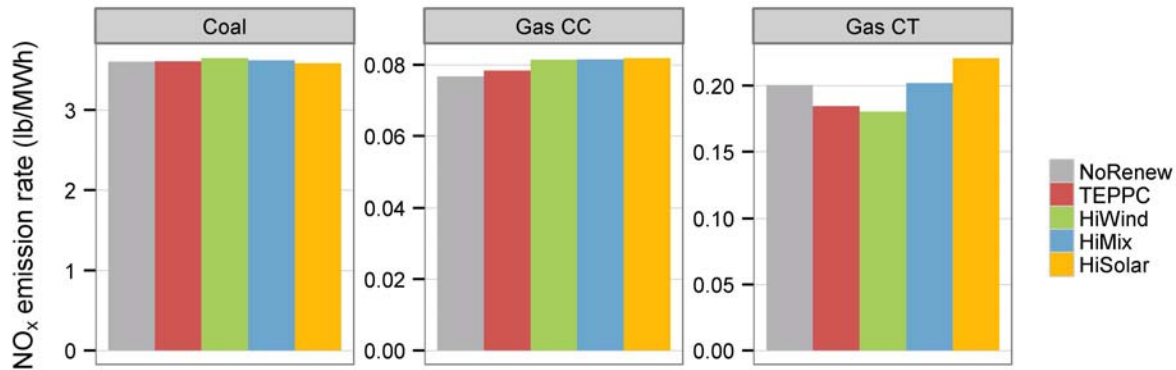
Figure 97. NO$_X$ emission rates from the average coal, gas CC, and gas CT unit
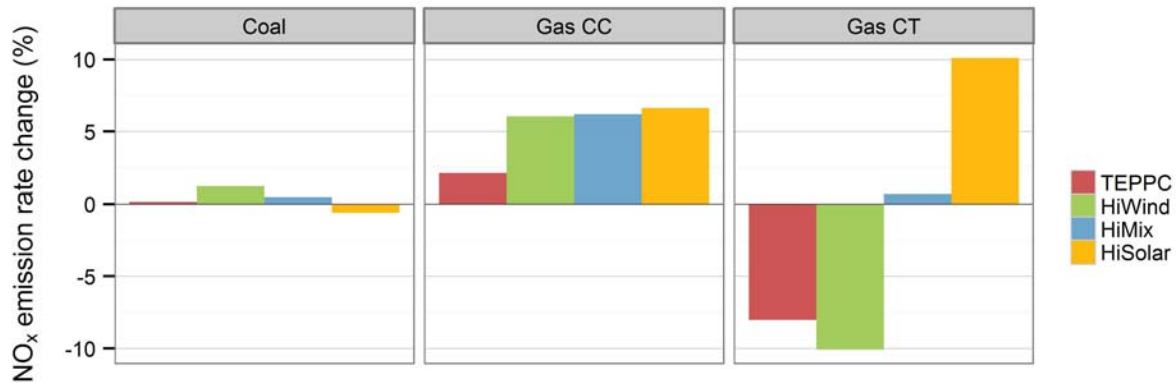
Figure 98. Change in NO$_X$ emission rates from the average coal, gas CC, and gas CT unit compared to the No Renewables Scenario

114

Figure 99 shows SO_2 emission rates from coal units by scenario and the change compared to the No Renewables Scenario. Gas units emit negligible amounts of SO_2. SO_2 emissions per MWh of generation lessen slightly (1%) in the High Wind Scenario and increase slightly (2%) in the High Solar Scenario.
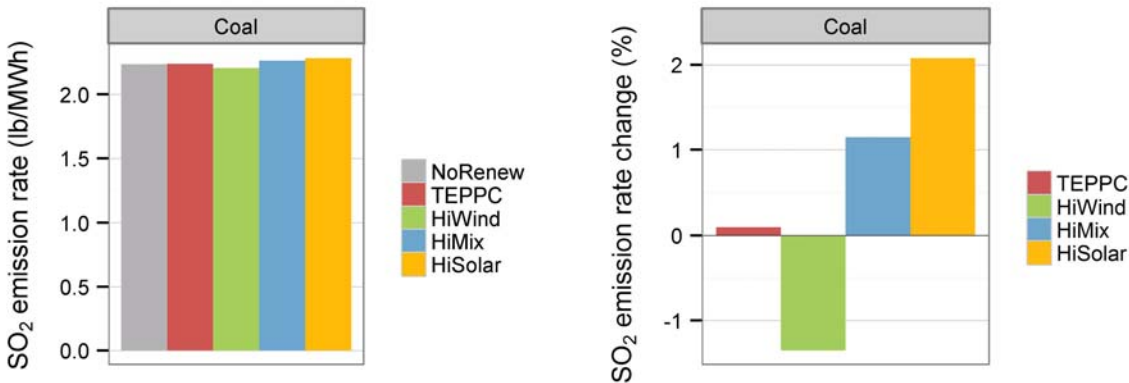
Figure 99. SO_2 emission rates from the (a) average coal unit and (b) change compared to the No Renewables Scenario

A 24%–26% penetration of wind and solar throughout all of the Western Interconnection (including Canada and Mexico) leads to a system-wide 29%–34% reduction in CO_2, a 16%–22% reduction in NO_x, and a 14%–24% reduction in SO_2. Wind penetration is more effective at reducing CO_2, SO_2, and NO_x emissions than solar because it displaces a greater fraction of coal generation. Wind- and solar-induced cycling has a very small impact (less than 5%) on the avoided CO_2, SO_2, and NO_x emissions from wind and solar, and wind/solar penetration has a small impact (always less than 10%, usually less than 2%) on emission rates (lb/MWh) of fossil-fueled generators. These are average results; cycling impacts on emissions can be smaller or greater for an individual generating unit.

6.6 Reserves and Unserved Load

There was no unserved load in any scenario. Contingency, regulating, and flexibility reserves were held using the methodology in Section 5. Figure 100 shows the reserve violations for contingency and regulating reserves. No regulating reserve violations were seen. Contingency reserve violations were very close to zero. They ranged from 2–4 MW-h of shortfall per 1 million MW-h required, and total shortfalls were less than 100 MW-h for all scenarios. This is in contrast to WWSIS-1 where contingency reserve violations totaled approximately 50 GWh. The difference is probably because WWSIS-2 held flexibility reserves in the unit commitment markets and also operated a 4HA market, neither of which was done in WWSIS-1.

Contingency reserve violations were much higher in the No Renewables Scenario because the power system was slightly underbuilt in this scenario. The wind and solar capacity removed from the TEPPC case was not replaced with equivalent thermal generator capacity because the scenario was used only for comparison purposes. Figure 100 does not show the No Renewables Scenario reserve violations.
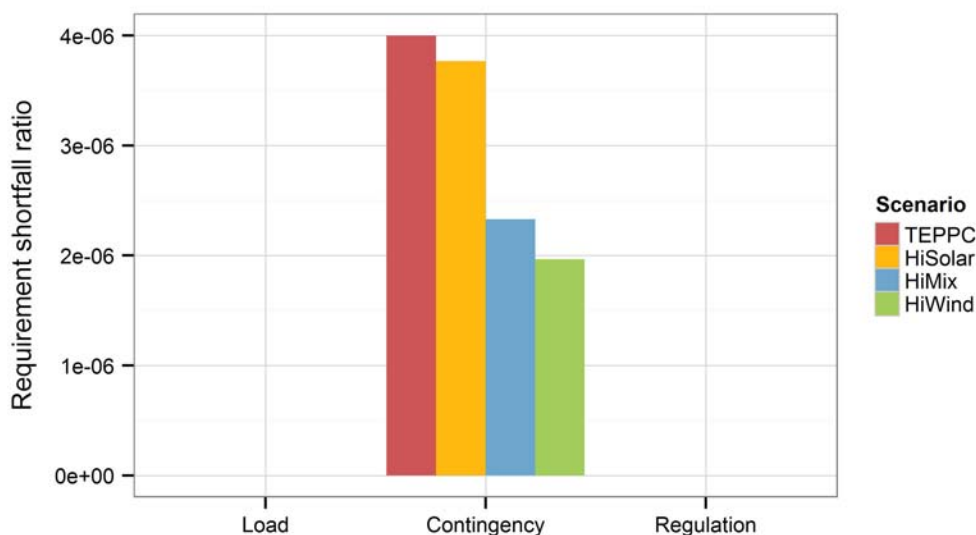
Figure 100. Unserved load and contingency and regulation reserve shortfalls, by scenario (as a fraction of total reserve requirement)

There was no unserved load or regulation reserve shortfalls in any scenario and contingency reserve shortfalls are negligible. For every 1 million MW-h of contingency reserves required by the statistical methodology, between 2 and 4 MW-h goes unserved in the scenarios. Holding flexibility reserves in the unit commitment markets and running a 4HA market likely contribute to minimizing the unserved contingency reserves.

6.7 Curtailment

This section investigates curtailment of wind and PV. We exclude CSP in these graphs because its thermal storage alleviates the need to curtail CSP, although some curtailment of CSP is expected based on the ratio of storage to turbine size. Figure 101 shows the percentage of total available PV and wind generation that is curtailed. Curtailment is highest with high solar penetrations but is still less than 5%. The High Wind Scenario has slightly more than 3% curtailment. Notably, the High Mix Scenario has the least curtailment (1.6%). This demonstrates that a more balanced mix of wind and solar may be helpful to reduce curtailment.

Figure 102 shows the annual average diurnal profile of curtailment. As expected, high solar penetrations result in midday curtailment, although interestingly, curtailment tends to occur before the solar peak. This is because the solar output is rising faster than the load, which peaks much later in the day. The High Wind Scenario illustrates wind curtailment in the late night/early morning when wind is high and load is low. Some midday curtailment also occurs because there is a modest amount of solar in this scenario as well. Curtailment assigned to wind or solar is not shown here because the marginal cost for both is zero; therefore, the selection made by the model is not meaningful.

Figure 103 depicts the average hourly curtailment by season. The highest curtailment for the High Solar and High Mix Scenarios occurs in the spring when solar irradiance is high and summer thunderstorms have not yet begun. The High Wind Scenario sees most of its curtailment in the winter and spring when winds are high.

116
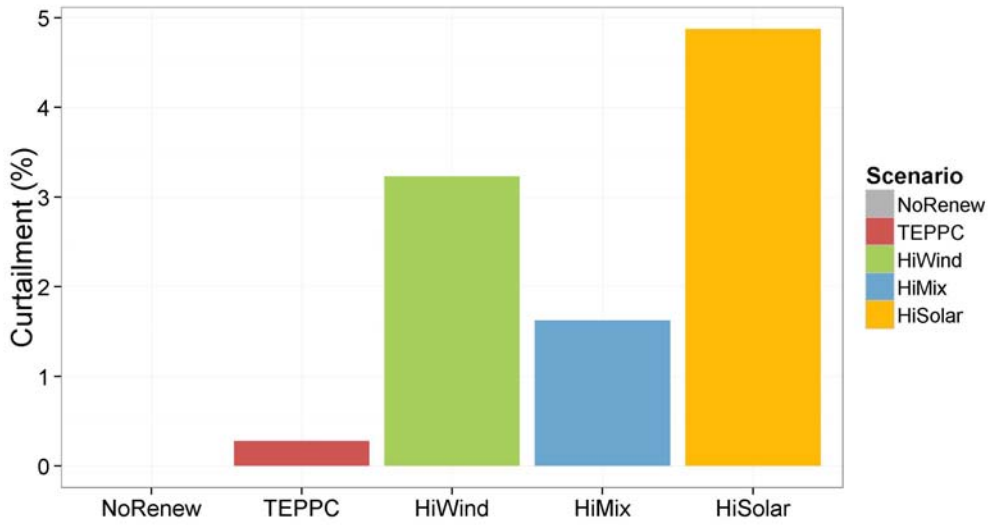
Figure 101. Curtailment as a percentage of available wind and PV generation
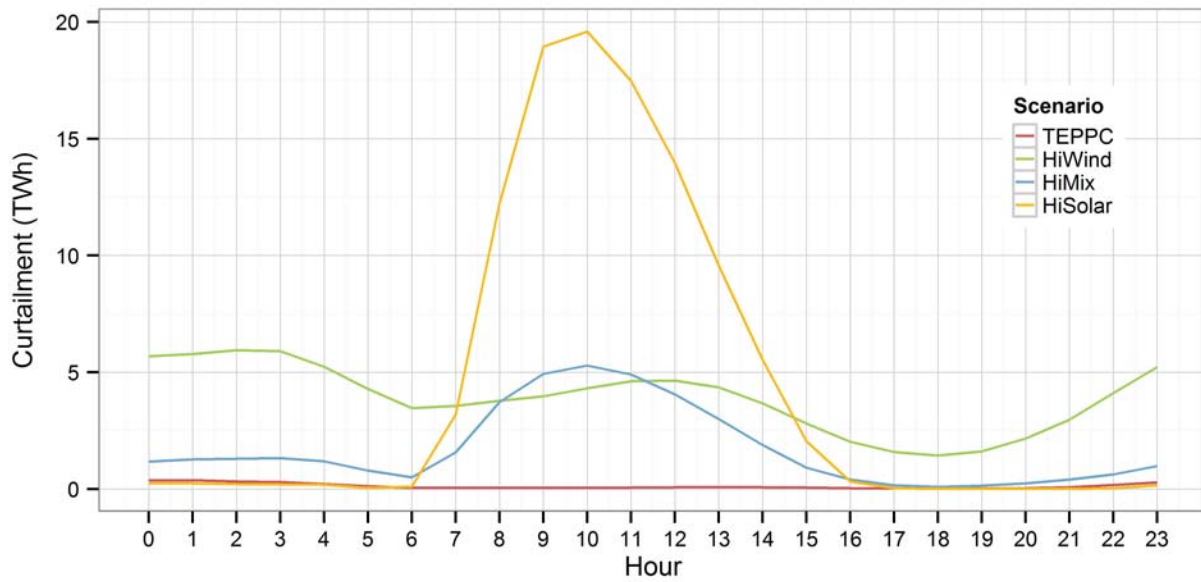
Figure 102. Curtailment diurnal profile for each scenario
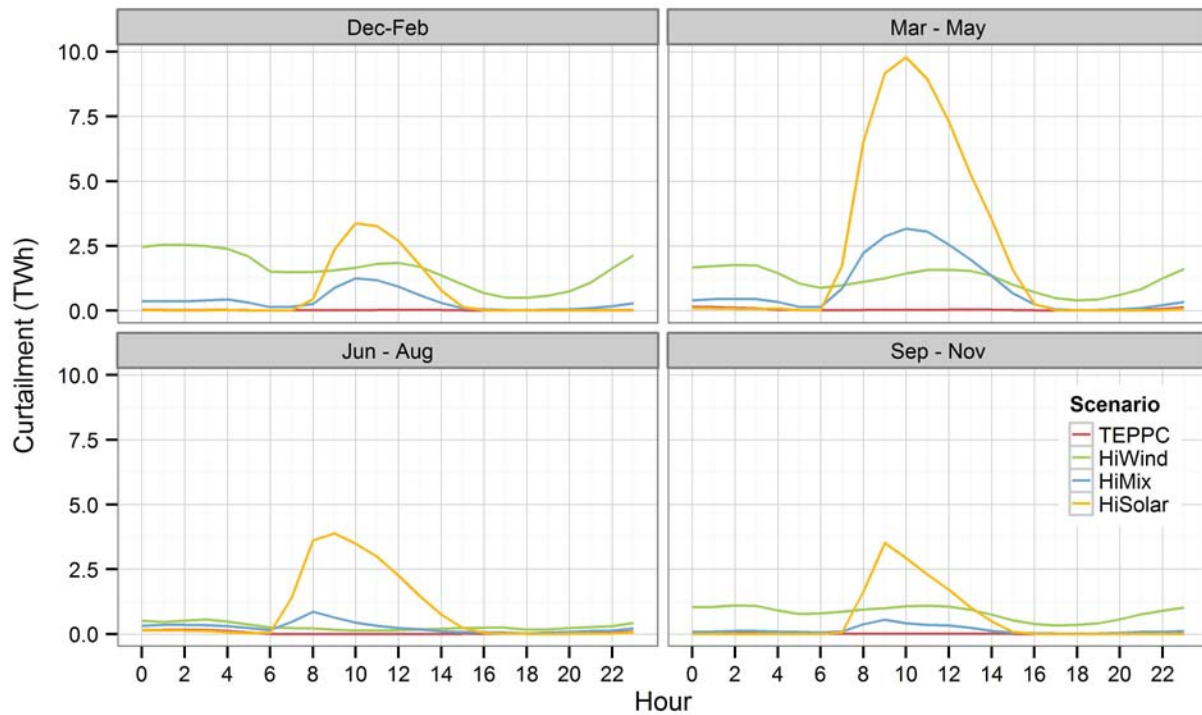
Figure 103. Average diurnal profile of curtailment by season for each scenario

Table 26 shows the curtailment by zone for the wind/solar scenarios. Most zones have very modest curtailment, but a few zones have curtailment of >10% in some of the scenarios. For example, Montana sees 13% curtailment in the High Wind Scenario and northern Nevada sees 16% curtailment in the High Solar Scenario.

Table 26. Curtailment by Zone

Region	TEPPC (%)	High Wind (%)	High Mix (%)	High Solar (%)
Arizona	0	1	2	9
California, North	0	0	0	0
California, South	0	0	0	1
Colorado	0	5	1	0
Idaho	0	0	0	0
IID	4	1	2	2
LAWP	0	0	0	0
Montana	2	13	5	2
Nevada, North	0	6	2	16
Nevada, South	0	1	1	2
New Mexico	0	1	3	12
Northwest	0	2	1	0
San Diego	0	0	1	4
San Francisco	0	3	3	3
Sacramento Municipal Utility District (SMUD)	0	0	0	0
Utah	0	0	0	0
Wyoming	0	5	1	0

Curtailment in the high-penetration scenarios is modest (2%–5%). We find the least curtailment with a balanced mixture of wind and solar. Solar curtailment occurs primarily during spring daylight hours. Wind curtailment is distributed more evenly throughout the days in the winter and spring.

6.8 Transmission Flows

The wind/solar scenarios show different patterns of congestion and flows. Figure 104 shows the interface flows (in annual TWh) in each direction between the transmission zones (from the WECC LRS zones). As more solar is added, average flows go down in most areas and some corridors experience more power flowing in both directions.
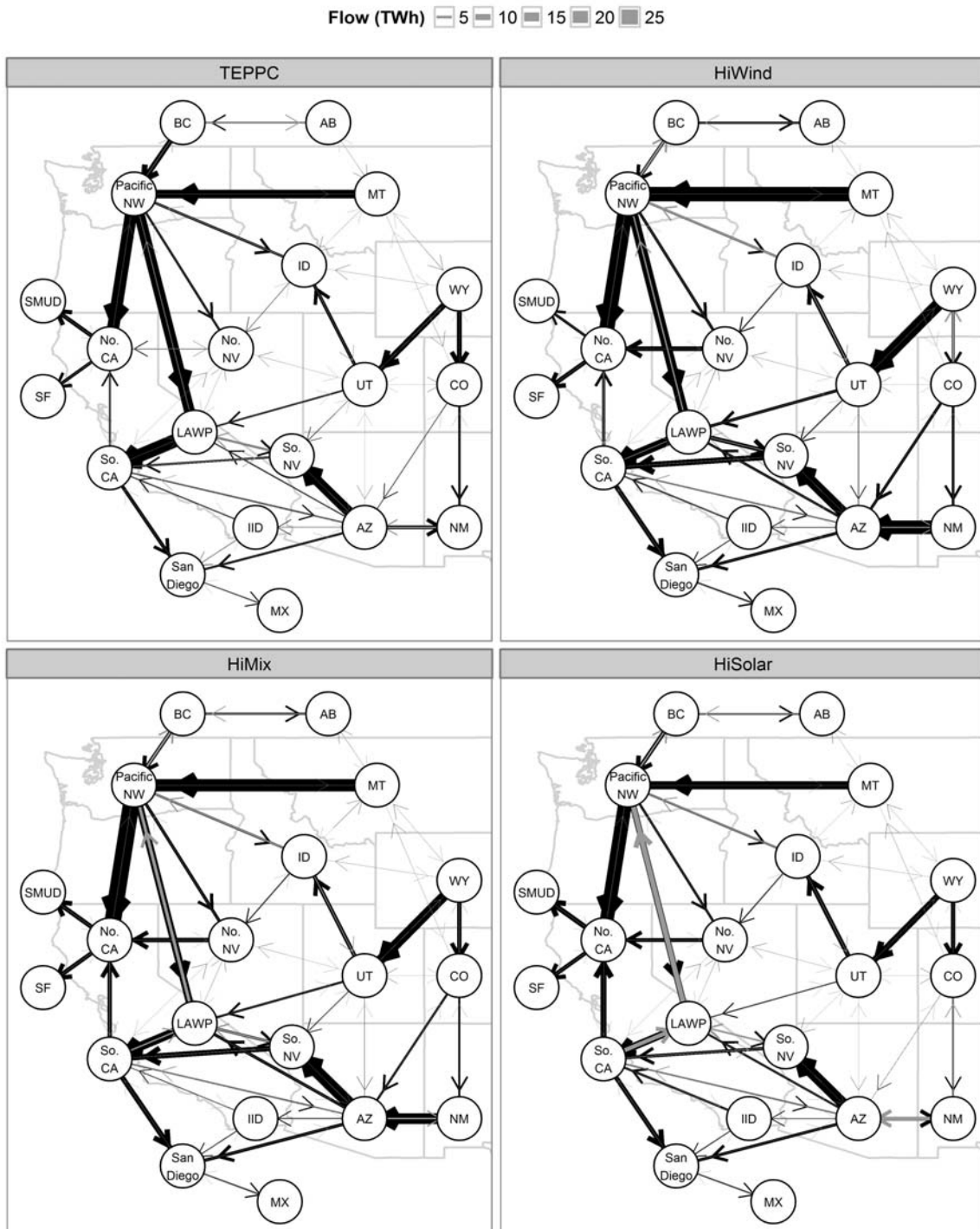
Figure 104. Interface flow map with prices for all scenarios

Notes: The width of the lines connecting zones denotes annual interface flows.
Bidirectional flows are shown with the smaller flow in gray and the larger flow in black.

Figure 105 shows flow duration curves across selected interfaces. Negative values represent flows in the opposite direction. In some scenarios, the flow limits are different because transmission build-outs differ. Flow limits can be seen on the plots when the curves flatten at the right or left side of the frame. For example, the MT to Pacific NW interface is congested approximately one-third of the time in all scenarios. Across some of the interfaces (e.g., AZ to Southern NV), there is very little change in flows between scenarios. Across others (e.g., Pacific NW to LAWP), the flows change significantly with scenario. Higher solar penetrations generally lead to lower flows and less congestion.
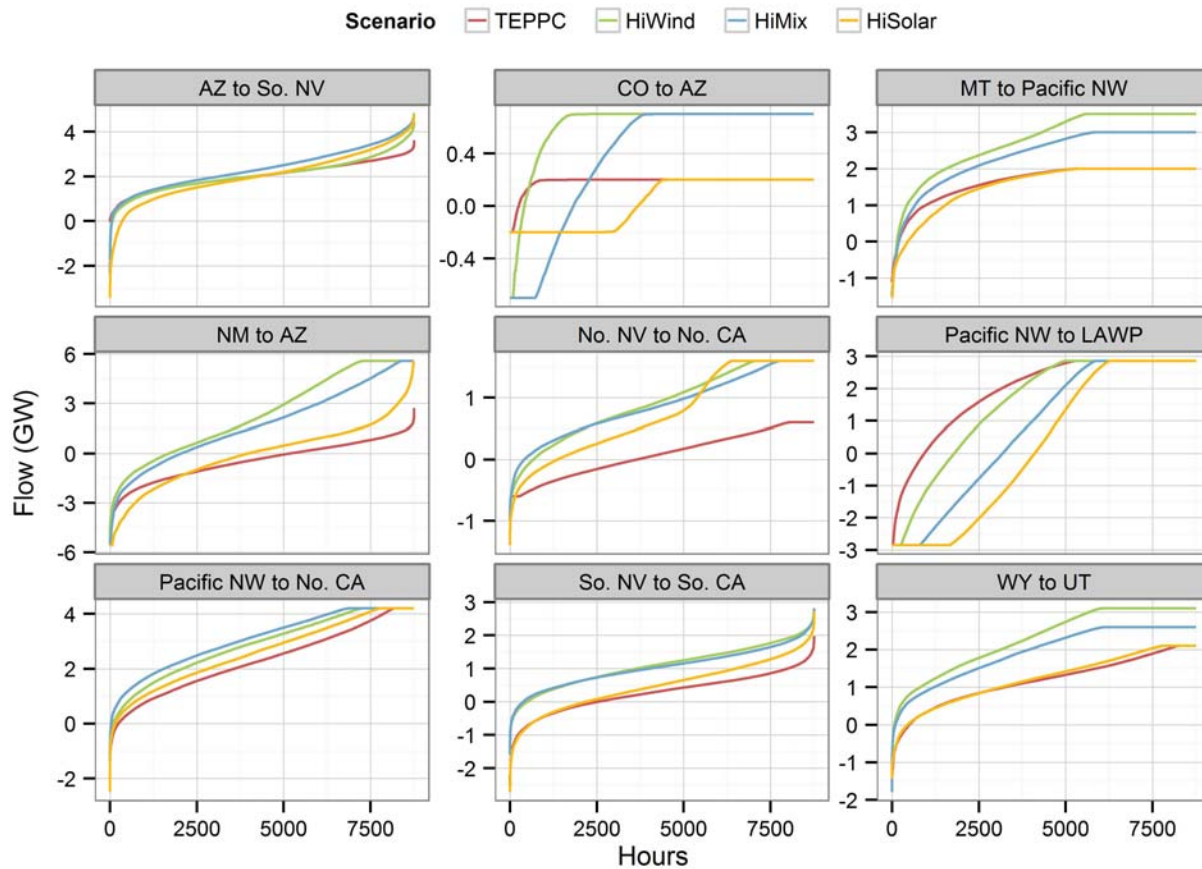
Figure 105. Flow duration curves across selected interfaces for each scenario

Higher wind penetrations generally lead to higher interface flows. Higher solar penetrations generally lead to slightly lower interface flows.

6.9 Gas Price Sensitivities

WWSIS-2 analysis is based on the WECC TEPPC assumption of an average natural gas price of $4.60/MMBtu across the Western Interconnection. Because operation is highly influenced by the ratio of coal to gas prices, we conducted a gas price sensitivity analysis using half and double the core gas price. We re-ran the production simulations for the No Renewables and High Mix Scenarios assuming an average natural gas price of $2.30/MMBtu (titled "$2.30 gas") and $9.20/MMBtu (titled "$9.20 gas").

121

Figure 106 shows the annual generation for all unit types. Very little difference is seen between the $4.60 and $9.20 gas cases because the natural gas units are already the most expensive and dispatch does not change dramatically if they become more expensive. With $2.30 gas, gas CC units are often cheaper than coal units, so generation from gas CC units replaces some generation from coal units in both the No Renewables and High Mix Scenarios. The differences in dispatch for other unit types are relatively minor.
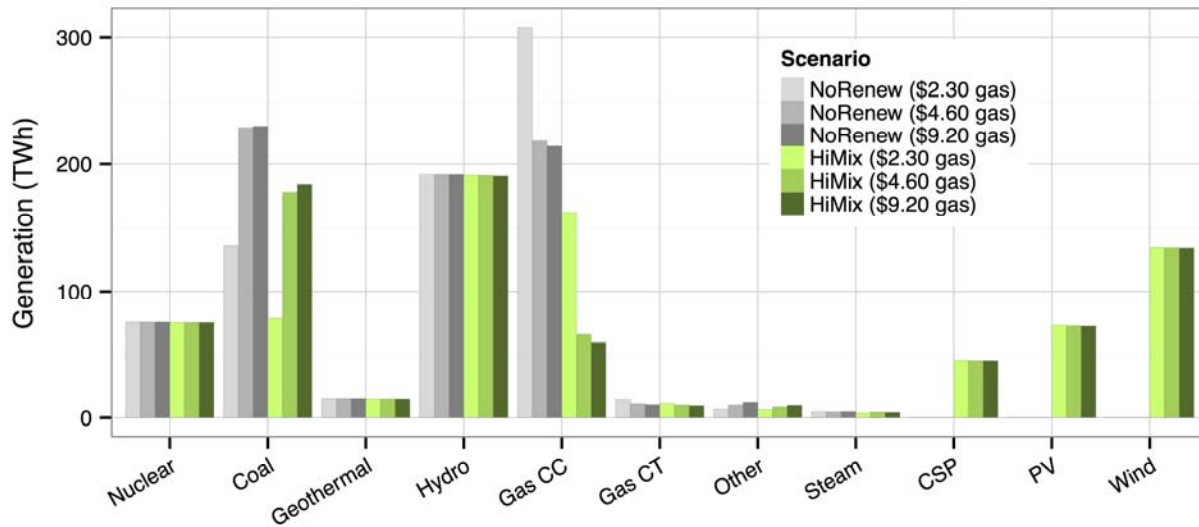
Figure 106. Annual generation by type in the gas price sensitivities

Figure 107 shows the generation that is displaced in the High Mix compared to the No Renewables Scenarios for each gas price assumption. Despite major differences in coal dispatch in the $2.30 and $4.60 scenarios, the amount of coal displaced by wind and solar is quite similar between the cases. As gas becomes cheaper, more coal is displaced because coal is more likely to be the marginal fuel type.
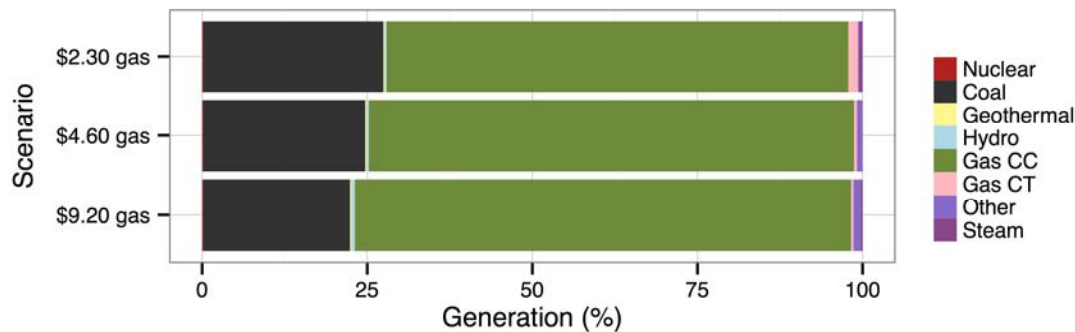
**Figure 107. Generation displaced by renewables in the High Mix
compared to No Renewables Scenarios for each gas price**

Figure 108 and Figure 109 show the capacity started and the number of ramps, respectively, in the gas price sensitivities. In the $2.30 gas cases, coal units are started less (and produce less energy). In the $9.20 gas cases, gas CC units are started more frequently because they are operated more as peaking units. The most noticeable change in the ramping patterns is that coal ramps more and gas CC units ramp less in the low gas price sensitivity. This is because gas CC units replace some of the coal units as baseload generation.
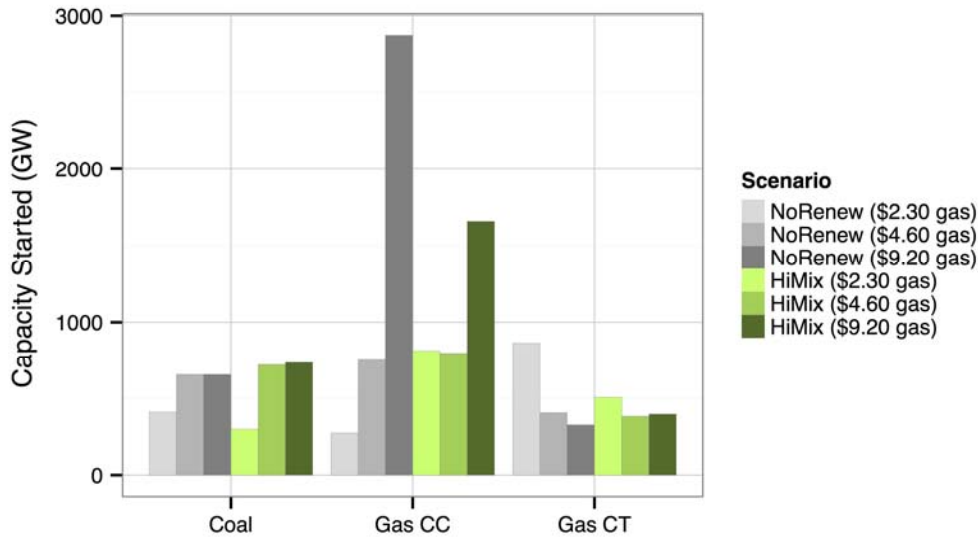
Figure 108. Capacity started in the gas price sensitivities
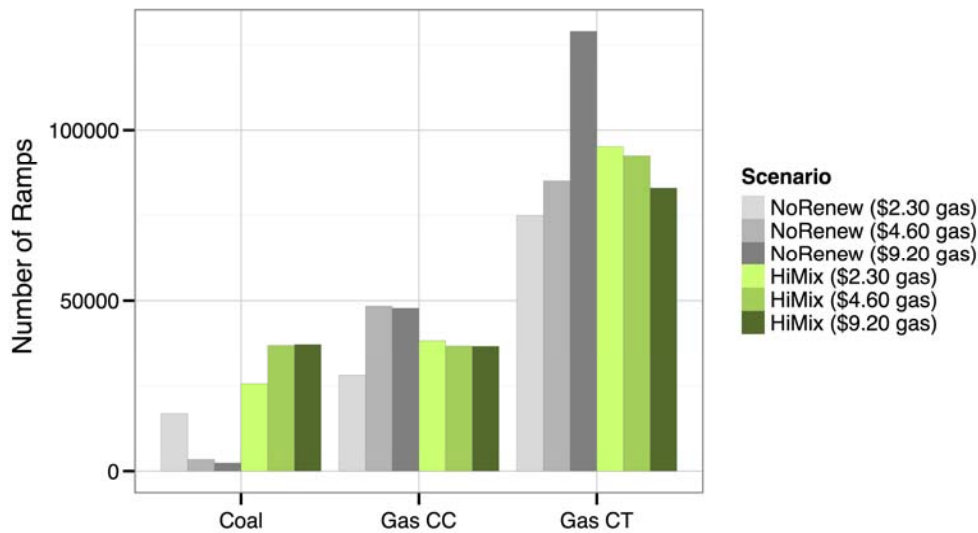
Figure 109. Number of ramps in the gas price sensitivities

Table 27 shows the increase in cycling costs resulting from renewable penetration compared to the corresponding No Renewables Scenario in each of the High Mix gas price sensitivities. In the original $4.60 case, adding wind and solar increased total cycling costs. In the $2.30 and $9.20 cases, adding renewables actually reduced total cycling costs. In the $2.30 case, the reduction was very small, and was partially caused by the coal units starting (and operating) less. In the $9.20 case, the reduction was more significant because the gas CC units started much less. In the

123

No Renewables $9.20 case, the gas CC units were used as peaking units when possible (started regularly), but this usage was displaced in the High Mix $9.20 case. As seen in Figure 110, the price of gas had a much larger impact on the total cycling cost than the addition of wind and solar generation to the system. This primarily resulted from the increased cycling of gas CC units in the different scenarios (as the pattern of operation changed from baseload to peaking).

Despite the significant difference in overall cycling costs between the cases, the impact on fossil-fueled generation was similar in all of the cases. The cycling costs per MWh of fossil-fueled generation increased by $0.30 to $1.16, depending on the gas price and cycling cost assumptions (lower versus upper bounds). The increase in cycling costs at fossil-fuel units occurs despite the reduction in overall cycling costs because generation from fossil-fuel units is significantly reduced in the High Mix Scenario.

Table 27. Cycling Cost Impacts of Wind and Solar in the High Mix Scenario (Gas Price Sensitivity)

Scenario	Increase in Cycling Costs (compared to corresponding No Renewables Scenario)		
	Total (million $)	Per MWh Wind and Solar Generation ($/MWh)	Per MWh Fossil-Fueled Generation ($/MWh)
High Mix, $2.30	−1 to −6	−0.02 to 0.00	0.30 to 0.81
High Mix, $4.60	34 to 95	0.14 to 0.38	0.47 to 1.16
High Mix, $9.20	−76 to −200	−0.30 to −0.80	0.47 to 0.92

* The PLEXOS model was updated before these gas price sensitivity runs, and very minor (<1%) differences exist between the numbers here for the $4.60 case and the original High Mix and No Renewables Scenarios.
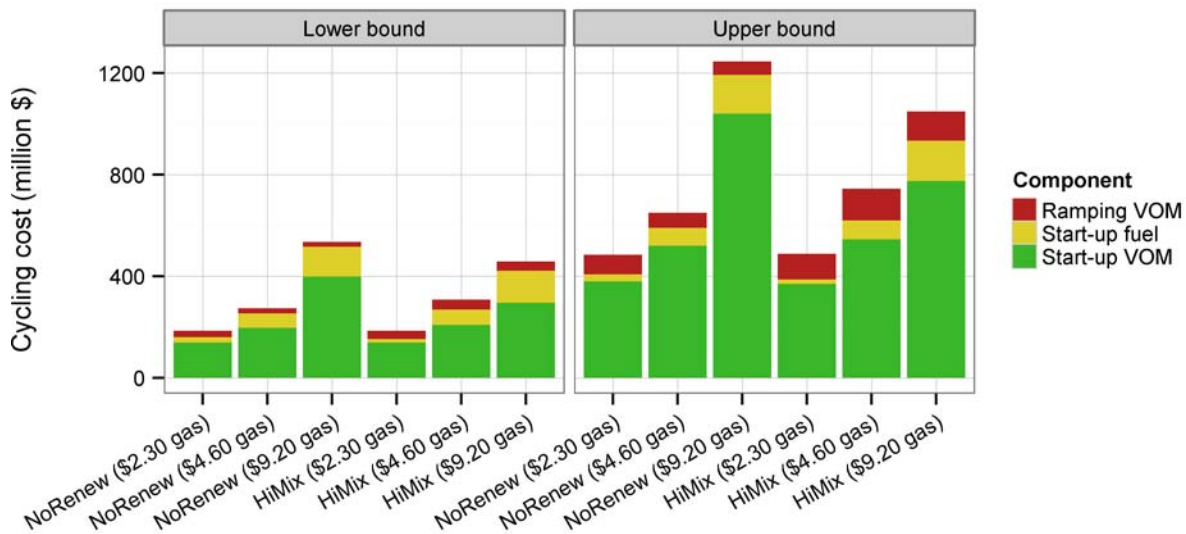
Figure 110. Cycling cost in the gas price sensitivities showing (left) lower and (right) upper bounds

Table 28 shows the emissions impacts of wind and solar for the different gas price assumptions. The avoided emissions depend primarily on whether gas CC or coal generation was displaced. Because the displaced energy was relatively similar in all cases, the avoided emissions are somewhat similar as well. The differences are mostly due to the emission rates of the displaced units, not because the impact of cycling is different in any of the gas price sensitivities.

**Table 28. Emissions Avoided per MWh of Wind and Solar Generation—
Considering Combined Part-Load, Ramping, and Start Impacts**

Scenario	Avoided CO_2 (lb/MWh)	Avoided NO_X (lb/MWh)	Avoided SO_2 (lb/MWh)
High Mix, $2.30	1,300	1.18	0.76
High Mix, $4.60	1,150	0.81	0.44
High Mix, $9.20	1,110	0.75	0.40

Figure 111 shows curtailment in the gas price sensitivities. Although energy becomes more expensive with higher gas prices, curtailment also increases. This correlates with the amount of coal online in the given cases. More coal generation is associated with more curtailment because the cost of shutting down coal units for a few hours is higher than the cost to keep them online, even when zero-cost energy is available.
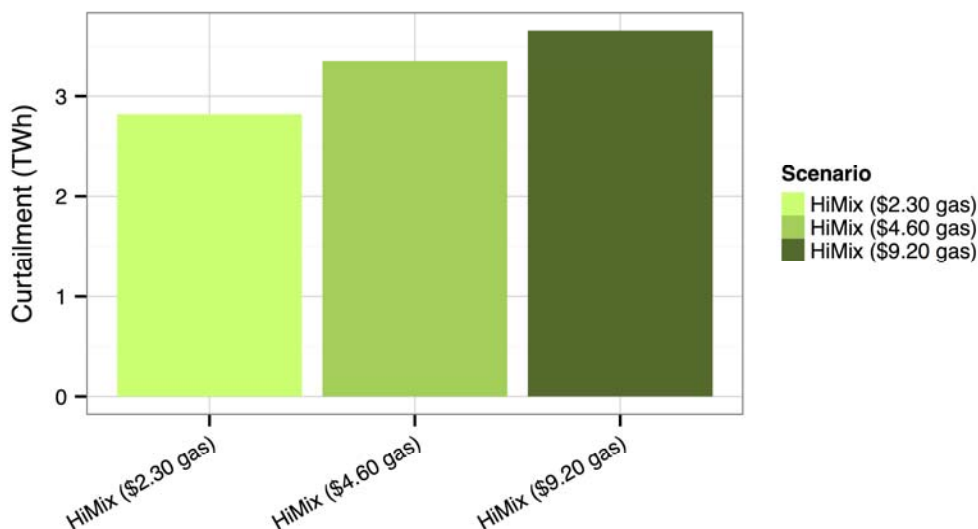
Figure 111. Curtailment in the gas price sensitivities

Figure 112 shows the production cost change per MWh of wind and solar generation for the High Mix case in the gas price sensitivities. Production cost reductions due to wind and solar become larger as gas price increases because of the increased value of the displaced fuel. Noncycling VOM and cycling costs have very little impact on the overall cost impacts. The total production cost reduction of wind and solar is approximately $18/MWh, $30/MWh, and $56/MWh for assumed natural gas prices of $2.30/MMBtu, $4.60/MMBtu, and $9.20/MMBtu, respectively.
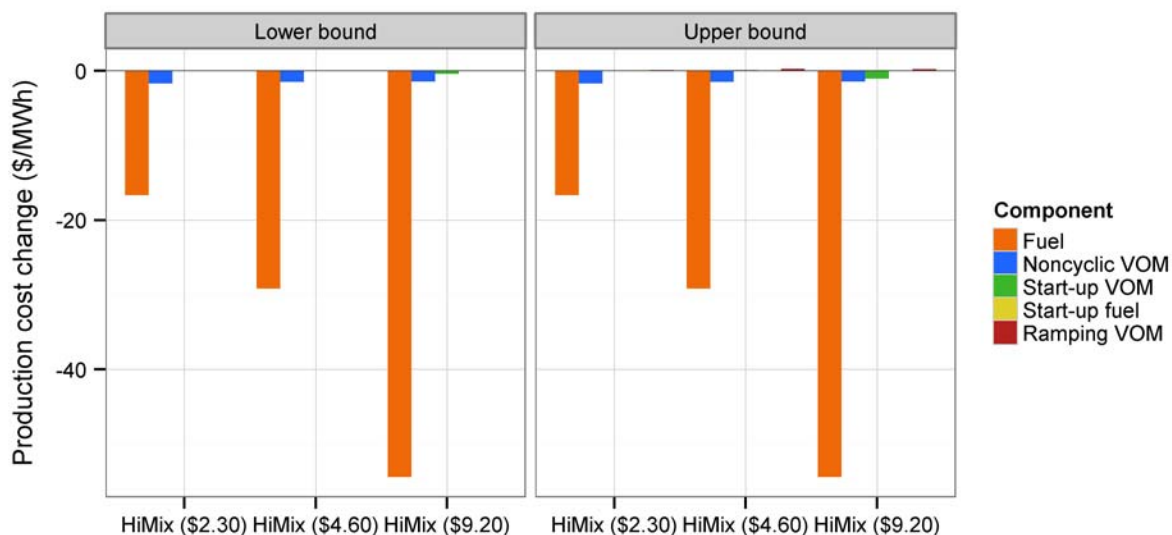
**Figure 112. Production cost change per MWh
of wind and solar generation in the gas price sensitivities**

*The price of gas had a much larger impact on the system cycling cost than the addition of wind and solar. With lower or higher gas prices, adding wind and solar actually **lowers** system cycling costs (up to $0.80/MWh of wind and solar). The effect that wind and solar have on the cycling cost per MWh of fossil-fuel generation is similar in all cases.*

6.10 Production Simulation Conclusions

We ran PLEXOS for the five scenarios to determine operational impacts of wind and solar generation. The Western Interconnection can operate with 33% wind and solar energy with no unserved load, no regulating reserve shortfalls, and only minimal contingency reserve shortfalls. Spring is the most challenging time for the high-penetration scenarios because of the high wind and solar output combined with the low load. The electric power system provides supply-side flexibility in a number of ways. Cycling is one of those methods, along with hydro flexibility, storage dispatch, and wind/solar curtailment.

We investigated the impacts of wind and solar on starts and ramping of fossil-fueled generators. The biggest impact of wind and solar on cycling is the increased ramping of coal units. Coal starts do not change appreciably. Coal units ramp daily in the spring down to minimum generation levels and back up to maximum capacity with high wind/solar penetrations, especially with high solar penetrations. Increasing wind penetrations are actually beneficial for gas CT cycling because they result in CTs being started and ramped less frequently. Gas CTs start more often with high solar penetration, helping to meet evening peaks as the sun sets. Gas CC units start more often and ramp more often per hour of operation with high wind/solar penetration. Wind and solar mostly displace gas CC generation. Instantaneous wind and solar penetration (averaged over a 5-minute interval) is below 60% in all scenarios.

126

Including wear-and-tear start costs within the production simulation optimization is important for conducting detailed analysis of high wind and solar penetration impacts. It is less important if the user is trying to understand high-level, system-wide impacts.

In this study, cycling (start, start fuel, and ramping) costs total between \$271–\$643 million (in the No Renewables Scenario) and \$324–\$800 million (in the High Solar Scenario). The cycling costs were dominated by start costs. These ranges represent the uncertainty in cycling costs. The cycling costs represent a relatively small fraction of total fuel costs (\$9–\$17 billion).

We can frame these costs from a system perspective, examining the impact of cycling on the change in production cost from wind and solar. Based on the specific system characteristics modeled for the Western Interconnection, these same cycling costs at low penetrations offset production cost reductions from wind and solar by \$0.41–\$1.05/MWh to \$32.6–\$33.2/MWh, and at high penetrations offset production cost reductions by \$0.14–\$0.67/MWh to \$29.4–\$30.6/MWh. Production cost does not include any capital costs or PPAs for thermal units, renewable generators, or transmission.

We can next frame these same cycling costs from the perspective of increased O&M of the fossil-fueled plants. High penetration levels of wind and solar could add to the O&M of the average fossil-fueled generator by up to \$1.28/MWh. At low penetrations, we find that the wind- and solar-induced cycling at the average fossil-fueled unit increases O&M by \$0.18–\$0.44/MWh. For high penetrations, this O&M increase is \$0.47–\$1.28/MWh.

With or without wind and solar, gas CTs have the highest cycling O&M because CTs undergo the most cycling. Compared to the system without wind or solar, cycling O&M for CTs actually decreases with low wind/solar penetrations and does not change for the High Wind Scenario. As solar penetration increases, the cycling O&M of CTs significantly increases because CTs were often started to handle the evening peak.

To determine emissions impacts, we had to aggregate emissions across the three countries in the Western Interconnection to capture the interchanges. The high penetration scenarios (24%–26% penetration of wind and solar throughout all of the Western Interconnection, including Canada and Mexico) leads to a 29%–34% reduction in CO_2, a 16%–22% reduction in NO_x, and a 14%–24% reduction in SO_2 system-wide. Because the High Wind Scenario displaces the most coal generation, the avoided emissions rates and overall reductions are the highest in this scenario.

Cycling impacts on CO_2, SO_2, and NO_x emissions were relatively small and ranged from –4.5% (reducing the avoided emissions of wind and solar by 4.5%) to +6.3% (increasing the avoided emissions of wind and solar). Start impacts were small in all cases (much less than 1%) because of the relatively modest change in the number of starts and the relatively small excess emissions caused by starting units for most pollutants. Cycling has a negligible impact on CO_2 emissions. NO_x reductions from wind and solar are actually 1%–2% higher than what would be expected if cycling is not considered because coal units in the West typically have lower NO_x emissions rates at part-load. Impacts of starts and ramping (part-load could not be assessed) on SO_2 were modest at high penetrations, reducing avoided SO_2 by 2%–5%. These are averaged results— cycling impacts on emissions could be smaller or greater for an individual generating unit.

We next view these same emissions from the perspective of a fossil-fueled generator that experiences emissions rate changes because of cycling. CO_2, SO_2, and NO_x emissions rate changes were very small. Interestingly, wind and solar sometimes increased and sometimes decreased average emissions rates, depending on pollutant, plant type, and scenario.

For CO_2 emissions, the largest wind and solar impacts were a 2% increase in the emissions rates for the average gas CT in the High Wind Scenario and a 1% decrease in the average gas CC unit emissions rates in the High Solar Scenario. For NO_x emissions, the largest wind and solar impacts were a 10% increase in the emissions rates for the average gas CT in the High Solar Scenario and a 10% decrease in the average gas CT emissions rates in the High Wind Scenario, although most types of units were affected by much less than 10%. For SO_2 emissions, the largest wind and solar impacts were a 2.1% increase in the emissions rates for the average coal unit in the High Solar Scenario and a 1.4% decrease in the average coal emissions rates in the High Wind Scenario. These are averaged results—individual units could be higher or lower.

We find modest curtailment up to 5% with high wind/solar penetrations. We find the least curtailment with a balanced mixture of wind and solar. Solar curtailment occurs primarily during spring daylight hours; wind curtailment is distributed more evenly throughout the days in the winter and spring.

Finally, we examined transmission flows and congestion. We found that higher wind penetrations generally lead to higher interface flows and higher solar penetrations generally lead to lower interface flows.

7 Conclusions

In this study, a detailed operational analysis of the Western Interconnection was conducted. The study focused on the wear-and-tear costs and emissions impacts from cycling of fossil-fueled plants. Increasing penetrations of wind and solar can induce increased cycling. Because some plants—especially many baseloaded coal plants in the West—were not designed for this type of cyclic operation, they can suffer increased repair and maintenance costs. Some analysts have asserted that the additional emissions from this type of operation can be significant compared with the emissions reductions from wind and solar. To the contrary, we found that the emissions reductions from wind and solar far outweigh emissions imposed by wind- and solar-induced cycling.

A detailed, consistent wear-and-tear cost and forced outage rate impact database was created for seven categories of plants for starts, ramps, and noncyclic operation. To our knowledge, this is the first public data set to calculate wear-and-tear costs and impacts for cycling, and one of the few integration studies that uses these explicit start costs to make unit commitment and economic dispatch decisions.

A detailed, plant-specific emissions database was created for nearly every plant in the West. The database describes the incremental emissions from starts and ramps as well as their emissions rates at part-loading.

Existing wind and solar output and forecast data sets were revised to reflect improvements in modeling utility-scale wind and solar plants and state-of-knowledge forecast errors. We developed a new reserves methodology for regulating and flexibility reserves that incorporates the short-term forecast error and the weather component of variability for wind and solar.

Next, these new data sets were used in a 5-minute unit commitment and economic dispatch model to examine subhourly impacts of wind and solar up to 33% energy penetration levels. We investigated the impacts on cycling and the resulting costs and emissions. We compared impacts of wind and solar on the rest of the power system. Under the scenarios studied, we found the following:

- Wind and solar increase cycling costs by \$35–\$157 million/year, or 13%–24%, across the Western Interconnection. Those costs are a small percentage of the displaced fuel costs of \$7 billion/year that result from wind and solar. For the average fossil-fueled plant, cycling costs increase by \$0.47–\$1.28/MWh of fossil-fueled generation, which is a significant increase. Starts, not ramps, drive total cycling costs. CTs incur the most cycling costs per MWh of operation, although CT cycling costs do not increase in the High Wind Scenario and actually decrease in the TEPPC Scenario. From a system perspective, the production cost reduction from wind and solar is \$29.4–\$33.2/MWh of wind and solar generated. Without considering cycling costs, the reduction would have been \$29.9–\$33.6/MWh. This does not account for fixed capital or PPA costs.

- Wind and solar lead to markedly increased ramping for coal generators, and coal runs fewer hours per start with high wind penetrations. Typical coal units ramp daily instead of weekly as wind and solar penetrations, especially solar, increase. Coal units do not start considerably more as renewable penetrations increase. With wind and solar, runtime per start for gas CC plants is halved from the No Renewables Scenario. At low wind and solar penetrations, gas CC units are started much more, but this impact decreases with high penetrations. Gas CTs start and ramp less often in scenarios with high ratios of wind to solar penetration. High solar penetrations, on the other hand, lead to more starts, shorter runtimes, and more ramping of CTs.

- This study finds that up to 33% wind and solar energy penetration in the United States' portion of the Western grid (which is equivalent to 24%–26% throughout the Western grid) avoids 29%–34% CO_2 emissions, 16%–22% NO_x emissions, and 14%–24% SO_2 emissions throughout the Western grid. Cycling impacts on CO_2 emissions were negligible. Considering cycling and part-load in detail results in 1%–2% more NO_x reduction from wind and solar than expected because, on average, coal plants in the West have lower NO_x emissions rates at part-load. Cycling results in 2%–5% less SO_2 reduction from wind and solar than expected.

- The impacts of wind and solar were compared, using new data sets that illuminated the subhourly variability of utility-scale PV. Wind and solar generation affect the system in different ways. They both mostly displace gas CC generation, but wind tends to displace more coal compared to solar. Solar tends to dominate variability extremes, but it can be mitigated because most of this variability is known and can be anticipated in the unit commitment. Wind tends to dominate uncertainty extremes, because of tail events in DA wind forecast errors. This can be mitigated by committing gas CC units in the 4HA time frame and gas CTs on shorter time frames. High wind and solar penetrations result in modest curtailment—up to 5%—and WWSIS-2 finds that a balanced mix of wind and solar reduces curtailment to 1.6%.

Future Work

Although system-wide impacts of cycling are modest, an individual unit might be cycled much more. In this case, plant owners will want to know whether they should retrofit their units or change their operations to better manage cycling at lower overall cost. Ongoing work includes research on potential retrofits or operational strategies to increase the flexibility of fossil-fueled generators. This includes analysis of the costs and benefits of retrofitting existing plants for options such as lower minimum generation levels or faster ramp rates.

Additional work that would illuminate the impacts of cycling and further compare wind and solar includes analysis of the following:

- Market impacts on fossil-fueled plants: How do increased O&M costs and reduced capacity factors affect cost recovery for fossil-fueled plants? What market structures might need revision in a high wind and solar paradigm? How do the economics look for those plants that were most affected?

- Different retirement scenarios: How are operations and results affected if significant coal capacity is retired or if the balance of plants is flexible versus inflexible?

- Storage: Does storage mitigate cycling and is it cost effective?

- Impacts of dispersed versus centralized PV: How does rooftop versus utility-scale PV affect the grid?

- Reserves requirement testing to fine tune flexibility reserves: What confidence levels of flexibility reserves are most cost effective and still retain reliable grid operation?

- Scenarios with constrained transmission build-outs: If transmission is constrained, how does the grid perform and how is cycling affected?

- Reserve-sharing options: How do different reserve-sharing options affect grid operations?

- Increased hydro flexibility and modeling assumptions: How does flexibility in the hydro fleet affect grid operations and what is the impact on cycling?

- Higher resolution representation of BA coordination and transmission: With higher hurdle rates to mimic less BA cooperation, how are grid operations and cycling affected? With nodal instead of zonal production simulations, how do operations change?

- Comparison of the detailed 5-minute production simulation modeling with cycling costs to hourly production simulation modeling without cycling costs: How much more accurate is the detailed modeling?

- Gas supply: Is additional gas storage needed? How does increased wind and solar affect gas scheduling and supply issues?

- Market sequence: How much does the system benefit from the 4HA market?

References

3Tier (2010). *Development of Regional Wind Resource and Wind Plant Output Data Sets.* NREL/SR-550-47676. Golden, CO: NREL. Accessed January 2013: www.nrel.gov/docs/fy10osti/47676.pdf.

Bentek Energy (2010). *How Less Became More…Wind, Power, and the Unintended Consequences in the Colorado Energy Market.* Evergreen, CO: Bentek Energy. Accessed January 2013: www.bentekenergy.com/windcoalandgasstudy.aspx.

Charles River Associates (2010). *SPP WITF Wind Integration Study.* Little Rock, AR: SPP. Accessed January 2013: http://www.uwig.org/CRA_SPP_WITF_Wind_Integration_Study_Final_Report.pdf.

Connolly, S.; Parks, K.; Janecek, C. (2011) *Wind Induced Coal Plant Cycling Costs and the Implications of Wind Curtailment for Public Service Company of Colorado.* Denver, CO: Xcel Energy. Accessed January 2013: http://www.xcelenergy.com/staticfiles/xe/Regulatory/Transmission/11M-710E_WindInducedCoalPlantCycling.pdf.

EnerNex Corporation (2006). *Wind Integration Study for Public Service Company of Colorado.* Denver, CO: Xcel Energy.

EnerNex Corporation (2011). *Eastern Wind Integration and Transmission Study.* NREL/SR-5500-47078. Golden, CO: NREL. Accessed January 2013: www.nrel.gov/docs/fy11osti/47078.pdf.

Edwards, R. (2009). *Characterization of Hurricane Gust Factors Using Observed and Analytical Data.* Ph.D. Dissertation. Lubbock, TX: Texas Tech University.

EIA (2009). *Form EIA-923 Detailed Data.* Data file. Retrieved from http://www.eia.gov/electricity/data/eia923/.

Ela, E.; Milligan, M.; Kirby, B. (2011). *Operating Reserves and Variable Generation.* NREL/TP-5500-51978. Golden, CO: NREL. Accessed January 2013: http://www.nrel.gov/docs/fy11osti/51978.pdf.

EPA (2009). *Continuous Emissions Monitoring Dataset.* Data files. Retrieved from http://www.epa.gov/airmarkets/.

EPRI (2001). *Damage to Power Plants Due to Cycling.* Product ID 1001507. Palo Alto, CA: EPRI. Accessed January 2013: http://www.epri.com/abstracts/Pages/ProductAbstract.aspx?ProductId=000000000001001507.

ERCOT (2012). "ERCOT Sets New Wind Power Record." News release, November 16. Accessed February 2013: http://www.ercot.com/news/press_releases/show/26342.

Estanqueiro, A.; Ardal, A.R.; O'Dwyer, C.; Flynn, D.; Huertas-Hernando, D.; Lew, D.; Gomez-Lazaro, E.; Carlini, E.M.; Solvang, E.; Ela, E.; Kiviluoma, J.; Rodrigues, L.; Amelin, M. (2012). "Contribution of Energy Storage for Large-Scale Integration of Variable Generation." *Proceedings of the 2nd International Workshop on Integration of Solar Power into Power Systems*. November 12–13, Lisbon, Portugal. 7pp.

Fripp, M. (2011). "Greenhouse Gas Emissions from Operating Reserves Used to Backup Large-Scale Wind Power." *Environmental Science and Technology* (45:21); pp. 9405–9412. Accessed January 2013: http://dx.doi.org/10.1021/es200417b.

GE Energy (2007). *Intermittency Analysis Project: Appendix B. Impact of Intermittent Generation on Operation of California Power Grid*. CEC-500-2007-081-APB. Work performed by GE Energy, Schenectady, New York. Sacramento, CA: The California Energy Commission. Accessed January 2013: http://www.energy.ca.gov/2007publications/CEC-500-2007-081/CEC-500-2007-081-APB.PDF.

GE Energy (2008). *Analysis of Wind Generation Impact on ERCOT Ancillary Services Requirements*. Work performed by GE Energy, Schenectady, New York. Taylor, TX: ERCOT. Accessed January 2013: www.uwig.org/AttchA-ERCOT_A-S_Study_Exec_Sum.pdf.

GE Energy (2010). *Western Wind and Solar Integration Study*. NREL/SR-550-47434. Golden, CO: NREL. Accessed January 2013: http://www.nrel.gov/docs/fy10osti/47434.pdf.

GE Energy (2011). "PJM Renewable Integration Study." Prepared for the PJM Stakeholder Meeting, July 19. Accessed January 2013: http://www.pjm.com/~/media/committees-groups/committees/mic/20110719/20110719-study-scenario-development-ge.ashx.

Goggin, M. (2012). "Southwest Power Pool Achieves Wind Penetration Record." The AWEA Blog: Into the Wind, December 20. Accessed February 2013: http://www.awea.org/blog/index.cfm?customel_dataPageID_1699=20642.

Hansen, C. (2012). *Validation of Simulated Irradiance and Power for the Western Wind and Solar Integration Study, Phase II*. SAND2012-8417. Albuquerque, NM: Sandia National Laboratories. Accessed January 2013: http://energy.sandia.gov/wp/wp-content/gallery/uploads/2012_Hansen_WWSIS_irradiance_sim_validation_final.pdf.

Hodge, B.-M.; Milligan, M. (2011a). "Wind Power Forecasting Error Distributions over Multiple Timescales." Prepared for the IEEE Power and Energy Society General Meeting, July 24–28, Detroit, Michigan. NREL/CP-5500-53784. Golden, CO: NREL. Accessed January 2013: http://dx.doi.org/10.1109/pes.2011.6039388.

Hodge, B.-M.; Ela, E.; Milligan, M. (2011b). "The Distribution of Wind Power Forecast Errors from Operational Systems." Prepared for the 10th International Workshop on Large-Scale Integration of Wind Power, October 25–26, Aarhus, Denmark. NREL/CP-5500-52749. Golden, CO: NREL.

Hodge, B.-M.; Ela, E.; Milligan, M. (2012). "Characterizing and Modeling Wind Power Forecast Errors from Operational Systems for Use in Wind Integration Planning Studies." *Wind Engineering* (36:5); pp. 509–524. Accessed January 2013: http://dx.doi.org/10.1260/0309-524X.36.5.509.

Hummon, M.; Ibanez, E.; Brinkman, G.; Lew, D. (2012). "Sub-Hour Solar Data for Power System Modeling From Static Spatial Variability Analysis: Preprint." Prepared for the 2nd International Workshop on Integration of Solar Power into Power Systems, November 12–13, Lisbon, Portugal. NREL/CP-6A20-56204. Golden, CO: NREL. 9 pp. Accessed January 2013: www.nrel.gov/docs/fy13osti/56204.pdf.

Ibanez, E.; Brinkman, G.; Hummon, M.; Lew, D. (2013). "Solar Reserve Methodology for Renewable Energy Integration Studies Based on Subhourly Variability Analysis: Preprint." Prepared for the 2nd Annual International Workshop on Integration of Solar Power into Power Systems, November 12–13, Lisbon, Portugal. NREL/CP-5500-56169. Golden, CO: NREL. 8 pp. Accessed January 2013: www.nrel.gov/docs/fy12osti/56169.pdf.

Intelligent Energy (2009). *Integrating Wind: Developing Europe's Power Market for the Large-Scale Integration of Wind Power.* Accessed January 2013: www.uwig.org/TradeWind.pdf.

Jaffe, M. (2011). "Xcel sets record for electricity from wind." The Denver Post, November 16. Accessed February 2013: http://www.denverpost.com/business/ci_19343828.

Jordan, G.; Piwko, R. (2013). *An Analysis of the Impact of Balancing Area Coordination on the Operation of the Western Electricity Coordinating Council and the Compounding Effects of Wind and Solar Generation*. NREL/SR-5500-53095. Golden, CO: NREL.

Katzenstein, W.; Apt, J. (2009). "Air Emissions Due to Wind and Solar Power." *Environmental Science and Technology* (43); pp. 253–258.

Kumar, N.; Besuner, P.; Lefton, S.; Agan, D.; Hilleman, D. (2012). *Power Plant Cycling Costs*. NREL/SR-5500-55433. Work performed by Intertek-APTECH, Sunnyvale, California. Golden, CO: NREL. Accessed January 2013: www.nrel.gov/docs/fy12osti/55433.pdf.

Lefton, S.; Besuner, P. (2001) *Power Plant Cycling Operations and Unbundling Their Effect on Plant Heat Rate*. APTECH Technical Paper TP134. Sunnyvale, CA: APTECH.

Lew, D.; Alonge, C.; Brower, M.; Frank, J.; Freeman, L.; Orwig, K.; Potter, C.; Wan, Y.-H. (2011). "Wind Data Inputs for Regional Wind Integration Studies: Preprint." Prepared for the Power and Energy Society Annual Meeting, July 24–29, Detroit, Michigan. 11 pp. NREL/CP-5500-50636. Golden, CO: NREL. Accessed January 2013: http://dx.doi.org/10.1109/pes.2011.6039695.

Lew, D.; Brinkman, G.; Ibanez, E.; Hummon, M.; Hodge, B.-M.; Heaney, M.; King, J. (2012). "Sub-Hourly Impacts of High Solar Penetrations in the Western United States: Preprint." Prepared for the 2nd Annual International Workshop on Integration of Solar Power into Power Systems, November 12–13, Lisbon, Portugal. NREL/CP-5500-56171. Golden, CO: National Renewable Energy Laboratory. 11 pp. Accessed January 2013: http://www.nrel.gov/docs/fy12osti/56171.pdf.

Milligan, M.; Ela, E.; Hodge, B.-M.; Kirby, B.; Lew, D.; Clark, C.; DeCesaro, J.; Lynn, K. (2011). "Integration of Variable Generation, Cost-Causation, and Integration Costs." *Electricity Journal* (24:9); pp. 51–63.

Milligan, M.; Clark, K.; King, J.; Kirby, B.; Guo, T.; Liu, G. (2012). *Examination of Potential Benefits of an Energy Imbalance Market in the Western Interconnection*. NREL/TP-5500-57115. Golden, CO: NREL. Accessed April 2013: http://www.nrel.gov/docs/fy13osti/57115.pdf.

MISO (2012). "Peak Wind Output Tops 10 GW in MISO." Press release, November 27. Accessed February 2012: https://www.midwestiso.org/AboutUs/MediaCenter/PressReleases/Pages/WindOutputSurpasses10GW.aspx.

Mur-Amada, J.; Bayod-Rújula, Á. (2007). "Characterization of Spectral Density of Wind Farm Power Output." *9th International Conference on Electrical Power Quality and Utilisation Proceedings*; October 9–11, Barcelona, Spain. Accessed February 2012: http://ieeexplore.ieee.org/xpls/abs_all.jsp?arnumber=4424187.

Navigant Consulting, Inc.; Sandia National Laboratories; Pacific Northwest National Laboratory (2011). *Large-Scale PV Integration Study*. Accessed January 2013: www.navigant.com/~/media/WWW/Site/Insights/NVE_PV_Integration_Report_Energy.ashx.

New York Independent System Operator. (2010.) *Growing Wind—Final Report of the NYISO 2010 Wind Generation Study*. Rensselaer, NY: New York Independent System Operator. Accessed January 2013: http://www.uwig.org/GROWING_WIND_-_Final_Report_of_the_NYISO_2010_Wind_Generation_Study.pdf.

Orwig, K. (2010). *Examining Strong Winds From a Time-Varying Perspective*. Ph.D. Dissertation. Lubbock, TX: Texas Tech University.

Orwig, K.; Corbus, D.; Piwko, R.; Schuerger, M.; Matsuura, M.; Roose, L. (2012). "Hawaii Solar Integration Study: Solar Modeling Developments and Study Results: Preprint." Prepared for the 2nd Annual International Workshop on Integration of Solar Power into Power Systems, November 12–13, Lisbon, Portugal. NREL/CP-5500-56311. Golden, CO: NREL. 10 pp. Accessed January 2013: www.nrel.gov/docs/fy13osti/56311.pdf.

Pehnt, M.; Oeser, M.; Swider, D. (2008). "Consequential Environmental System Analysis of Expected Offshore Wind Electricity Production in Germany." *Energy* (33:5); pp. 747–759. doi:10.1016/j.energy.2008.01.007.

Perez, R. (2002). "Time-Specific Irradiances Derived From Geostationary Satellite Images." *Journal of Solar Energy Engineering—Transactions of the ASME* (124:1); pp. 1–1.

Perez, R.; Ineichen, P.; Moore, K.; Kmiecik, M.; Chain, C.; George, R.; Vignola, F. (2002). "A New Operational Satellite-to-Irradiance Model." *Solar Energy* (75:5); pp. 307–317.

Potter, C.; Gil, H.; McCaa, J. (2007). "Wind Power Data for Grid Integration Studies." *IEEE Power Engineering Society General Meeting Proceedings*, June 24–28, Tampa, Florida.

Potter, C.; Lew, D.; McCaa, J.; Cheng, S.; Eichelberger, S.; Grimit, E. (2008). "Creating the Dataset for the Western Wind and Solar Integration Study." *Wind Engineering* (32:4). Accessed January 2013: http://dx.doi.org/10.1260/0309-524X.32.4.325.

Short, W.; Sullivan, P.; Mai, T.; Mowers, M.; Uriarte, C.; Blair, N.; Heimiller, D.; Martinez, A. (2011). *Regional Energy Deployment Systems (ReEDS)*. NREL/TP-6A20-46534. Golden, CO: NREL. Accessed January 2013: www.nrel.gov/docs/fy12osti/46534.pdf.

United Kingdom Department of Enterprise, Trade, and Investment. (2008). *All Island Grid Study*. Accessed January 2013: www.uwig.org/Irish_All_Island_Grid_Study/Study_Overview.pdf.

Wan, Y.-H. (2005). *A Primer on Wind Power for Utility Applications*. NREL/TP-500-36230. Golden, CO: NREL. Accessed January 2013: www.nrel.gov/docs/fy06osti/36230.pdf.

WECC (2011). *Assumptions Matrix for the 2020 TEPPC Dataset.* Accessed January 2013: www.wecc.biz/library/StudyReport/Documents/Assumptions%20Matrix%20for%20the%202020%20TEPPC%20Dataset.pdf.

Zavadil, R.; King, J.; Samaan, N.; Lamoree, J. (2006). *Final Report—2006 Minnesota Wind Integration Study, Volume I.* Work performed by EnerNex Corporation, Knoxville, TN. Knoxville, TN: EnerNex Corp. Accessed January 2013: www.uwig.org/windrpt_vol%201.pdf.

Appendix A: Correction of the WWSIS Wind Production Data Seams Issue

3TIER (2010) developed a large wind speed and wind power database using an NWP model applied to the West. The model simulates a re-creation of the weather at any time or space, and wind speed data were sampled every 10 minutes for a 3-year period on a 2-km spatial resolution at representative hub heights for modern wind turbines. The resulting high-resolution data set captured the chronological behavior of the wind seen at locations around the West. The data set was then used to construct the various wind scenarios described throughout the report.

The NWP model of the Western Interconnection contained temporal seams that were not possible to resolve. This resulted in unrealistic wind energy ramps near the temporal boundaries, which occurred every 3 days. A continuous annual record was needed to obtain a complete reserves and ramping analysis, so a method to smooth those ramps below statistical significance was required. Statistical comparisons to surround "correct" data can be used to improve on the correction that the data vendor applied. The goal is to reduce the variability of the output around the anomalies while leaving data outside the window of the anomalies unaffected.

The temporal seams occurred every third day at the same time of day. We counted the days into 3-day sections, starting on January 1, 2004, and continuing through the end of 2006. We ended up with 363 days labeled "1," 363 days labeled "2," and 363 days labeled "3." The seam was found to be at midnight Coordinated Universal Time going from Day 3 to Day 1.[5] It was empirically determined that the 3TIER smoothing can cover a period of up to 6 hours (36 10-minute intervals), 2 hours before and 4 hours after the seam.

To illustrate the seam issue, consider Figure 113, which shows the 10-minute changes of output for a particular site. This plot shows the change in output verses the 10-minute interval of the 3-day period, 1 to 432 (there are 144 10-minute intervals in a day). The first 10-minute intervals of all Type 1s were interval 1, and so on. Note the greater variability around the Day 3 to Day 1 transition, highlighted by the circles.

---

[5] When counting from the beginning of each year individually, the seam was at midnight on Day 3 to Day 1 for 2004 and 2005. If counting began on January 1, 2006, the seam would have appeared at midnight on Day 1 to Day 2. This is because 2004 had 366 (divisible by three) days and 2005 had 365 (divisible by three, with a remainder of 2) days.
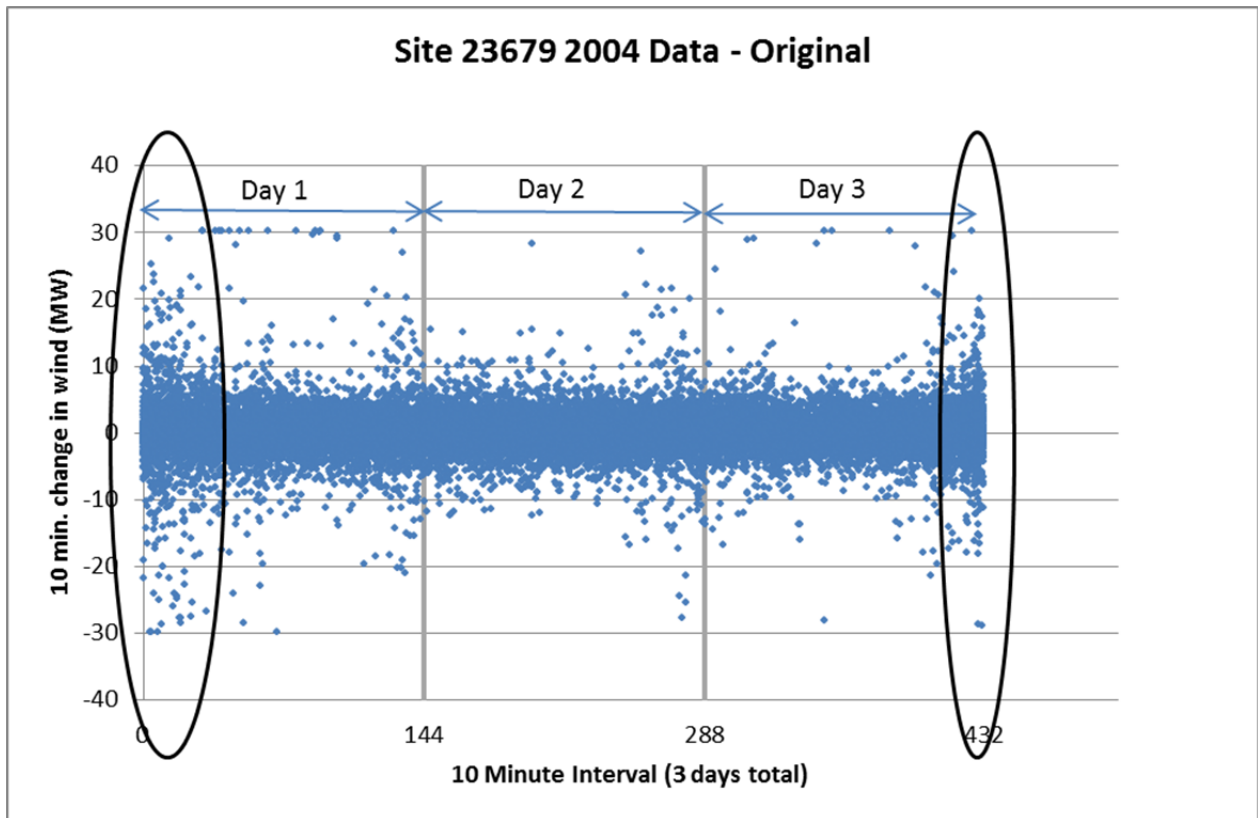
Figure 113. Distribution of wind changes by 10-minute interval number

Figure 114 shows the standard deviation for the data at each interval. The first point is the standard deviation for all interval 1 data points, and so on. This figure clearly shows the higher variability around the seam, as indicated by the higher standard deviation values just before and after the seam.

A number of approaches to mitigate the higher variability at the seam were evaluated. These included filtering the 3TIER supplied data, synthesizing new data based on the average sigma of the 10-minute changes, and randomly splicing data from "good" days to the affected ranges.

The filtering was successful at the individual site level; however, as sites were aggregated to larger areas, it was found that the correlation between sites in the seam area was much higher than in the rest of the data. This resulted in increasingly higher variability as more sites were aggregated. This is an artifact of the method 3TIER used to smooth the seams, which led to unacceptable results as sites were aggregated to a BA level.
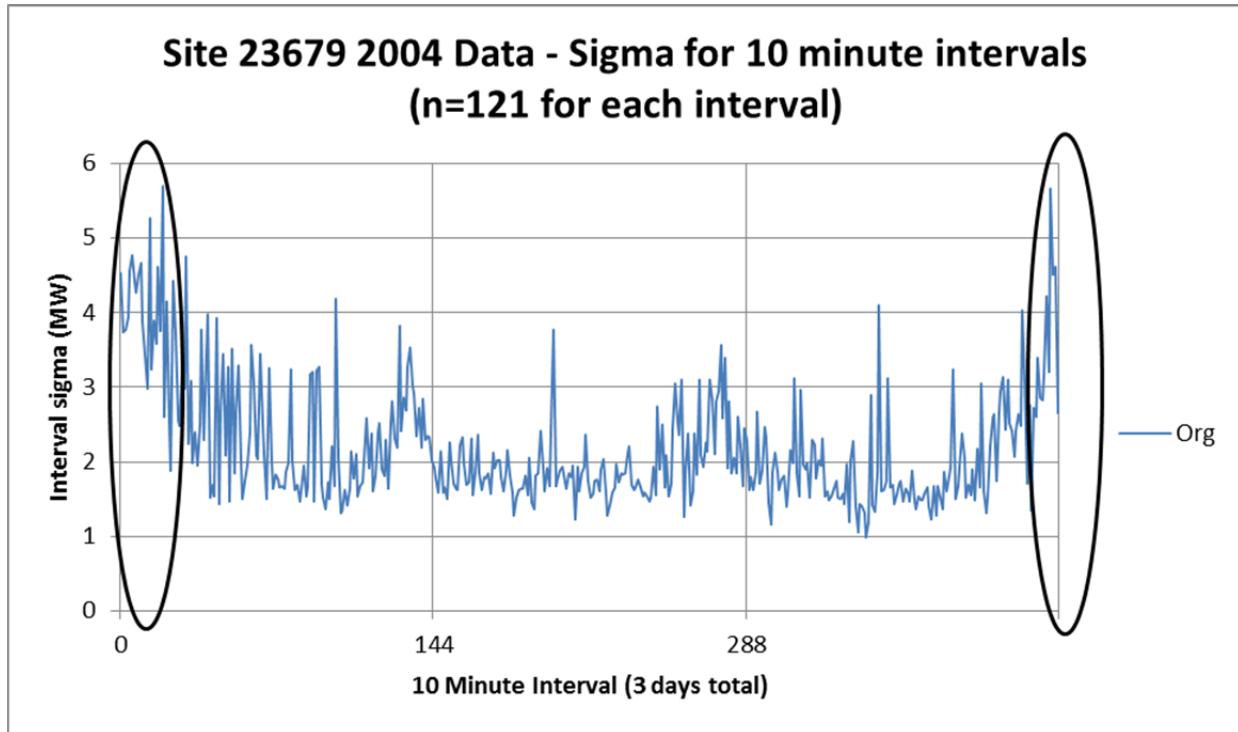
Figure 114. Standard deviation of 10-minute wind deltas by 10-minute interval number

To limit the correlation, an approach of synthesizing new data was evaluated. This was done by calculating the average sigma for the 10-minute changes and then generating normally distributed values to add to a trend that matched the beginning and end of the seam-smoothing region. This approach showed no correlation between the sites and resulted in too little variability as aggregation level increased. Several distributions were tried, and none yielded satisfactory results.

To match the correlation between sites, it was determined that splicing segments of the good days into the seams was a practical approach that should have the desired characteristics. Code was built that randomly selected a good day from the two-thirds of days that did not have seams. Care was taken to use splice data from only the same time of day of the good days. The variability of the splice data was isolated by subtracting the trend, then the splice was blended into the "bad" day by adding an appropriate trend to match the beginning and ending values surrounding the seam.

Figure 115 shows results of the correction method applied to the sample site. The red dots are the synthesized intervals plotted on top of the original data (blue dots). As shown, only data surrounding the anomaly were affected.

139
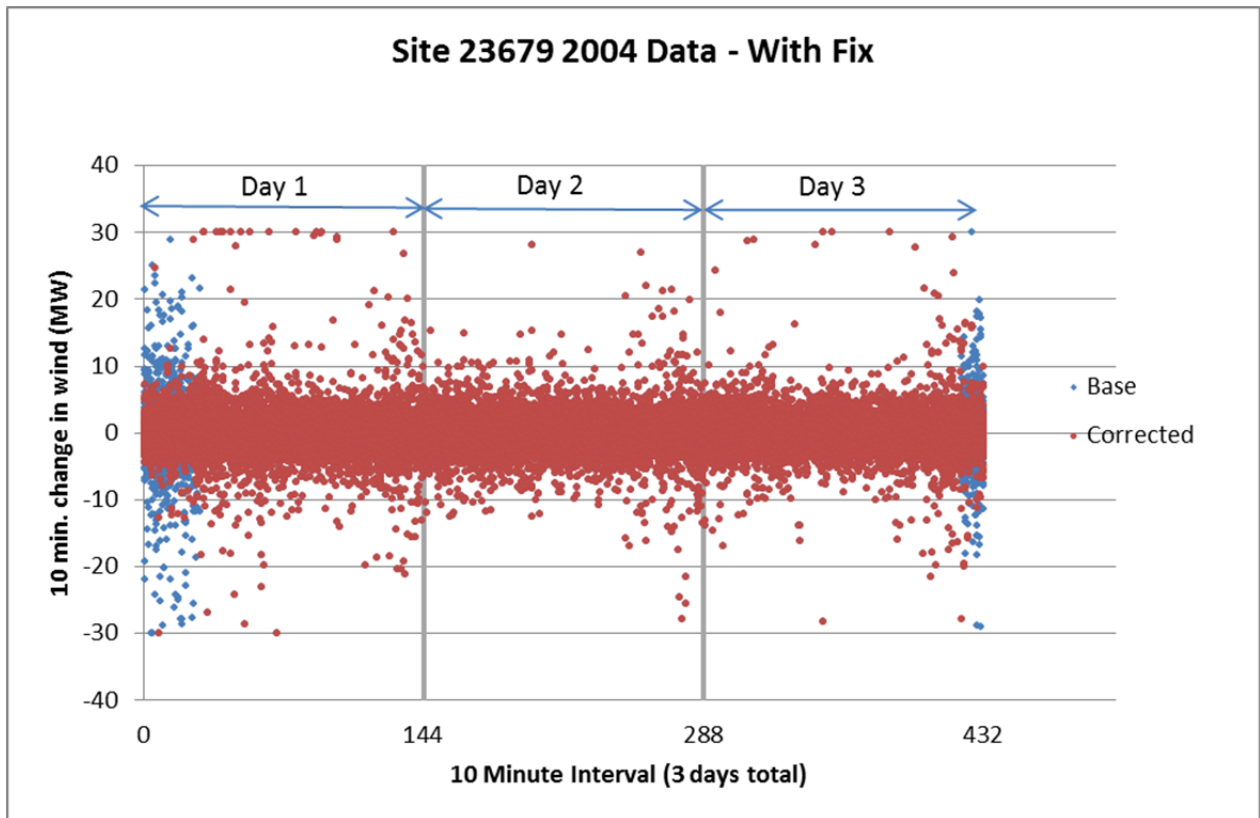
Figure 115. Corrected site data

To validate the results, we calculated the standard deviation for all the points in each interval of the 3-day window across the entire year of data. Figure 116 shows the interval standard deviations for both the uncorrected and spliced data. As expected, the values were identical except when the spliced data were substituted. Observing the spliced area shows that the variability in the anomaly has been reduced to approximately the same range as for the Day 1 to 2 and the Day 2 to 3 transitions.
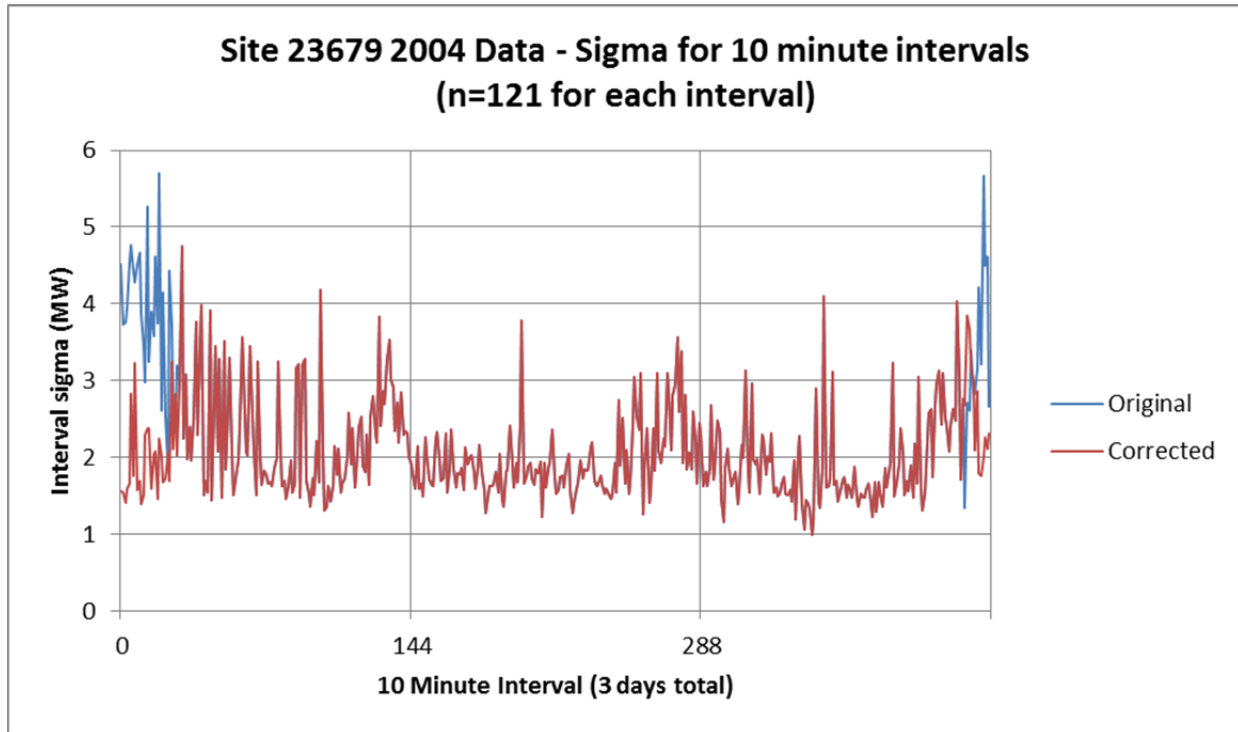
Figure 116. Standard deviation for 10-minute intervals for a single site

This detailed analysis was done for 10 randomly selected sites for each year (2004–2006) with equally good performance for each site.

The preceding analysis shows that the method produced reasonable results for a single site; however, it is very important that the method provides similar results for all levels of aggregation. To verify this performance, the detailed analysis was run for a number of regional combinations and for all of the wind assigned to the Western Interconnection for this study.

Figure 117 shows the results for the aggregation of all BAs into approximately 25% penetration into the Western Interconnection. Note that the red dots are the corrected data plotted over the original data in blue.

The performance of the method seemed quite good. There is a small "notch" in the negative side of the corrected data at the point where the correction ends (approximately Interval 24). This is probably because some sites had a smoothing period (3TIER correction) that was longer than the empirically determined 6 hours. This effect is shown in Figure 118, when the standard deviation for the 10-minute intervals of the original data slowly decayed from the high level shown in the anomaly region.

141
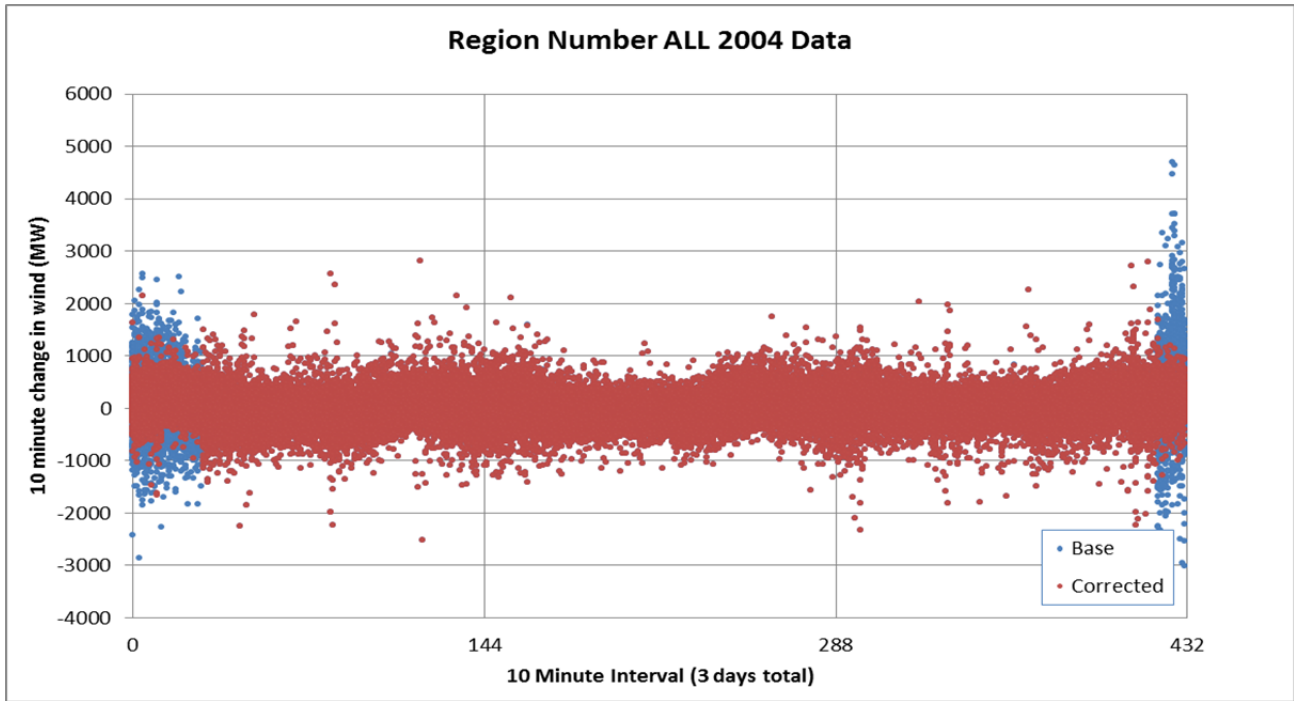
Figure 117. Ten-minute wind change distribution by interval for all regions aggregated
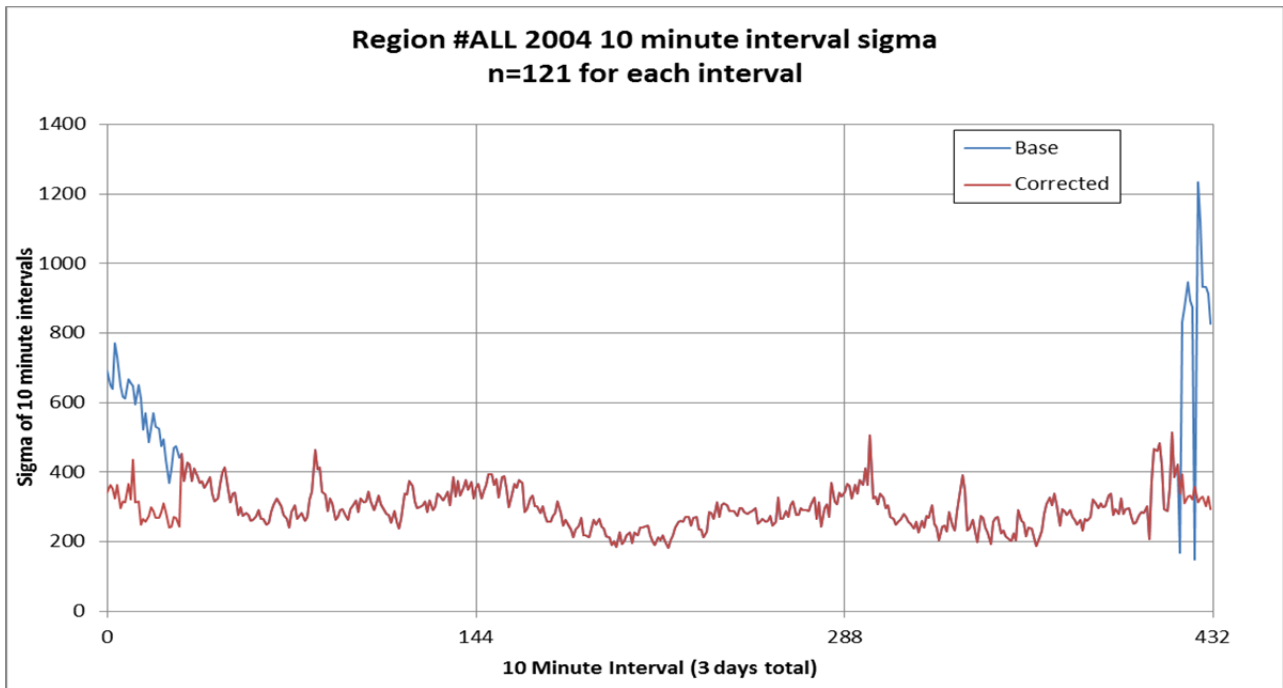
Figure 118. Standard deviation by 10-minute interval for all regions aggregated

142

It is also important to ensure that the method yields acceptable results with 1-hour averaged data as well as the 10-minute data. Figure 119 shows the distribution of hourly changes for each hour of the 3-day period. Figure 120 shows the standard deviation of the data at each hour of the 72 hours of the 3-day period.
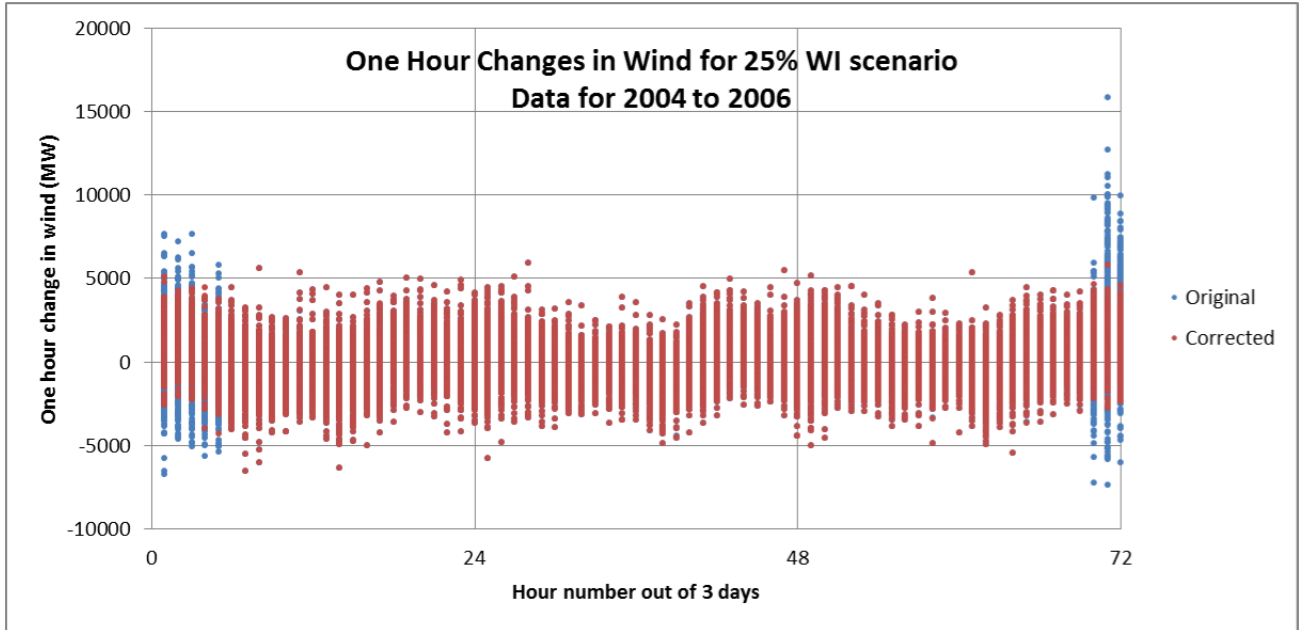
Figure 119. One-hour changes in wind for 25% Western Interconnection scenario by hour number
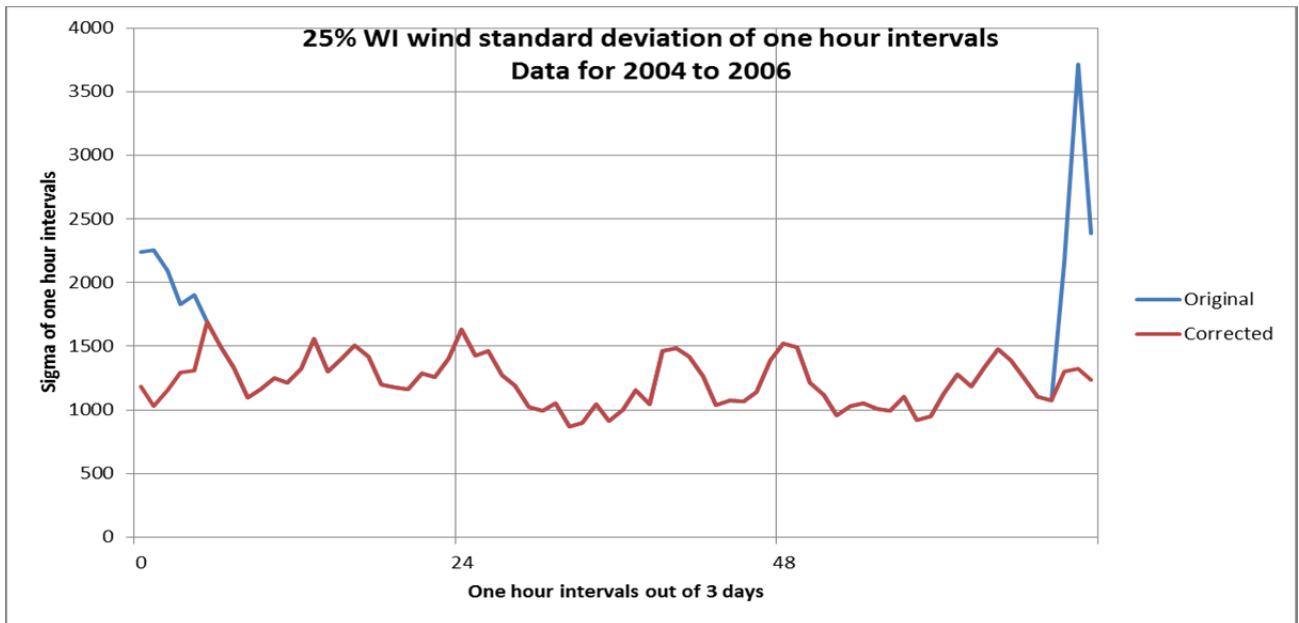
Figure 120. Sigma for 1-hour wind changes for 25% Western Interconnection scenario by hour number

143

In WWSIS-1, GE Energy (2010) provided a different visualization of the hourly data to demonstrate the problem with the 3TIER smoothing. The bar-and-whisker plots in Figure 121 and Figure 122 show the original and corrected average 1-hour change in wind output for the hour. The whiskers are the minimum and maximum values for each hour of the 3-day intervals. The bars show the mean value plus and minus one standard deviation.
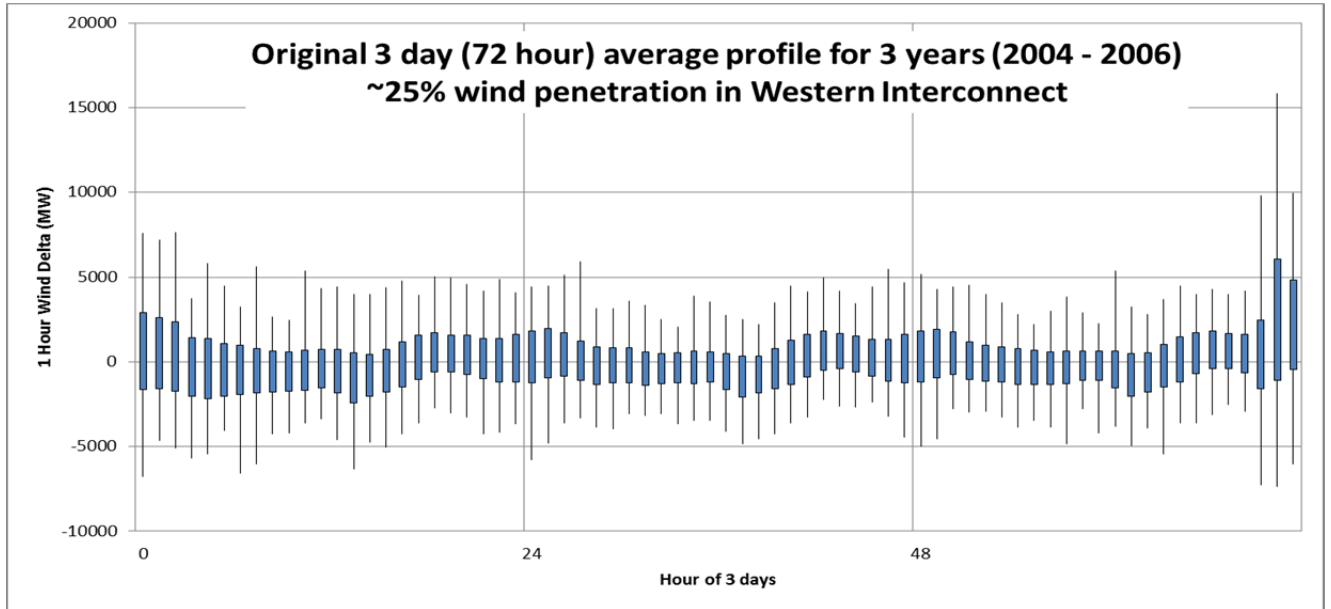
Figure 121. Bar and whisker for hourly changes for original data
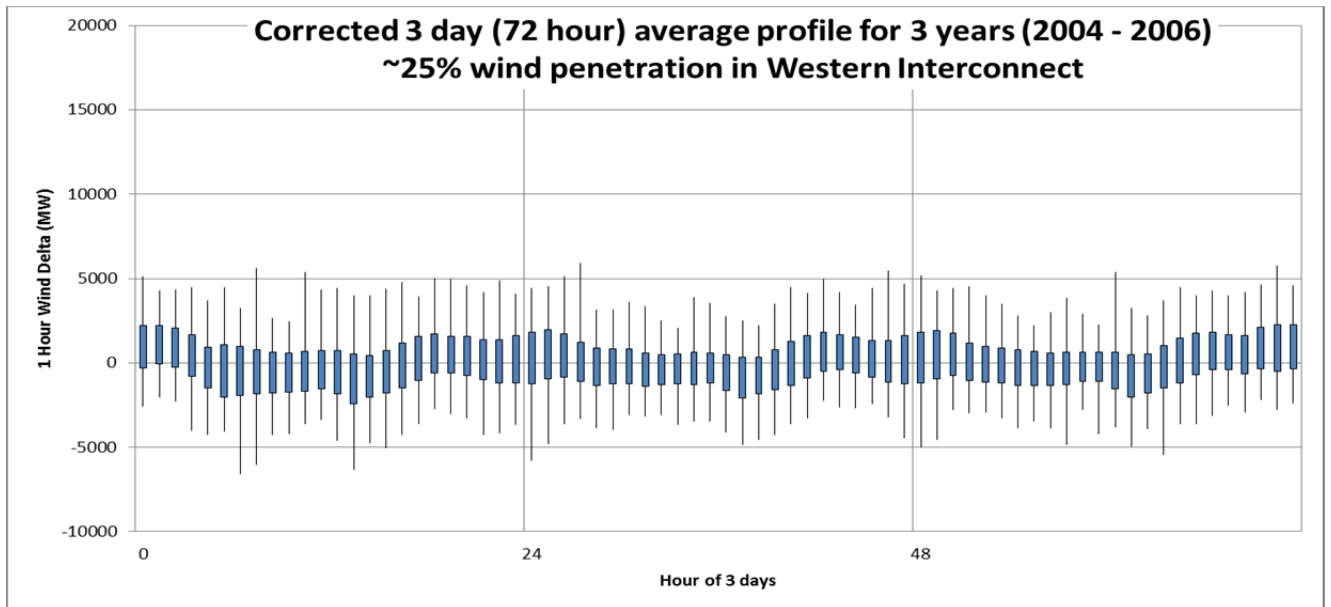
Figure 122. Bar and whisker for hourly changes for corrected data

Appendix B: One-Minute Wind Data Development

This section describes the method used for simulating 1-minute wind power data. The WWSIS wind power data provided by 3TIER contained data at 10-minute intervals. A method was needed to interpolate data between each 10-minute interval and to simulate power variability from a set of real wind turbines with a total capacity of 30 MW.

One-minute interval power data from several GE 1.5-MW wind turbines located at the Cedar Creek Wind Farm were analyzed. To achieve a capacity of 30 MW, data from 20 GE turbines were summed. Data from a second set of 20 GE turbines were summed to evaluate repeatability of profiles.

Wind turbine power spectrums can be generated from turbine power data using a number of different types of Fourier transform methods (Orwig 2010). An FFT proved to be suitable for power spectrums of wind data (Edwards 2009), so an FFT method was applied to the Cedar Creek data. To check for differences throughout time, data from August 2011 and December 2011 were analyzed. The FFT generated a magnitude and phase from the time series wind power data. The frequency range was limited by the time interval of the data and number of observations. Plots of magnitude versus frequency are referred to as power spectrums (Mur-Amada and Bayod-Rújula 2007).

Wind data have a characteristic spectrum, and the high-frequency range of actual data can be used to simulate the high-frequency variability between the 10-minute intervals of wind power data supplied by 3TIER. Figure 123 shows power spectrums from Cedar Creek turbines for the two different time periods. In general, the spectrums were similar. There appeared to be a slight upturn in magnitude at the highest frequency range for the December 2011 data. Because the low-frequency profile (10 minutes and greater) existed in the supplied wind power data, only the high-frequency portion needed to be used for noise simulation.

The general approach was to first apply a cubic spline interpolation to the 10-minute data to obtain power estimates at 1-minute intervals. The second step used high-frequency magnitude data combined with randomized phase to generate the noise component of the wind power data. Magnitude and phase are needed to calculate real and imaginary components that result in the high-frequency noise after applying the inverse Fourier transform. This noise was then added to the cubic spline interpolation to give the simulated wind power data.
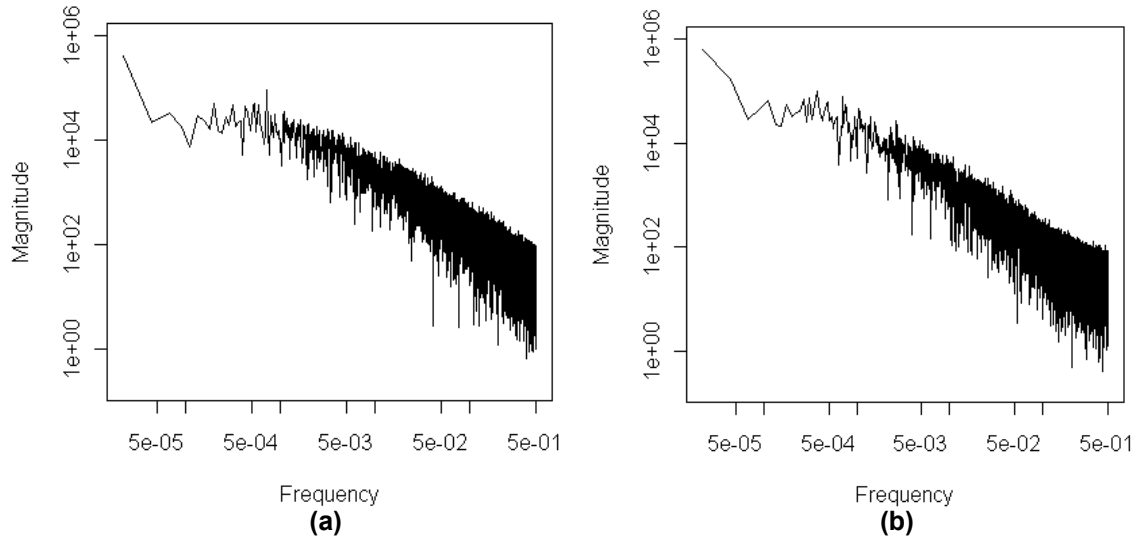
**Figure 123. Power spectrums of the Cedar Creek turbines
for (a) August 2011 and (b) December 2011**

Note: Frequency is in Hz.

An experimental approach was used to determine a reasonable cutoff frequency for the high-frequency portion of the spectrum to be used for simulating noise. The Cedar Creek wind turbine power data were used to test the cutoff frequency by extracting observations at 10-minute intervals and then simulating the high-frequency noise using different values for cutoff frequency. Actual noise was determined by subtracting the cubic spline fit away from the actual 1-minute interval data. Table 29 compares the standard deviation of the actual noise to the standard deviation for simulated noise using different cutoff frequencies.

**Table 29. Comparison of Actual Noise Standard Deviation
to Simulated Noise Standard Deviation for August 2011 and December 2011**

Noise	Cutoff Frequency (Hz)	August 2011 Standard Deviation (MW)	December 2011 Standard Deviation (MW)
Actual		0.943	0.554
Simulated	0.10	0.308	0.185
Simulated	0.05	0.504	0.296
Simulated	0.04	0.588	0.357
Simulated	0.02	0.946	0.604

Based strictly on the standard deviation results, it appears that a cutoff frequency gives standard deviations comparable to actual noise. Nevertheless, comparisons of actual data to simulated data indicated that (1) the variability is not always uniform throughout time and (2) a cutoff frequency of 0.02 was resulting in some additional undesirable oscillations. Therefore, a cutoff frequency of 0.04 (less than 25 minutes) was selected, which gave reasonable noise simulations.

Figure 124 shows the power spectrums from August 2011 and December 2011, with simulated high-frequency noise overlaid on the original power spectrums from Figure 123. As shown, the power spectrums from 1-minute interpolated data agreed reasonably well with the power spectrums of actual data. The magnitude for the interpolated August 2011 data shows a broader range than actual but it is not excessive.
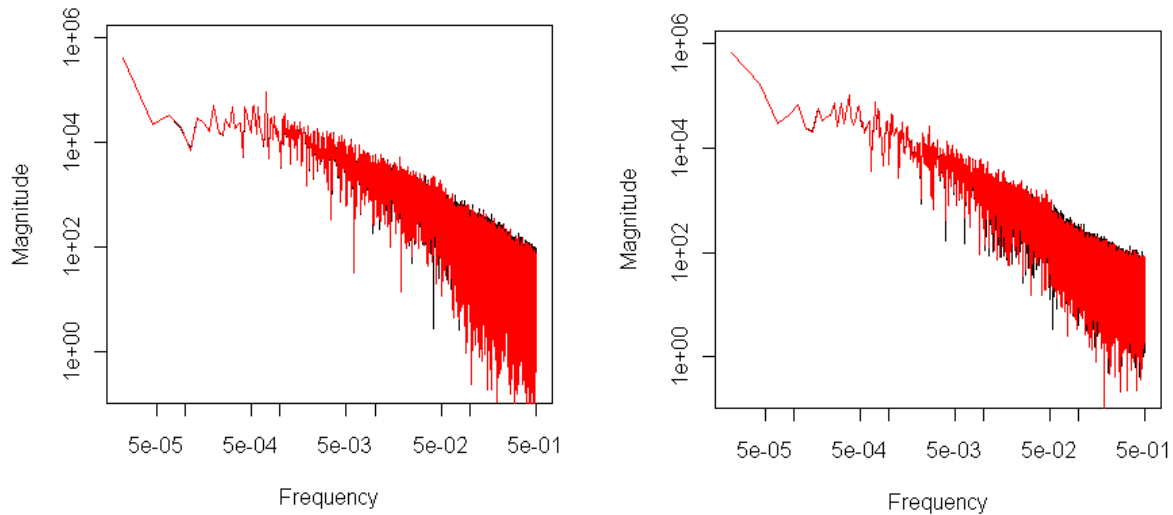
(a) (b)

Figure 124. Power spectrums using simulated (red) high-frequency noise overlaid on (black) power spectrums from actual data for (a) August 2011 and (b) December 2011

Note: Frequency is in Hz.

Figure 125 compares the simulated interpolated data to actual data for a short segment of time during August 2011. Also plotted were actual noise—which was the actual data minus the cubic spline fit—and the simulated noise. Although the noise of the simulated data was more uniform and less in magnitude than that from the actual data, in general, the simulated data resembled the actual data. Figure 126 compares simulated data to actual data for a short segment of time in December 2011. Again, there was reasonable resemblance between the simulated data and the actual data.

147
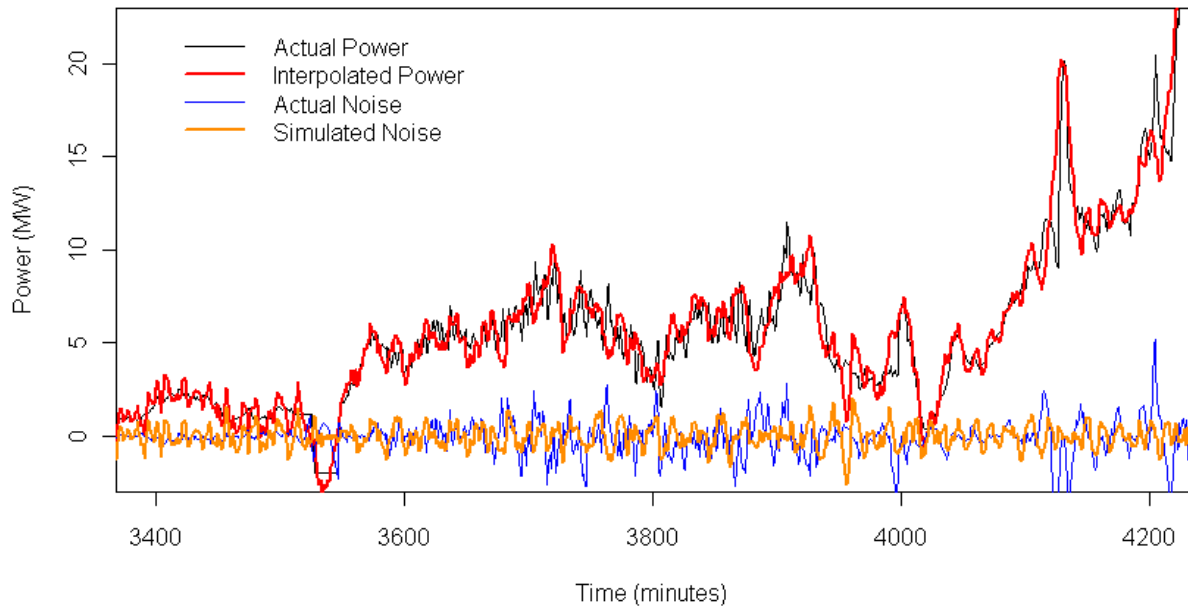
Figure 125. Comparison of interpolated 1-minute wind power data to actual data for August 2011 (time between 3,400 and 4,200 minutes)
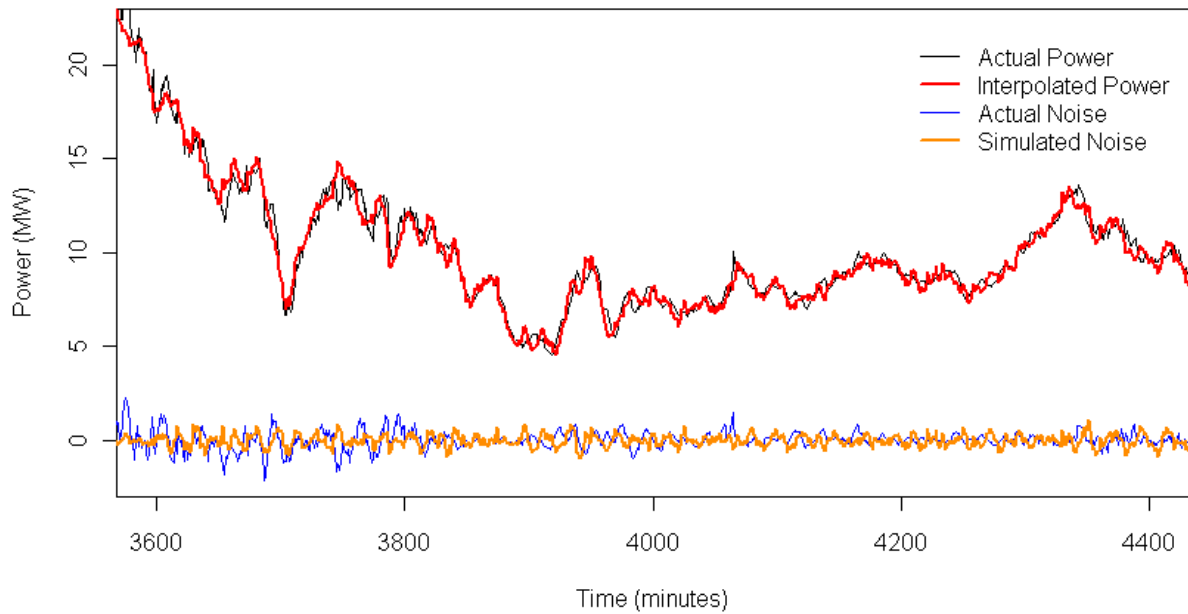

Figure 126. Comparison of interpolated 1-minute wind power data to actual data for December 2011 (time between 3,600 and 4,400 minutes)

148

Because the 10-minute data from 3TIER is stored in files containing 1 full year of data, it was desirable to process these files in one step. This required a file containing 1 full year of magnitudes to generate 1 full year of simulated noise. Only about one-half of a year of 1-minute data were collected at the time the interpolation was done. Available wind power data followed an annual cycle with more power being available in the winter, then declining in the spring, reaching a minimum in the summer, and increasing again in the fall. To approximate this trend, Cedar Creek data from July 2011 through December 2011 were combined. To approximate the time period from January 2011 through June 2011, the combined data were then reversed and reassigned to the time period of January 2011 through June 2011. This gave 1 full year of data from which simulated noise could be generated. Figure 127 shows the power spectrum from this spliced together data set. It resembles reasonably well the power spectrums of monthly data shown in Figure 123.
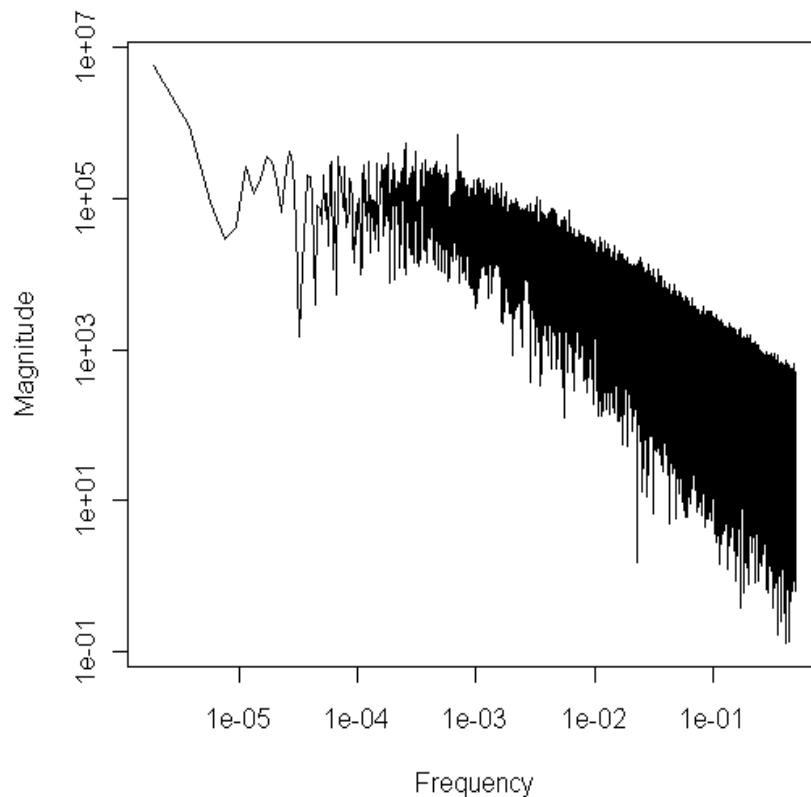
Figure 127. Power spectrum from spliced Cedar Creek turbine data for 1 full year

Appendix C: Transmission Graphs

This appendix details the transmission expansion for each scenario, showing the path capability added at each iteration of the PLEXOS runs. Figure 128 through Figure 131 show the iterative transmission expansion for each shadow price cutoff value for the TEPPC, High Wind, High Mix, and High Solar Scenarios.
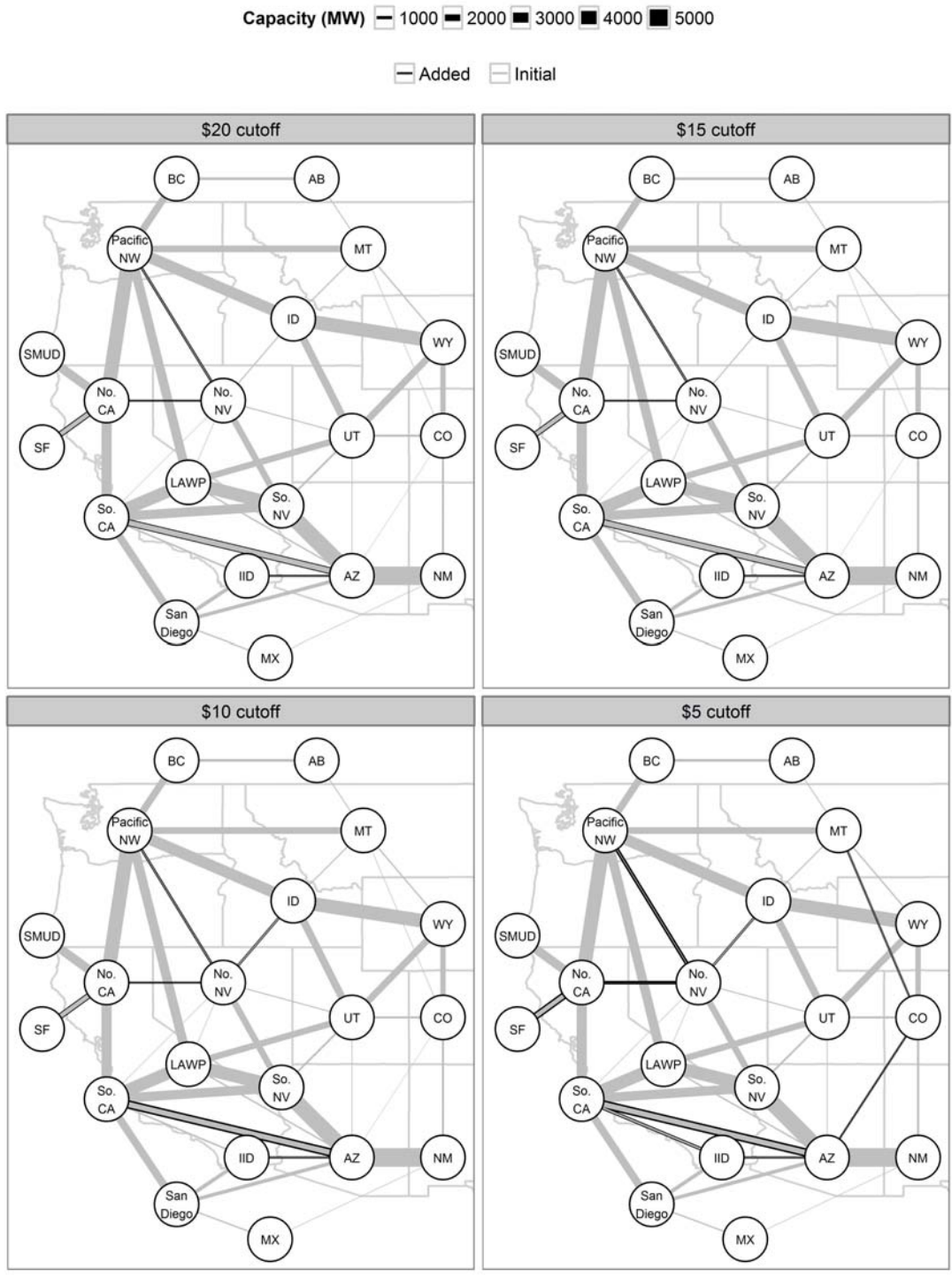
Figure 128. Transmission expansion for the TEPPC Scenario showing the (gray) initial and (black) additional transmission for each shadow price cutoff value tested

151
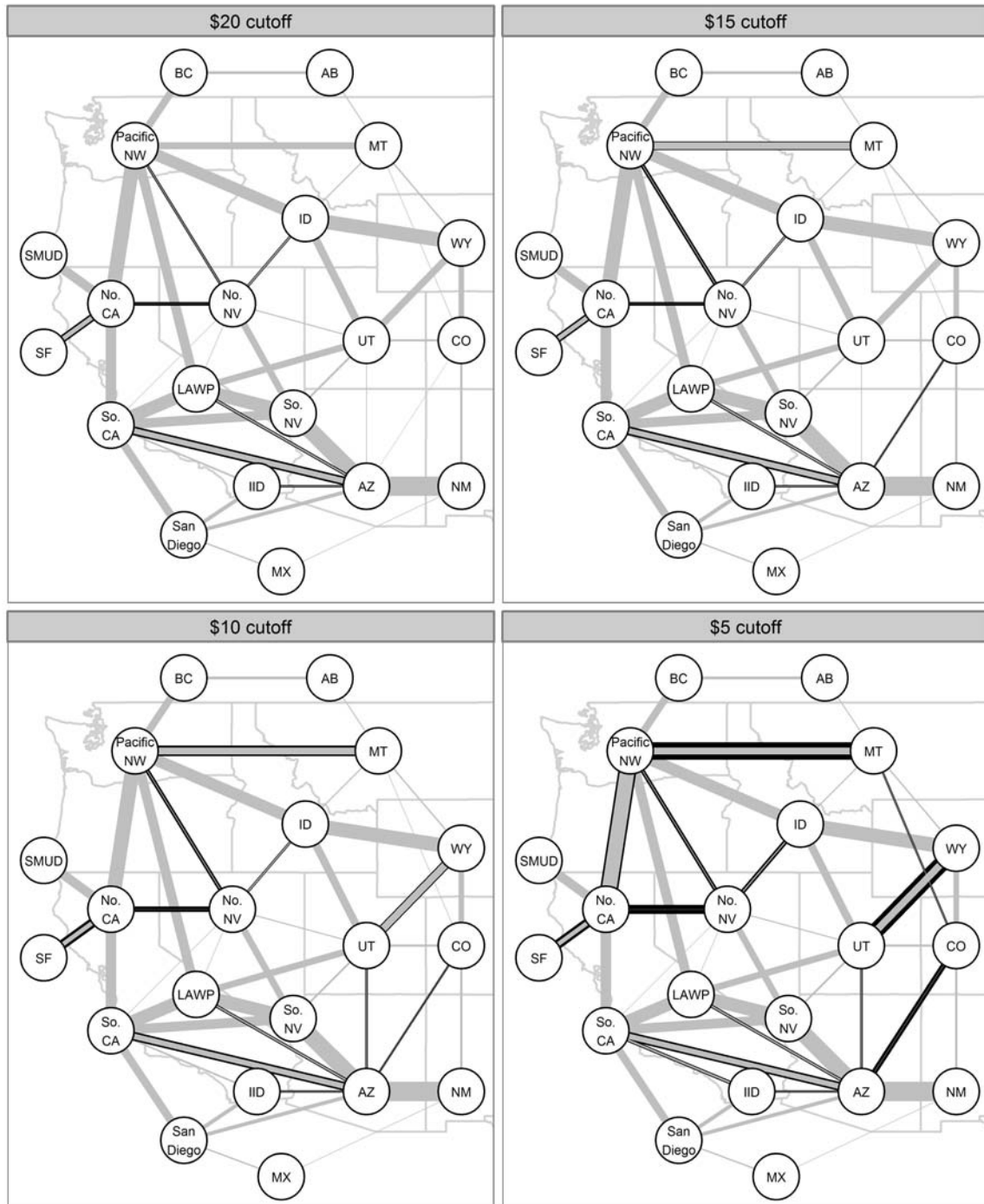
Figure 129. Transmission expansion for the High Wind Scenario showing the (gray) initial and (black) additional transmission for each shadow price cutoff value tested
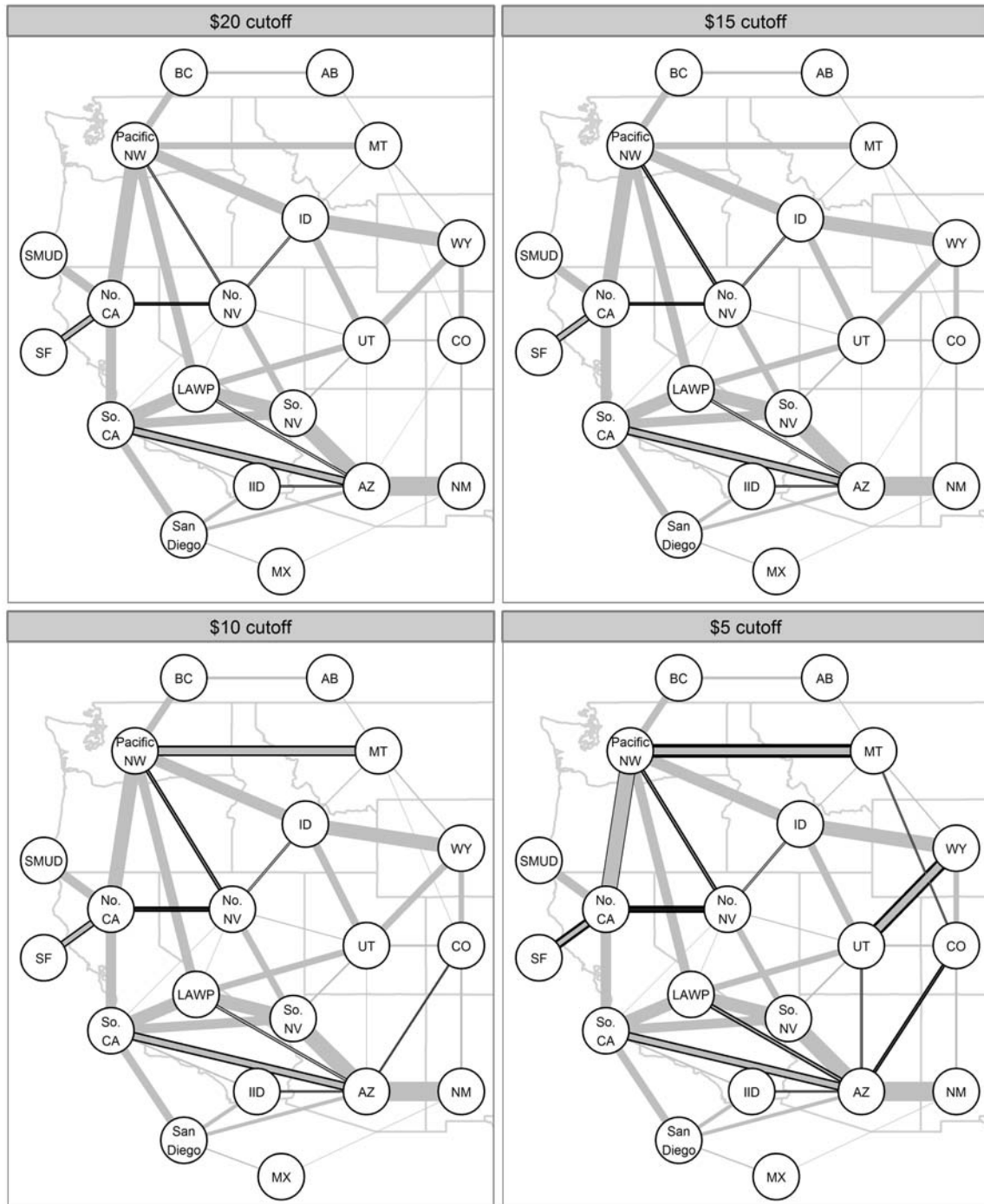
Figure 130. Transmission expansion for the High Mix Scenario showing the (gray) initial and (black) additional transmission for each shadow price cutoff value tested

153
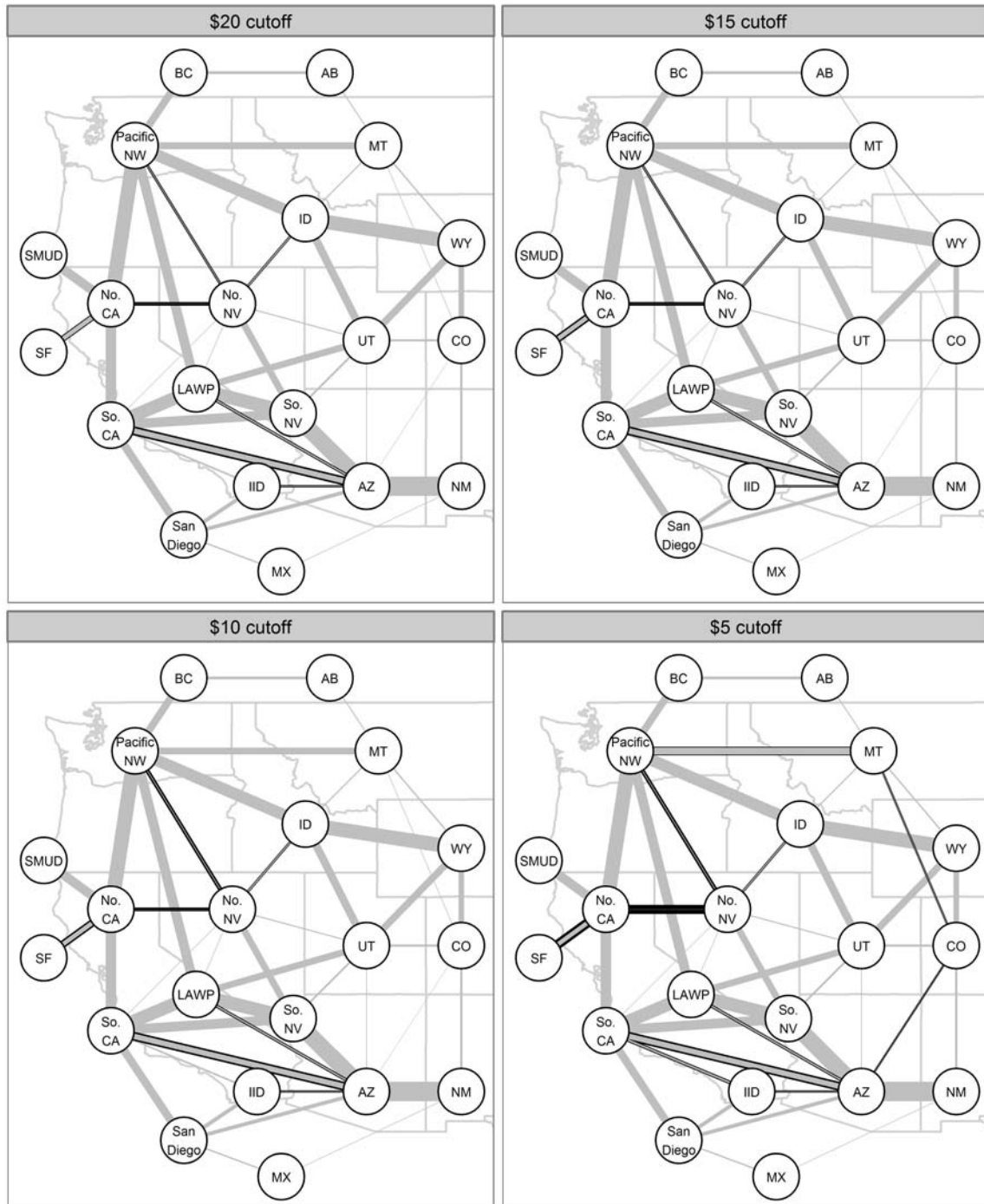
Figure 131. Transmission expansion for the High Solar Scenario showing the (gray) initial and (black) additional transmission for each shadow price cutoff value tested

154

Table 30 and Table 31 show the tabular values for each path from Figure 128 through Figure 131. Table 30 shows the transmission expansion by Scenario and Table 31 shows the expansion by shadow price cutoff value.

Table 30. Transmission Expansion for Each Scenario Showing the Increased Path Capabilities for Different Shadow Price Cutoff Values

|	Initial	High Wind				High Solar				High Mix				TEPPC		
		$20 Cutoff	$15 Cutoff	$10 Cutoff	$5 Cutoff	$20 Cutoff	$15 Cutoff	$10 Cutoff	$5 Cutoff	$20 Cutoff	$15 Cutoff	$10 Cutoff	$5 Cutoff	$20/$15 Cutoff	$10 Cutoff	$5 Cutoff
Alberta to British Columbia	800	0	0	0	0	0	0	0	0	0	0	0	0	0	0	0
Alberta to Montana	325	0	0	0	0	0	0	0	0	0	0	0	0	0	0	0
Arizona to California_South	1,600	1,000	1,000	1,000	1,000	1,000	1,000	1,000	1,000	1,000	1,000	1,000	1,000	1,000	1,000	1,000
Arizona to Colorado	200	0	500	500	1,500	0	0	0	500	0	0	500	1,000	0	0	500
Arizona to IID	195	500	500	500	500	500	500	500	500	500	500	500	500	500	500	500
Arizona to LAWP	468	500	500	500	500	500	500	500	500	500	500	500	1,000	0	0	0
Arizona to Nevada_South	4,785	0	0	0	0	0	0	0	0	0	0	0	0	0	0	0
Arizona to New Mexico	5,582	0	0	0	0	0	0	0	0	0	0	0	0	0	0	0
Arizona to San Diego	1,168	0	0	0	0	0	0	0	0	0	0	0	0	0	0	0
Arizona to Utah	250	0	500	500	500	0	0	0	500	0	0	500	500	0	0	500
British Columbia to Northwest	2,200	0	0	0	0	0	0	0	0	0	0	0	0	0	0	0
California_North to California_South	3,000	0	0	0	0	0	0	0	0	0	0	0	0	0	0	0
California_North to Nevada_North	100	1,000	1,500	1,500	2,500	1,000	1,000	1,500	2,500	1,000	1,000	1,500	2,000	500	500	1,000
California_North to Northwest	4,200	0	0	0	1,000	0	0	0	0	0	0	0	500	0	0	0
California_North to San Francisco	1,272	1,000	1,000	1,500	1,500	1,000	1,000	1,000	1,500	1,000	1,000	1,500	1,500	500	500	1,000
California_North to SMUD	2,750	0	0	0	0	0	0	0	0	0	0	0	0	0	0	0
California_South to IID	600	0	0	500	500	0	0	500	500	0	0	0	0	0	0	500
California_South to LAWP	3,750	0	0	0	0	0	0	0	0	0	0	0	0	0	0	0
California_South to Nevada_North	200	0	0	0	0	0	0	0	0	0	0	0	0	0	0	0
California_South to Nevada_South	2,814	0	0	0	0	0	0	0	0	0	0	0	0	0	0	0
California_South to San Diego	2,440	0	0	0	0	0	0	0	0	0	0	0	0	0	0	0

155

Colorado to Montana	200	0	0	0	500	0	0	0	500	0	0	0	500	0	0	500
Colorado to New Mexico	664	0	0	0	0	0	0	0	0	0	0	0	0	0	0	0
Colorado to Utah	650	0	0	0	0	0	0	0	0	0	0	0	0	0	0	0
Colorado to Wyoming	1,595	0	0	0	0	0	0	0	0	0	0	0	0	0	0	0
Idaho to Montana	325	0	0	0	0	0	0	0	0	0	0	0	0	0	0	0
Idaho to Nevada_North	350	500	500	500	1,000	500	500	500	500	500	500	500	1,000	500	500	500
Idaho to Northwest	3,400	0	0	0	0	0	0	0	0	0	0	0	0	0	0	0
Idaho to Utah	2,250	0	0	0	0	0	0	0	0	0	0	0	0	0	0	0
Idaho to Wyoming	4,100	0	0	0	0	0	0	0	0	0	0	0	0	0	0	0
IID to San Diego	1,150	0	0	0	0	0	0	0	0	0	0	0	0	0	0	0
LAWP to Nevada_North	200	0	0	0	0	0	0	0	0	0	0	0	0	0	0	0
LAWP to Nevada_South	3,883	0	0	0	0	0	0	0	0	0	0	0	0	0	0	0
LAWP to Northwest	2,858	0	0	0	0	0	0	0	0	0	0	0	0	0	0	0
LAWP to Utah	1,920	0	0	0	0	0	0	0	0	0	0	0	0	0	0	0
Mexico (CFE) to New Mexico	200	0	0	0	0	0	0	0	0	0	0	0	0	0	0	0
Mexico (CFE) to San Diego	408	0	0	0	0	0	0	0	0	0	0	0	0	0	0	0
Montana to Northwest	2,000	0	500	1,500	3,000	0	0	0	500	0	500	1,000	2,000	0	0	0
Montana to Wyoming	400	0	0	0	0	0	0	0	0	0	0	0	0	0	0	0
Nevada_North to Nevada_South	2,000	0	0	0	0	0	0	0	0	0	0	0	0	0	0	0
Nevada_North to Northwest	300	1,000	1,000	1,000	1,000	500	1,000	1,000	1,000	1,000	1,000	1,000	1,000	500	1,000	1,000
Nevada_North to Utah	360	0	0	0	0	0	0	0	0	0	0	0	0	0	0	0
Nevada_South to Utah	600	0	0	0	500	0	0	0	0	0	0	0	0	0	0	0
Utah to Wyoming	2,100	0	0	1,000	2500	0	0	0	0	0	0	500	1,500	0	0	0

Note: CFE, Comisión Federal de Electricidad

Table 31. Transmission Expansion for Each Shadow Price Cutoff Values Showing the Increased Path Capabilities for Different Scenarios

	Initial	$20 Cutoff				$15 Cutoff				$10 Cutoff				$5 Cutoff			
		High Wind	High Solar	High Mix	Ref	High Wind	High Solar	High Mix	Ref	High Wind	High Solar	High Mix	Ref	High Wind	High Solar	High Mix	Ref
Alberta to British Columbia	800	0	0	0	0	0	0	0	0	0	0	0	0	0	0	0	0
Alberta to Montana	325	0	0	0	0	0	0	0	0	0	0	0	0	0	0	0	0
Arizona to California_South	1,600	1,000	1,000	1,000	1,000	1,000	1,000	1,000	1,000	1,000	1,000	1,000	1,000	1,000	1,000	1,000	1,000
Arizona to Colorado	200	0	0	0	0	500	0	0	0	500	0	500	0	1,500	500	1,000	500
Arizona to IID	195	500	500	500	500	500	500	500	500	500	500	500	500	500	500	500	500
Arizona to LAWP	468	500	500	500	0	500	500	500	0	500	500	500	0	500	500	1,000	0
Arizona to Nevada_South	4,785	0	0	0	0	0	0	0	0	0	0	0	0	0	0	0	0
Arizona to New Mexico	5,582	0	0	0	0	0	0	0	0	0	0	0	0	0	0	0	0
Arizona to San Diego	1,168	0	0	0	0	0	0	0	0	0	0	0	0	0	0	0	0
Arizona to Utah	250	0	0	0	0	500	0	0	0	500	0	500	0	500	500	500	500
British Columbia to Northwest	2,200	0	0	0	0	0	0	0	0	0	0	0	0	0	0	0	0
California_North to California_South	3,000	0	0	0	0	0	0	0	0	0	0	0	0	0	0	0	0
California_North to Nevada_North	100	1,000	1,000	1,000	500	1,500	1,000	1,000	500	1,500	1,500	1,500	500	2,500	2,500	2,000	1,000
California_North to Northwest	4,200	0	0	0	0	0	0	0	0	0	0	0	0	1,000	0	500	0
California_North to San Francisco	1,272	1,000	1,000	1,000	500	1,000	1,000	1,000	500	1,500	1,000	1,500	500	1,500	1,500	1,500	1,000
California_North to SMUD	2,750	0	0	0	0	0	0	0	0	0	0	0	0	0	0	0	0
California_South to IID	600	0	0	0	0	0	0	0	0	500	500	0	0	500	500	0	500
California_South to LAWP	3,750	0	0	0	0	0	0	0	0	0	0	0	0	0	0	0	0
California_South to Nevada_North	200	0	0	0	0	0	0	0	0	0	0	0	0	0	0	0	0
California_South to Nevada_South	2,814	0	0	0	0	0	0	0	0	0	0	0	0	0	0	0	0
California_South to San Diego	2,440	0	0	0	0	0	0	0	0	0	0	0	0	0	0	0	0
Colorado to Montana	200	0	0	0	0	0	0	0	0	0	0	0	0	500	500	500	500
Colorado to New Mexico	664	0	0	0	0	0	0	0	0	0	0	0	0	0	0	0	0
Colorado to Utah	650	0	0	0	0	0	0	0	0	0	0	0	0	0	0	0	0
Colorado to Wyoming	1,595	0	0	0	0	0	0	0	0	0	0	0	0	0	0	0	0
Idaho to Montana	325	0	0	0	0	0	0	0	0	0	0	0	0	0	0	0	0

Idaho to Nevada_North	350	500	500	500	500	500	500	500	500	500	500	500	500	1,000	500	1,000	500
Idaho to Northwest	3,400	0	0	0	0	0	0	0	0	0	0	0	0	0	0	0	0
Idaho to Utah	2,250	0	0	0	0	0	0	0	0	0	0	0	0	0	0	0	0
Idaho to Wyoming	4,100	0	0	0	0	0	0	0	0	0	0	0	0	0	0	0	0
IID to San Diego	1,150	0	0	0	0	0	0	0	0	0	0	0	0	0	0	0	0
LAWP to Nevada_North	200	0	0	0	0	0	0	0	0	0	0	0	0	0	0	0	0
LAWP to Nevada_South	3,883	0	0	0	0	0	0	0	0	0	0	0	0	0	0	0	0
LAWP to Northwest	2,858	0	0	0	0	0	0	0	0	0	0	0	0	0	0	0	0
LAWP to Utah	1,920	0	0	0	0	0	0	0	0	0	0	0	0	0	0	0	0
Mexico (CFE) to New Mexico	200	0	0	0	0	0	0	0	0	0	0	0	0	0	0	0	0
Mexico (CFE) to San Diego	408	0	0	0	0	0	0	0	0	0	0	0	0	0	0	0	0
Montana to Northwest	2,000	0	0	0	0	500	0	500	0	1,500	0	1,000	0	3,000	500	2,000	0
Montana to Wyoming	400	0	0	0	0	0	0	0	0	0	0	0	0	0	0	0	0
Nevada_North to Nevada_South	2,000	0	0	0	0	0	0	0	0	0	0	0	0	0	0	0	0
Nevada_North to Northwest	300	1,000	500	1,000	500	1,000	1,000	1,000	500	1,000	1,000	1,000	1,000	1,000	1,000	1,000	1,000
Nevada_North to Utah	360	0	0	0	0	0	0	0	0	0	0	0	0	0	0	0	0
Nevada_South to Utah	600	0	0	0	0	0	0	0	0	0	0	0	0	500	0	0	0
Utah to Wyoming	2,100	0	0	0	0	0	0	0	0	1,000	0	500	0	2,500	0	1,500	0

Note: The Ref scenario refers to the TEPPC scenario.

Appendix D: Statistical Graphs

This section contains a more complete set of statistical graphs than the body of the report. Each group of graphs is accompanied by a short introduction giving any interpretation information and special comments. Note that some information is labeled as Reference Scenario or Intermediate Scenario. For this study, the Reference Scenario was renamed as the TEPPC Scenario and the Intermediate Scenario was renamed as the High Mix Scenario.

Figure 132 through Figure 135 show the siting of wind and solar plants by state for each scenario. The darker colors show higher installed capacity. The number of states at each installed capacity range is shown in parentheses in the legend.
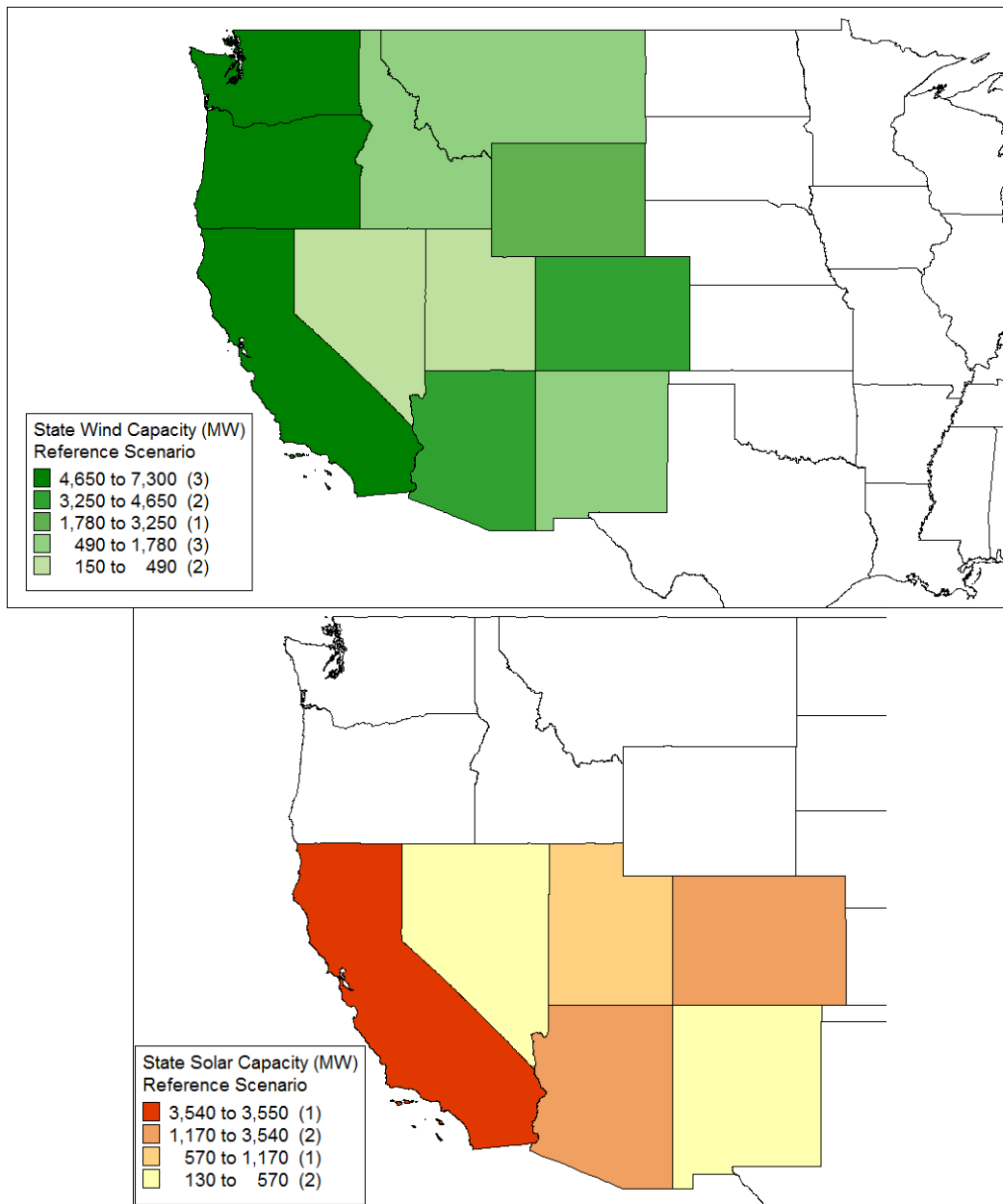
Figure 132. TEPPC Scenario—installed capacity by state
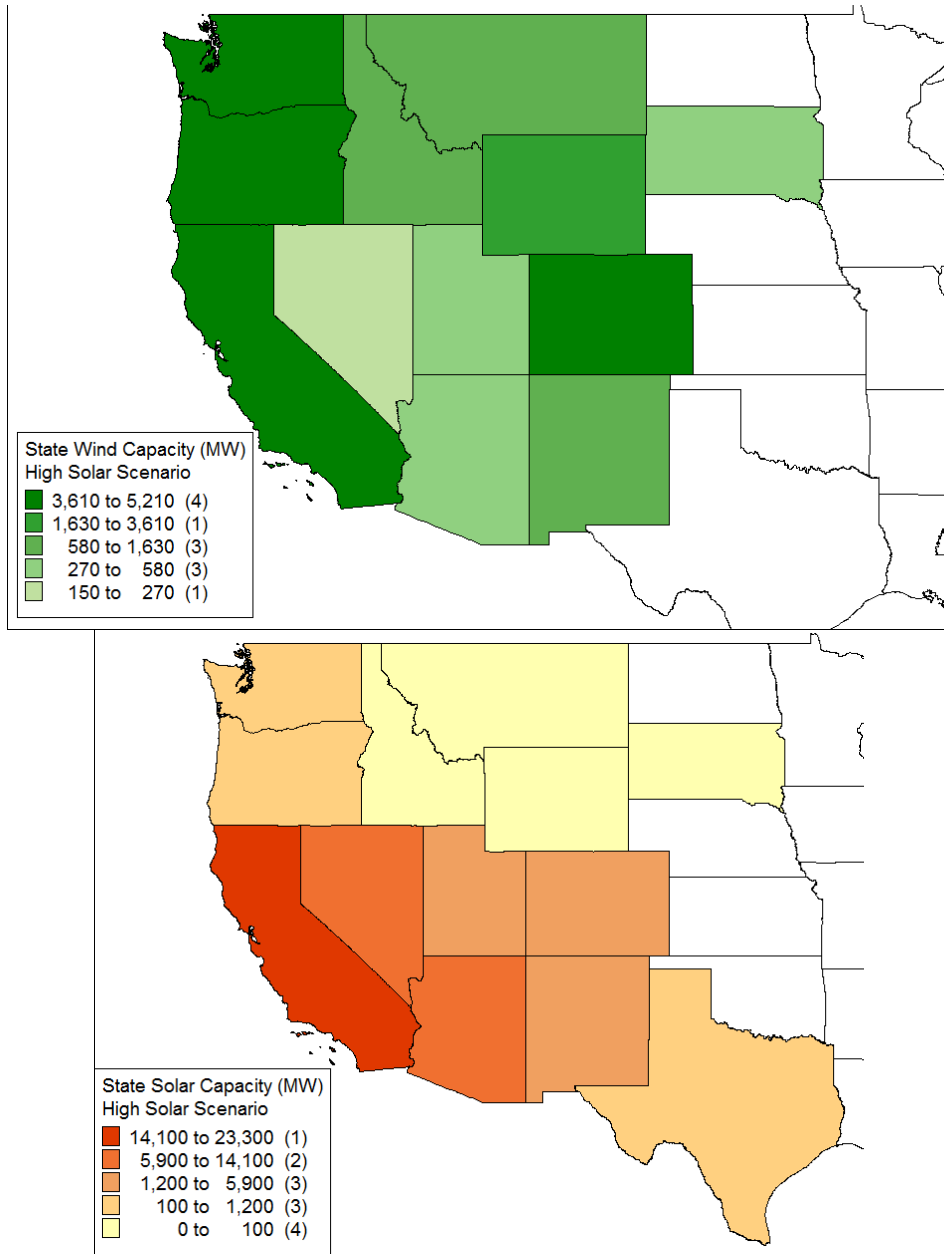
Figure 133. High Solar Scenario—installed capacity by state

State Wind Capacity (MW)
Intermediate Scenario
- 5,410 to 7,250 (4)
- 3,130 to 5,410 (3)
- 1,440 to 3,130 (3)
- 1,090 to 1,440 (1)
- 680 to 1,090 (1)

State Solar Capactiy (MW)
Intermediate Scenario
- 9,000 to 18,100 (2)
- 2,800 to 9,000 (1)
- 1,100 to 2,800 (4)
- 100 to 1,100 (2)
- 0 to 100 (4)
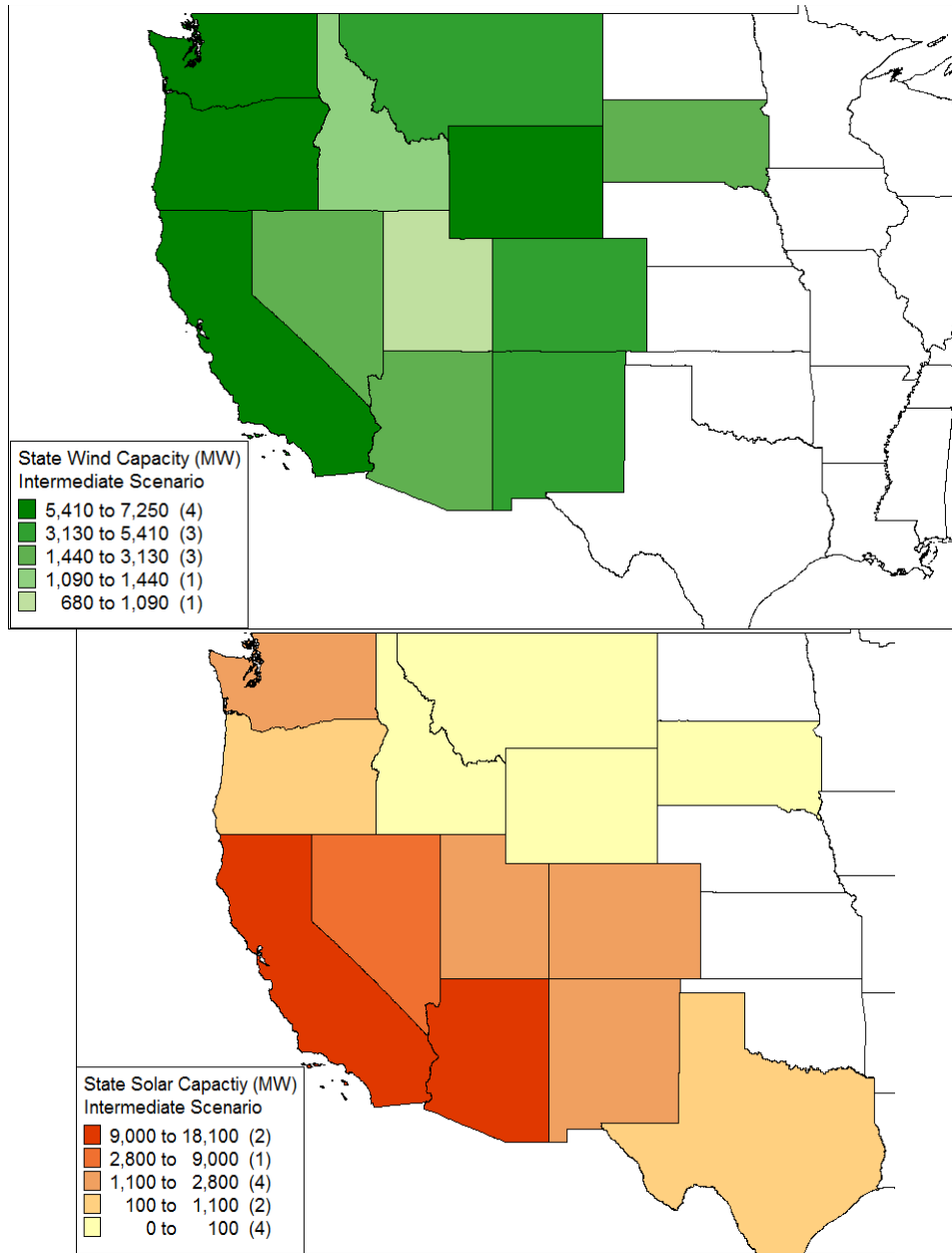
Figure 134. High Mix Scenario—installed capacity by state

State Wind Capacity (MW)
High Wind Scenario

10,100 to 11,200 (2)	
5,800 to 10,100 (3)	
4,700 to 5,800 (3)	
2,600 to 4,700 (2)	
1,300 to 2,600 (2)	

State Solar Capacity (MW)
High Wind Scenario

10,200 to 10,300 (1)	
2,100 to 10,200 (2)	
700 to 2,100 (3)	
100 to 700 (3)	
0 to 100 (4)	
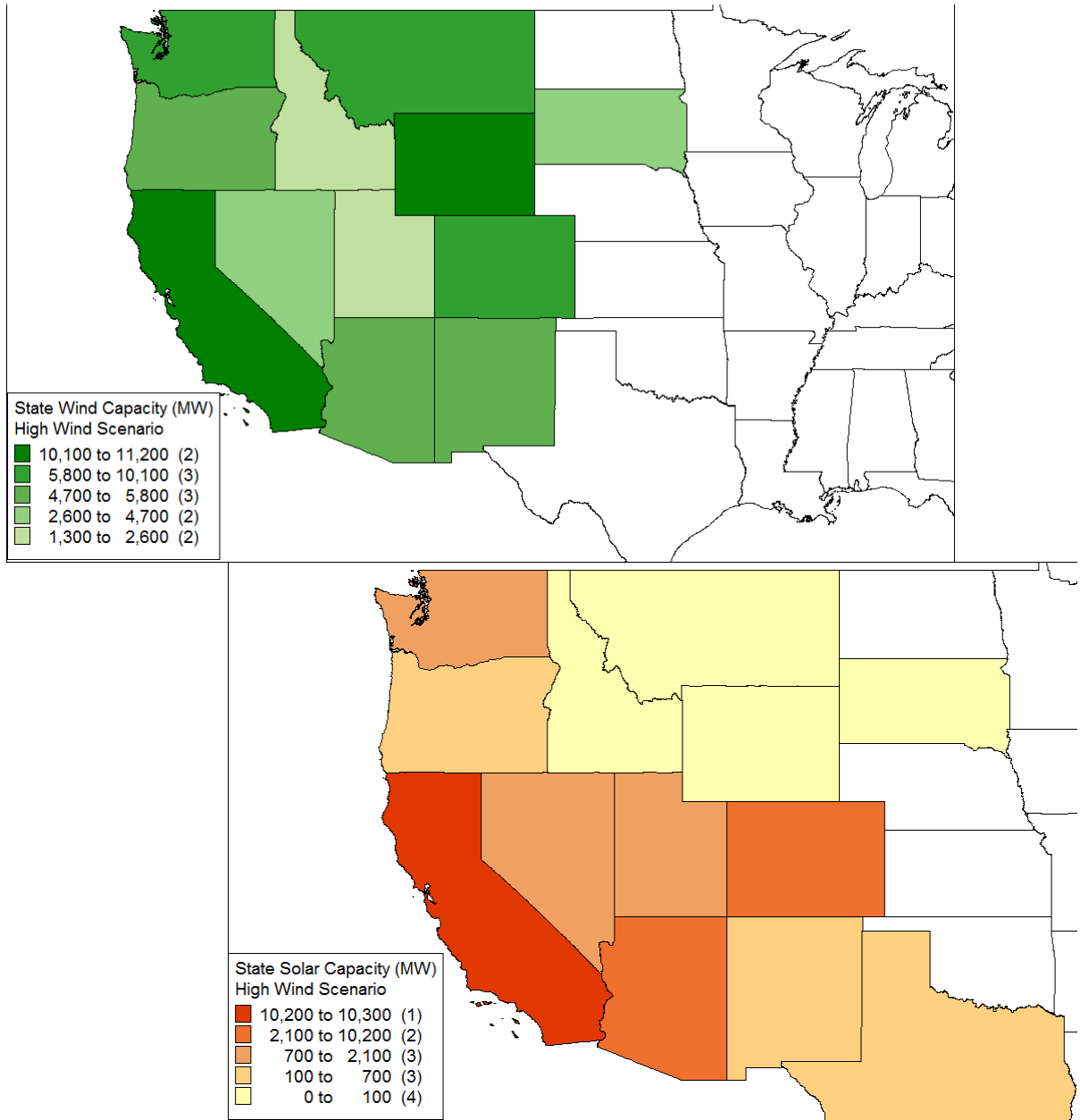
Figure 135. High Wind Scenario—installed capacity by state

Figure 136 through Figure 139 show the monthly wind and solar energy production for several subregions: WC, CG, NTTG, and CAISO. The percentage of energy penetration for each month is labeled on the graphs. The aggregated wind and solar energy production across the Western Interconnection is also shown, in GWh and as a percentage of load. VG in these plots includes wind, PV and CSP.
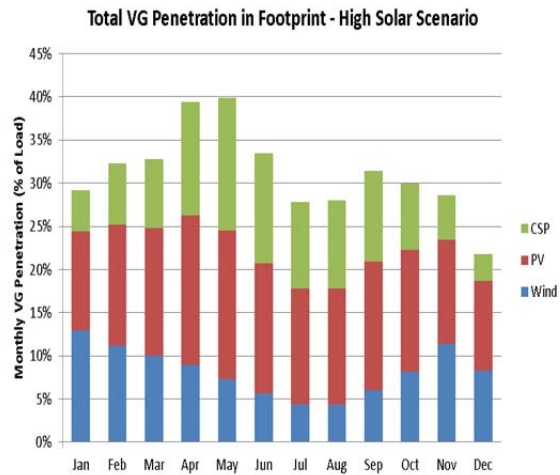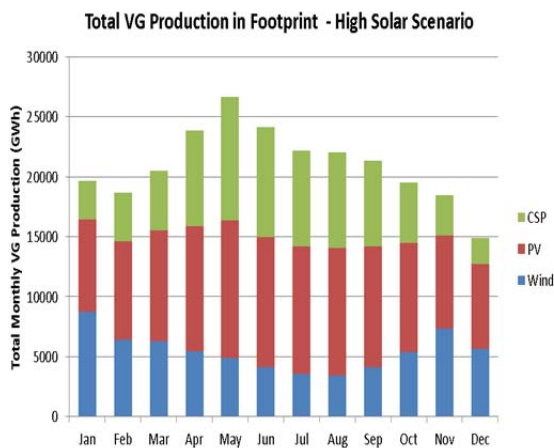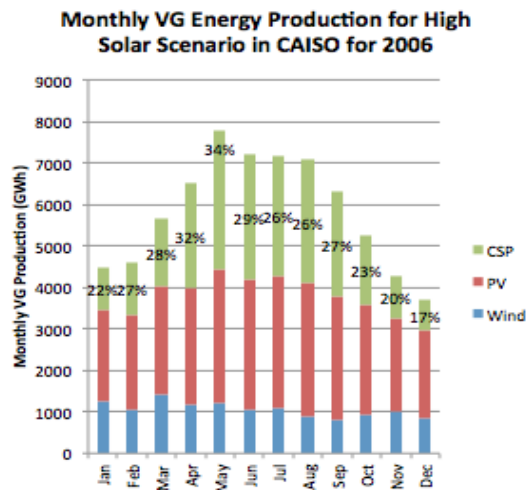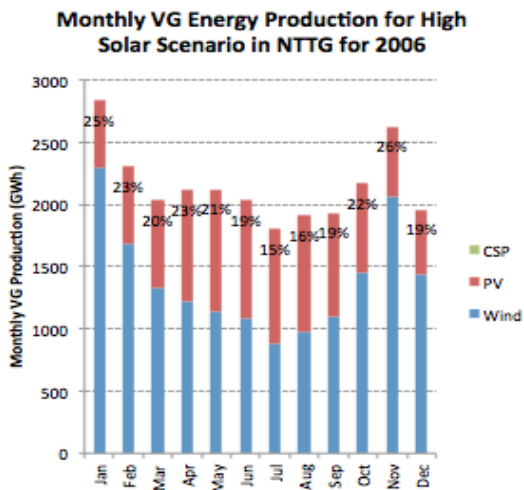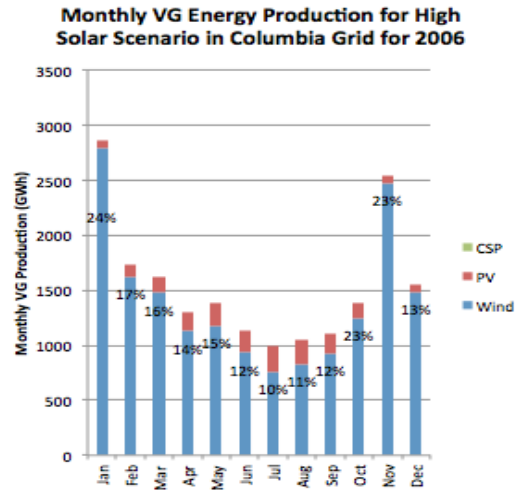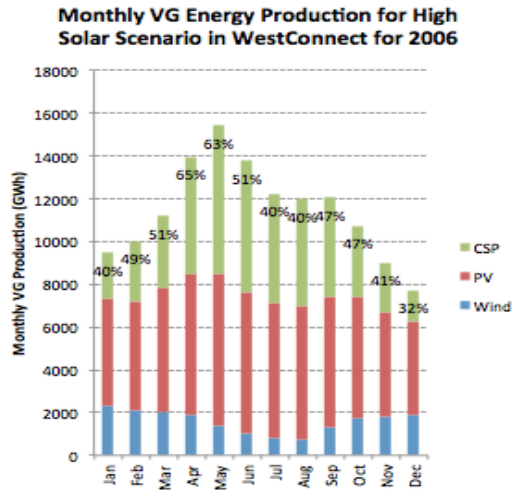
Figure 136. High Solar Scenario—monthly profiles

163
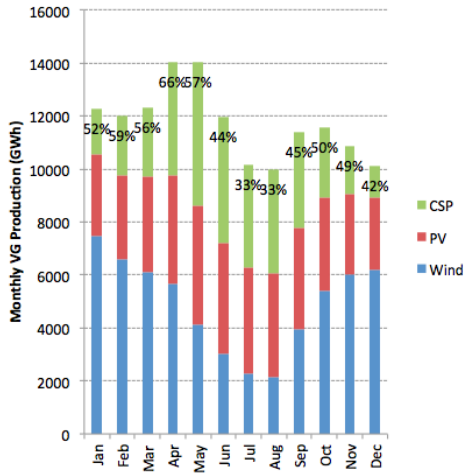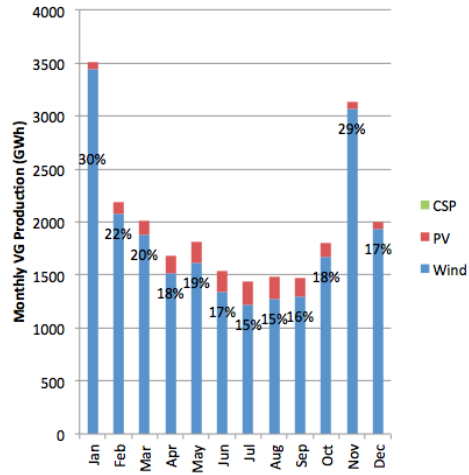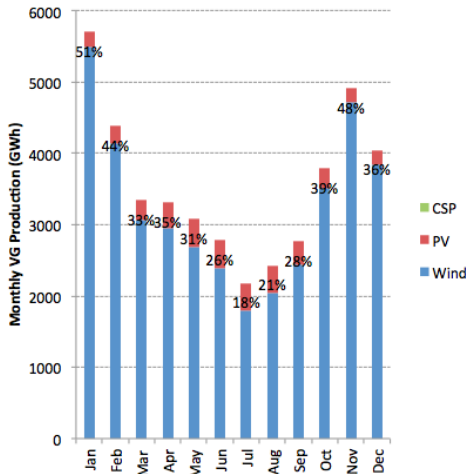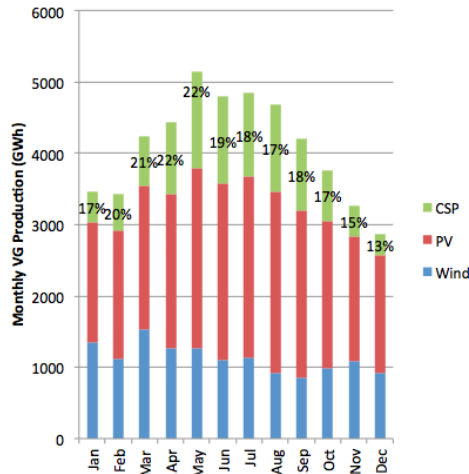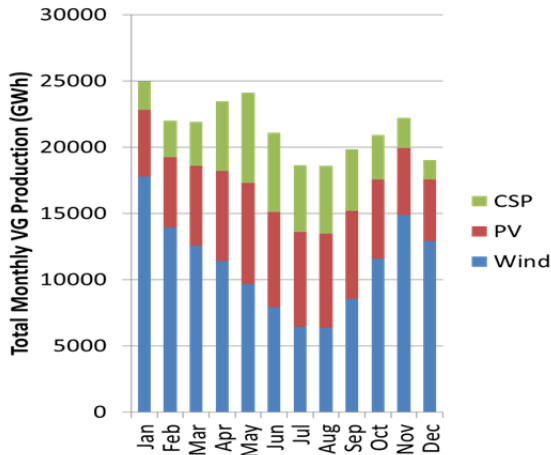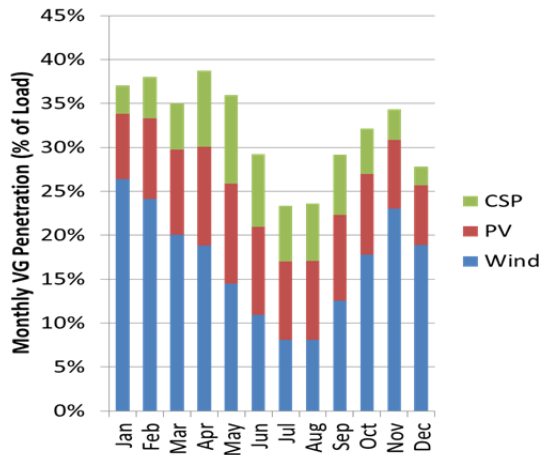
Figure 137. High Mix Scenario—monthly profiles

164
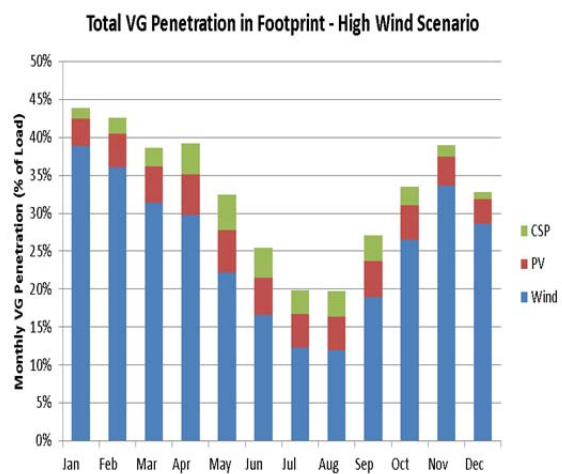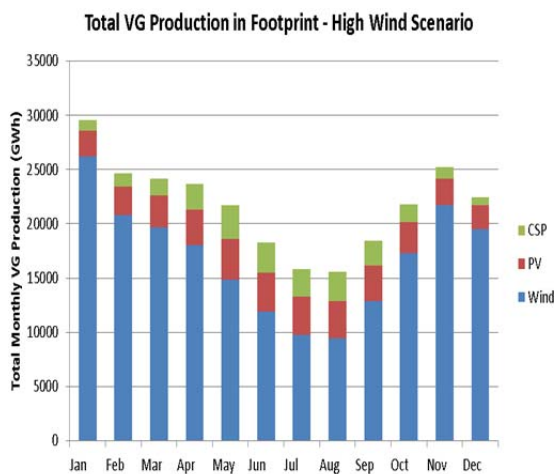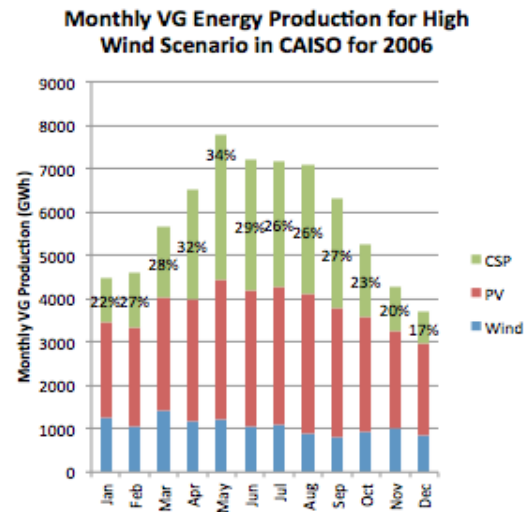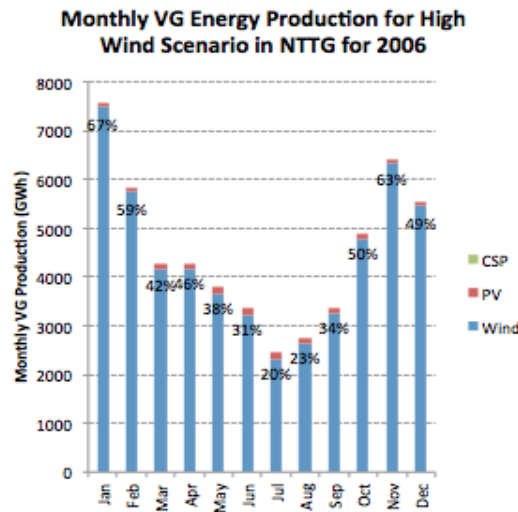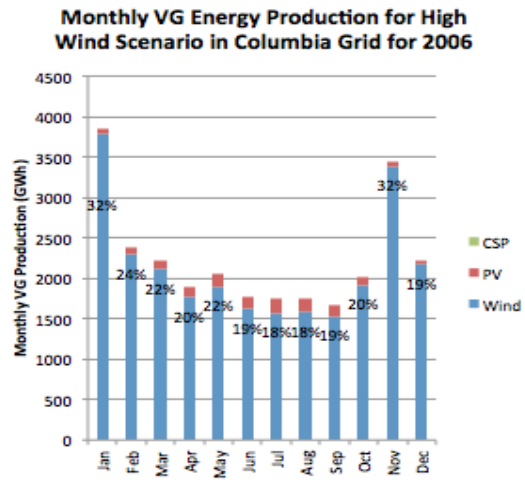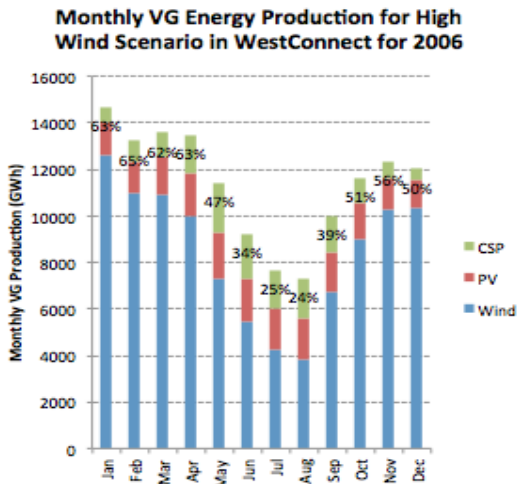
Figure 138. High Wind Scenario—monthly profiles

165
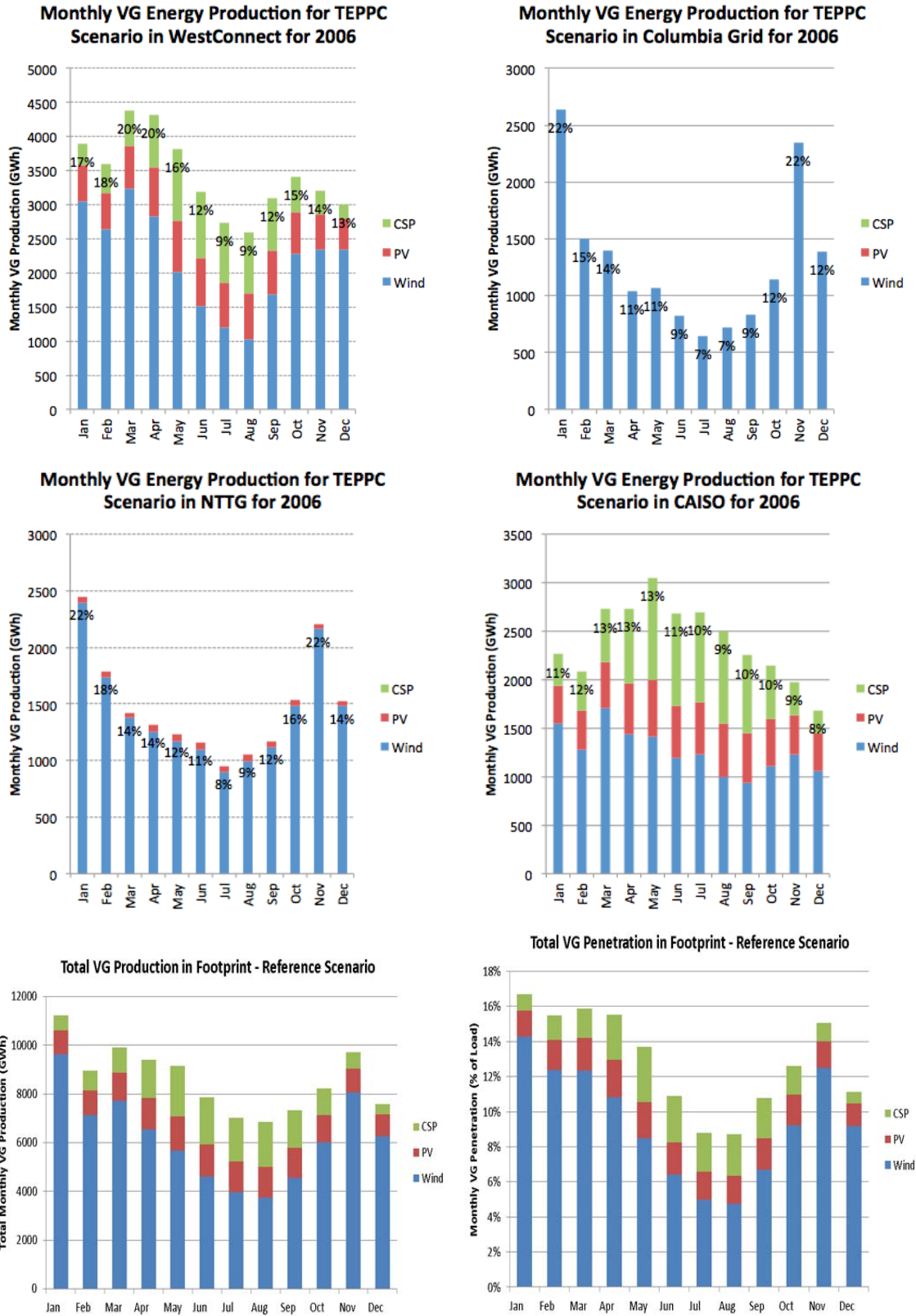
Figure 139. TEPPC Scenario—monthly profiles

166

Figure 140 through Figure 143 show the average diurnal profiles of the load, wind, PV, and CSP for each scenario. The CSP shown in these profiles was dispatched by NREL's System Advisor Model and does not reflect the final dispatch as modeled by PLEXOS.
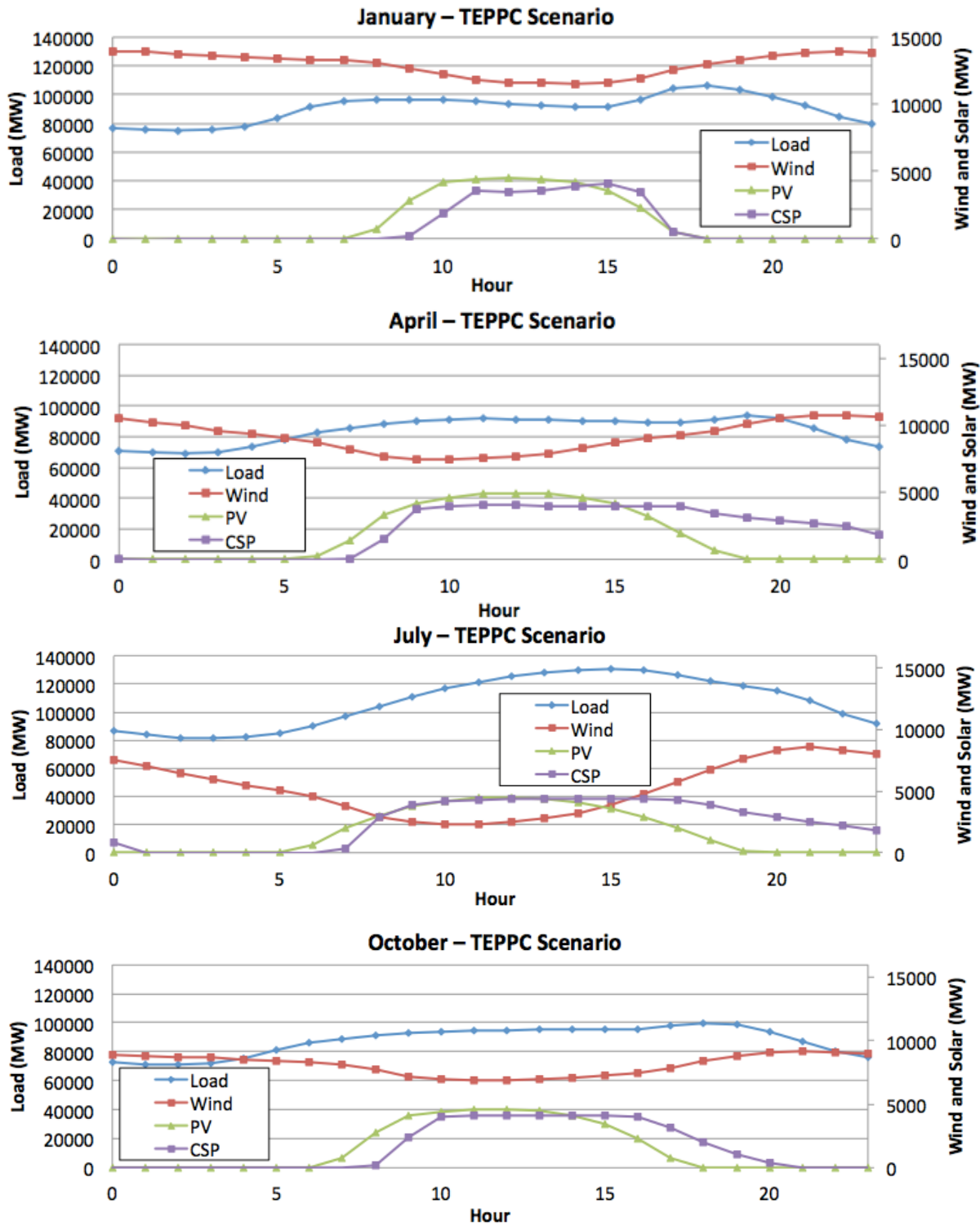
Figure 140. TEPPC Scenario—average diurnal profile
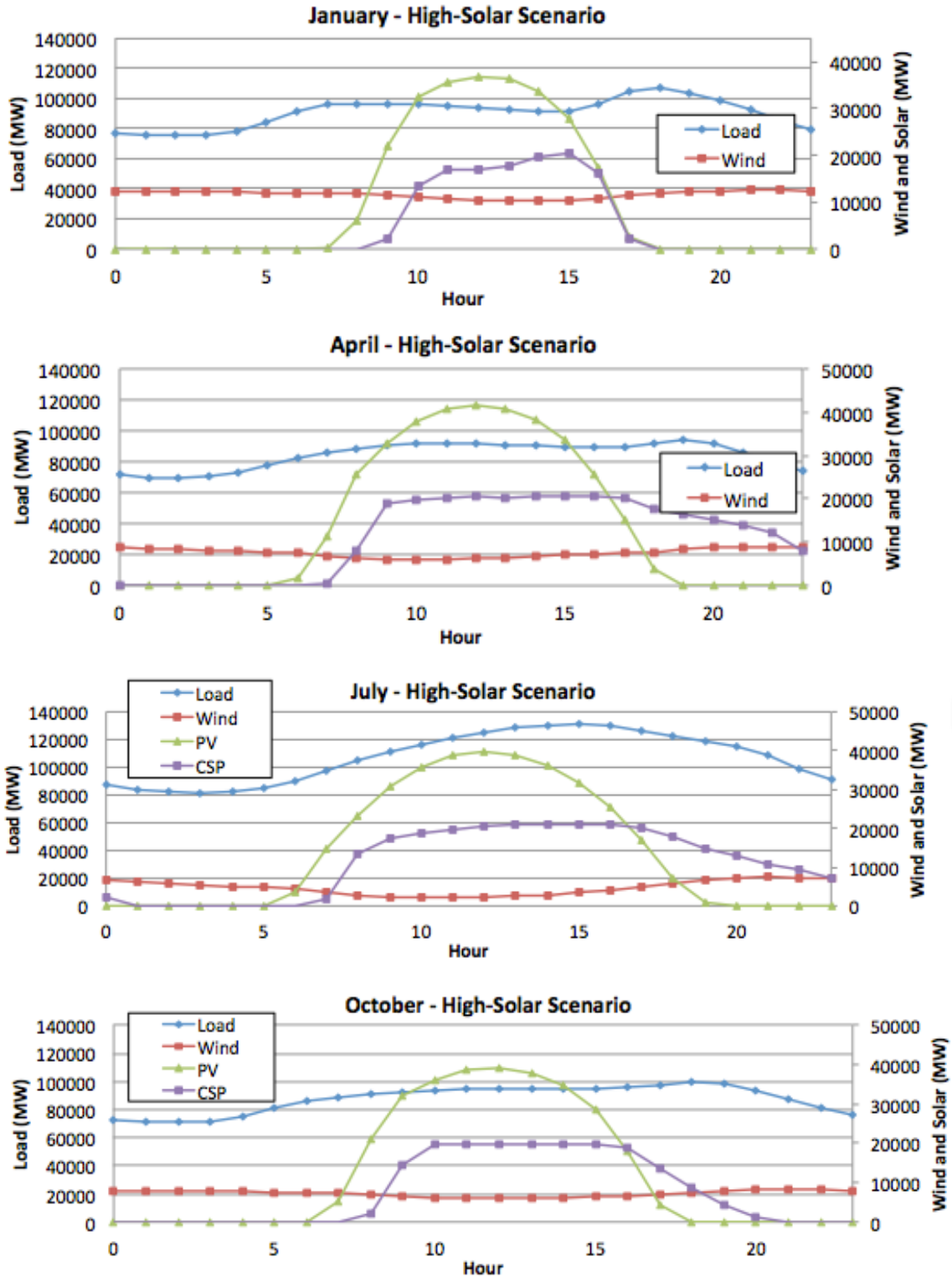
Figure 141. High Solar Scenario—average diurnal profile

168
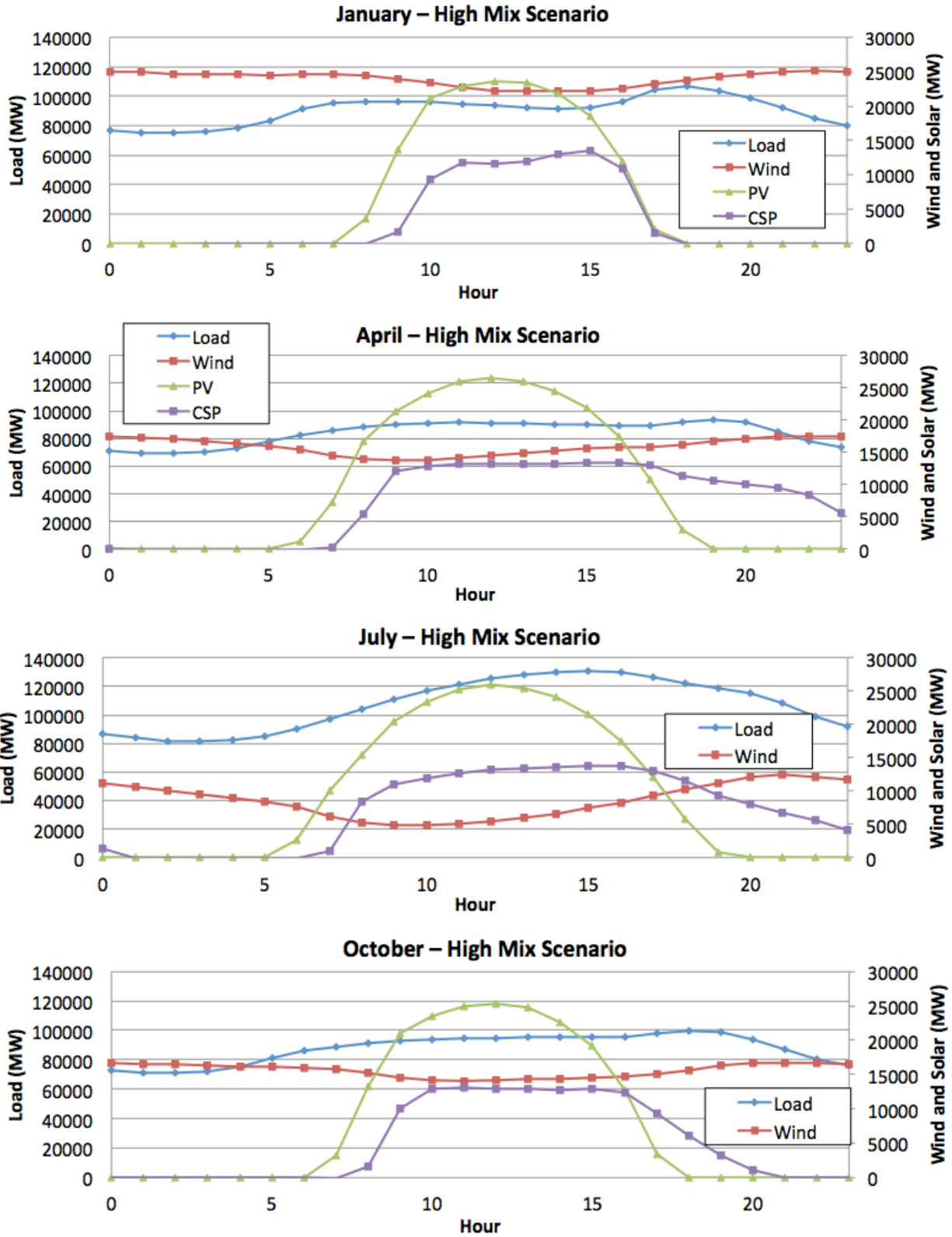
Figure 142. High Mix Scenario—average diurnal profile
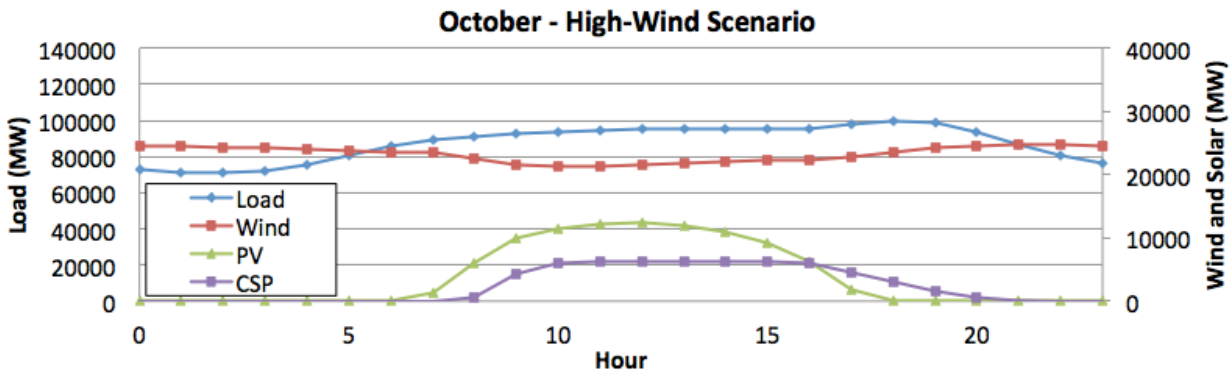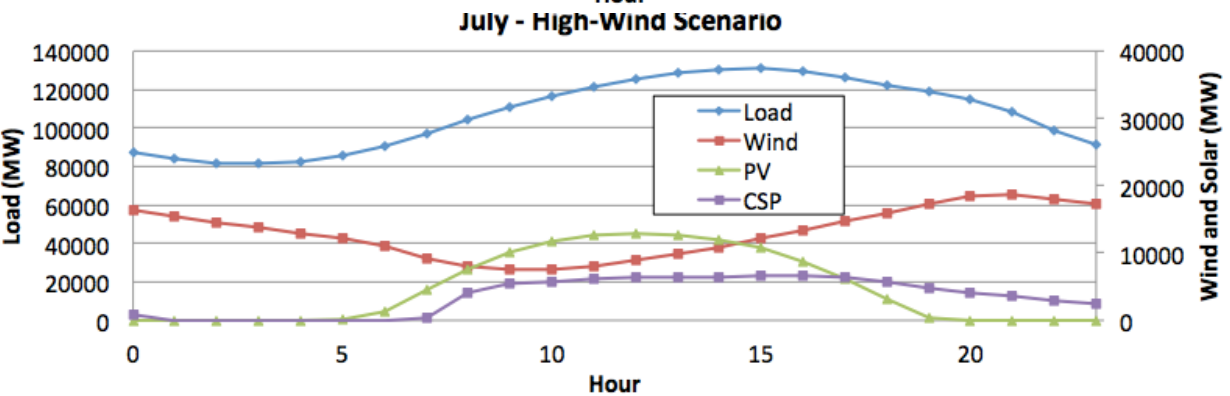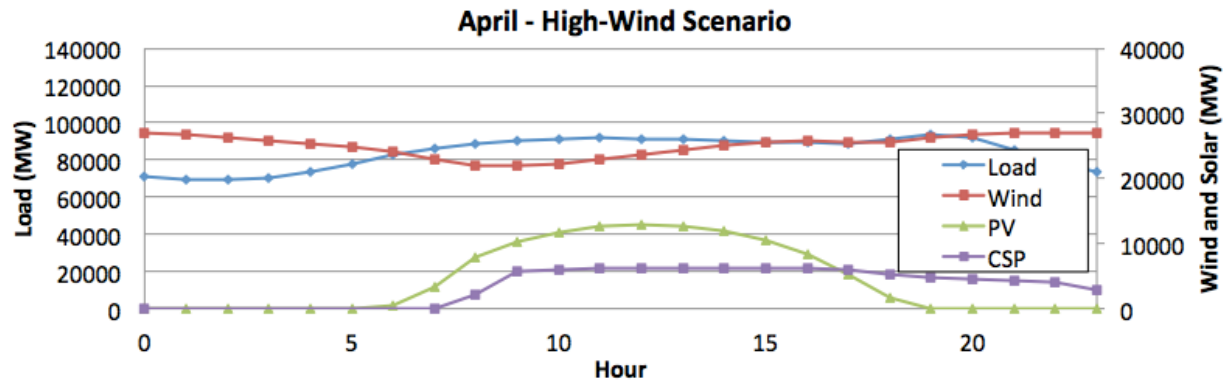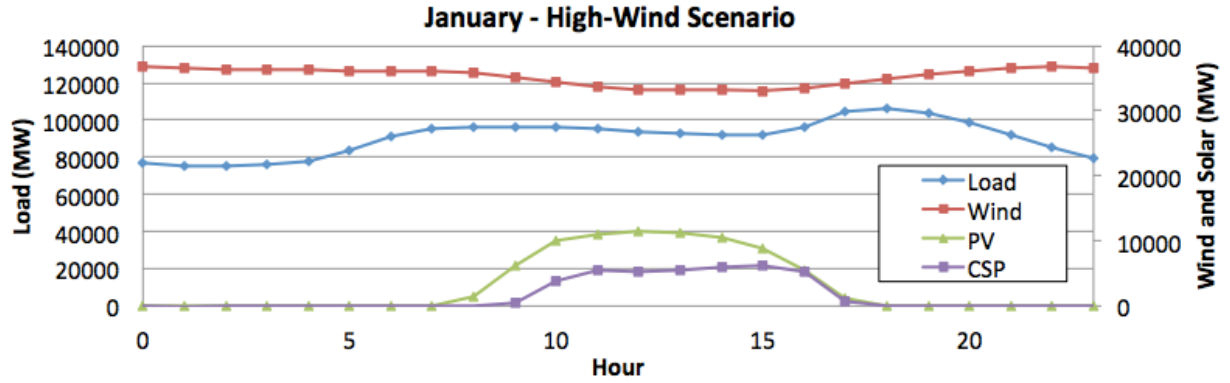
Figure 143. High Wind Scenario—average diurnal profile

170

Figure 144 through Figure 146 show the seasonal variability of wind, PV, and wind plus PV for the high-penetration scenarios. Each point on the plots represents a single ordered pair of load deltas with the time-synchronized resource deltas.
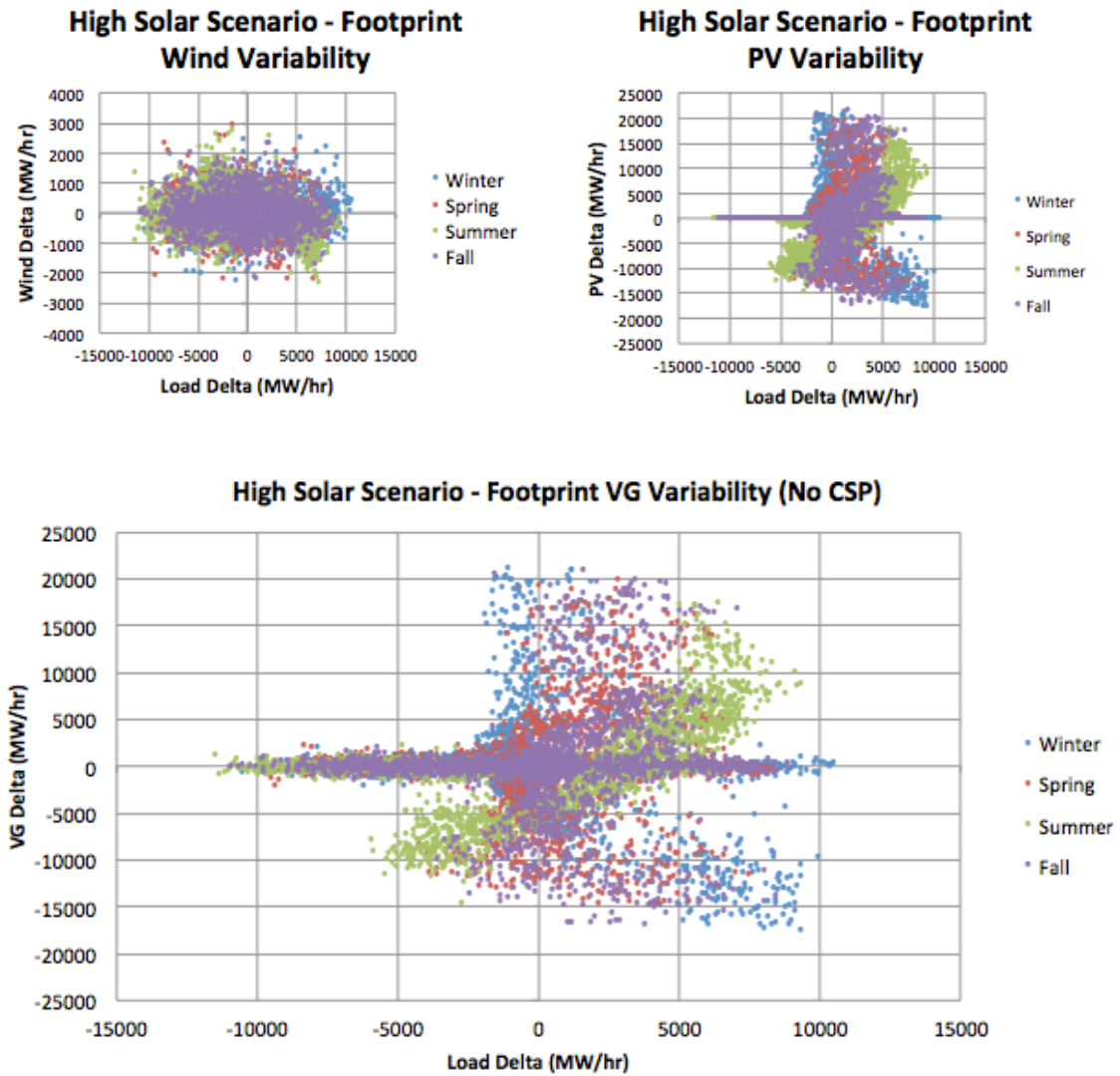
Figure 144. High Solar Scenario—hourly variability by season

High Mix Scenario Footprint Wind Variability

High Mix Scenario Footprint PV Variability

High Mix Scenario Footprint VG Variability (No CSP)
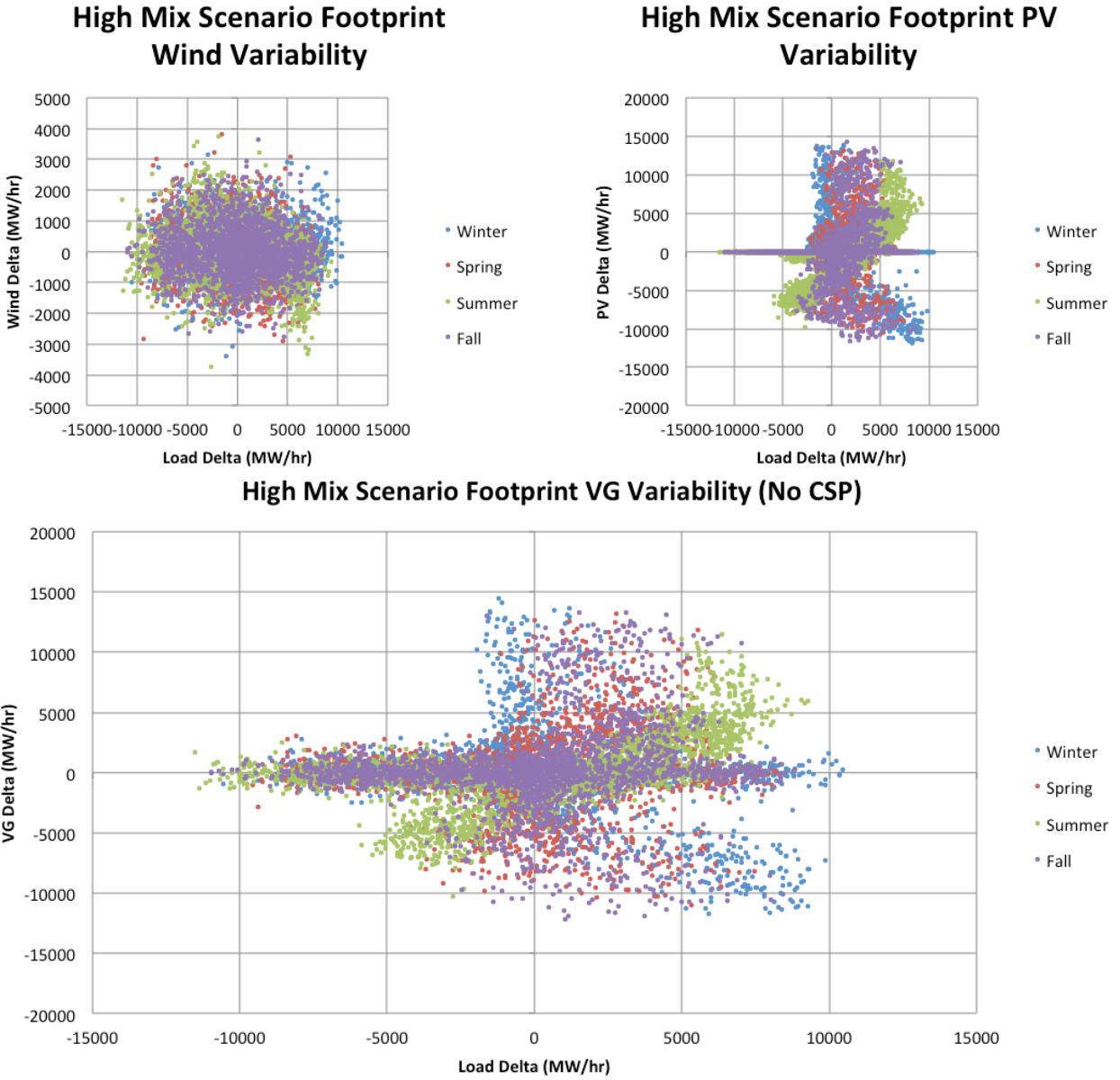
Figure 145. High Mix Scenario—hourly variability by season

High Wind Scenario Footprint Wind Variability

High Wind Scenario Footprint PV Variability

High Wind Scenario Footprint VG Variability (No CSP)
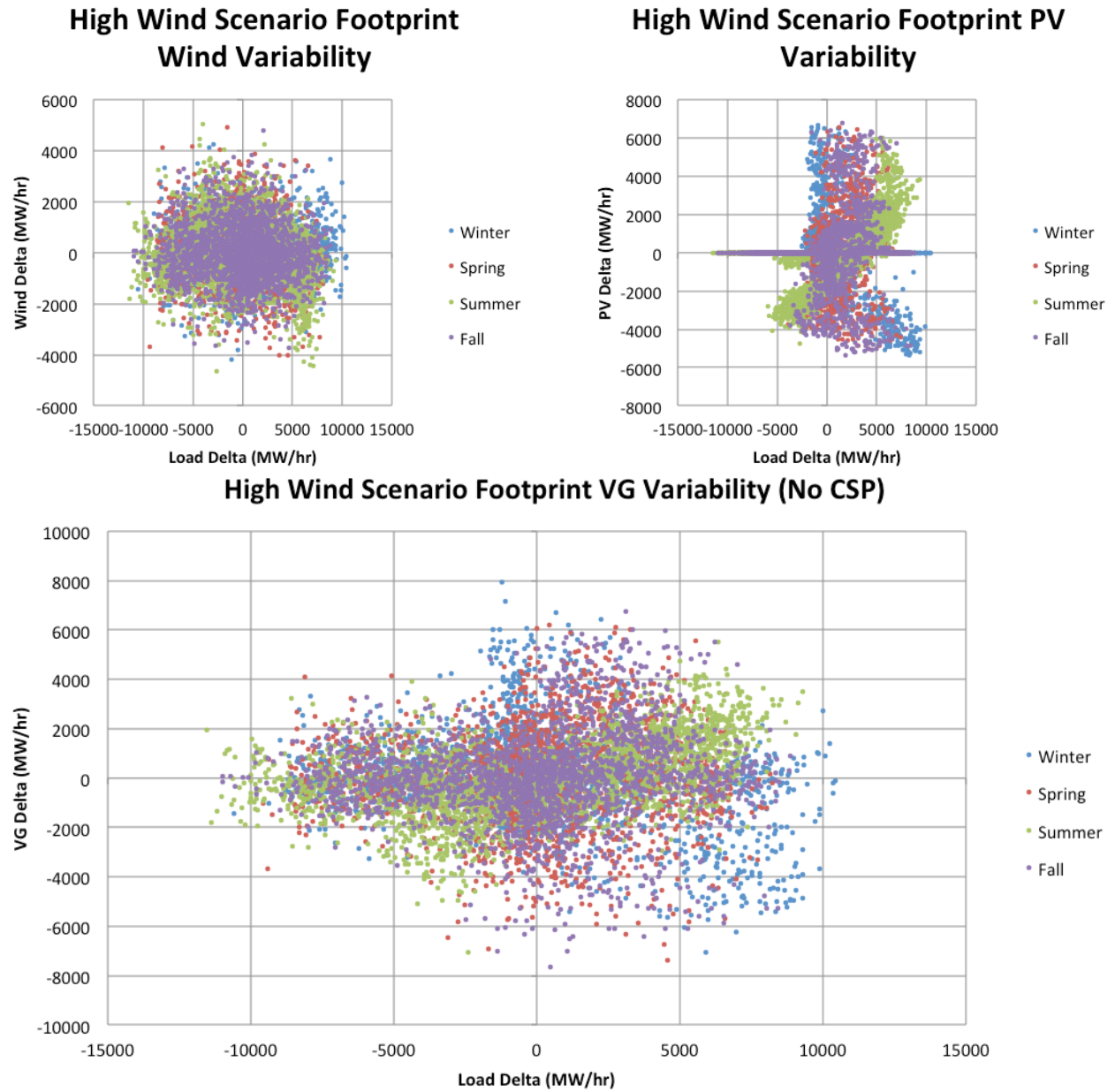
Figure 146. High Wind Scenario—hourly variability by season

Figure 147 and Figure 148 show a surface indicating when load and net load values occur over the year of data used in the study. The x-axis is the hour of the day and the y-axis is the month of the year. The color scale shows the average monthly value of load or net load in the hour.
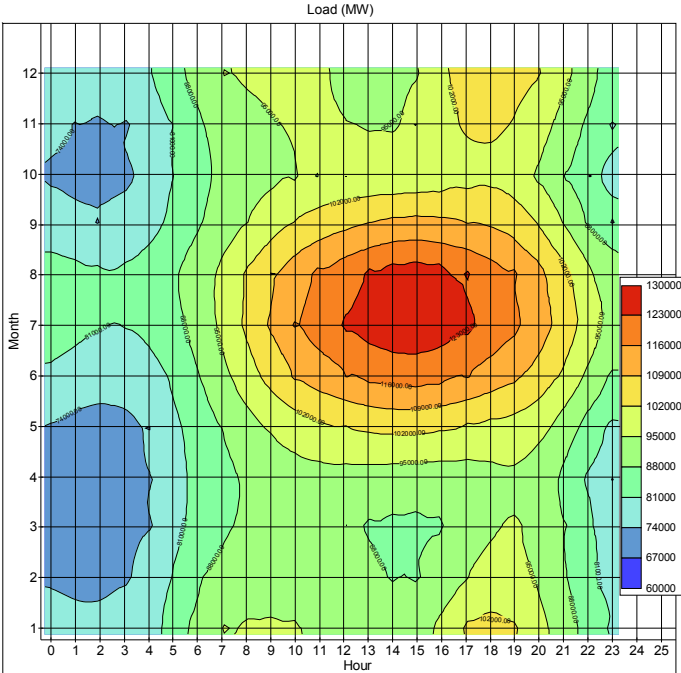
Figure 147. Load alone with monthly average values in MW
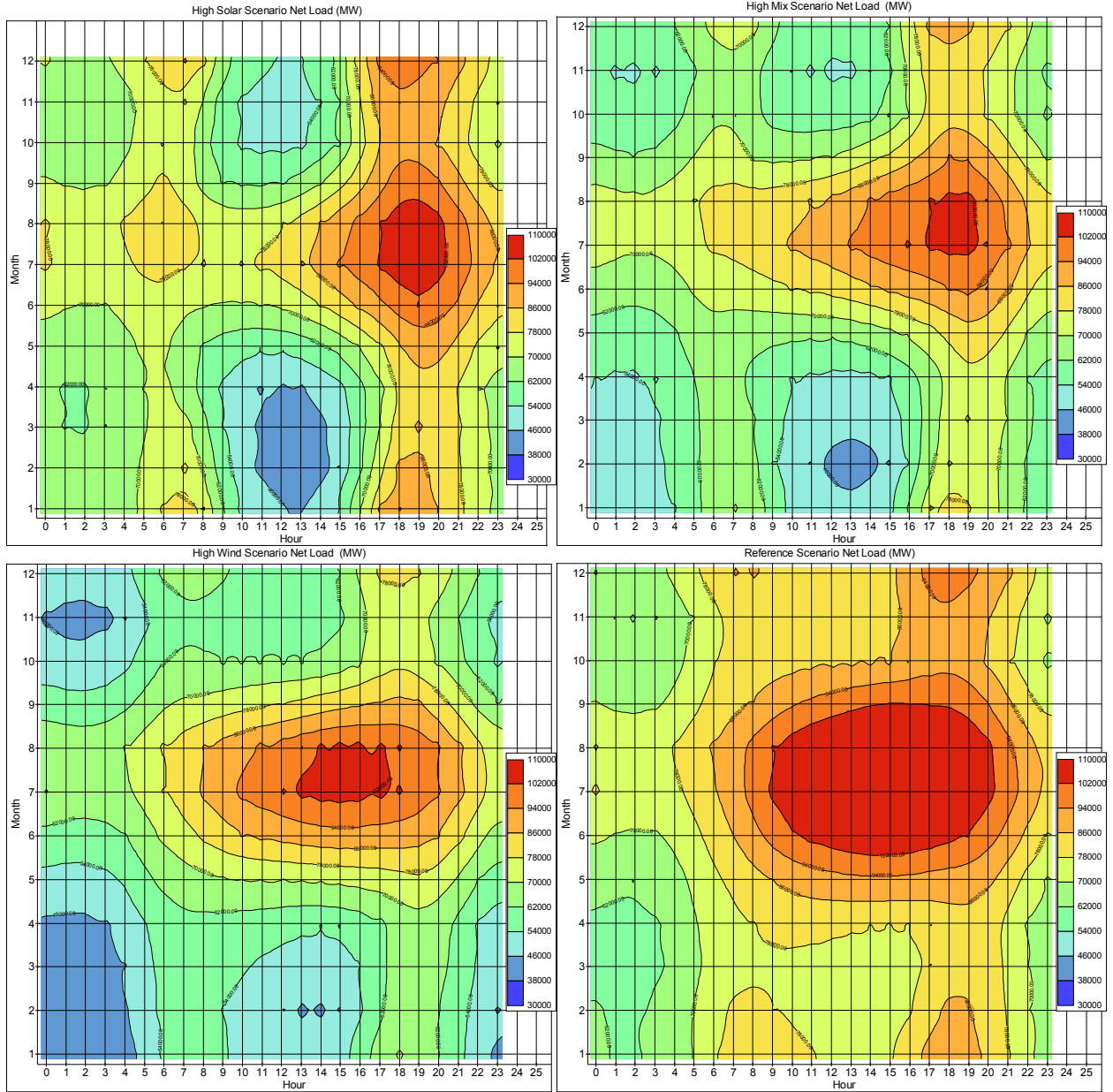
Figure 148. Net load with monthly average values in MW for each scenario

175

Figure 149 and Figure 150 show a surface indicating when load and net load changes occur over the year of data used in the study. The x-axis is the hour of the day and the y-axis is the month of the year. The color scale shows the monthly average change in load or net load in the hour.
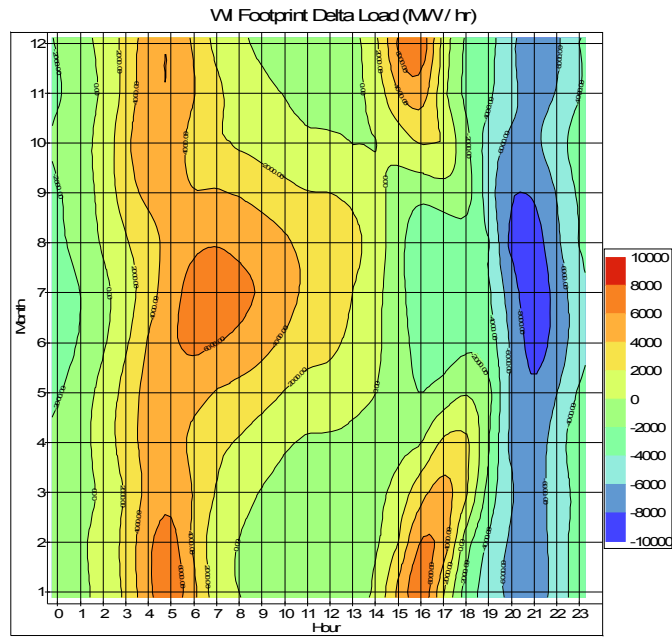
Figure 149. Delta load only with monthly average changes in MW/h
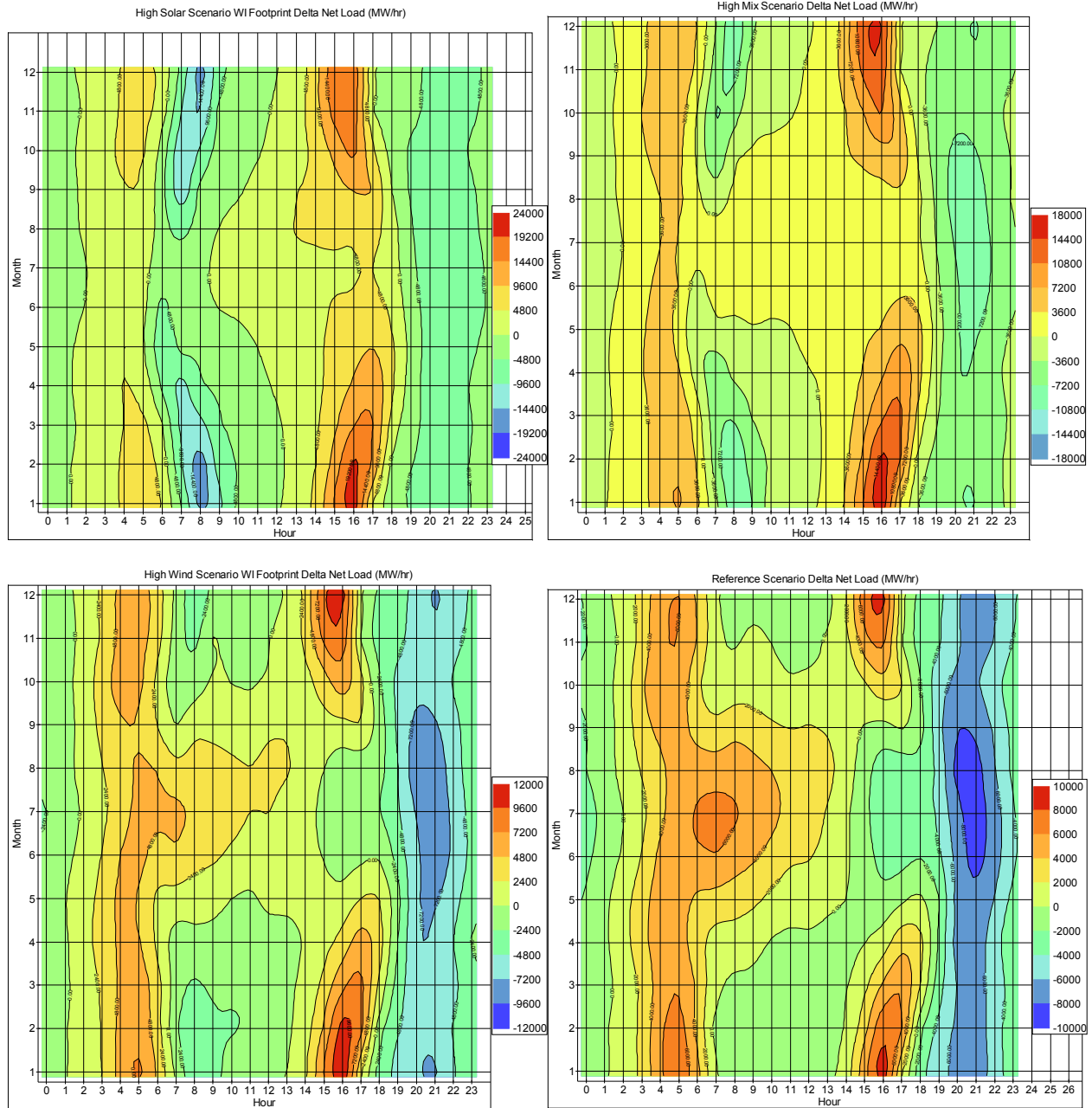
Figure 150. Delta net load with monthly average changes in MW/h for each scenario

Note: Observe the difference in scales between the scenarios.

177

The next section focuses on the DA forecast error analysis. Figure 151 through Figure 153 show DA forecast error analysis for wind, PV, and wind plus PV forecast errors. CSP is not included in this forecast error analysis because CSP has storage that allows it to be dispatched. Statistics by subregion are shown in Table 32 through Table 35.
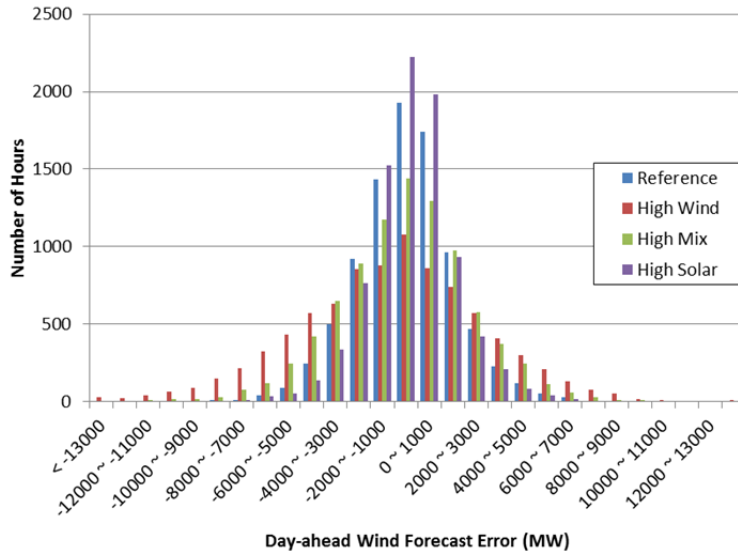
Figure 151. Distribution of DA wind forecast errors
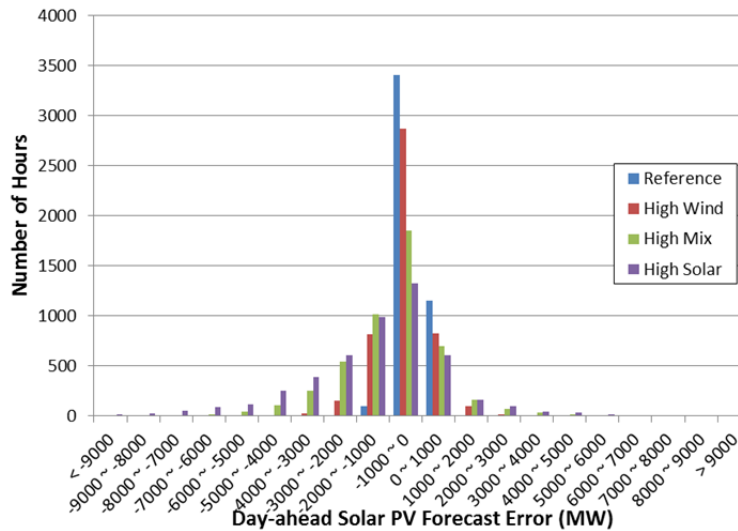
Figure 152. Distribution of DA PV forecast errors
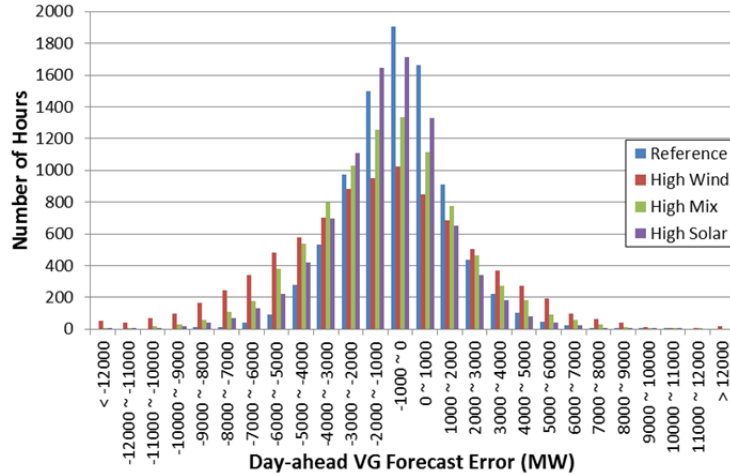
Figure 153. Distribution of DA wind plus PV forecast errors

Table 32. DA Forecast Error Statistics for the High Solar Scenario

Region	Capacity (MW)	MAE (MW)	MAE (%)	RMSE (MW)	RMSE (%)	Maximum Negative Error (MW)	Negative Error (%)	Maximum Positive Error (MW)	Maximum Positive Error (%)
Wind									
CA	4,406	451	10	649	15	−2,384	−54	2,958	67
CG	6,581	631	10	946	14	−4,973	−76	5,101	78
NTTG	5,787	495	9	711	12	−3,807	−66	3,052	53
WC	6,584	403	6	562	9	−2,848	−43	2,726	41
U.S. Western Interconnection	23,357	1,387	6	1,849	8	−8,169	−35	8,458	36
Solar (PV)									
CA	17,134	713	4	1,055	6	−6,589	−38	5,310	31
CG	1,211	105	9	156	13	−619	−51	667	55
NTTG	5,270	285	5	440	8	−2,070	−39	2,103	40
WC	36,526	1,248	3	1,771	5	−9,189	−25	6,018	16
U.S. Western Interconnection	60,141	1,882	3	2,628	4	−16,974	−28	9,867	16
Total									
CA	21,539	692	3	989	5	−7,592	−35	5,243	24
CG	7,792	639	8	947	12	−4,973	−64	5,101	65
NTTG	11,057	560	5	771	7	−3,807	−34	3,169	29
WC	43,110	936	2	1,435	3	−9,576	−22	6,168	14
U.S. Western Interconnection	83,498	2,004	2	2,676	3	−17,714	−21	10,806	13

Table 33. DA Forecast Error Statistics for the High Mix Scenario

Region	Capacity (MW)	MAE (MW)	MAE (%)	RMSE (MW)	RMSE (%)	Maximum Negative Error (MW)	Negative Error (%)	Maximum Positive Error (MW)	Maximum Positive Error (%)
Wind									
CA	4,788	478	10	680	14	−2,462	−51	2,983	62
CG	8,261	757	9	1,106	13	−5,550	−67	5,908	72
NTTG	12,414	905	7	1,218	10	−6,123	−49	4,474	36
WC	18,314	1,073	6	1,442	8	−6,763	−37	5,471	30
U.S. Western Interconnection	43,778	2,207	5	2,874	7	12,232	−28	11,098	25
Solar (PV)									
CA	13,588	306	2	641	5	−5,172	−38	4,731	35
CG	1,161	51	4	106	9	−588	−51	637	55
NTTG	2,976	61	2	130	4	−814	−27	903	30
WC	23,165	427	2	821	4	−6,173	−27	3,687	16
U.S. Western Interconnection	40,890	704	2	1,323	3	−11,373	−28	8,441	21
Total									
CA	18,376	668	4	931	5	−6,228	−34	4,760	26
CG	9,422	761	8	1,105	12	−5,550	−59	5,908	63
NTTG	15,390	915	6	1,225	8	−6,123	−40	4,519	29
WC	41,479	1,271	3	1,670	4	−7,047	−17	6,113	15
U.S. Western Interconnection	84,668	2,429	3	3,133	4	−12,525	−15	11,098	13

Table 34. DA Forecast Error Statistics for the High Wind Scenario

Region	Capacity (MW)	MAE (MW)	MAE (%)	RMSE (MW)	RMSE (%)	Maximum Negative Error (MW)	Negative Error (%)	Maximum Positive Error (MW)	Maximum Positive Error (%)
Wind									
CA	7,970	693	9	977	12	−3,756	−47	4,832	61
CG	9,101	822	9	1,188	13	−5,895	−65	6,587	72
NTTG	16,854	1,179	7	1,582	9	−7,584	−45	6,501	39
WC	32,224	1,838	6	2,438	8	−10,078	−31	9,558	30
U.S. Western Interconnection	66,150	3,183	5	4,115	6	−17,381	−26	16,574	25
Solar (PV)									
CA	9,772	188	2	384	4	−2,885	−30	2,776	28
CG	969	42	4	86	9	−491	−51	507	52
NTTG	2,312	23	1	49	2	−305	−13	377	16
WC	14,979	199	1	382	3	−2,356	−16	1,992	13
U.S. Western Interconnection	28,032	362	1	673	2	−5,340	−19	4,550	16
Total									
CA	17,743	766	4	1,042	6	−4,963	−28	4,879	28
CG	10,070	825	8	1,188	12	−5,895	−59	6,587	65
NTTG	19,167	1,181	6	1,583	8	−7,584	−40	6,501	34
WC	47,203	1,875	4	2,477	5	−10,078	−21	9,545	20
U.S. Western Interconnection	94,183	3,229	3	4,161	4	−17,381	−18	16,574	18

Table 35. DA Forecast Error Statistics for the TEPPC Scenario

Region	Capacity (MW)	MAE (MW)	MAE (%)	RMSE (MW)	RMSE (%)	Maximum Negative Error (MW)	Negative Error (%)	Maximum Positive Error (MW)	Maximum Positive Error (%)
Wind									
CA	5,630	524	9	744	13	−2,725	−48	3,341	59
CG	6,161	591	10	896	15	−4,762	−77	5,057	82
NTTG	6,054	513	8	739	12	−3,912	−65	3,260	54
WC	10,054	692	7	955	9	−4,150	−41	4,804	48
U.S. Western Interconnection	27,900	1,612	6	2,118	8	−8,929	−32	10,182	36
Solar (PV)									
CA	2,798	63	2	144	5	−1,309	−47	1,078	39
CG	0	0	-	0	-	0	-	0	-
NTTG	364	12	3	28	8	−215	−59	187	51
WC	3,912	84	2	169	4	−1,418	−36	827	21
U.S. Western Interconnection	7,074	135	2	272	4	−2,265	−32	1,170	17
Total									
CA	8,428	545	6	762	9	−2,873	−34	3,194	38
CG	6,161	591	10	896	15	−4,762	−77	5,057	82
NTTG	6,418	514	8	738	12	−3,912	−61	3,260	51
WC	13,967	719	5	980	7	−4,150	−30	4,804	34
U.S. Western Interconnection	34,974	1,640	5	2,144	6	−8,929	−26	10,182	29

Figure 154 through Figure 159 show the wind and solar DA forecast errors as a function of load, net load, wind, and solar levels.
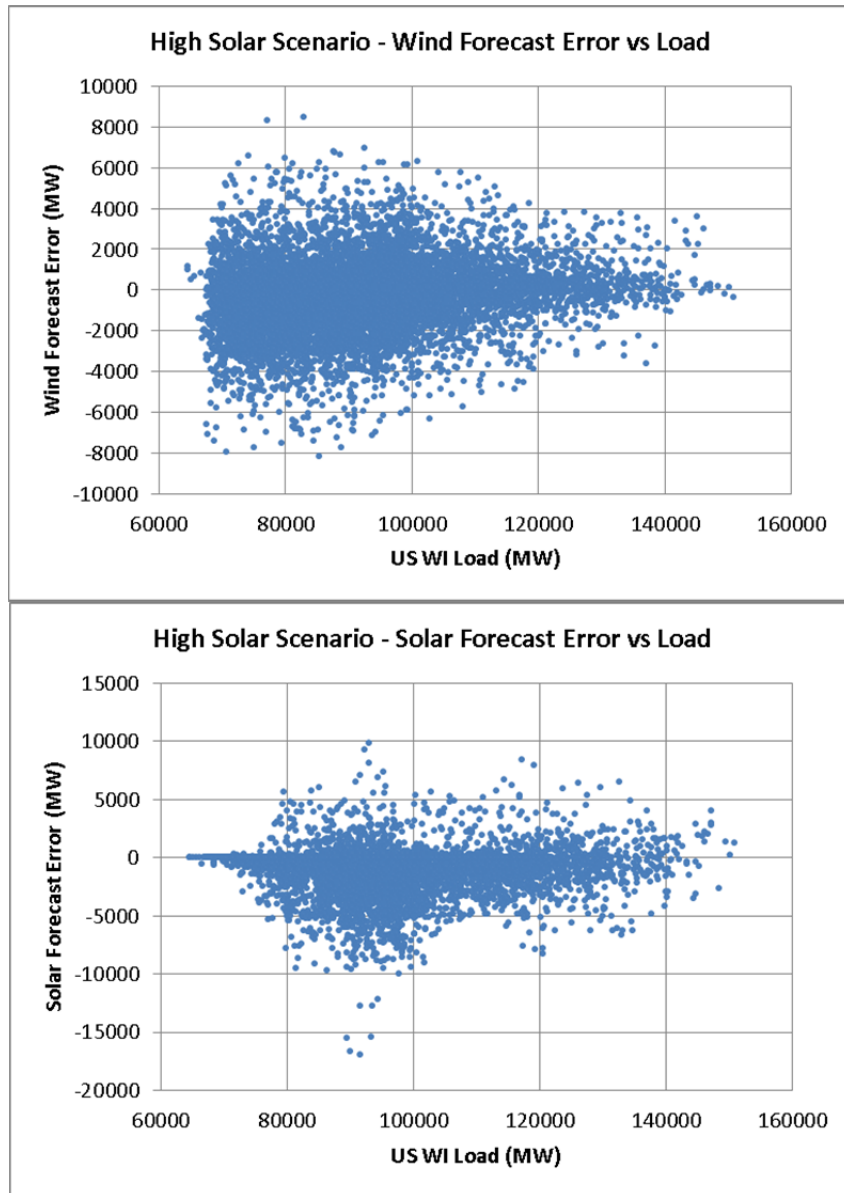
**Figure 154. Wind and PV DA forecast error
as a function of load level for the High Solar Scenario**
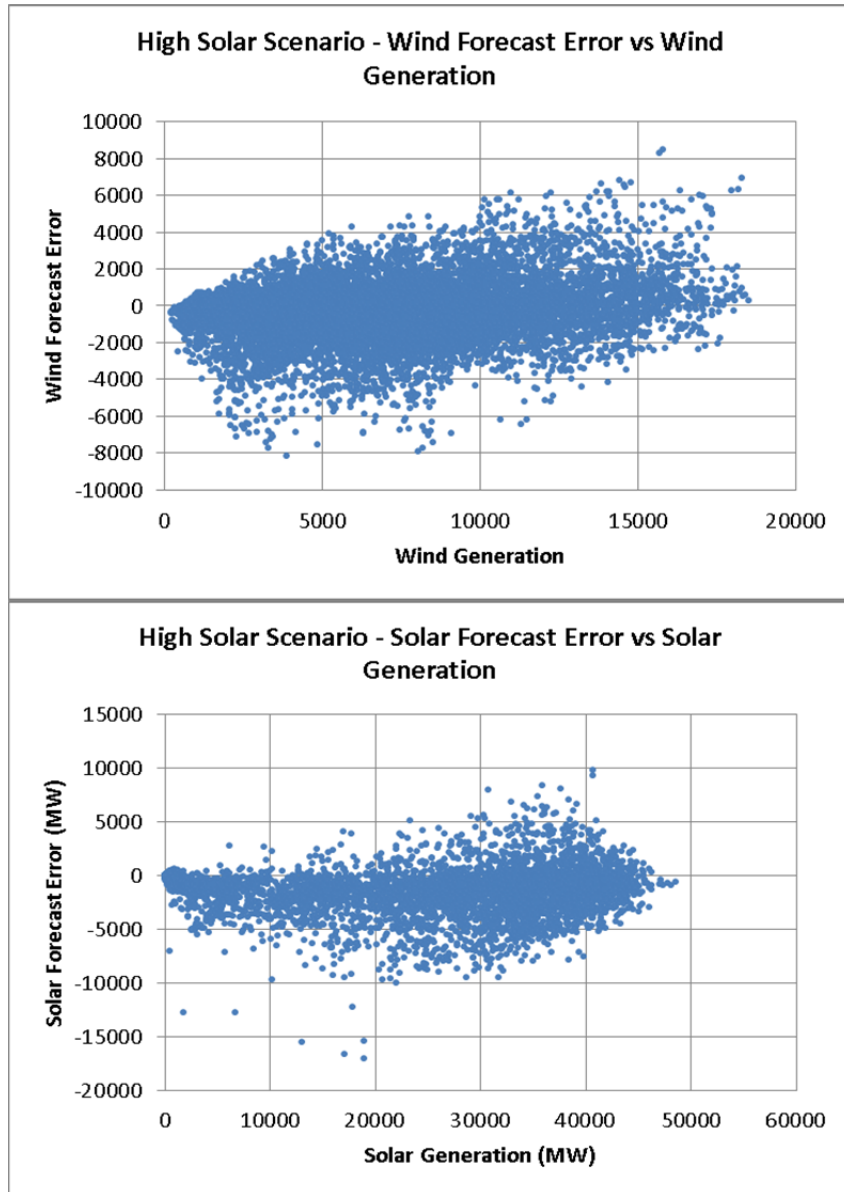
Figure 155. Wind and PV DA forecast error as a function of wind and PV output level for the High Solar Scenario
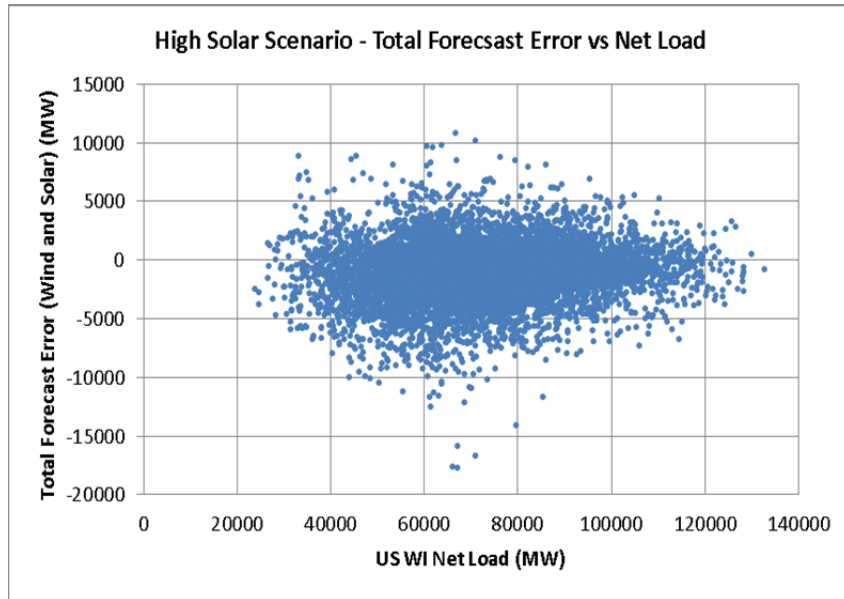
**Figure 156. Wind plus PV DA forecast error
as a function of net load for the High Solar Scenario**
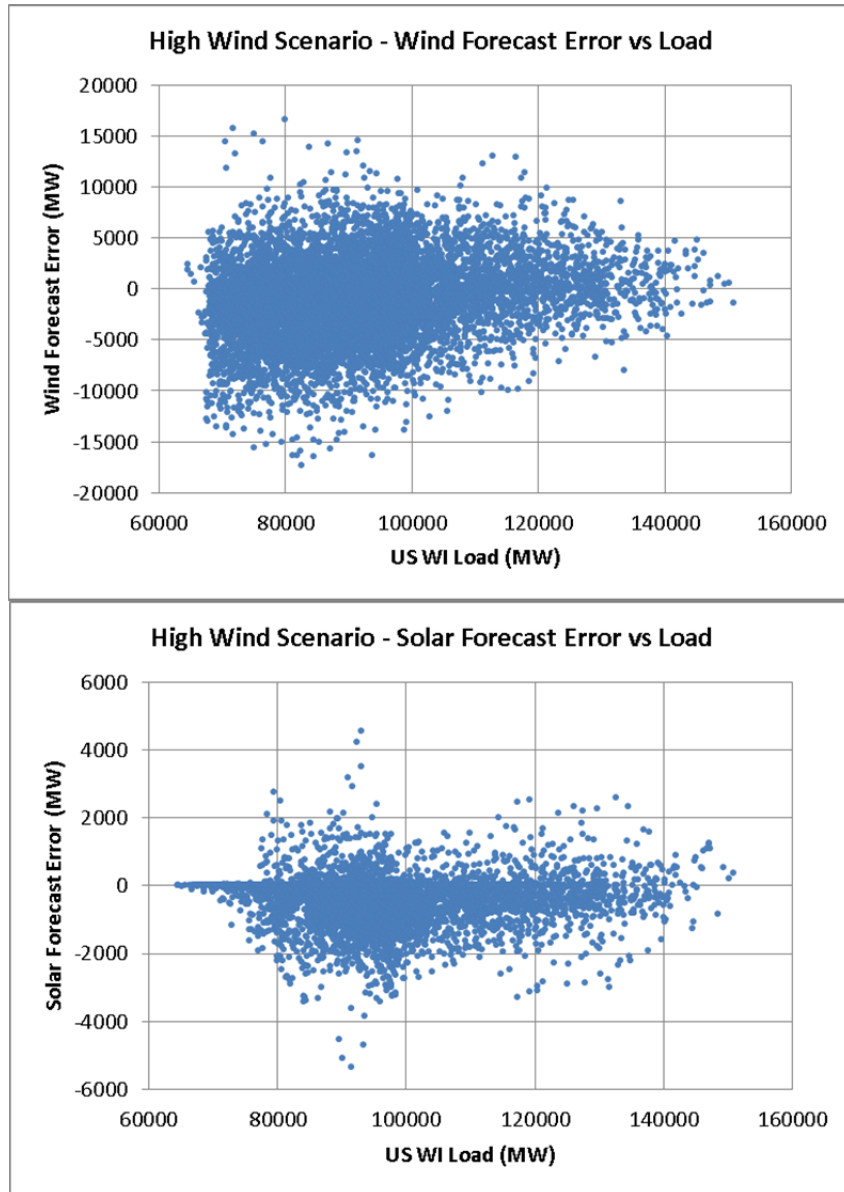
**Figure 157. Wind and PV DA forecast error
as a function of load level for the High Wind Scenario**
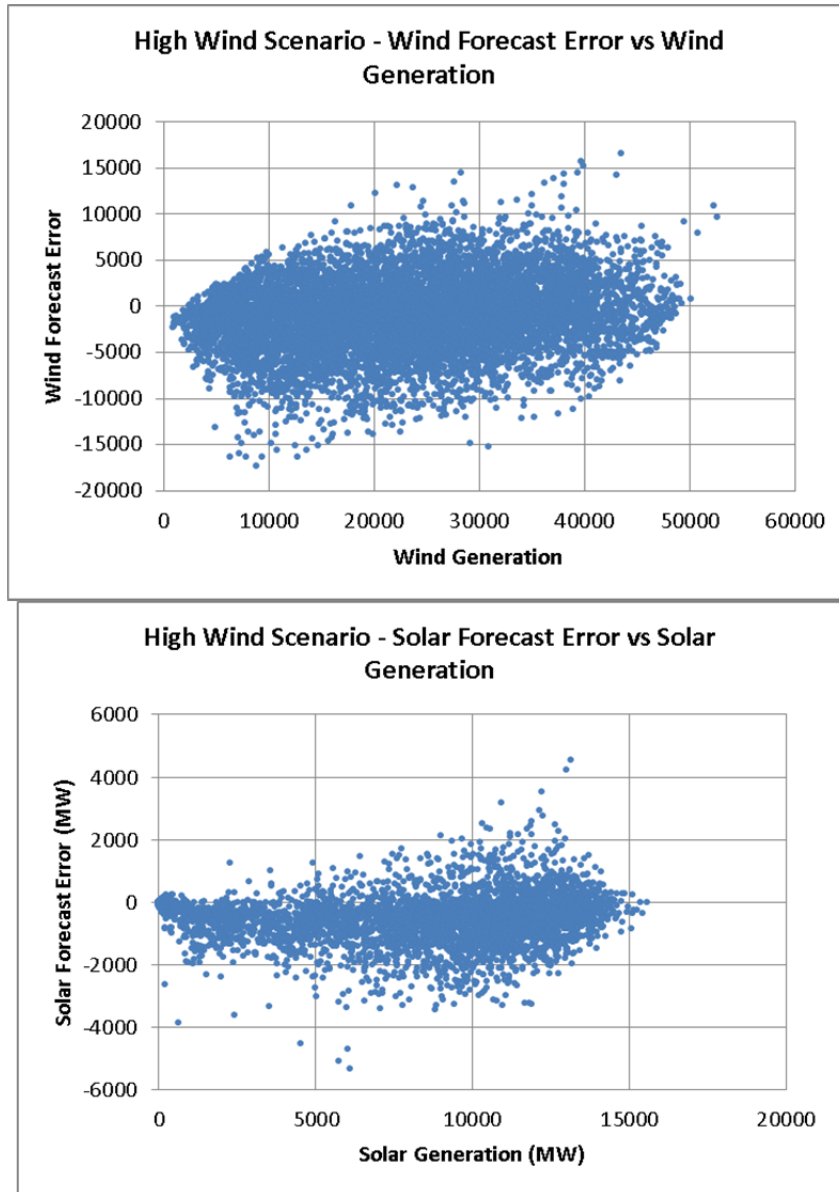
Figure 158. Wind and solar DA forecast error as a function of wind and solar output level for the High Wind Scenario
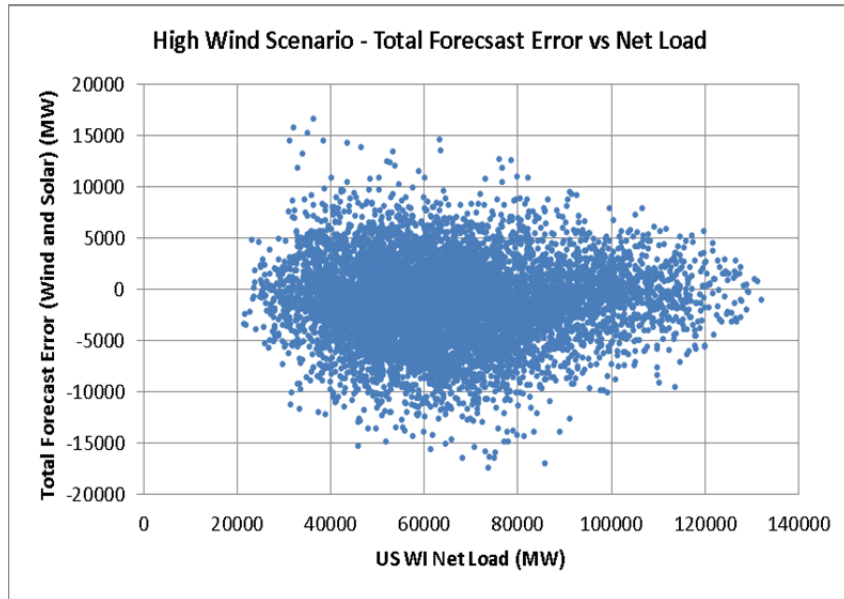
**Figure 159. Wind plus PV DA forecast error
as a function of net load for the High Wind Scenario**

The next section focuses on the 4HA forecast error analysis. Figure 160 through Figure 162 show the 4HA forecast error analysis for wind, PV, and wind plus PV forecast errors. CSP is not included in this forecast error analysis. Statistics by subregion are shown in Table 36 through Table 39.
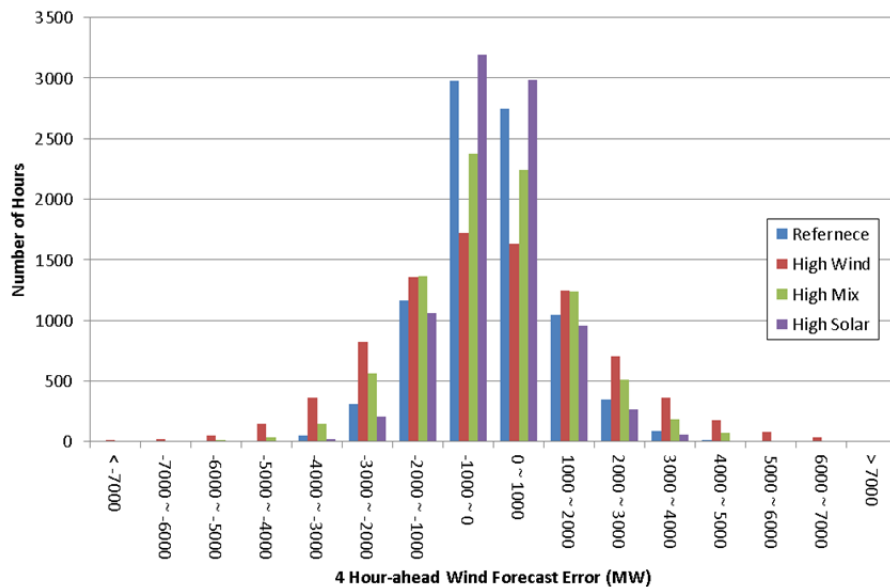
Figure 160. Distribution of 4HA wind forecast errors
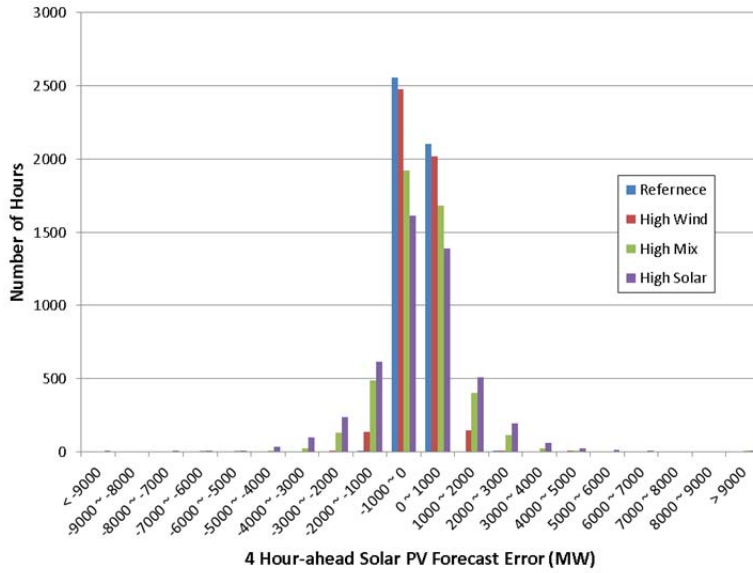
Figure 161. Distribution of 4HA solar forecast errors
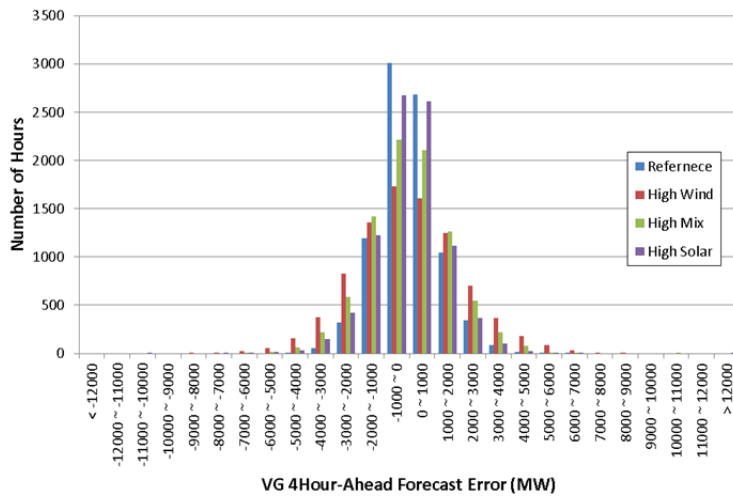
Figure 162. Distribution of 4HA wind plus PV forecast errors

Table 36. 4HA Forecast Error Statistics for the High Solar Scenario

| Region	Capacity (MW)	MAE (MW)	MAE (%)	RMSE (MW)	RMSE (%)	Maximum Negative Error (MW)	Negative Error (%)	Maximum Positive Error (MW)	Maximum Positive Error (%)
Wind									
CA	4,406	299	7	438	10	−2,200	−50	2,306	52
CG	6,581	312	5	454	7	−2,485	−38	3,352	51
NTTG	5,787	248	4	353	6	−2,034	−35	2,102	36
WC	6,584	269	4	356	5	−1,688	−26	1,772	27
U.S. Western Interconnection	23,357	785	3	1,038	4	−4,280	−18	5,153	22
Solar (PV)									
CA	17,134	418	2	597	3	−2,658	−16	3,788	22
CG	1,211	46	4	69	6	−368	−30	339	28
NTTG	5,270	157	3	249	5	−1,573	−30	1,906	36
WC	36,526	667	2	966	3	−7,711	−21	14,380	39
U.S. Western Interconnection	60,141	991	2	1,423	2	−10,323	−17	19,982	33
Total									
CA	21,539	424	2	596	3	−3,247	−15	3,728	17
CG	7,792	316	4	456	6	−2,485	−32	3,352	43
NTTG	11,057	282	3	392	4	−2,040	−18	2,102	19
WC	43,110	516	1	776	2	−7,631	−18	13,643	32
U.S. Western Interconnection	83,498	1,020	1	1,382	2	−10,544	−13	19,156	23

Table 37. 4HA Forecast Error Statistics for the High Mix Scenario

Region	Capacity (MW)	MAE (MW)	MAE (%)	RMSE (MW)	RMSE (%)	Maximum Negative Error (MW)	Negative Error (%)	Maximum Positive Error (MW)	Maximum Positive Error (%)
Wind									
CA	4,788	308	6	450	9	−2,244	−47	2,356	49
CG	8,261	355	4	506	6	−2,523	−31	3,439	42
NTTG	12,414	423	3	561	5	−3,241	−26	2,563	21
WC	18,314	637	3	829	5	−3,590	−20	3,597	20
U.S. Western Interconnection	43,778	1,173	3	1,516	3	−5,951	−14	6,637	15
Solar (PV)									
CA	13,588	356	3	510	4	−2,290	−17	2,507	18
CG	1,161	45	4	67	6	−352	−30	321	28
NTTG	2,976	66	2	104	3	−548	−18	545	18
WC	23,165	438	2	634	3	−5,376	−23	8,820	38
U.S. Western Interconnection	40,890	696	2	989	2	−6,900	−17	11,781	29
Total									
CA	18,376	407	2	567	3	−2,959	−16	2,825	15
CG	9,422	357	4	508	5	−2,518	−27	3,439	37
NTTG	15,390	425	3	564	4	−3,148	−20	2,563	17
WC	41,479	708	2	929	2	−5,367	−13	7,991	19
U.S. Western Interconnection	84,668	1,261	1	1,631	2	−6,600	−8	10,996	13

Table 38. 4HA Forecast Error Statistics for the High Wind Scenario

Region	Capacity (MW)	MAE (MW)	MAE (%)	RMSE (MW)	RMSE (%)	Maximum Negative Error (MW)	Negative Error (%)	Maximum Positive Error (MW)	Maximum Positive Error (%)
Wind									
CA	7,970	441	6	619	8	−3,052	−38	2,956	37
CG	9,101	377	4	532	6	−2,608	−29	3,464	38
NTTG	16,854	550	3	725	4	−3,878	−23	3,273	19
WC	32,224	988	3	1,275	4	−5,412	−17	5,691	18
U.S. Western Interconnection	66,150	1,637	2	2,100	3	−7,685	−12	7,864	12
Solar (PV)									
CA	9,772	217	2	307	3	−1,388	−14	1,596	16
CG	969	37	4	55	6	−300	−31	261	27
NTTG	2,312	26	1	40	2	−193	−8	232	10
WC	14,979	201	1	289	2	−1,880	−13	3,132	21
U.S. Western Interconnection	28,032	352	1	496	2	−2,617	−9	4,179	15
Total									
CA	17,743	477	6	651	4	−3,089	−17	2,853	16
CG	10,070	378	4	533	5	−2,608	−26	3,464	34
NTTG	19,167	550	3	725	4	−3,851	−20	3,273	17
WC	47,203	990	3	1,281	3	−5,412	−11	5,691	12
U.S. Western Interconnection	94,183	1,650	2	2,115	2	−8,499	−9	8,021	9

Table 39. 4HA Forecast Error Statistics for the TEPPC Scenario

Region	Capacity (MW)	MAE (MW)	MAE (%)	RMSE (MW)	RMSE (%)	Maximum Negative Error (MW)	Negative Error (%)	Maximum Positive Error (MW)	Maximum Positive Error (%)
Wind									
CA	5,630	337	6	487	9	−2,470	−44	2,526	45
CG	6,161	298	5	436	7	−2,431	−39	3,335	54
NTTG	6,054	255	4	363	6	−2,110	−35	2,152	36
WC	10,054	371	4	493	5	−2,336	−23	2,267	23
U.S. Western Interconnection	27,900	888	3	1,171	4	−4,636	−17	6,192	22
Solar (PV)									
CA	2,798	82	2	132	5	−767	−27	1,063	38
CG	0	0	-	0	-	0	-	0	-
NTTG	364	16	3	27	8	−148	−41	201	55
WC	3,912	90	2	130	4	−893	−23	1,561	40
U.S. Western Interconnection	7,074	145	2	218	4	−1,482	−21	2,824	40
Total									
CA	8,428	347	4	494	6	−2,409	−29	2,445	29
CG	6,161	298	5	436	7	−2,431	−39	3,335	54
NTTG	6,418	255	4	363	6	−2,094	−33	2,152	34
WC	13,967	376	3	499	4	−2,336	−17	2,184	16
U.S. Western Interconnection	34,974	889	3	1,172	3	−4,490	−13	6,192	18

Figure 163 through Figure 168 show how the wind and solar 4HA forecast errors vary with load, net load, wind, and PV output.
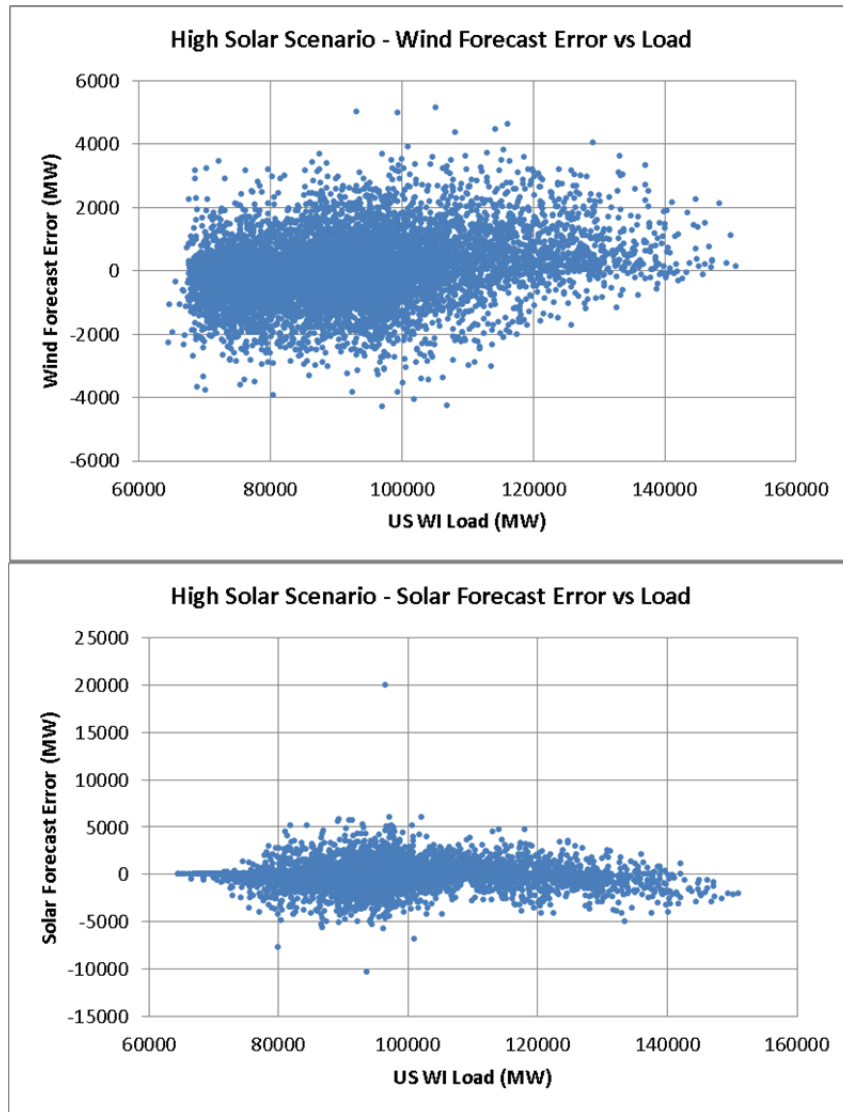

Figure 163. Wind and PV 4HA forecast errors as a function of load level for the High Solar Scenario
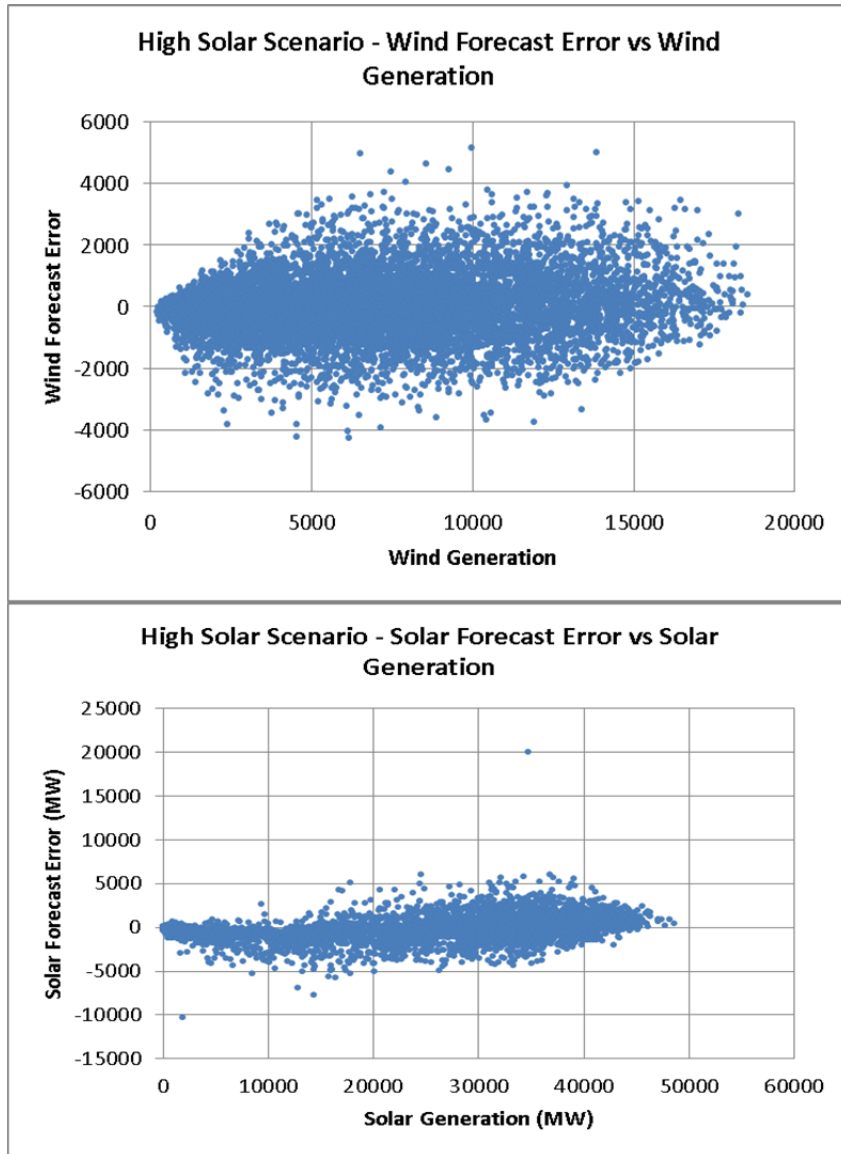
Figure 164. Wind and PV 4HA forecast error as a function of wind and PV output level for the High Solar Scenario
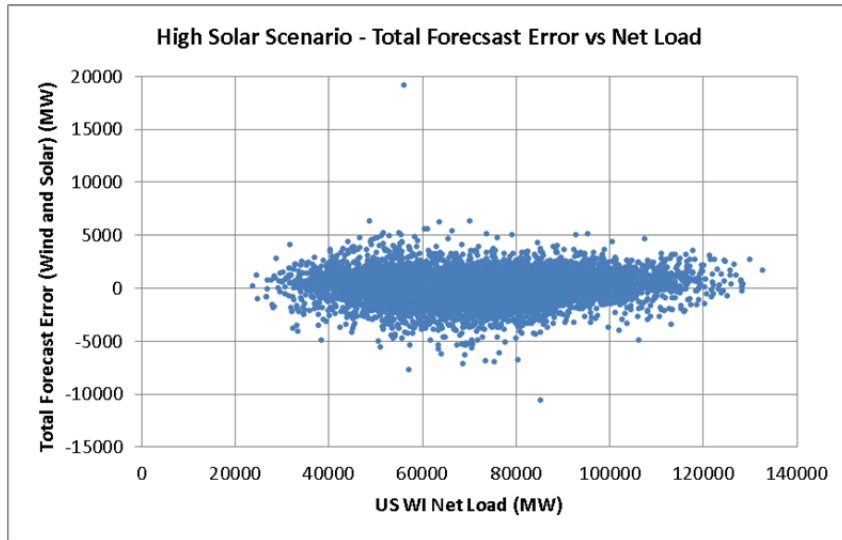
**Figure 165. Wind plus PV 4HA forecast error as a function
of net load level for the High Solar Scenario**
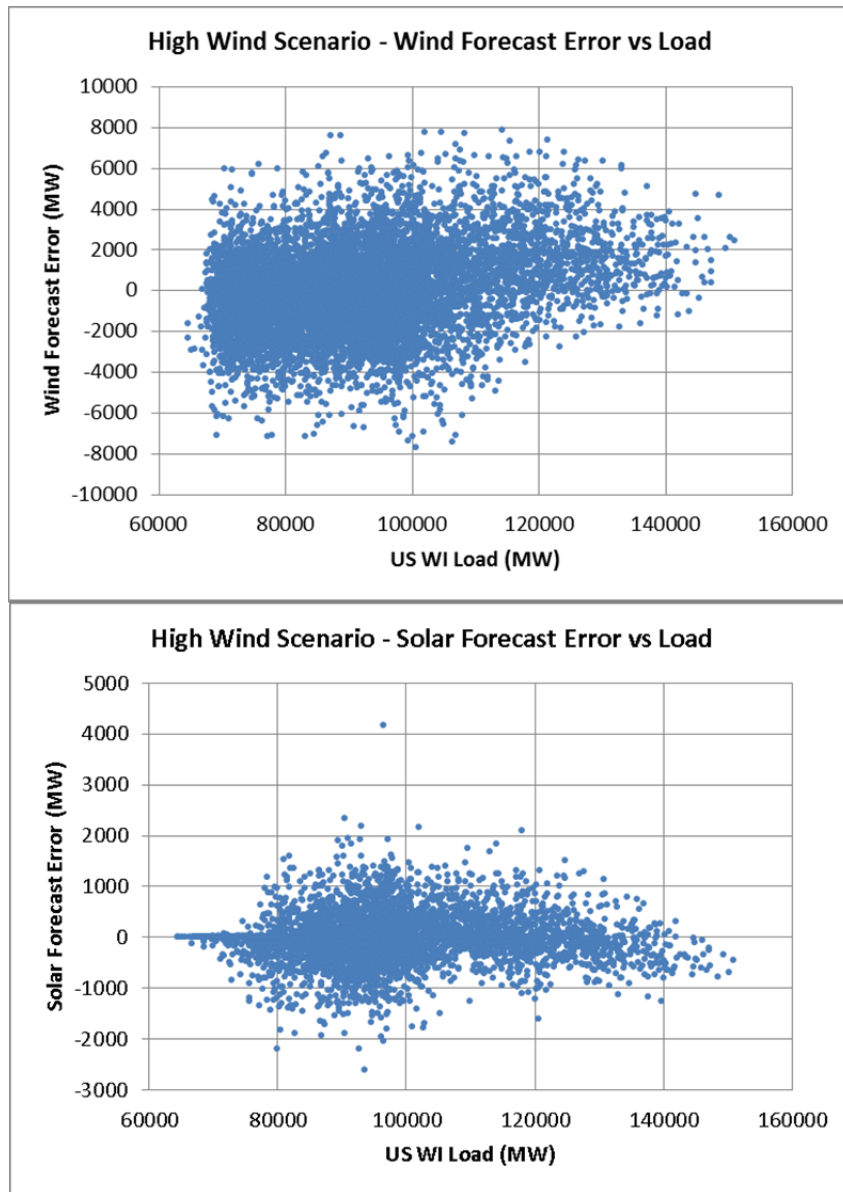
**Figure 166. Wind and PV 4HA forecast error
as a function of load level for the High Wind Scenario**
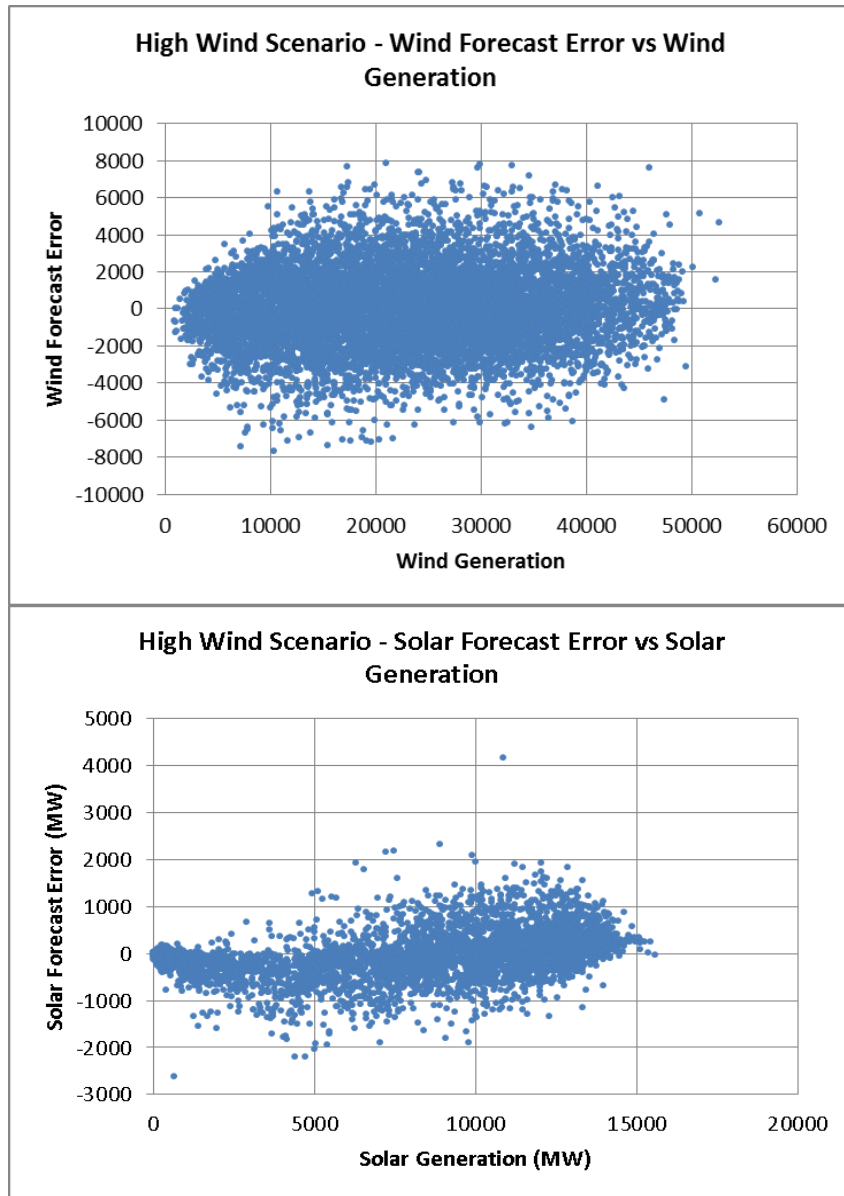
Figure 167. Wind and PV 4HA forecast error as a function of wind and solar output level for the High Wind Scenario
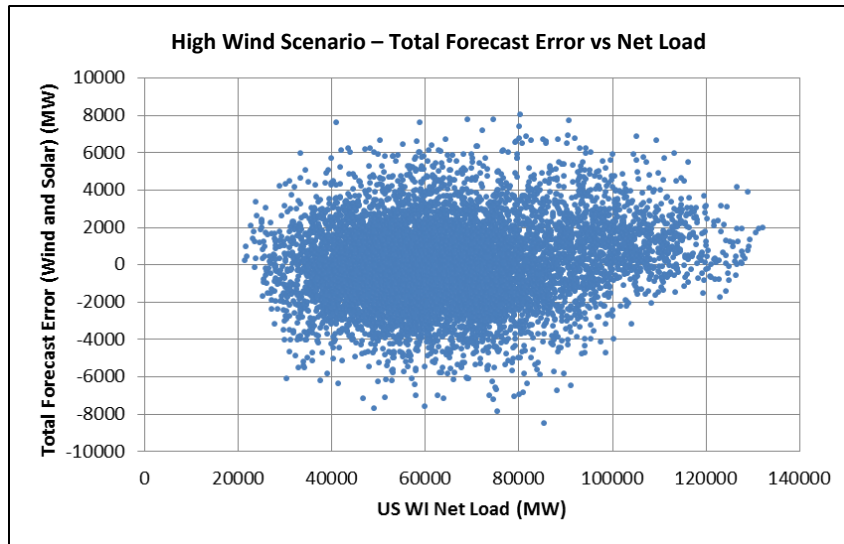
Figure 168. Wind plus PV 4HA forecast error as a function of net load level for the High Wind Scenario